Motion Coordination of Mechanical Systems

Leader-Follower Synchronization of Euler-Lagrange Systems using Output Feedback Control

Erik Kyrkjebø

A Dissertation Submitted in Partial Fulfillment of
the Requirements for the

Philosophiae Doctor Degree (PhD)

Department of Engineering Cybernetics
Norwegian University of Science and Technology

March 21, 2007

NTNU
Norwegian University of Science and Technology

Thesis for the degree of philosophiae doctor

Faculty of Information Technology, Mathematics, and Electrical Engineering
Department of Engineering Cybernetics

ISBN 978-82-471-1318-9 (printed ver.)
ISBN 978-82-471-1321-9 (electronic ver.)
ISSN 1503-8181

ITK Report 2007-1-w

Theses at NTNU, 2007:60

Summary

This thesis proposes two motion synchronization approaches to coordinate the motion of a follower to a leader within the Euler-Lagrange system framework. The information requirements from the leader are that of position and orientation only, i.e. the mathematical model with its parameters and the velocity and acceleration of the leader are considered unknown and unmeasured. The follower is responsible for the control action necessary to coordinate the systems, and the leader system is free to manoeuvre independently of the follower. There is no off-line synchronization of the systems through predefined paths or trajectories.

The concept of motion control of multiple objects is discussed in terms of the different forms of synchronization; cooperation (where all objects contribute equally) and coordination (where one object governs the motion of the others). Motivating examples and literature provide the motivation for the definition of two motion coordination problems. The output reference state feedback synchronization problem is defined by utilizing only output feedback from the desired motion reference, while assuming state feedback for the follower in the coordination control law. Furthermore, to increase the usefulness of the proposed control schemes and to provide robustness towards loss or poor quality of velocity measurements, the requirements of state information for the follower are alleviated in the definition of the output reference output feedback synchronization problem utilizing only output information of both the leader and the follower in the synchronization design. Furthermore, the necessary tools of stability are presented to prove that the proposed coordination schemes are uniformly ultimately bounded or practically asymptotically stable closed-loop systems.

In order to solve the output reference state feedback and the output reference output feedback synchronization problems, an observer-controller scheme is proposed that estimates the unknown states of the leader indirectly through a nonlinear model-based error observer. The observer-controller approach makes the follower system a physical observer of the leader system through the coupled observer and controller error-dynamics. A second nonlinear model-based observer is introduced for the follower to remove the state feedback assumption. The observer-controller scheme is proven to be uniformly globally ultimately bounded when utilizing state feedback of the follower in the coordination control law, and to be uniformly semiglobally ultimately bounded when utilizing only output feedback of the follower in the coordination control law. The observer-controller approach to motion coordination is studied through simulations and experiments, and a back-to-back comparison between ideal simulations and practical experiments is presented to allow for a discussion on the performance of the scheme under modelling errors, measurement noise and external disturbances. The observer-controller scheme is demonstrated to be suitable

for practical applications.

Furthermore, a virtual vehicle scheme is proposed to solve the output reference state/output feedback synchronization problems through a cascaded approach. The virtual vehicle approach is based on a two-level control structure to decouple the estimation and coordination error dynamics in the stability analysis and the tuning process. The virtual vehicle scheme estimates the unknown states of the leader through a virtual kinematic vehicle stabilized to the output of the leader system. A stable first-order velocity filter is introduced for the follower to remove the state feedback assumption. The virtual vehicle scheme is proven to be uniformly globally practically asymptotically stable when utilizing state feedback of the follower in the coordination control law, and to be uniformly semiglobally practically asymptotically stable when utilizing only output feedback of the follower in the coordination control law. Application of the virtual vehicle scheme to both vehicle coordination and robot manipulator coordination is presented, and the virtual vehicle approach to motion coordination is studied through simulations and experiments. The virtual vehicle scheme is demonstrated to be suitable for practical applications. In addition, an extension to a dynamic synchronization scheme is proposed to impose a smooth behaviour on the follower during a change of relative position.

The proposed coordination schemes are compared in terms of estimation principle, performance and robustness. Simulation studies compare the performance of the proposed schemes in terms of gain tuning and bounds on the closed-loop errors, and in terms of impact from external disturbances, modelling errors and measurement noise. The two coordination schemes are distinguished by concept rather than by performance, and both of the proposed schemes are believed to be suitable for practical implementation in coordination applications.

Preface

The research presented in this thesis is the result of my doctoral studies from October 2003 to December 2006 at the department of Engineering Cybernetics at the Norwegian University of Science and Technology, partially supported through the strategic university program CM-in-MC and the European Community Marie Curie Fellowship under contract number HPMT-CT-2001-00278.

I have been blessed with a supervisor, Professor Kristin Y. Pettersen, that not only has inspired me and guided me professionally, but has endured my slow, but hopefully progressive, maturing in the field of control. That she is meticulous in her feedback, enthusiastic and motivating in her supervision, and including in her personality is the main reasons why three years have passed without looking back, and ended just when I started raising my eyes. I also wish to thank my co-supervisor Professor Henk Nijmeijer at the Technische Universiteit Eindhoven (TU/e) for providing the inspiration for this work, and express my gratitude by borrowing one of his quotes *"Let all the credit of this work go to them, and all the criticism come to me"*.

The invitation of Dr. Elena Panteley and Dr. Antonio Loría to visit them at Laboratoire de Signaux et Systèmes at C.N.R.S/Supèlec outside Paris introduced me to many valuable topics and top researchers, and for this I am particularly grateful. I would also like to thank Dr. Antoine Chaillet at C.N.R.S/Supèlec for explaining the concepts of practical stability a sufficient and necessary number of times, and for providing the adaptations of his work that proved instrumental in some of the proofs of this thesis.

My work has benefited greatly from the discussions, corrections and inputs from many. In particular, I wish to thank Even Børhaug for setting the bar too high, Bjørnar Bøhagen for sharing his understanding and challenging mine, and Raymond Kristiansen for asking all the questions I should have asked.

I would like to thank my colleagues at SINTEF Applied Cybernetics, in particular Research Director Sture Holmstrøm, for the encouragement and opportunity, and all the faculty and PhD-students at the department of Engineering Cybernetics and Centre for Ship and Ocean Structures, in particular Dr. Maria V. Ottermo. I am also very grateful to Tove K. Johnsen and Eva Amdahl for clearing all the administrative issues and letting me focus on my work.

The experimental results presented in this thesis are the result of cooperation with Michiel Wondergem, Kjetil A. Knudsen and Jialu Do, and could not have been performed without the help of Stefano Bertelli at the Department of Engineering Cybernetics and Torgeir Wahl at the Department of Marine Technology.

I would like to thank the members of my doctoral evaluation committee; Professor António M. Pascoal, Dr. Jann Peter Strand and Professor Thor Inge Fossen for their constructive comments and feedback that have improved the quality of this thesis.

I would like to thank my entire family for their love, support and encouragement, and my girlfriend Mariann for her love and patience. The long-time friendly competition from Dr. Harald Takle is a big part of the reason why my doctoral studies were commenced, and for this I am forever indebted.

Trondheim, March 21, 2007 Erik Kyrkjebø

Contents

List of Figures

List of Tables

Chapter 1

Introduction

This thesis considers the problem of coordinating two or more mechanical systems in a leader-follower structure. The information requirements from the *leader* are that of position and orientation only, i.e. the mathematical model with its parameters and the velocity and acceleration of the leader are considered unknown and unmeasured. Thus, the coordination problem is a problem of the *followers*; fully actuated systems where the mathematical models with parameters are known, and only position/orientation measurements are required.

Coordinating multiple mechanical systems is important in providing flexibility through saleability and reliability through redundancy for many operations. However, this thesis focuses on the problem where coordination of several mechanical systems is a *requirement* to complete an operation. Tele-manipulation of surgical robots, lifting large structures by using two robot manipulators, towing large structures by using a large number of tugboats or transferring parts, fuel and personnel between moving ships, are all operations that require a high degree of coordination to be completed successfully.

1.1 Motivation

"Would you like to dance?" is a question that could be the beginning of a highly complex ritual where two or more people move their body in time to music. Dancing requires a high degree of coordination between the participants to synchronize their motion, not to collide with their partner or others on the dance floor, and to stay in time with the music. Most dance routines designate one of the dance partners to be the leading partner who governs the motion of the couple around the dance floor. However, in some dances, all partners take an equal part in deciding where to move and what moves to execute. Nevertheless, both strategies involve following an accepted global leader; the music. This synchronization behaviour is an example of a behaviour not only found among humans, animals or in nature in general, but it is also the goal of many control tasks in robotic, marine or aerospace systems; motion coordination.

1.1.1 Motivating examples

Coordinated motion of formations or groups of mechanical systems has been a topic of great interest in many applications over the last few years. Military applications have been predominant in employing coordinated motion schemes to increase endurance, flexibility and reliability of operations, and battle formations exist for almost all branches of the military; army, cavalry, navy and air force. Furthermore, many of the strategic techniques are inspired by natural phenomena, e.g. the flock of birds flying in formation to reduce air drag is an inspiration for the fighter jet pilots flying in close formation. However, recently coordinated motion has transitioned into civil applications such as the manufacturing and automotive industry through coordination of production lines, into medicine through artificial pacemakers and robotic surgery, and into multi-vehicle control in space and maritime environments.

Example 1.1 (Robot manipulator coordination) *In the manufacturing industry and especially in the automotive sub-supplier sector, there is a clear trend towards systems with two or more robots to increase performance quality and time-cycle issues. One of the main applications requiring precise robot coordination is arc-welding (Figure 1.1), especially in exhaust pipe, axle and seat production. The coordinated multi-robot systems offer advantages in terms of product quality, production rate and total system cost.*

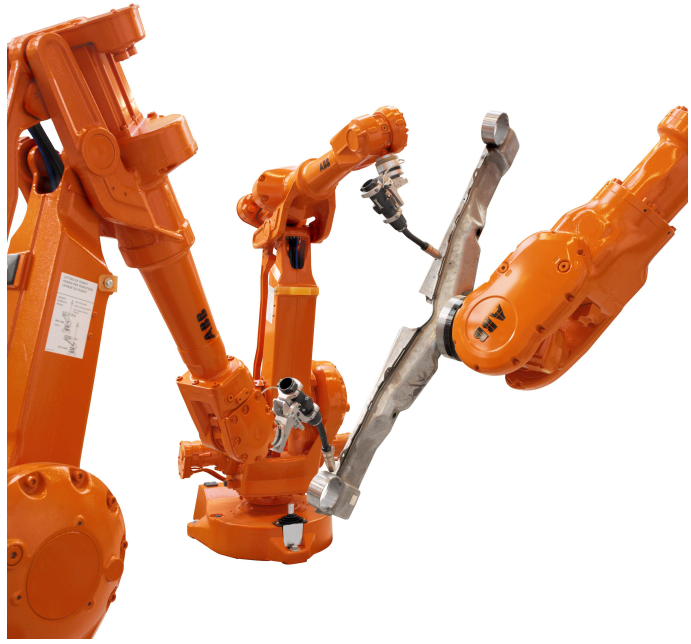

Figure 1.1: Multiple robots operating on an object moved by another robot. Photo: ABB, www.abb.com

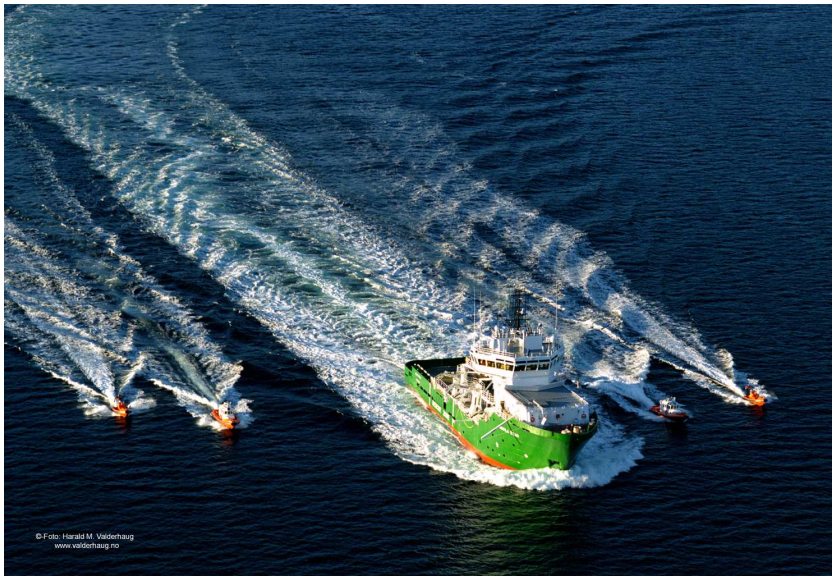

Figure 1.2: Illustration of marine vessels in formation. Photo: Harald M. Valderhaug, `www.valderhaug.no`.

Example 1.2 (Marine vessel formations) *Formation control of marine vessels has its application in many different operations that are traditionally piloted manually. In convoys over the Atlantic Ocean during World War I and II, every ship was closely piloted to stay in the convoy formation to gain protection from the accompanying battle ships, which proved a tiresome and nerve-racking task for already strained crews. The convoy formation has it parallel in today's ice-breaking escorts making a passage for larger freight ships in arctic areas.*

During the crossing of the Atlantic in convoys, another coordination task arouse in transferring fuel, supplies or ammunition between the ships. The operation of Underway Replenishment (UNREP) was taken on[1]*, and has since been a way of effectively increasing range and reducing port-time for vessels where it is impractical or impossible to return to base to replenish storage due to mission requirements.*

Recently, techniques for two-boat seining have improved fishing techniques in coastal and high-sea waters by coordinating two fishing boats towing a single seine to allow for larger seines and faster setting of the net. Also, the operation of oil booms and skimmers to contain oil spills requires a close coordination between the oil pollution vessel and the tug boat deploying the boom. The speed should be kept under 1 knot to reduce the risk of oil escaping the skimmers, and the oil spill containment booms are very sensitive to deviations from the desired formation. Any error in speed or heading reduces the efficiency of the equipment. The concept of coordinated towing operations can also be extended to more participants and larger structures, e.g. to manoeuvre oil platforms safely through narrow fjords and straits.

[1] See Section 1.1.2 for a closer look at underway replenishment.

Example 1.3 (Spacecraft formations) *Formations of spacecraft have primarily been used in monitoring the Earth and its surrounding atmosphere, but recently the focus is set on using distributed spacecraft infrastructures to form single sensing systems for all types of space applications: geodesy, deep-space imaging, exploration and data acquisition. The Cluster spacecraft (ESA) in Figure 1.3 is a collection of four spacecraft flying in formation to investigate the magnetosphere of the Earth, giving detailed information on how the solar winds affect our planet in three dimensions. The Cluster tetrahedron formation can be expanded using the two Double Star satellites (China/ESA) to form a larger sensing array, and due to the complementary Cluster and Double Star orbits, scientists can for the first time obtain a global view of the structure and physical processes at work in the magnetic shield of the Earth, with the Cluster tetrahedron studying these processes at small scales, and Double Star at large scales.*

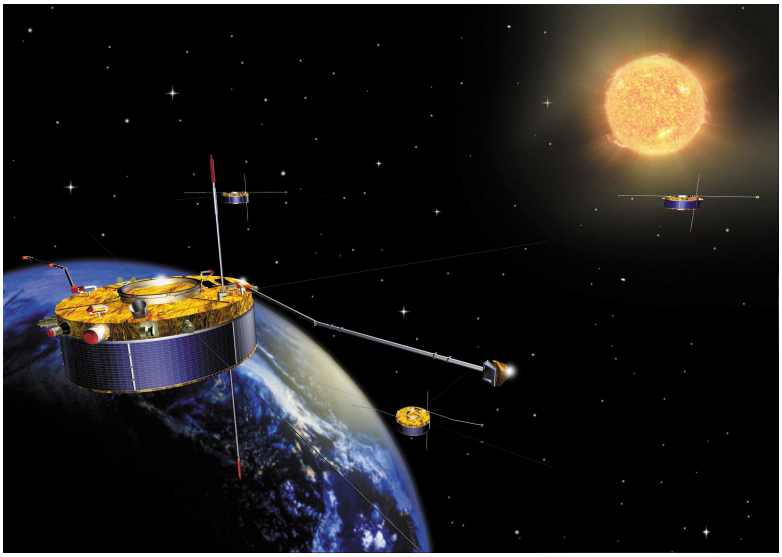

Figure 1.3: The Cluster satellites, a collection of four spacecraft flying in formation around Earth to investigate how the solar winds affect our planet in three dimensions. Photo: ESA, `www.esa.int`.

Note that the original four Cluster spacecraft were destroyed when the Ariane-5 rocket exploded during its maiden launch on 4 June 1996. A replacement spacecraft was build to recover some of the unique science of the mission, and this was equipped with flight spares of the experiments and subsystems prepared for the Cluster mission. However, recognizing that the scientific objectives of the Cluster mission could not be met by a single spacecraft, all four full-size Cluster spacecraft were rebuilt and launched in 2000.

Other distributed spacecraft systems include the two STEREO spacecraft (NASA) studying the extraordinary solar events known as Coronal Mass Ejections (CMEs) simultaneously from two different viewpoints to construct stereoscopic images. A third eye in this sensor array can be formed by the SOHO spacecraft (ESA/NASA), or even further expanded using the two Double Star spacecraft.

1.1.2 Underway Replenishment

A main motivation for the work presented in this thesis is the underway replenishment operation. An underway replenishment operation is an operation where fuel, food, parts or personnel are transferred from one vessel to another while both vessels are moving, and is common in space, aerospace and marine operations. These rendezvous operations are essential in situations where it is impractical or impossible to return to base to replenish storage or personnel due to mission requirements. In particular, underway replenishment (UNREP) operations at sea are essential for long-term military operations to shorten or avoid port time. The military has the luxury of having complete knowledge and control over all vessels participating in an UNREP operation, and can thus afford cooperative schemes to be employed through proper training and procedures for all personnel involved in the operation.

Figure 1.4: A military underway replenishment (UNREP) operation between an aircraft carrier and a dedicated supply ship. Photo: US Navy's Military Sealift Command, `www.msc.navy.mil`

However, facilitating civilian underway replenishment operations to replenish or offload commercial freighters or oil-tankers requires a different approach to the motion control problem. Faced with unknown vessels to be replenished, untrained personnel for the operation, and little information of the unknown vessels available, a cooperative scheme is ill-fitted to the application. In a motion control scheme for a civilian underway replen-

ishment operation, the parameters of the mathematical model of the replenished vessel can not be expected to be known, and no knowledge or influence over the control input from the captain steering the replenished vessel should be required. Furthermore, one cannot assume that all internal states for the replenished vessel are known to the supply vessel, and should thus employ a motion control scheme that relies only on the available output information from the replenished vessel.

A civilian underway replenishment operation thus demands a motion control strategy that requires no information of the future motion of the ship to be replenished and no knowledge of internal ship states or commanded control forces. In the simulation and model experiments section of the succeeding chapters we will use the civilian underway replenishment operation for surface vessels as an example to illustrate the theoretical contributions of this thesis.

We will designate the ship to be replenished as the leader in a leader-follower coordinated synchronization motion control scheme. The leader is allowed to move freely, and we will assume that we can only access its position and heading as output information from its internal states. Furthermore, we will assume that the replenished ship is unknown to the follower in the sense that there is no knowledge of the parameters of the mathematical model of the replenished ship, and no knowledge of the commanded control forces from the captain of this ship. The captain of the replenished ship is free to manoeuvre independently during the underway replenishment operation, and any predefined paths, trajectories or manoeuvres executed by the captain is assumed unknown to the follower supply vessel.

In turn, we will assume that the follower vessel is the supply vessel responsible for all the control action to coordinate the behaviour of the vessels, and that this ship is fully actuated in all degrees of freedom, the parameters of the mathematical model are known, and that we have access to state information of the follower vessel. Furthermore, to increase the usefulness of the control scheme and to provide robustness towards loss or poor quality of velocity measurements, we will alleviate the requirements on state information for the follower vessel and show how the motion control scheme can be expanded to utilize only output information from both the leader and the follower.

The history of underway replenishment

The replenishment problem dates back to the early days of sail, when the sailing ships were replenished at anchor by boats rowing out supplies from storages onshore, or exchanging personnel and mail by ship boats at sea. Through the development of the modern mechanized ship, the replenishment problem has changed character from a joint civil and naval operation at anchor in the early days, to nowadays primarily being a naval operation desirably conducted when the ships are underway.

During the US Quasi-War with France (1799-1801) (Hill (1989)), the US Navy used civil merchant ships to replenish their ships protecting their trade interests in the Caribbean. The merchant ships were taken under tow, and the ships were replenished using ship boats. Later during the war with Tripoli, the US Navy used a reduced armoured naval ship to shuttle men and supplies across the Atlantic to their fleet in the Mediterranean.

The introduction of the mechanized fleet introduced a new limited resource to the ships, and from this emerged the operations of coaling-at-sea and refuelling-at-sea. The former was usually conducted by bringing merchant colliers alongside the ships and lashing the ships together using fenders and mooring lines to transfer the coal using booms on the

collier. This approach was particularly vulnerable to weather conditions, and during the Spanish-American war off Cuba in 1899 one-quarter of the US ships were useless in the blockade when they were forced to seek calmer water for coaling-at-sea. This led to the development of a tension rig in 1904 designed to transfer the coal in bags, but poor operation and the introduction of fuel oil stopped further developments.

From this point on, the refuelling-at-sea operation required that the ships were specially equipped for the operation, and during World War I in 1916 a diesel powered oiler was used to replenish destroyers south of Greenland during their crossing of the Atlantic. World War II introduced the first real underway replenishment operations, but it was not until the Korean War that the concept of "designed-for-purpose" replenishment ships was fully utilized.

These early ships still lacked a robust underway replenishment system, and a new multi-product underway replenishment system providing UNREP for a broader set of weather conditions was introduced in 1957, when the standard tensioned replenishment alongside method (STREAM) was based upon the tension rig from 1904. This formed the basis for UNREP operations nowadays aided by helicopters in vertical replenishment (VERTREP) operations. See Hill (1989) and references therein for a thorough review of the history of underway replenishment, FAS (1999) and NROTC (2003) for a introduction to current replenishment techniques, and Miller and Combs (1999) for an evaluation of today's UNREP systems and the challenges faced when designing the next generation of underway replenishment systems.

Underway replenishment control approaches

Accurate control of the two ships during an underway replenishment operation is essential to avoid critical situations endangering personnel and materiel (Chen (2003)). The control approaches of underway replenishment have up to now used flags and signals to communicate control commands between ships (FAS (1999), NROTC (2003)) while being manually steered by the captains. Automatic control approaches have proposed utilizing some sort of tracking control of both ships in order to maintain trajectories that provide joint motion suitable for replenishment. Some of the earliest references to automated replenishment can be found as simulations studies of ship manoeuvring and steering control for underway replenishment operations in Brown and Alvestad (1978) and Dimmick *et al.* (1978), while Uhrin and Thaler (1976) designed a nonlinear speed control system for UNREP operations. Skjetne *et al.* (2004*c*) have expanded on traditional tracking methods with predefined paths, and introduced a feedback from the actual position of a ship (subject to disturbances) to the other ships in a formation through a path parameterization variable. All ships have predefined paths with individual tracking controllers requiring mathematical models and control availability, and the ships synchronize in terms of progression along the path.

Any two physical systems which are not identical in their design will experience different impacts from environmental forces such as wind, drag, current, terrain or waves. This difference may possibly lead to critical situations when employing simple tracking controllers to predefined reference paths where the coordination of the leader and follower is only done at the path planning stage, and not through active control. The schemes presented in this thesis do not require any predefined paths, and thus the effects of any divergence from an ideal path due to disturbances, unmodelled dynamics, actuator limi-

tations, poor control design or actuator failure is inherently cancelled in the coordination approaches of Section 3 and 4. Through this, civilian underway replenishment operations may be facilitated, and the performance of existing UNREP operations may be improved by introducing automatic control systems.

Sensor systems

Underway replenishment at sea requires a close coordination of two vessels, and has up to now been conducted using manual control together with control flags to exchange instructions between the vessels. Recent advances in control theory and measurement systems, in particular the introduction of the Global Positioning System (GPS) (Parkinson and Spilker (1995)) and the Automatic Identification System (AIS) (Harre (2000)) allows automatic control approaches for replenishment purposes to be designed. These autopilots are faced with the goal of suppressing effects of external disturbances due to wind, waves and currents, while achieving the accuracy demands of the operation using a reduced set of measurements. The introduction of autopilots and advanced measurement systems expand the range of operating conditions for safe replenishment in terms of increased manoeuvrability in close waters or in the proximity of other vessels, and in the robustness towards environmental disturbances.

The Automatic Identification System is a system used by ships and vessel traffic systems principally for identification of vessels at sea. AIS helps to resolve the difficulty of identifying ships when not in sight (e.g. at night, in fog, in radar blind arcs or shadows or at distance) by providing a means for ships to exchange ID, position, course, speed and other ship data with nearby ships. It works by integrating a standardized VHF transceiver system with a GPS receiver and other navigational equipment on board the ship (gyro compass, rate of turn indicators, etc.), and transmits position and course at fixed intervals depending on the operation. The AIS transceiver transmits the following data every 2 to 10 seconds depending on the speed of the vessels while underway, and every 3 minutes while the vessel is at anchor (USCG (2005)):

- MMSI number of vessel - a unique identification for the vessel
- Navigation status - "at anchor", "under way using engine(s)", "not under command"
- Rate of turn - right or left, ranging from 0 to 720 degrees per minute
- Speed over ground - with a 0.1 knot resolution from 0 to 102 knots
- Position accuracy
- Longitude and Latitude - with a resolution of 1/10000 minute
- Course over ground - relative to true north to with a resolution of 0.1 degrees
- True Heading - 0 to 359 degrees from e.g. a gyro compass
- Time stamp - UTC time accurate to nearest second when this data was generated

AIS is required aboard all ships greater than/equal to 300 gross tons for international voyages, and it is estimated that more than 40,000 ships currently carry AIS class A equipment.

1.2 Background

1.2.1 Synchronized motion

The concept of synchronized motion has been discussed for artificial systems since Huygens (1673) designed an experiment with two pendulum clocks exhibiting (anti-)frequency synchronization after a short time when hanging from a light weighted beam. The pendulum clock was a breakthrough in timekeeping, and became instrumental in naval navigation to determine the latitude of a ship by measuring the angular altitude of the star Polaris at a given time. In the last century, synchronization has received a lot of attention in the Russian scientific community (Blekhman (1971)) through its observation in balanced and unbalanced rotors and vibro-exciters. Recently, several papers have been published relating to synchronization of rotation bodies and electromechanical systems (Blekhman *et al.* (1997), Huijberts *et al.* (2000)). Synchronized motion can be exhibited in unbalanced rotors in milling machines, vibro-machinery in production plants or in electrical generators (Blekhman (1971)) as uncontrolled vibrations, while for mechanical machines that cooperate to increase flexibility and manoeuvrability (Nijmeijer and Rodriguez-Angeles (2003)) it is instrumental in completing the task.

Synchronization can be seen as a type of time conformity between systems, and can be divided into the concepts of cooperation or coordination. *Cooperation* requires that all participants interact to share information and cooperate on equal terms toward achieving the goal. In many systems this is desirable, as in controlling multi-fingered robot hands and multi-actuated platforms lifting large structures (Brunt (1998), Tan *et al.* (2004)). Cooperative (internal) synchronization describes a situation where the failure of one of the participants is detrimental to the whole group. *Coordination* requires that one object takes the role of a leader that governs the motion of the others, and the behaviour of this leader is independent of the motion of the other objects. This is desirable in groups where the participants should copy or react to the behaviour of a single object, as in teleoperated systems (Xi and Tarn (2000)) and surgery (Hills and Jensen (1998)). Coordinated (external) synchronization control is often referred to as *leader-follower* control, and describes a situation where the failure of a follower will not affect the behaviour of the leader.

In a cooperative approach, all participants have two tasks; achieve the goal of the group *and* control the geometry of the group. In a coordinated approach the tasks are distributed; the leader is responsible for achieving the goal of the group, while the followers are responsible for the coordination within the group. The information flow in a coordinated control scheme is unidirectional from the leader to the followers, as opposed to the bidirectional information flow between the participants in a cooperative control scheme. The coordination approach thus alleviates some of the information requirements placed on the participants in a cooperative approach; in a cooperative scheme, all participants must have some knowledge of the states of the other participants in order to cooperate.

All cooperating participants must achieve the goal of the group through active control in a cooperative approach. This means, depending on the degree of cooperation, that if one of the participants in a redundant group fails, the group behaviour is affected. On the other hand, in a strictly coordinated redundant group, the failure of a follower does not affect the behaviour of the group. The degree of cooperation or coordination thus determines the behaviour in the case of failure of one of the participants in a group.

Note that we can design a cooperative system so that it disregards faulty objects and

thus leaves the group unaffected, and we can design coordinated systems so that the failure of one of the followers changes the behaviour of the group through a feedback from the followers to the leader. Thus, a nominally cooperative system may behave as a coordinated system in a situation of failure, and a nominally coordinated system may behave as a cooperative system in a situation of failure, as illustrated in Figure 1.5.

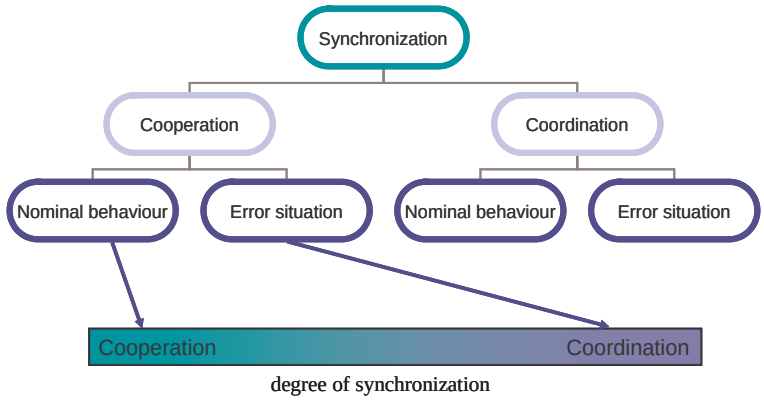

Figure 1.5: The degree of synchronization ranges from strictly cooperative to strictly coordinated motion control schemes. The figure depicts a nominally cooperative scheme, but for a redundant group with a faulty participant, a sleeping leader is awoken to govern the motion of the group. The group has now changed its motion control scheme to a coordinated scheme to avoid being slowed down by a faulty unit.

The focus of this thesis is on systems that lend themselves naturally to the leader-follower coordination approach to successfully achieve the synchronization goal, rather than to those systems that require a larger degree of cooperation in their nominal behaviour. The choice of synchronization strategy as cooperative and coordinated should reflect the nominal behaviour of the system, while the degree of synchronization should determine the behaviour in situations where one of the participants fail. Furthermore, the degree of synchronization for a system may depend on the degree of failure. This thesis will only focus on the nominal behaviour of coordinated systems. However, it will also deal with loss of state information for the followers. For this purpose, a loss of state information of the followers is not considered as a failure, but rather as a degradation of the system.

For synchronized moving objects, it is natural to think of all the objects in terms of a formation or a group, which relates closely to the concepts of fish schools, flocks of birds or large herds of animals. However, for other synchronized systems e.g. two robot manipulator arms, the concept of a formation is not so apparent, and in some cases misleading. Thus, this thesis uses the concept of *synchronization* to describe the motion of two or more objects *in time* with each other. Synchronized motion is further divided into the concepts of coordination and cooperation to describe the governing factor in the behaviour of the systems. The concepts of formations and groups are to be understood as synchronized motion in applications which naturally lend themselves to these concepts, but for the development of the coordination control schemes in the succeeding chapters, these concepts do not exclude other applications such as the robot manipulator case. Formations and groups are

merely intellectual concepts providing the intuitive basis for understanding the concepts discussed.

1.2.2 Coordination as a natural phenomenon

Synchronized motion is not only found in artificial systems induced by active control or resonance effects, but maybe foremost as a natural phenomenon in biological systems. The book of Camazine *et al.* (2001) provides an excellent overview of cooperation as self-organization in the synchronized flashing of fireflies, fish schooling and trail formations of ants, and the concept of coordination in biological systems through "Leaders, Blueprints, Recipes and Templates" (Camazine *et al.*, 2001, Chapter 4). Strict coordination in biological systems can be observed in the queuing behaviour of ducklings or chicks where each of the young individuals blindly follows their mother, and leadership has also been proposed as the governing factor in coordinated movements of individuals in large groups such as schools of fish or flocks of birds. In insect societies of honey bees or wasps, the mother queen is the "central pacemaker and coordinator of colony activity" to her workers.

In biological systems, it is believed that groups move from coordination to cooperation due to limited communication and cognitive abilities of the individuals in the group. In particular, the individuals may have problems in making and using blueprints, recipes and templates, or the limitation may be that one of the individuals must have excellent cognitive skills, an effective communication network and thorough knowledge of the master plan to function as a leader. In many systems, these skills are not present in a single individual allowing a centralized coordination scheme, but rather as pieces spread out between the individuals suggesting a distributed cooperative scheme.

Group synchronized motion in biological systems is beneficiary not only pertaining to the performance of the group, but also to the survival of the group individuals. One survival strategy is the swift, evasive manoeuvre at the approach of predators (Partridge (1982)) called the Trafalgar Effect (Treherne and Foster (1981)) by analogy to the rapid transfer of battle-flag signals along a chain of ships in Admiral Nelson's fleet at Trafalgar. However, coordinated behaviour can also be observed among the predators, as in schools of killer whales hunting dolphins by encircling their prey and gradually constricting the circle before one of the whales rush into the middle of the school while the others continue to circle (Martinez and Klinghammer (1970)).

In addition, there may be the effect of increased hydrodynamic swimming efficiency that could increase the endurance up to six times for fish travelling in schools (Wiehs (1973)), although contradictory data to this fact for several species has been reported in Partridge and Pitcher (1979)). For flocks of birds flying in their V-shaped flight formation (see Figure 1.6) it is suggested that the energy savings for a group of twenty-five individuals will allow them to increase their flight range by 70 percent over that of a solitary bird (Lissaman and Shollenberger (1970), May (1979)). A prime example of motion coordination to increase performance is found in the migrations of spiny lobsters in Bill and Herrnkind (1976), where as many as sixty-five lobsters line up in single-file formations maintained by tactile feedback. The study shows that a formation of nineteen lobster individuals can maintain a pace of 35 cm/s with the same hydrodynamic drag as individual lobsters travelling only 25 cm/s.

The principle of reduced drag has not been lost on professional cyclists who can be seen maintaining single-line formations, and changing formations to adjust for wind direction

Figure 1.6: A flock of birds flying in a V-shaped formation. Photo: www.potomacs.com

and wind speed. Closing the gap between a natural phenomena and artificial coordination is the use of pacemakers; an artificial system implanted in the human body to provide proper heart rhythm when the natural pacemaker of the body is not functioning properly.

1.2.3 Artificial coordination

The works of Blekhman (1971) spawned interest in the synchronization concept from Huygens (1673), and synchronization has lately been introduced to many fields within control theory and physics. In communication systems, synchronization is used to improve efficiency of the transmitter-receiver system, and to encrypt information to improve security in the transmissions (Kocarev *et al.* (1992), Celikovský and Chen (2005)). The applications in mechanical systems range from the synchronization of rotation bodies and electromechanical systems (Blekhman *et al.* (1997), Huijberts *et al.* (2000)), mobile robot vehicles in formation (Yamaguchi *et al.* (2001)) and formation control of satellites (Wang *et al.* (1996), Kang and Yeh (2002), Lawton and Beard (2002)), to telerobotic surgery giving more precise and less invasive surgery (Hills and Jensen (1998)).

In a synchronized motion scheme, the group of participants must achieve two objectives; the group objective and the geometry objective. The geometry objective determines the position of each individual within the group, while the group objective is usually strongly determined by the application, and ranges from the simple strategy to get from point A to point B, to more elaborate strategies executing complex motion paths. The interaction between the geometry objective and the group objective is one of the determining factors in classifying motion control schemes into different categories.

Classic motion categories for single-object control are the path-following or trajectory tracking strategies (Spong and Vidyasagar (1989), Fossen (2002), Aguiar and Hespanha (2004)) or the manoeuvring strategy (Hauser and Hindman (1995), Skjetne (2005)), which have been adopted into multi-object strategies (cf. Frezza (1999), Encarnacao and Pascoal (2001) and Skjetne *et al.* (2003)). See Appendix D for more details on the concepts of multi-object path-following, trajectory tracking and manoeuvring. The multi-object control schemes based on classic motion control strategies all requires, due to their original single-object design, a predefined group motion objective in the form of a path, trajectory or a manoeuvre.

Due to this predefined information, these strategies are for some applications more suited to a cooperative approach, as all participants must follow this predefined motion pattern which is the group objective. Should the environment or group objective change, this requires a recalculation of the motion pattern, and in turn this new motion pattern must be communicated to all participants of the group.

There also exists freedom in the synchronization strategy of classic motion control schemes. Predefining a motion pattern for each individual can be seen as off-line synchronization, while true coordination or cooperation can only be achieved through on-line feedback. Due to the predefined information, it is often only necessary to synchronize the motion of individuals along the path (Encarnacao and Pascoal (2001), Skjetne *et al.* (2003)) using some path parameterization variable to limit the communication flow substantially. However, this only guarantees synchronization along the path, and large cross-track errors due to external disturbances may not be compensated for in the synchronization control.

These motion synchronization approaches all come from the classic single-object control strategies, while an inherently multi-object approach was introduced by Rodriguez-Angeles (2002) using a leader-follower synchronization approach which does not require any predefined motion patterns for the participants in a leader-follower coordinated scheme. The followers are coordinated to the leader of the group through the geometry objective, while only the leader is responsible for obtaining the group objective. The motion coordination is based purely on on-line information from the leader, and any disturbances affecting the ability of the leader to fulfil the group objective does not affect the geometry control objective of the followers.

In the literature, we can to some extent distinguish between model-based and behavioural based motion synchronization approaches, which both have utilized the concept of a *virtual* object to aid in the synchronization schemes.

Behavioural based approach The behavioural based methods prescribe a set of desired behaviours for each individual of a group, and weigh the individual behaviour such that desirable group behaviour emerges without an explicit model of the individuals or the environment. The desired group objective can be trajectory tracking, neighbour tracking, collision and obstacle avoidance or formation control. In Justh and Krishnaprasad (2004) and Sepulchre *et al.* (2006), identical (point wise) objects in the plane moving at constant speed are considered, and the objects are subject to steering controls that change their orientation. Motion is stabilized to isolated relative equilibriums corresponding to either parallel or circular motion. Tracking control is treated in Paley *et al.* (2004), and formation control in Balch and Arkin (1998), Leonard and Fiorelli (2001) and Olfati-Saber and Murray (2002), while an application to unmanned sensor networks is presented in Øgren *et al.* (2004). The behavioural rules are often given as algorithms, and stability can be hard to analyze since the group behaviour is not given explicitly. This issue has been addressed in Stilwell and Bishop (2002) by introducing a system-theoretic approach to control a platoon of underwater vehicles. Note that due to the nature of this approach, most control schemes should be regarded as cooperative schemes.

Model-based synchronization The model-based synchronization methods utilize the explicit mathematical model of the participants in synchronizing their motion. This approach allows for nonlinear model-based controllers (cf. Marino and Tomei (1995)) and

nonlinear model-based observers (cf. Nijmeijer and Fossen (1999)) to be constructed in order to synchronize the motion of multiple objects. Synchronization schemes are applied to a wide range of applications from the synchronization of spacecraft motion (Wang *et al.* (1996), Lawton and Beard (2002), Kristiansen *et al.* (2006), Krogstad and Gravdahl (2006) to the synchronization of windshield wipers (Levine (2004)), oscillators (Kumon *et al.* (2002)), pendulums (Loría *et al.* (1998)), or moving gantry stages (Tan *et al.* (2004)).

Synchronized motion control schemes for fixed robots have been applied to both industrial manipulators (Connolly and Pfeiffer (1994), Brunt (1998), Caccavale *et al.* (1998), Nijmeijer and Rodriguez-Angeles (2003), Bondhus *et al.* (2004)), applications in medicine such as telerobotic surgery (Hills and Jensen (1998)) and to mobile subsea manipulators (Lizarralde *et al.* (1995)). Mobile vehicles have been synchronized in applications ranging from mobile robots (Yamaguchi *et al.* (2001), Hu *et al.* (2003)), aircrafts (Frezza (1999), Giulietti *et al.* (2000), Seiler *et al.* (2004) and marine vessels (Stilwell and Bishop (2000), Encarnacao and Pascoal (2001), Skjetne *et al.* (2002), Flakstad Ihle (2006)).

Some approaches focus on communication requirements and constraints between objects (Fax and Murray (2004), Ghabcheloo *et al.* (2006)), or limiting the information flow or state measurements (Encarnacao and Pascoal (2001), Nijmeijer and Rodriguez-Angeles (2003), Skjetne *et al.* (2004*c*)). Through the use of dynamic models for the participants in model-based control approaches, stability can in most cases be investigated through classic Lyapunov analysis (cf. Khalil (2002)). Most of the model-based approaches to synchronization have been employed in both cooperative schemes and coordinated schemes, and thus the choice of strategy is generally determined by the application.

Virtual object synchronization Virtual objects are used in both the behavioural and the model-based approaches, where a virtual model or object to govern the motion of the individual participants in a group, or the motion of the group as a whole. This virtual object can be a vehicle, manipulator or a group structure depending on the application, and specifies the behaviour of the participants in formations and groups by providing a virtual control reference.

The virtual object approach has been utilized both as an abstraction vehicle (Crowley (1989), Salichs *et al.* (1991)) and as an intermediate level between the desired trajectories of a system and the controller. In a way, it can be considered as a low-level controller in a two-level control structure (Fradkov *et al.* (1991), Gusev *et al.* (1998)), and was used in Sakaguchi *et al.* (1999) as the mapping of a physical vehicle, and in Egerstedt *et al.* (2001) to control a reference point on a planned path. Each member of the formation tracks a virtual element, while the motion of the virtual elements is governed by the formation function specifying the geometry of the formation.

The approach of Egerstedt *et al.* (2001) has been utilized in Hu *et al.* (2003) to combine the task of path following and obstacle avoidance, and in Cheng *et al.* (2004) with a modified goal point to improve practical robustness to path diversity. A virtual leader together with artificial potentials was used in the behavioural approaches of Leonard and Fiorelli (2001) to coordinate a group of vehicles, and by Olfati-Saber and Murray (2002) to manipulate vehicles in a formation through cost graphs.

The virtual object synchronization control schemes can also be seen from a dynamical synchronization viewpoint as in Efimov (2005), where the control errors exhibit a specified

dynamical behaviour rather than being stabilized to zero. Thus, oscillatory motion around a (virtual) leader can be obtained in a formation or group.

1.3 Contributions and scope of thesis

The focus of this thesis is motion coordination of mechanical systems using only the available output information from the leader. No knowledge of mathematical parameters in the model of the leader, or any velocity or acceleration information, is assumed to be available to the follower. The proposed coordination approaches assume no knowledge of any predefined paths for the leader (or the follower), and no knowledge or control of the actuator forces of the leader. This last assumption suggests that the follower can not rely on the leader to actively participate in the synchronization of the two systems, and thus the synchronization schemes become coordinated schemes where the followers are responsible for all the synchronization control action. The synchronization schemes presented in this thesis focus on applications where coordination between multiple systems is a *requirement* for completing the objective of the application. This is in contrast to control schemes where multiple systems provide redundancy in an application. Thus, the focus of this thesis is on coordinating the follower to the leader, and the problem of what motion the leader-follower system executes is subordinate to this coordination objective.

The synchronization approaches proposed in Encarnacao and Pascoal (2001), Skjetne (2005) and Flakstad Ihle (2006) are based on classic single object control schemes with predefined paths or trajectories. All systems are responsible for synchronization control action through a path variable designed to minimize the communication flow between the systems, and state information is only utilized locally through each path following controller. Thus, synchronized motion requires in most cases cooperation between all the individuals of the group, or at least some knowledge of the future behaviour of the other participants. This assumption is removed in the proposed coordination schemes of this thesis to facilitate synchronization to a system where the parameters of the mathematical model are unknown, and the velocities and accelerations are unmeasured.

The coordination approach proposed in Nijmeijer and Rodriguez-Angeles (2003) provides synchronized motion for systems with no dissipative forces in the system model. This thesis extends these results to systems with dissipation to further generalize the result. In addition, velocity measurements of the follower are introduced to the coordination scheme and shown to give global stability results. Furthermore, a sliding surface is introduced to provide additional design freedom in the complex tuning process of the observer-controller scheme. The proposed coordination scheme is experimentally verified, and thus a discussion of performance in terms of modelling errors, measurement noise and external disturbances can be presented for the observer-controller coordination scheme.

The two-level motion control scheme of Gusev *et al.* (1998) provides a simple kinematic control law for a single vehicle to stabilize to a desired trajectory. This thesis utilizes a two-level motion control scheme to coordinate multiple systems in a leader-follower coordination scheme, utilizing a more general kinematic controller and the concepts of a virtual vehicle and a reference vehicle with reference kinematics. Furthermore, practical stability of the closed-loop errors is proven for the coordination scheme, and the assumption of state measurements of the follower is removed to generalize the stability results.

1.3.1 Delimitations

This thesis proposes solutions for the motion coordination problem where the reference is a physical system (a leader) experiencing disturbances, model errors etc. that may cause deviations from ideal paths or trajectories. The coordination schemes assume coordination within a local frame of reference, and hence the external disturbances experienced by the participants are likely to be similar in magnitude and direction, albeit of different influence to the participants depending on their physical structure. The focus of the thesis is to present motion coordination solutions that can be applied to a large number of systems in general, and not to address the implementation issues associated with each application in particular. This section briefly summarizes some of the aspects of motion coordination for physical systems that are not the focus of this thesis.

Situations where the number of degrees-of-freedom in the control objective is unmatched by the actuators of the system (underactuation or redundancy) are not addressed in this thesis. A collision avoidance scheme between the leader and the follower system is inherent in the motion coordination schemes proposed. However, this thesis does not focus on designing collision avoidance systems between multiple followers. The representation of attitude and orientation of the systems described is assumed to be mathematically non-singular, in the sense that the representation of attitude is in the form of non-singular representations, or in that the systems are assumed never to approach singular configurations. Although the discussion of the control systems assumes continuous-time plants, the control schemes are implemented in discrete-time, and thus the sampling time is assumed sufficient for this simplification. Furthermore, communication issues regarding limited bandwidth and loss of communication packages are not discussed explicitly in this thesis.

In the control schemes presented, no explicit treatment is given to the impact of force saturations in actuators, measurement noise, model parameter errors or external disturbances. However, the effect of such perturbations is discussed in a simulation study when comparing the two proposed control schemes in terms of robustness, and in the practical experiments presented.

In the application of robot manipulators, the effects of nonlinear dissipative forces are studied, but no explicit analysis is done on the effects of flexible manipulators. Motion coordination of aerospace and aeronautical applications are not studied explicitly in this thesis, but fits into the general framework of the Euler-Lagrange system models. In the application of coordinating marine vehicles, no explicit wave-filtering has been applied to the surface applications to reduce controller action, chattering etc. However, experiments with waves illustrate the performance under the influence of motions in the uncontrolled degrees-of-freedom (roll and pitch).

An adaptation of the proposed coordination control schemes to utilize relative measurements (range measurements) rather than absolute position measurements is not presented in this thesis. Relative measurements provide position coordinates relative to the observer's position, and providing the introduction of an attitude measurement or attitude observer, the problem reduces to that of absolute measurements.

Note also that gains and gain restrictions presented in this thesis are not necessarily optimal in the sense of performance, energy consumption or transient behaviour. Gains are chosen to illustrate the behaviour of the motion coordination schemes under ideal conditions in the simulations, and to attenuate disturbances while maintaining good performance during the experiments.

1.3.2 Contributions

The main purpose of this thesis has been to achieve leader-follower coordination of systems using a minimal set of measurements and model parameters. For the entirety of the thesis, the leader is assumed to be a system for which only the position/orientation is available as output information, while the mathematical model parameters and the velocity and acceleration of the leader are unknown. The position/orientation and the parameters of the mathematical model of the follower are assumed known, while the coordination schemes are developed using both estimates and measurements of the follower velocity to make the results applicable for a larger set of operation scenarios, and to provide safety and reliability in the case of sensor failures. The contributions of this thesis can thus be summarized as follows:

- Chapter 2: The definition of output feedback state tracking forms the basis for two new definitions of output feedback problems where the states of the reference are unknown; the output reference state feedback synchronization problem in Definition 2.7 and the output reference output feedback synchronization problem in Definition 2.8. Furthermore, the concept of a reference vehicle with kinematics is introduced, where the reference vehicle is uniquely determined by the position of the leader. The reference vehicle defines the desired position for the follower in the motion coordination schemes proposed in Chapter 3 and Chapter 4.

- Chapter 3: Results on observer-controller synchronization of mechanical systems are extended to include dissipative terms in the Euler-Lagrange model, and to incorporate available velocity measurements of the follower which is shown to provide global stability results. Furthermore, simulations and experiments are presented in a back-to-back comparison to investigate the performance of the observer-controller scheme in terms of robustness towards measurement noise, modelling errors and external disturbances. The complex tuning process of the coupled closed-loop system is investigated in detail, and a sliding surface is introduced to the scheme to provide additional design freedom. The observer-controller approach to motion coordination is shown to give uniform ultimate boundedness of the closed-loop errors. This chapter is based on joint work with Michiel Wondergem, Henk Nijmeijer and Kristin Y. Pettersen.

- Chapter 4: A virtual kinematic observer is introduced as a controlled virtual vehicle to provide estimates of the unknown states of the leader in a motion coordination scheme. The virtual vehicle is an estimator based on the kinematics of the follower, and through the definition of a virtual control law, estimates of the unknown states of the leader can be utilized in a control law to coordinate the motion of the follower to the leader. The virtual vehicle design provides a two-level cascaded control structure that decouples the stability analysis and tuning process of the estimator and the coordination controller. Simulations and practical experiments verify the theoretical results of practical stability of the closed-loop errors, and the domain of attraction and the bound on the closed-loop errors can be enlarged and diminished as desired through the tuning process. Furthermore, a dynamic synchronization scheme is proposed to impose a smooth dynamic behaviour on the follower when changing position relative to the leader. This chapter is based on joint work with Elena Panteley, Antoine Chaillet and Kristin Y. Pettersen.

- Chapter 5: The observer-controller approach of Chapter 3 and the virtual vehicle approach of Chapter 4 are compared in terms of estimation principles, performance and robustness in practical applications. A discussion is presented on the estimation principles employed to estimate the unknown states of the leader, and the benefits and drawbacks associated with each approach are discussed. Simulation studies investigating the performance and robustness of the proposed motion coordination schemes are presented. This chapter is based on joint work with Kristin Y. Pettersen.

1.3.3 Publications

The following is a list of the pertinent publications produced during the work contained in this thesis. The list includes both accepted and submitted papers.

Journal Papers and Book Chapters

- Kyrkjebø, E., E. Panteley, A. Chaillet and K. Y. Pettersen (2006 *a*). *Group Coordination and Cooperative Control*. Chap. A Virtual Vehicle Approach to Underway Replenishment, pp. 171 – 189. Vol. 336 of *Lecture Notes in Control and Information Systems*. Springer Verlag. Tromsø, Norway.

- Kyrkjebø, E., K. Y. Pettersen, M. Wondergem and H. Nijmeijer (2006 *b*). Output synchronization control of ship replenishment operations: Theory and experiments. *Control Engineering Practice*. Accepted

Refereed conference papers

- Kyrkjebø, E. and K. Y. Pettersen (2003). Ship replenishment using synchronization control. In: *Proc. 6th IFAC Conf. on Manoeuvring and Control of Marine Craft*. Girona, Spain. pp. 286–291.

- Kyrkjebø, E., M. Wondergem, K. Y. Pettersen and H. Nijmeijer (2004). Experimental results on synchronization control of ship rendezvous operations. In: *Proc. IFAC Conf. on Control Applications in Marine Systems*. Ancona, Italy. pp. 453 – 458.

- Danielsen, A. L., E. Kyrkjebø and K. Y. Pettersen (2004). MVT: A marine visualization toolbox for matlab. In: *Proc. IFAC Conf. on Control Applications in Marine Systems*. Ancona, Italy. pp. 515 – 519.

- Kyrkjebø, E. and K. Y. Pettersen (2005 *a*). Output synchronization control of Euler-Lagrange systems with nonlinear damping terms. In: *Proc. 44th IEEE Conf. on Decision and Control and European Control Conf.* Sevilla, Spain. pp. 4951 – 4957.

- Kyrkjebø, E. and K. Y. Pettersen (2005 *b*). Tracking from a synchronization perspective. In: *Proc. 17th IMACS World Congress on Scientific Computation, Applied Mathematics and Simulation*. Paris, France.

- Kyrkjebø, E. and K. Y. Pettersen (2006 *a*). Leader-follower dynamic synchronization of surface vessels. In: *Proc. 7th IFAC Conf. on Manoeuvring and Control of Marine Craft*. Lisboa, Portugal.

- Kyrkjebø, E. and K. Y. Pettersen (2006 *b*). A virtual vehicle approach to output synchronization control. In: *Proc. 45th IEEE Conf. on Decision and Control*. San Diego, USA.

- Kyrkjebø, E. and K. Y. Pettersen (2007 *a*). Leader-follower synchronization control of Euler-Lagrange systems with leader position measurements only. In: *Proc. Mediterranean Conf. on Control and Automation*. Athens, Greece. *Submitted*

- Kyrkjebø, E. and K. Y. Pettersen (2007 *b*). Operational space synchronization of two robot manipulators through a virtual velocity estimate. In: *Proc. 46th IEEE Conf. on Decision and Control*. New Orleans, USA. *Submitted*

1.4 Organization of thesis

This thesis is organized as follows:

Chapter 2 presents the necessary definitions and theorems providing preliminaries for the stability analysis of the succeeding chapters. Furthermore, the fundamental properties of Euler-Lagrange systems are presented along with the definition of reference frames and reference kinematics.

Chapter 3 presents an observer-controller approach to solve the problems stated in Definition 2.7 and Definition 2.8. It introduces a nonlinear model-based error observer used to indirectly estimate the unknown states of the leader, and proposes control schemes to coordination the motion of the follower to the leader with and without state measurements of the follower. Stability results are presented, and the results are verified through simulations and experimental results.

Chapter 4 presents a virtual vehicle approach to solve the problems stated in Definition 2.7 and Definition 2.8. It introduces a virtual vehicle, a controlled vehicle that provides estimates of the unknown leader states through a kinematic control law, and proposes control schemes to coordination the motion of the follower to the leader with and without state measurements of the follower. Stability results are presented, and the results are verified through simulations and experimental results. Furthermore, an extension to a dynamic synchronization scheme is presented.

Chapter 5 compares the proposed observer-controller approach of Chapter 3 and the virtual vehicle approach of Chapter 4 in terms of the estimation principles, performance and robustness. The performance of the two proposed schemes is discussed based on simulations and practical experience from experiments.

Chapter 6 presents some concluding remarks on the motion coordination schemes proposed in this thesis.

Appendix A presents some mathematical tools and definitions.

Appendix B presents further details on the reference kinematics of Section 2.2.5.

Appendix C presents details of the proofs of Section 3 and 4.

Appendix D presents background material on single-object motion control strategies.

Appendix E presents the mathematical models and the simulation and experimental environments used to verify the proposed motion coordination schemes.

Chapter 2

Preliminaries

This chapter presents the necessary definitions and theorems to make this thesis self-contained by providing preliminaries for the stability analysis of the succeeding chapters. Furthermore, the fundamental properties of Euler-Lagrange systems are presented along with the definition of reference frames and reference kinematics.

2.1 Mathematical preliminaries

This section presents the notation used in this thesis, and a brief introduction to general stability concepts. For a formal definition of stability and uniformity, please see Khalil (2002). The stability analysis of the proposed control schemes in this thesis will deal with non-vanishing perturbations, and thus the concepts of uniform ultimate boundedness and uniform practical asymptotic stability are discussed in detail.

2.1.1 Notation

The set $\mathbb{N}$ denotes all nonnegative integers and $\mathbb{R}$ all real numbers. The set $\mathbb{N}_{\leq N}$ designates all nonnegative integers less than or equal to the integer N, and $\mathbb{R}_{\geq 0}$ is the set of all nonnegative real numbers. The matrix $\mathbf{I}$ denotes the identity matrix of appropriate dimension. The space $\mathbb{R}^n$ is the Euclidean n-dimensional space, and $\mathrm{SO}(3)$ is the special orthogonal group of order three. Note that $\mathbb{R}^3$ is a local map of $\mathrm{SO}(3)$.

The minimum and maximum eigenvalue of a positive definite matrix $\mathbf{M}$ will be denoted as $\mathbf{M}_m$ and $\mathbf{M}_M$, respectively. The norm of a vector $\mathbf{x}$ is defined as $\|\mathbf{x}\| = \sqrt{\mathbf{x}^T\mathbf{x}}$ and the induced norm of a matrix $\mathbf{M}$ is $\|\mathbf{M}\| = \max_{\|\mathbf{x}\|=1} \|\mathbf{M}\mathbf{x}\|$.

We denote by $\mathscr{B}_\delta$ the closed ball in $\mathbb{R}^n$ of radius δ centred at the origin, i.e. $\mathscr{B}_\delta := \{\mathbf{x} \in \mathbb{R}^n | \, \|\mathbf{x}\| \leq \delta\}$, and we use the notation $\mathscr{H}(\delta, \Delta) := \{\mathbf{x} \in \mathbb{R}^n : \delta \leq \|\mathbf{x}\| \leq \Delta\}$. For a nonnegative constant δ we define $\|\mathbf{x}\|_\delta := \inf_{z \in \mathscr{B}_\delta} \|\mathbf{x} - \mathbf{z}\|$, and $\mathbf{x}(t, t_0, \mathbf{x}_0)$, denotes the solutions of the differential equation $\dot{\mathbf{x}} = \mathbf{f}(t, \mathbf{x})$ with initial conditions $\mathbf{x}(t_0, t_0, \mathbf{x}_0) = \mathbf{x}_0$.

A continuous function $\alpha : \mathbb{R}_{\geq 0} \to \mathbb{R}_{\geq 0}$ is of class $\mathscr{K}$ ($\alpha \in \mathscr{K}$) if it is strictly increasing and $\alpha(0) = 0$. Moreover, α is of class $\mathscr{K}_\infty$ ($\alpha \in \mathscr{K}_\infty$) if, in addition, $\alpha(s) \to \infty$ as $s \to \infty$. A continuous function $\sigma : \mathbb{R}_{\geq 0} \to \mathbb{R}_{\geq 0}$ is of class $\mathscr{L}$ ($\sigma \in \mathscr{L}$) if it is strictly decreasing and $\sigma(s) \to 0$ as $s \to \infty$. A continuous function $\beta : \mathbb{R}_{\geq 0} \times \mathbb{R}_{\geq 0} \to \mathbb{R}_{\geq 0}$ is said to be a class

$\mathcal{KL}$ function ($\beta \in \mathcal{KL}$) if $\beta(\cdot, t) \in \mathcal{K}$ for any fixed $t \in \mathbb{R}_{\geq 0}$, and $\beta(s, \cdot) \in \mathcal{L}$ for any fixed $s \in \mathbb{R}_{\geq 0}$.

A function $\mathbf{f} : \mathbb{R}^n \to \mathbb{R}^n$ is said to be *locally Lipschitz* if, for any compact set $\mathbb{U} \subset \mathbb{R}^n$, there exists a nonnegative constant L_U such that

$$\|\mathbf{f}(\mathbf{x}) - \mathbf{f}(\mathbf{y})\| \leq L_U \|\mathbf{x} - \mathbf{y}\|, \qquad \forall \quad \mathbf{x}, \mathbf{y} \in \mathbb{U} \tag{2.1}$$

2.1.2 General stability

The concept of stability in this thesis should be understood in the sense of Lyapunov (cf. Loría and Panteley (2006)), which is the property of a point, a set or a trajectory that any solution starting sufficiently close remains arbitrarily close for all future time. We adopt from Chaillet (2006) the intuitive concept of a ball on a non-flat surface (Figure 2.1) to illustrate different concepts of stability.

An equilibrium point is *stable* if, after any sufficiently small perturbation on the position of the ball, it remains for ever arbitrarily close to it. The equilibrium point is *asymptotically stable* (AS) if, in addition, the ball approaches it asymptotically. The *domain of attraction* is the region of the state space that leads to asymptotic convergence. If the domain of attraction is the whole state-space, then the equilibrium is said to be *globally asymptotically stable* (GAS).

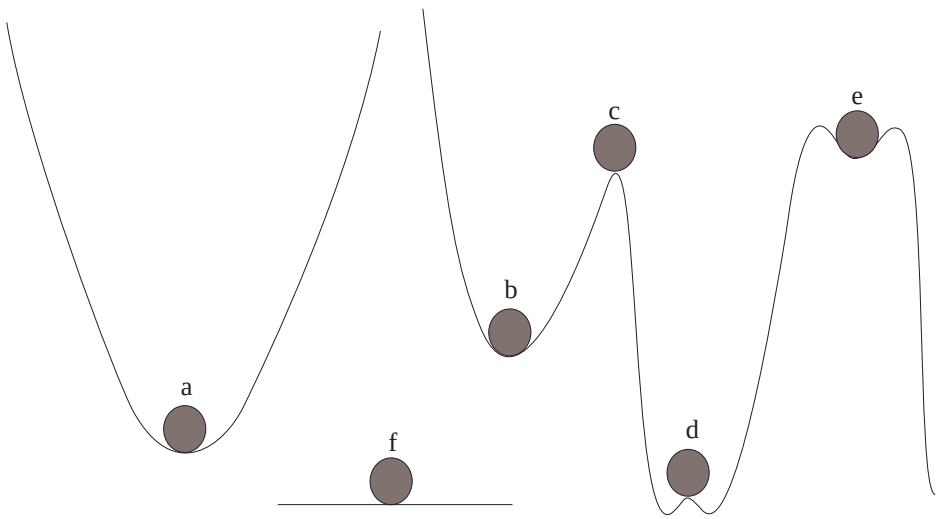

Figure 2.1: Global asymptotic stability (a), asymptotic stability (b), instability (c), instability with a small steady-state error (d), asymptotic stability with a small domain of attraction (e), and stability (f).

In addition, if the trajectory of the ball is independent of the time t_0 that the perturbation is imposed, the equilibrium is said to be *uniformly (globally asymptotically) stable* (U(GA)S).

Domain of attraction and region of instability Global asymptotic stability is a notion that to some extent is only a necessity from a theoretical viewpoint, and for control systems in practice (often due to neglected high-order dynamics) it is often only necessary to have an estimate of the domain of attraction, and to prove that by tuning certain parameters of the control system, this estimate of the domain of attraction can be arbitrarily enlarged. This is the concept of *semiglobal asymptotic stability*, and such a tuning parameter is often, but not always, a control gain.

A small region of instability that gives a small steady-state error, see Figure 2.1(d), may be present in controlled systems due to non-vanishing perturbations acting on the plant, or measurement imprecisions, that impedes convergence to the origin. This region of instability gives a set to which the solutions of the system converge, and the stability of the controlled system can thus be characterized through the concepts of *ultimate boundedness* and *practical stability*.

2.1.3 Uniform ultimate boundedness

Uniform asymptotic stability implies a natural robustness to small external disturbances. However, it provides no information on the behaviour of the system subject to larger perturbations. The presence of a non-vanishing perturbation impedes asymptotic stability to the origin, and leads to the definition of *ultimate boundedness* as the convergence to a neighbourhood of the operating point (cf. Khalil (2002), Chaillet (2006)).

Definition 2.1 (Uniform Ultimate Boundedness) *The solutions $\mathbf{x}(t) \in \mathbb{R}^n$ of the differential equation $\dot{\mathbf{x}} = \mathbf{f}(t, \mathbf{x}(t))$ are said to be **uniformly ultimately bounded (UUB)** with ultimate bound δ if there exists positive constants Δ_0 and δ, independent of $t_0 \geq 0$, such that for every $\Delta \in (0, \Delta_0)$, there exists a nonnegative constant $T(\delta, \Delta)$, independent of t_0, such that for all initial conditions $\mathbf{x}(t_0) = \mathbf{x}_0 \in \mathscr{B}_\Delta$ and all $t_0 \in \mathbb{R}_{\geq 0}$, they satisfy*

$$\|\mathbf{x}(t)\| \leq \delta, \qquad \forall t \geq t_0 + T \tag{2.2}$$

*If this holds for arbitrarily large Δ, then the solutions are **uniformly globally ultimately bounded (UGUB)**.*

The following result will be useful in the stability analysis of succeeding chapters. It is a modified version of a theorem by Chen and Leitman (1987), and is also found in Berghuis and Nijmeijer (1994) and Nijmeijer and Rodriguez-Angeles (2003)

Lemma 2.1 *Consider the following function $g : \mathbb{R} \to \mathbb{R}$*

$$g(y) = \alpha_0 - \alpha_1 y + \alpha_2 y^2, \qquad y \in \mathbb{R}^+ \tag{2.3}$$

where $\alpha_i > 0, i = 0, 1, 2$. Then $g(y) < 0$ if $y_1 < y < y_2$, where

$$y_1 = \frac{\alpha_1 - \sqrt{\alpha_1^2 - 4\alpha_2\alpha_0}}{2\alpha_2} \qquad y_2 = \frac{\alpha_1 + \sqrt{\alpha_1^2 - 4\alpha_2\alpha_0}}{2\alpha_2} \tag{2.4}$$

with $y_1, y_2 > 0$.

Proposition 2.1 *Let $\mathbf{x}(t) \in \mathbb{R}^n$ be the solution of the differential equation $\dot{\mathbf{x}} = \mathbf{f}(\mathbf{x}(t), t)$ where $\mathbf{f}(\mathbf{x}(t), t)$ is Lipschitz and under initial conditions $\mathbf{x}(t_0) = \mathbf{x}_0$, and assume that there exists a function $V(\mathbf{x}(t), t)$ that satisfies*

$$\begin{aligned} \mathbf{P}_m \|\mathbf{x}(t)\|^2 \leq V(\mathbf{x}(t), t) \leq \mathbf{P}_M \|\mathbf{x}(t)\|^2 \\ \dot{V}(\mathbf{x}(t), t) \leq \|\mathbf{x}(t)\| \cdot g(\|\mathbf{x}(t)\|) < 0, \qquad \forall y_1 < \|\mathbf{x}(t)\| < y_2 \end{aligned} \tag{2.5}$$

*with P_m and P_M positive constants, $g(\cdot)$ as in (2.3) and y_1, y_2 as in (2.4). Define $\delta := \sqrt{\mathbf{P}_m^{-1}\mathbf{P}_M}$. If $y_2 > \delta y_1$, then $\mathbf{x}(t)$ is **uniformly locally ultimately bounded (ULUB)**, that is, given $d_m = \delta y_1$, there exists $d \in (d_m, y_2)$ such that*

$$\|\mathbf{x}_0\| \leq \Delta_0 \Rightarrow \|\mathbf{x}(t)\| \leq d, \qquad \forall t \geq t_0 + T(d, \Delta_0) \tag{2.6}$$

where

$$T(d, \Delta_0) = \begin{cases} 0 & \Delta_0 \leq R \\ \frac{\mathbf{P}_M \Delta_0^2 - \mathbf{P}_m R^2}{-\alpha_0 R + \alpha_1 R^2 - \alpha_2 R^3} & R < \Delta_0 < \delta^{-1} y_2 \end{cases} \tag{2.7}$$

and $R = \delta^{-1} d$.

This implies that a system is uniformly ultimately bounded if it has a Lyapunov function whose time derivative is negative in an annulus of a certain width around the origin.

2.1.4 Practical asymptotic stability

The definitions presented in this section are adopted from Chaillet (2006). Motivated by the concept of instability with a small steady-state error in Figure 2.1(d), we state a definition of uniform global asymptotic stability of nonlinear time-varying systems with respect to a ball. Consider the system

$$\dot{\mathbf{x}} = \mathbf{f}(t, \mathbf{x}) \tag{2.8}$$

where $\mathbf{x} \in \mathbb{R}^n$, $t \in \mathbb{R}_{\geq 0}$ and $f : \mathbb{R}_{\geq 0} \times \mathbb{R}^n \to \mathbb{R}^n$ is piecewise continuous in t and locally Lipschitz in $\mathbf{x}$ uniformly in t. Let $\Delta > \delta > 0$.

Definition 2.2 (US w.r.t. ball) *The closed ball $\mathscr{B}_\delta$ is **uniformly stable** on $\mathscr{B}_\Delta$ for the system (2.8) if there exists a class $\mathscr{K}_\infty$ function α such that the solution of (2.8) from any initial state $\mathbf{x}_0 \in \mathscr{B}_\Delta$ and initial time $t_0 \in \mathbb{R}_{\geq 0}$ satisfies*

$$\|\mathbf{x}(t, t_0, \mathbf{x}_0)\|_\delta \leq \alpha(\|\mathbf{x}_0\|), \qquad \forall t \geq t_0$$

Definition 2.3 (UA w.r.t. ball) *The closed ball $\mathscr{B}_\delta$ is **uniformly attractive** on $\mathscr{B}_\Delta$ for the system (2.8) if there exists a class $\mathscr{L}$ function σ such that the solution of (2.8) from any initial state $\mathbf{x}_0 \in \mathscr{B}_\Delta$ and initial time $t_0 \in \mathbb{R}_{\geq 0}$ satisfies*

$$\|\mathbf{x}(t, t_0, \mathbf{x}_0)\|_\delta \leq \sigma(t - t_0), \qquad \forall t \geq t_0$$

Definition 2.4 (UAS w.r.t. ball) *The closed ball $\mathscr{B}_\delta$ is **uniformly asymptotically stable** on $\mathscr{B}_\Delta$ (UAS on $\mathscr{B}_\Delta$) for the system (2.8) if there exists a class $\mathscr{KL}$ function β such that the solution of (2.8) from any initial state $\mathbf{x}_0 \in \mathscr{B}_\Delta$ and initial time $t_0 \in \mathbb{R}_{\geq 0}$ satisfies*

$$\|\mathbf{x}(t, t_0, \mathbf{x}_0)\|_\delta \leq \beta(\|\mathbf{x}_0\|, t - t_0), \qquad \forall t \geq t_0$$

*If $\Delta \to \infty$, then $\mathscr{B}_\Delta = \mathbb{R}^n$ and the closed ball $\mathscr{B}_\delta$ is **uniformly globally asymptotically stable** for the system (2.8).*

Thus, the ball $\mathscr{B}_\delta$ is UAS for system (2.8) on $\mathscr{B}_\Delta$ if it is US and UA on $\mathscr{B}_\Delta$. While Definition 2.4 implies the property of ultimate boundedness in Definition 2.1 (with any $\delta^\star > \delta$ as the ultimate bound), it actually constitutes a stronger property. Notably, the transient is guaranteed to remain arbitrarily near $\mathscr{B}_\delta$ for any sufficiently small initial state, which is a stability property not covered by the notion of ultimate boundedness.

Stability with respect to a ball is often satisfied in perturbed systems where the nominal system is UGAS, and has motivated the introduction of the concept of *practical stability* as defined in Chaillet (2006). Consider parametrized nonlinear time-varying systems of the form

$$\dot{\mathbf{x}} = f(t, \mathbf{x}, \theta) \tag{2.9}$$

where $\mathbf{x} \in \mathbb{R}^n$, $t \in \mathbb{R}_{\geq 0}$, $\theta \in \mathbb{R}^m$ is a constant parameter vector, and $f : \mathbb{R}_{\geq 0} \times \mathbb{R}^n \times \mathbb{R}^m \to \mathbb{R}^n$ is locally Lipschitz in $\mathbf{x}$ and piecewise continuous in t.

Definition 2.5 (Uniform Practical Asymptotic Stability) *Let $\Theta \subset \mathbb{R}^m$ be a set of parameters. The system (2.9) is said to be **uniformly semiglobally practically asymptotically stable (USPAS)** on Θ if, given any $\Delta > \delta > 0$, there exists $\theta^\star(\delta, \Delta) \in \Theta$ such that the ball $\mathscr{B}_\delta$ is UAS on $\mathscr{B}_\Delta$ for the system $\dot{\mathbf{x}} = f(t, \mathbf{x}, \theta^\star)$.*

*Moreover, if $\Delta = \infty$ and $\theta^\star$ is independent of Δ, i.e. $\theta^\star = \theta^\star(\delta)$, such that the ball $\mathscr{B}_\delta$ is UGAS for the system $\dot{\mathbf{x}} = f(t, \mathbf{x}, \theta^\star)$, the system (2.9) is said to be **uniformly globally practically asymptotically stable (UGPAS)** on Θ.*

The following result will be useful in the stability analysis of succeeding chapters. It is a modified version of Proposition 2 from Chaillet and Loría (2006), and can be found in Kyrkjebø *et al.* (2006*a*) for UGPAS systems and in Kristiansen *et al.* (2006) for USPAS systems.

Corollary 2.1 *Let $\sigma_i : \mathbb{R}^m \to \mathbb{R}_{\geq 0}$, $i \in \mathbb{N}_{\leq N}$ be continuous functions positive over Θ, and a_m, a_M and q be positive constants. Assume that, for any $\theta^\star \in \Theta$, there exists a continuously differentiable Lyapunov function $V : \mathbb{R}_{\geq 0} \times \mathbb{R}^n \to \mathbb{R}_{\geq 0}$ satisfying, for all $\mathbf{x} \in \mathbb{R}^n$ and all $t \in \mathbb{R}_{\geq 0}$,*

$$a_m \min\{\sigma_i(\theta)\} \|\mathbf{x}\|^q \leq V(t, \mathbf{x}) \leq a_M \max\{\sigma_i(\theta)\} \|\mathbf{x}\|^q \tag{2.10}$$

Assume that for any $\Delta > \delta > 0$ there exists $\theta^\star(\delta, \Delta) \in \Theta$ and a class $\mathscr{K}$ function $\alpha_{\delta,\Delta}$ such that, for all $\mathbf{x} \in \mathscr{B}_\Delta \setminus \mathscr{B}_\delta$, i.e. $\|\mathbf{x}\| \in [\delta, \Delta]$, and all $t \in \mathbb{R}_{\geq 0}$,

$$\frac{\partial V}{\partial t}(t, \mathbf{x}) + \frac{\partial V}{\partial \mathbf{x}}(t, \mathbf{x}) f(t, \mathbf{x}, \theta^\star) \leq -\alpha_{\delta,\Delta}(\|\mathbf{x}\|) \tag{2.11}$$

Assume also that for all $i \in \mathbb{N}_{\leq N}$, and for every fixed $\Delta > 0$,

$$\lim_{\delta \to 0} \sigma_i(\theta^\star(\delta, \Delta)) \delta^q = 0, \qquad \text{and} \qquad \lim_{\delta \to 0} \sigma_i(\theta^\star(\delta, \Delta)) \neq 0 \tag{2.12}$$

and, for every fixed $\delta > 0$,

$$\lim_{\Delta \to \infty} \frac{\sigma_i(\theta^\star(\delta, \Delta))}{\Delta^q} = 0, \qquad \text{and} \qquad \lim_{\Delta \to \infty} \sigma_i(\theta^\star(\delta, \Delta)) \neq 0. \tag{2.13}$$

then the system $\dot{\mathbf{x}} = f(t, \mathbf{x}, \theta^\star)$ is USPAS on the parameter set Θ.

Moreover, if $\Delta = \infty$ and $\theta^\star$ is independent of Δ, i.e. $\theta^\star = \theta^\star(\delta)$, the conditions in (2.13) are no longer required, $\mathscr{B}_\Delta = \mathbb{R}^n$, and the system $\dot{\mathbf{x}} = f(t, \mathbf{x}, \theta^\star)$ is UGPAS on the parameter set Θ.

Note that the assumptions of Corollary 2.1 are more conservative than those of the original result (Chaillet and Loría, 2006, Proposition 2). However, the assumptions of Corollary 2.1 are easier to verify for systems described by the Euler-Lagrange equations, and will thus be used in the stability analysis of this thesis. See Chaillet (2006) for a thorough discussion on practical stability.

In the above definition and corollary, the parameter θ represents the tuning parameters, e.g. control gains or any free design parameter, while the set Θ is the set of allowed tuning parameters, which may be bounded due to physical constraints such as actuators limitations. The set $\mathscr{B}_\Delta$ is an estimate of the domain of attraction. In most applications a larger Δ induces better performance since the operating bandwidth is enlarged. In contrast, δ represents the radius of the ball to which the solutions ultimately converge; therefore it is typically required to be small in order to reduce the steady-state error as much as possible.

The functions $\sigma_i(\theta)$ refer in many cases to the minimum eigenvalues of gain matrices in θ, and thus, roughly speaking, it is imposed that the dependency of Δ and $1/\delta$ in the minimum eigenvalues of the gain matrices should be polynomial and of a lower order than the bounds on V.

Ultimate boundedness and practical stability considerations

The definition of uniform ultimate boundedness in Definition 2.1 requires that the solutions of a system eventually enter a ball without leaving it anymore. Thus, the errors of the closed-loop system remain in some neighbourhood of the origin after a sufficiently long time. This has been the *de facto* interpretation of many definitions of practical stability in the literature (cf. Khalil (1996)). However, practical stability as defined in Definition 2.5 requires, in addition, that the size of this neighbourhood is reducible at will by tuning some parameter (typically control gains), and also that the ball $\mathscr{B}_\delta$ is not only attractive, but also stable. Thus, solutions remain arbitrarily close to a small neighbourhood of the origin for all time provided that its initial state was sufficiently close. This suggests a "reasonable" behaviour of the transient dynamics which is not necessarily the true in the definition of ultimate boundedness. Note that we can also define the property of practical stability with respect to design parameters, e.g. the sampling time in discrete-time systems.

For uniform semiglobal practical asymptotic stability or uniform semiglobal ultimate boundedness we impose that the estimate of the domain of attraction $\mathscr{B}_\Delta$ can be arbitrarily enlarged by a convenient choice of parameters. This situation is fairly common in continuous-time feedback control problems using static control gains as the tuning parameter, and most notably in the case of UGAS (with respect to the origin) controlled systems perturbed by bounded external disturbances.

Notice also that, with a slight abuse of notation, from $\delta = 0$ we recover from Definition 2.5 the notion of uniform semiglobal asymptotic stability (USAS), and when $\Delta \to \infty$ we recover the definition of uniform global practical asymptotic stability (UGPAS). If both $\delta = 0$ and $\Delta \to \infty$ we recover the definition of uniform global asymptotic stability (UGAS).

2.1.5 Output feedback control

Output feedback control is a well studied subject throughout the literature (cf. Ortega *et al.* (1994), Loría (1996), Lefeber (2000)), and has been a way of constructing feedback control laws with a reduced set of measurements. An accurate system model is assumed to

be given for the system under consideration; a mobile robot, a spacecraft, a ship or a robot manipulator of the form

$$\dot{\mathbf{x}} = \mathbf{f}(t, \mathbf{x}, \mathbf{u}) \tag{2.14a}$$
$$\mathbf{y} = \mathbf{h}(t, \mathbf{x}, \mathbf{u}) \tag{2.14b}$$

where $\mathbf{x} \in \mathbb{R}^n$ is the state of the system, $\mathbf{u} \in \mathbb{R}^r$ is the input vector that controls the system and $\mathbf{y} \in \mathbb{R}^m$ denotes the output of the system which represents the measurements. Assume that a reference input $\mathbf{u}_r(t)$ exists, and generates a feasible reference trajectory

$$\dot{\mathbf{x}}_r = \mathbf{f}_r(t, \mathbf{x}_r, \mathbf{u}_r) \tag{2.15a}$$
$$\mathbf{y}_r = \mathbf{h}_r(t, \mathbf{x}_r, \mathbf{u}_r) \tag{2.15b}$$

For the system (2.14-2.15), we can recall the definition of the output feedback state tracking control problem from Lefeber (2000) as

Definition 2.6 (Output feedback state tracking problem) *Find an appropriate dynamic control law*

$$\mathbf{u} = \mathbf{u}(t, \mathbf{x}_r, \mathbf{u}_r, \mathbf{y}, \mathbf{z}) \tag{2.16a}$$
$$\dot{\mathbf{z}} = \mathbf{g}(t, \mathbf{x}_r, \mathbf{u}_r, \mathbf{y}, \mathbf{z}) \tag{2.16b}$$

such that for the resulting closed-loop system (2.14, 2.16)

$$\lim_{t \to \infty} \|\mathbf{x}(t) - \mathbf{x}_r(t)\| = 0 \tag{2.17}$$

This renders the zero tracking error equilibrium asymptotically stable. Note that a feasible reference state trajectory $\mathbf{x}_r(t)$ is assumed to exist, i.e. that once being on the reference trajectory it is possible to stay on that trajectory. Note also that the output feedback state tracking problem extends the output feedback output tracking problem of finding a control law for the input $\mathbf{u}$ such that as t tends to infinity the output $\mathbf{y}(t)$ converges to $\mathbf{y}_r(t)$.

Based on Definition 2.6, we can now define two output feedback state synchronization problems to be addressed in this thesis; the output reference state feedback synchronization problem and the output reference output feedback synchronization problem.

Definition 2.7 (Output reference state feedback synchronization problem) *Consider the system (2.14). Assume that a feasible reference trajectory exists with output (2.15b). Find an appropriate dynamic control law*

$$\mathbf{u} = \mathbf{u}(t, \mathbf{y}_r, \mathbf{x}, \mathbf{z}) \tag{2.18a}$$
$$\dot{\mathbf{z}} = \mathbf{g}(t, \mathbf{y}_r, \mathbf{x}, \mathbf{z}) \tag{2.18b}$$

such that for the resulting closed-loop system (2.14, 2.18) there exists a $\delta > 0$ such that

$$\lim_{t \to \infty} \|\mathbf{x}(t) - \mathbf{x}_r(t)\| \leq \delta \tag{2.19}$$

Definition 2.8 (Output reference output feedback synchronization problem) *Consider the system (2.14). Assume that a feasible reference trajectory exists with output (2.15b). Find an appropriate dynamic control law*

$$\mathbf{u} = \mathbf{u}(t, \mathbf{y}_r, \mathbf{y}, \mathbf{z}) \tag{2.20a}$$
$$\dot{\mathbf{z}} = \mathbf{g}(t, \mathbf{y}_r, \mathbf{y}, \mathbf{z}) \tag{2.20b}$$

such that for the resulting closed-loop system (2.14, 2.20) there exists a $\delta > 0$ such that

$$\lim_{t\to\infty} \|\mathbf{x}(t) - \mathbf{x}_r(t)\| \leq \delta \tag{2.21}$$

Remark 2.1 *The control laws (2.18) of Definition 2.7 and (2.20) of Definition 2.8 render the tracking error uniformly ultimately bounded with bound δ, or asymptotically stable with respect to the closed ball $\mathscr{B}_\delta$.*

For the motion coordination control problem where the reference states $\dot{\mathbf{x}}_r(t)$ and $\ddot{\mathbf{x}}_r(t)$ are unknown and unmeasured, we can consider the output reference feedback control problem as controlling the measured states $\mathbf{x}$ and $\dot{\mathbf{x}}$ of a follower system to an unknown reference system based only on the *output* $\mathbf{y}_r(t)$ of the reference system as defined in Definition 2.7. Furthermore, we can design the same output reference feedback control system while assuming only output measurements $\mathbf{y}$ of the follower system, as defined in Definition 2.8.

Note that the reference in the motion coordination schemes presented in this thesis is generated by a physical leader system. The physical nature of the leader as a mechanical system subject to moment of inertia and actuator limitations restricts the attainable velocities and accelerations of the leader. Thus, for the leader system

$$\dot{\mathbf{x}}_m = \mathbf{f}_m(t, \mathbf{x}_m, \mathbf{u}_m) \tag{2.22a}$$
$$\mathbf{y}_m = \mathbf{h}_m(t, \mathbf{x}_m, \mathbf{u}_m) \tag{2.22b}$$

the following assumptions are made on the states as

Assumption 2.1 *The unmeasured states $\dot{\mathbf{x}}_m$ and $\ddot{\mathbf{x}}_m$ are bounded such that*

$$\sup_t \|\dot{\mathbf{x}}_m(t)\| = V_M < \infty \tag{2.23}$$
$$\sup_t \|\ddot{\mathbf{x}}_m(t)\| = A_M < \infty \tag{2.24}$$

The bounds on the velocity and acceleration of the leader system in Assumption 2.1 can be established based on the knowledge of a desired trajectory for the leader, or by the limitations imposed by the maximum acceleration and velocity given by the actuators. The boundedness assumption of the acceleration and velocity thus has a clear physical interpretation in mechanical control systems.

Remark 2.2 *Note that Assumption 2.1 is an assumption on the attainable velocity and acceleration of the leader system, and do not impose any restrictions on the system states $\mathbf{x}$ and $\dot{\mathbf{x}}$ of the coordination control schemes of Chapter 3 and 4.*

2.2 Kinematic and kinetic preliminaries

The study of motion is twofold; kinematics, which is the geometrical aspect of motion, and kinetics, which is the analysis of the forces causing the motion. We will first treat the kinematic relationships between motions in different reference frames, and then discuss the kinetics for Euler-Lagrange systems in general, and for robot manipulators and marine vehicles in particular.

2.2.1 Reference frames

Describing the motion of a system requires at least one frame of reference. For terrestrial motion (not excluding earth-orbiting satellites) we can define two Earth-centred reference frames as

ECI The Earth-centred inertial reference frame. When Newton (1687) stated his famous laws of motion, he referred them to a non-accelerating inertial reference frame which moved at either zero or constant velocity. This reference frame has motivated the definition of the ECI reference frame located in the centre of the Earth with its z-axis pointing towards the geographic north pole (*Boreal*), its x-axis directed towards the vernal equinox[1], and the y-axis completing the dextral triad.

ECEF The Earth-centred Earth-fixed reference frame. This frame rotates with the Earth, and its origin and z-axis coincide with the ECI-frame, while the x-axis points towards the Greenwich meridian at 0° longitude, and the y-axis completes the dextral triad.

For local terrestrial motion we can define more convenient reference frames as

NED The north-east-down reference frame. A fixed reference frame defined relative to the Earth's reference ellipsoid, where the x^n-axis points toward true North, the y^n-axis toward East, and the z^n-axis points downwards normal to the Earth's surface. For local navigation close to the surface it is common to assume that this frame is inertial, and this is usually referred to as flat Earth navigation.

Path/Orbit The path reference frame or the orbit reference frame. The origin is at a point along a given path or orbit, and its x-axis is directed along the tangent vector, the y-axis along the principal normal vector and the z-axis along the binormal vector. This is often referred to as the *Serret-Frenet frame* (Frenet (1847)).

Body This is a body-fixed moving reference frame where the origin is chosen in the centre of gravity of the object, and the axes coincide with the principal axes of inertia. The x^b-axis is chosen along the principal axis of inertia in the forward direction, the y^b-axis directed towards the principal axis in the sideways right direction, and the z^b-axis to complete the dextral triad system pointing downwards along the principal axis. Rotation of the axes in the body frame relative to a different reference frame (NED or path/orbit) describes the orientation or attitude of the object, and is given as *roll* around the body-fixed x-axis, *pitch* around the y-axis and *yaw* around the z-axis.

[1]The direction parallel to the line from the centre of the Earth to the Sun at the first day of spring. The gravitational force of the Sun and Moon cause a slow rotation of the Earth's spin axis with a period of approx. 26 000 years. This suggests that the vernal equinox moves approx. 50 seconds of arc each year and that the ECI is not an inertial reference frame, but the approximation is sufficient for most terrestrial applications, and certainly for the applications treated in this thesis.

Note that for robot manipulators, the base of manipulation is usually fixed, and the kinematic transformation of positions and velocities for the end-effector is between the *operational* and the *joint* space of the manipulator. The joint space is the configuration space where the joint variables are defined, and the operational space is defined by the reachable postures for the manipulator, and this is where the task is typically specified.

2.2.2 Euler-Lagrange systems

In this thesis, we consider mechanical systems that can be described by the Euler-Lagrange equations (cf. Goldstein *et al.* (2002)) of the form

$$\frac{d}{dt}\left(\frac{\partial \mathscr{L}(\mathbf{x},\dot{\mathbf{x}})}{\partial \dot{\mathbf{x}}}\right) - \frac{\partial \mathscr{L}(\mathbf{x},\dot{\mathbf{x}})}{\partial \mathbf{x}} + \frac{\partial \mathscr{F}(\dot{\mathbf{x}})}{\partial \dot{\mathbf{x}}} = \tau \tag{2.25}$$

where $\mathbf{x} \in \mathbb{R}^n$ are generalized coordinates assumed measurable, and $\tau \in \mathbb{R}^n$ are generalized forces acting on the system. $\mathscr{L}(\mathbf{x},\dot{\mathbf{x}}) = \mathscr{T}(\mathbf{x},\dot{\mathbf{x}}) - \mathscr{V}(\mathbf{x})$ is the Lagrangian function of potential energy $\mathscr{V}(\mathbf{x})$ and kinetic energy $\mathscr{T}(\mathbf{x},\dot{\mathbf{x}})$. We assume that the kinetic energy function is of the quadratic form

$$\mathscr{T}(\mathbf{x},\dot{\mathbf{x}}) = \frac{1}{2}\dot{\mathbf{x}}^T \mathbf{M}(\mathbf{x})\dot{\mathbf{x}}, \qquad \mathbf{M}(\mathbf{x}) = \mathbf{M}^T(\mathbf{x}) > 0 \tag{2.26}$$

where the inertia matrix $\mathbf{M}(\mathbf{x})$ is positive definite and uniformly bounded. Using the Christoffel symbols of the first kind (Spong and Vidyasagar (1989)) and (2.26), we can rewrite (2.25) in the form of a Euler-Lagrange systems with dynamics as

$$\mathbf{M}(\mathbf{x})\ddot{\mathbf{x}} + \mathbf{C}(\mathbf{x},\dot{\mathbf{x}})\dot{\mathbf{x}} + \mathbf{d}(\mathbf{x},\dot{\mathbf{x}}) + \mathbf{g}(\mathbf{x}) = \tau \tag{2.27}$$

where $\mathbf{C}(\mathbf{x},\dot{\mathbf{x}})\dot{\mathbf{x}}$ is the vector of Coriolis and centripetal forces, and the vector of potential forces are given by

$$\mathbf{g}(\mathbf{x}) = \frac{\partial V(\mathbf{x})}{\partial \mathbf{x}} \tag{2.28}$$

The dissipative or frictional forces in the system are derived from the scalar dissipation function $\mathscr{F}(\dot{\mathbf{x}})$, defined from the rate of energy $\mathscr{E}$ dissipating from the system, as in (Sagatun (1992))

$$\frac{d\mathscr{E}}{dt} = -\mathscr{F}(\dot{\mathbf{x}}) = \frac{1}{n+1}\sum_{i=1}^{n} c_i |\dot{x}_i|^{n+1} \tag{2.29}$$

where $\mathscr{F}$ is a power function and in general a function of the velocity and c_i, $i = 1,\ldots n$ are positive damping coefficients. For $n = 1$ this is known as Rayleigh's dissipation function. The dissipative forces

$$\mathbf{d}(\mathbf{x},\dot{\mathbf{x}}) = \mathbf{D}(\mathbf{x},\dot{\mathbf{x}})\dot{\mathbf{x}} = \frac{\partial \mathscr{F}(\dot{\mathbf{x}})}{\partial \dot{\mathbf{x}}} \tag{2.30}$$

are dry friction or Coulomb damping for $n = 0$ in

$$\frac{\partial \mathscr{F}(\dot{\mathbf{x}})}{\partial \dot{\mathbf{x}}_i} = c_i |\dot{x}_i|^{n-1}\dot{x}_i \tag{2.31}$$

linear viscous friction (Newtonian damping) for $n = 1$, and quadratic damping for $n = 2$.

Although (2.27) is a complex nonlinear equation, it satisfies several fundamental properties (cf. Ortega and Spong (1989)) which can be exploited to facilitate control system design. These properties are as follows

P1 The inertia matrix $\mathbf{M}(\mathbf{x})$ is symmetric, positive definite, differentiable in $\mathbf{x}$, and uniformly bounded as

$$0 < \mathbf{M}_m \leq \|\mathbf{M}(\mathbf{x})\| \leq \mathbf{M}_M < \infty, \qquad \forall\, \mathbf{x} \in \mathbb{R}^n \tag{2.32}$$

where $\mathbf{M}_m$ and $\mathbf{M}_M$ are positive constant bounds on the eigenvalues of $\mathbf{M}(\mathbf{x})$.

P2 The Coriolis- and centripetal matrix $\mathbf{C}(\mathbf{x},\dot{\mathbf{x}})$ can always be parametrized in terms of Christoffel symbols, and thus satisfies

$$\mathbf{C}(\mathbf{x},\mathbf{y})\,\mathbf{z} = \mathbf{C}(\mathbf{x},\mathbf{z})\,\mathbf{y}, \qquad \forall\, \mathbf{x},\mathbf{y},\mathbf{z} \in \mathbb{R}^n \tag{2.33}$$

P3 The matrix $\mathbf{N}(\mathbf{x},\dot{\mathbf{x}}) = \dot{\mathbf{M}}(\mathbf{x}) - 2\mathbf{C}(\mathbf{x},\dot{\mathbf{x}})$ is skew-symmetric, and thus

$$\mathbf{y}^T\left(\dot{\mathbf{M}}(\mathbf{x}) - 2\mathbf{C}(\mathbf{x},\dot{\mathbf{x}})\right)\mathbf{y} = 0, \qquad \forall\, \mathbf{x},\dot{\mathbf{x}},\mathbf{y} \in \mathbb{R}^n \tag{2.34}$$

P4 The Coriolis- and centripetal matrix $\mathbf{C}(\mathbf{x},\dot{\mathbf{x}})$ is bounded in $\mathbf{x}$ and linear in $\dot{\mathbf{x}}$, and satisfies for some positive constant $\mathbf{C}_M$

$$\|\mathbf{C}(\mathbf{x},\dot{\mathbf{x}})\| \leq \mathbf{C}_M \|\dot{\mathbf{x}}\|, \qquad \forall\, \mathbf{x},\dot{\mathbf{x}} \in \mathbb{R}^n \tag{2.35}$$

In addition, the following assumption is made on the dissipative term in the system (2.27)

Assumption 2.2 *The dissipative term $\mathbf{d}(\mathbf{x},\dot{\mathbf{x}})$ is continuously differentiable in $\mathbf{x}$ and $\dot{\mathbf{x}}$, and satisfies for some $k_d \geq 0$*

$$\mathbf{y}^T \frac{\partial\, \mathbf{d}(\mathbf{x},\dot{\mathbf{x}})}{\partial \dot{\mathbf{x}}}\mathbf{y} \geq k_d\, \mathbf{y}^T\mathbf{y}, \qquad \forall\, \mathbf{x},\dot{\mathbf{x}},\mathbf{y} \in \mathbb{R}^n \tag{2.36}$$

and for a continuous function $\beta_d(\mathbf{s}) : \mathbb{R}_{\geq 0} \to \mathbb{R}_{\geq 0}$

$$\left\| \frac{\partial \mathbf{d}(\mathbf{x},\dot{\mathbf{x}})}{\partial \dot{\mathbf{x}}} \right\| \leq \beta_d(\|\dot{\mathbf{x}}\|), \qquad \forall\, \mathbf{x},\dot{\mathbf{x}} \in \mathbb{R}^n \tag{2.37}$$

Note that Assumption 2.2 is a generalization based on practical considerations regarding the dissipative terms in most Euler-Lagrange systems, and that the presence of dissipative forces are mainly due to friction or hydro- and aerodynamic damping effects. In particular, the restrictiveness of Assumption 2.2 is addressed for friction effects in Section 2.2.3, and for hydrodynamic damping effects in Section 2.2.4.

2.2.3 Robot manipulators

A robot manipulator is an Euler-Lagrange system satisfying Properties **P1**-**P4**. This thesis considers n-degree-of-freedom manipulators with revolute joints only. The robot manipulator dynamics are usually treated in two different configuration spaces; the joint space and the operational space. We will assume that the dimension of the operational space is

equal to the dimension of the joint space ($n = r$), and thus the manipulator acts in non-singular configurations. The joint angles $\mathbf{q} \in \mathbb{R}^r$ and the operational space coordinates $\mathbf{x} \in \mathbb{R}^n \times \mathrm{SO}(3)$ constitutes two different sets of generalized coordinates for the robot manipulator, and the generalized positions in a six degree of freedom system are

$$\mathbf{q} := [q_1, q_2, q_3, q_4, q_5, q_6]^T \in \mathbb{R}^6 \tag{2.38}$$

$$\mathbf{x} := [x, y, z, \phi, \theta, \psi]^T \in \mathbb{R}^3 \times \mathrm{SO}(3) \tag{2.39}$$

Note that the vector $\mathbf{x}$ of generalized coordinates has a position sub-vector $\mathbf{p} = [x, y, z]^T \in \mathbb{R}^3$, and an orientation sub-vector $\Theta = [\phi, \theta, \psi]^T \in \mathrm{SO}(3)$ (roll, pitch, yaw). The dynamic model of a robot manipulator in the joint space can be written (Sciavicco and Siciliano (1996))

$$\mathbf{M_q}(\mathbf{q})\ddot{\mathbf{q}} + \mathbf{C_q}(\mathbf{q}, \dot{\mathbf{q}})\dot{\mathbf{q}} + \mathbf{d_q}(\dot{\mathbf{q}}) + \mathbf{g_q}(\mathbf{q}) = \tau_\mathbf{q} \tag{2.40}$$

where $\mathbf{q}$ are the joint coordinates, $\mathbf{M_q}(\mathbf{q})$ is the inertia matrix, $\mathbf{C_q}(\mathbf{q}, \dot{\mathbf{q}})$ is the matrix of Coriolis and centripetal forces, $\mathbf{d_q}(\dot{\mathbf{q}})$ is a general function of friction or other dissipative forces, and the gravitational forces are given in $\mathbf{g_q}(\mathbf{x})$. The joint space model (2.40) belongs to the class of Euler-Lagrange systems described by (2.27), and the matrices satisfies Properties **P1**-**P4**.

The joint space and the operational space are related through the kinematic relationship

$$\mathbf{x} = \mathbf{f}(\mathbf{q}) \tag{2.41}$$

computed from the geometric structure of the manipulator, and enables us to compute the end-effector position and orientation $\mathbf{x} \in \mathbb{R}^3 \times \mathrm{SO}(3)$ based on the joint variables $\mathbf{q} \in \mathbb{R}^6$. The differential kinematic relationship

$$\dot{\mathbf{x}} = \mathbf{J}(\mathbf{q})\dot{\mathbf{q}} \tag{2.42}$$

relates the joint space velocities $\dot{\mathbf{q}}$ to the operational space velocities $\dot{\mathbf{x}}$ (Khatib (1987)) through the Jacobian matrix $\mathbf{J}(\mathbf{q}) = \frac{\partial \mathbf{f}(\mathbf{q})}{\partial \mathbf{q}}$. Through (2.42) we can write the dynamic model of the manipulator in the operational space as

$$\mathbf{M}(\mathbf{x})\ddot{\mathbf{x}} + \mathbf{C}(\mathbf{x}, \dot{\mathbf{x}})\dot{\mathbf{x}} + \mathbf{d}(\mathbf{x}, \dot{\mathbf{x}}) + \mathbf{g}(\mathbf{x}) = \tau \tag{2.43}$$

where $\mathbf{x}$ are the operational space coordinates, $\mathbf{M}(\mathbf{x})$ is the inertia matrix, $\mathbf{C}(\mathbf{x}, \dot{\mathbf{x}})$ is the matrix of Coriolis and centripetal forces, $\mathbf{d}(\mathbf{x}, \dot{\mathbf{x}})$ is a general function of friction or other dissipative forces, and the gravitational forces are given in $\mathbf{g}(\mathbf{x})$. The control input vector τ is the generalized forces and moments acting on the system. The operational space model (2.43) belongs to the class of Euler-Lagrange systems described by (2.27), and the matrices satisfies Properties **P1**-**P4**.

The operational space model is related to the joint space model through the transformations

$$\begin{aligned}
\mathbf{M}(\mathbf{x}) &= \mathbf{J}^{-T}(\mathbf{q})\mathbf{M_q}(\mathbf{q})\mathbf{J}^{-1}(\mathbf{q}) \\
\mathbf{C}(\mathbf{x}, \dot{\mathbf{x}}) &= \mathbf{J}^{-T}\mathbf{C_q}(\mathbf{q}, \dot{\mathbf{q}})\dot{\mathbf{q}} - \mathbf{M_q}(\mathbf{q})\dot{\mathbf{J}}(\mathbf{q})\dot{\mathbf{q}} \\
\mathbf{d}(\mathbf{x}, \dot{\mathbf{x}}) &= \mathbf{J}^{-T}(\mathbf{q})\mathbf{d_q}(\dot{\mathbf{q}}) \\
\mathbf{g}(\mathbf{x}) &= \mathbf{J}^{-T}(\mathbf{q})\mathbf{g_q}(\mathbf{q}) \\
\tau &= \mathbf{J}^{-T}(\mathbf{q})\tau_\mathbf{q}
\end{aligned} \tag{2.44}$$

Friction in a robot manipulator can be classified as viscous or static friction torques (Sciavicco and Siciliano (1996)). A viscous friction torque is given as $\mathbf{F}_v\dot{\mathbf{q}}$ where $\mathbf{F}_v$ is a diagonal matrix of viscous friction coefficients. Static friction is often simplified as $\mathbf{F}_s \operatorname{sign}(\dot{\mathbf{q}})$ where $\mathbf{F}_s$ is a diagonal matrix and $\operatorname{sign}(\dot{\mathbf{q}})$ is a vector of sign-functions of single joint velocities. Assuming that both effects are present in a manipulator gives the dissipative forces in the form

$$\mathbf{d}_{\mathbf{q}}(\dot{\mathbf{q}}) = \mathbf{F}_v\dot{\mathbf{q}} + \mathbf{F}_s \operatorname{sign}(\dot{\mathbf{q}}) \tag{2.45}$$

Remark 2.3 *Note that the friction term in (2.45) does not satisfy Assumption 2.2 due to the discontinuous nature of the sign-function. However, static or dry friction is always dissipative and can be compensated for without introducing any stability problems (cf. Paulsen and Egeland (1995)). Thus, the static friction terms can be dealt with separately or left out of the dissipative term in the stability analysis. The dissipative forces in (2.45) satisfies Assumption 2.2 when the stabilizing static friction term is ignored or dealt with separately.*

2.2.4 Marine vessels

A marine vessel is an Euler-Lagrange system satisfying Properties **P1**-**P4**. This thesis uses the vectorial notation from Fossen (2002) to express the equations of motion for a marine vessel in both the body-fixed frame and the NED frame. The generalized position vector $\mathbf{x} \in \mathbb{R}^3 \times \mathrm{SO}(3)$ and the velocity vector $\nu \in \mathbb{R}^6$ in six degrees of freedom are

$$\mathbf{x} := [x, y, z, \phi, \theta, \psi]^T \in \mathbb{R}^3 \times \mathrm{SO}(3) \tag{2.46}$$

$$\nu := [u, v, w, p, q, r]^T \in \mathbb{R}^6 \tag{2.47}$$

Note that the vector $\mathbf{x}$ of generalized coordinates has a position sub-vector $\mathbf{p} = [x, y, z]^T \in \mathbb{R}^3$, and an orientation sub-vector $\Theta = [\phi, \theta, \psi]^T \in \mathrm{SO}(3)$ (roll, pitch, yaw). The body-fixed velocity vector ν has a linear velocity sub-vector $\mathbf{v} = [u, v, w]^T \in \mathbb{R}^3$ (surge, sway, heave), and an angular velocity sub-vector $\omega = [p, q, r]^T \in \mathbb{R}^3$. The 6 DOF model of a marine vessel in the body-fixed reference frame can be written (Fossen (2002))

$$\mathbf{M}_\nu \dot{\nu} + \mathbf{C}_\nu(\nu)\nu + \mathbf{D}_\nu(\nu)\dot{\nu} + \mathbf{g}_\nu(\mathbf{x}) = \tau_\nu \tag{2.48}$$

where $\mathbf{x}$ is the NED position and orientation vector, and ν is the body-fixed velocity vector. The inertia matrix $\mathbf{M}_\nu(\nu)$ includes added mass effects, and is positive definite and constant. The Coriolis and centripetal matrix $\mathbf{C}_\nu(\nu)$ is skew-symmetric ($\mathbf{C}_\nu(\nu) = -\mathbf{C}_\nu^T(\nu)$), and the hydrodynamic damping matrix $\mathbf{D}_\nu(\nu)$ is non-symmetric and strictly positive ($\mathbf{D}_\nu(\nu) > 0,\ \forall\, \nu \in \mathbb{R}^6$). The gravitational/buoyancy forces are collected in $\mathbf{g}_\nu(\mathbf{x})$. Note that ν is does not constitute a set of generalized coordinates, and thus the model (2.48) does not in general satisfy Properties **P1**-**P4**.

The Jacobian transformation matrix $\mathbf{J}(\mathbf{x})$ relates the body reference frame to the NED reference frame through

$$\dot{\mathbf{x}} = \begin{bmatrix} \dot{\mathbf{p}} \\ \dot{\Theta} \end{bmatrix} = \begin{bmatrix} \mathbf{R}_b^n(\Theta) & \mathbf{0} \\ \mathbf{0} & \mathbf{T}_\Theta(\Theta) \end{bmatrix} \begin{bmatrix} \mathbf{v} \\ \omega \end{bmatrix} = \mathbf{J}(\mathbf{x})\nu \tag{2.49}$$

where $\mathbf{R}_b^n(\Theta)$ is the rotation matrix from the body frame to the NED frame, and $\mathbf{T}_\Theta(\Theta)$ is a transformation matrix. The relation can be written out in full as

$$\begin{bmatrix} \dot{x} \\ \dot{y} \\ \dot{z} \\ \dot{\phi} \\ \dot{\theta} \\ \dot{\psi} \end{bmatrix} = \begin{bmatrix} c\psi c\theta & -s\psi c\phi + c\psi s\theta s\phi & s\psi s\phi + c\psi c\phi s\theta & 0 & 0 & 0 \\ s\psi c\theta & c\psi c\phi + s\phi s\theta s\psi & -c\psi s\phi + s\theta s\psi c\phi & 0 & 0 & 0 \\ -s\theta & c\theta s\phi & c\theta c\phi & 0 & 0 & 0 \\ 0 & 0 & 0 & 1 & s\phi t\theta & c\phi t\theta \\ 0 & 0 & 0 & 0 & c\phi & -s\phi \\ 0 & 0 & 0 & 0 & \frac{s\phi}{c\theta} & \frac{c\phi}{c\theta} \end{bmatrix} \begin{bmatrix} u \\ v \\ w \\ p \\ q \\ r \end{bmatrix} \tag{2.50}$$

where $c\cdot$ and $s\cdot$ denotes the cosine and sine functions, respectively. Substituting the kinematic equation (2.49) and its derivative into (2.48) yields the dynamic model in the NED reference frame as

$$\mathbf{M}(\mathbf{x})\ddot{\mathbf{x}} + \mathbf{C}(\mathbf{x},\dot{\mathbf{x}})\dot{\mathbf{x}} + \mathbf{D}(\mathbf{x},\dot{\mathbf{x}})\dot{\mathbf{x}} + \mathbf{g}(\mathbf{x}) = \tau \tag{2.51}$$

The inertia matrix $\mathbf{M}(\mathbf{x})$ is positive definite but no longer constant, and the Coriolis and centripetal matrix $\mathbf{C}(\mathbf{x},\dot{\mathbf{x}})$ is defined in terms of Christoffel symbols. The dissipative vector $\mathbf{D}(\mathbf{x},\dot{\mathbf{x}})\dot{\mathbf{x}} = \mathbf{d}(\mathbf{x},\dot{\mathbf{x}})$ collects the dissipative forces, while $\mathbf{g}(\mathbf{x})$ is the vector of gravitational forces. The control input vector τ is the generalized forces and moments acting on the system. The dynamic model (2.51) belongs to the class of Euler-Lagrange systems described by (2.27), and the matrices satisfies Properties **P1**-**P4**.

The body-fixed representation of (2.48) is related to the NED reference frame representation of (2.51) through the transformations

$$\begin{aligned} \mathbf{M}(\mathbf{x}) &= \mathbf{J}^{-T}(\mathbf{x})\mathbf{M}_\nu\mathbf{J}^{-1}(\mathbf{x}) \\ \mathbf{C}(\mathbf{x},\dot{\mathbf{x}}) &= \mathbf{J}^{-T}\left[\mathbf{C}_\nu\left(\mathbf{J}^{-1}(\mathbf{x})\dot{\mathbf{x}}\right) - \mathbf{M}_\nu\mathbf{J}^{-1}(\mathbf{x})\dot{\mathbf{J}}^{-1}(\mathbf{x})\right]\mathbf{J}^{-1}(\mathbf{x}) \\ \mathbf{D}(\mathbf{x},\dot{\mathbf{x}}) &= \mathbf{J}^{-T}(\mathbf{x})\mathbf{D}_\nu\left(\mathbf{J}^{-1}(\mathbf{x})\dot{\mathbf{x}}\right)\mathbf{J}^{-1}(\mathbf{x}) \\ \mathbf{g}(\mathbf{x}) &= \mathbf{J}^{-T}(\mathbf{x})\mathbf{g}_\nu(\mathbf{x}) \\ \tau &= \mathbf{J}^{-T}(\mathbf{x})\tau_\nu \end{aligned} \tag{2.52}$$

Damping in a marine vessel is mainly caused by potential damping forces, skin friction, wave-drift damping and damping due to vortex shedding as defined in Fossen (2002). The contribution from potential damping terms is usually negligible compared to other dissipative terms. Linear skin friction is important in the low-frequency motion of the vessel, and in addition there is a high-frequency nonlinear (quadratic) skin friction contribution. Wave drift damping is the added resistance for surface vessels advancing in waves, and contributes heavily to damping in surge for higher sea-states due to the proportional dependency on the square of the significant wave height. Wave drift damping in sway and yaw is small relative to the viscous damping due to vortex shedding (drag). The damping terms contribute to both linear and nonlinear dissipative effects, but in many cases it can be difficult to separate these effects, and it is convenient to write the hydrodynamic damping term in the body-fixed frame of the vessel as

$$\mathbf{D}_\nu(\nu) = \mathbf{D}_l + \mathbf{D}_n(\nu) \tag{2.53}$$

where $\mathbf{D}_l$ is the linear part of the damping matrix, and $\mathbf{D}_n(\nu)$ is the remaining nonlinear damping effects. Note that for a rigid body moving through an ideal fluid, the hydrodynamic damping matrix of (2.53) will be real, non-symmetric and strictly positive. Note also that the damping term of (2.51) satisfies $\mathbf{D}(\mathbf{x},\dot{\mathbf{x}}) > 0\ \forall\ \mathbf{x},\dot{\mathbf{x}} \in \mathbb{R}^6$.

Nonlinear dissipative terms are in practice difficult to identify beyond the contribution from quadratic damping terms for marine vessels, and in the discussion on dissipative terms in succeeding chapters, we will thus make the following assumption

Assumption 2.3 *The bound on the dissipation vector in (2.37) satisfies for marine vessels*

$$\beta_d(\|\dot{\mathbf{x}}\|) = k_{D1} + k_{D2}\|\dot{\mathbf{x}}\|, \qquad k_{D1}, k_{D2} > 0 \tag{2.54}$$

Thus, we restrict the damping in the system to linear and quadratic damping.

Note that Assumption 2.3 satisfies Assumption 2.2 with $\beta_d(\cdot)$ as defined in (2.54).

2.2.5 Reference kinematics

In the development of a leader-follower coordinated synchronization control scheme, we desire that the motion of the follower is coordinated to the leader. In dynamic docking operations where vehicles are docked in moving vehicles, as for autonomous underwater vehicles docking in submarines, the coordination reference will coincide with the leader, and the control objective is just that of making the follower converge to the leader. In a many practical situations, however, the follower should not converge to the leader, but rather to a reference position relative to and uniquely determined by the leader. We will use the concept of a *reference* vehicle (see Figure 2.2) to designate this position.

Remark 2.4 *Note that we will use the term vehicle as a generalization of a marine vessel, a spacecraft or any detached mechanical system, while structures like robot manipulators, that does not always lend themselves to the concept of a vehicle, will be given special attention in the definition of a reference position for such situations.*

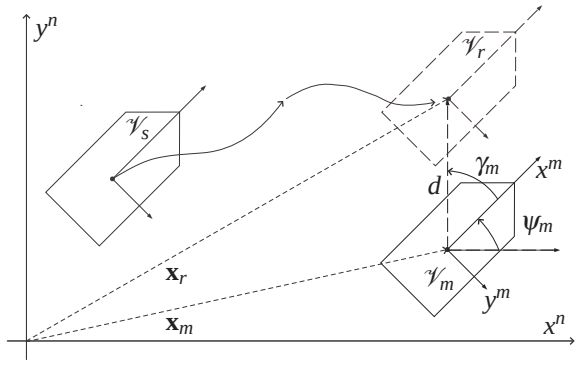

Figure 2.2: The leader vehicle $\mathcal{V}_m$, the follower vehicle $\mathcal{V}_s$ and the reference vehicle $\mathcal{V}_r$.

$\mathcal{V}_m$ The leader vehicle with position $\mathbf{x}_m = (x, y, \psi)^T$.

$\mathcal{V}_r$ The reference vehicle shifted a distance d in the direction given by the angle γ_m relative to the position of the leader vessel.

$\mathcal{V}_s$ The follower vehicle that coordinates to the reference vehicle.

The reference vehicle in a 3DOF applications can be illustrated through the control problem: Given the position and orientation (x,y) and heading angle ψ of the leader vehicle, we want the follower vehicle to converge to a position shifted by a distance d at an angle γ_m relative to the leader.

The position and heading in the NED frame of a reference vehicle placed at a constant distance d from the leader vehicle is given by the vector $\mathbf{d}_r^m$ from the leader vehicle to the reference vehicle

$$\mathbf{d}_r^m = \begin{bmatrix} d\cos\gamma_m \\ d\sin\gamma_m \\ 0 \end{bmatrix} \tag{2.55}$$

through the relation

$$\mathbf{x}_r = \mathbf{x}_m + \mathbf{J}(\mathbf{x}_m)\,\mathbf{d}_r^m \tag{2.56}$$

where $\mathbf{J}(\mathbf{x}_m)$ is the Jacobian transformation matrix from (2.49). The position and heading of the reference vehicle is thus uniquely determined by the position and heading $\mathbf{x}_m$ of the leader vehicle and the vector $\mathbf{d}_r^m$. We can obtain the differential kinematic relation for the reference vehicle using (2.49), and recognizing that for a 3DOF application the Jacobian matrix $\mathbf{J}(\mathbf{x}_m)$ of (2.50) reduces to a simple rotation matrix in heading $\mathbf{J}(\psi_m)$ Differentiating (2.56) gives

$$\dot{\mathbf{x}}_r = \dot{\mathbf{x}}_m + \mathbf{J}(\mathbf{x}_m)\,\mathbf{S}(r_m)\,\mathbf{d}_r^m \tag{2.57}$$

where $\mathbf{S}(\cdot)$ is a skew-symmetric matrix.

The differential kinematic relationship for the leader vehicle in the NED frame can be written in component form using (2.49)

$$\begin{aligned} \dot{x}_m &= u_m\cos\psi_m - v_m\sin\psi_m \\ \dot{y}_m &= u_m\sin\psi_m + v_m\cos\psi_m \\ \dot{\psi}_m &= r_m \end{aligned} \tag{2.58}$$

Consider the case where the reference vehicle is chosen at a position orthogonally off one of the sides of the leader, i.e. with $\gamma_m = \pm\frac{\pi}{2}$, to achieve parallel motion between the leader and follower. The vector from the leader vehicle to the reference vehicle in (2.55) now becomes

$$\mathbf{d}_r^m = \begin{bmatrix} 0 \\ \pm d \\ 0 \end{bmatrix} \tag{2.59}$$

and the component form of (2.57) is then

$$\begin{aligned} \dot{x}_r &= \dot{x}_m \pm d r_m\cos\psi_m \\ \dot{y}_r &= \dot{y}_m \pm d r_m\sin\psi_m \\ \dot{\psi}_r &= r_m \end{aligned} \tag{2.60}$$

Substituting $\dot{\mathbf{x}}_m$ from (2.58) in (2.57) and defining $u_r = u_m \pm d r_m$, $v_r = v_m$ and $r_r = r_m$ gives

$$\begin{aligned} \dot{x}_r &= u_r\cos\psi_m - v_r\sin\psi_m \\ \dot{y}_r &= u_r\sin\psi_m + v_r\cos\psi_m \\ \dot{\psi}_r &= r_r \end{aligned} \tag{2.61}$$

It is easy to see from (2.61) that for parallel motion only the forward velocity of the reference vehicle is changed ($u_r = u_m \pm dr_m$) with respect to that of the leader vehicle. Note that this is necessary for the follower vehicle to maintain its position parallel to the leader vehicle during turns due to the difference in turn radius. The differential kinematic model of the reference vehicle can now be written as

$$\dot{\mathbf{x}}_r = \mathbf{J}(\mathbf{x}_m)\, \nu_r \tag{2.62}$$

where $\nu_r = [u_m \pm dr_m,\ v_m,\ r_m]^T$. See Appendix B for a complete discussion on the kinematics of the reference vehicle for $\lambda_m \in [0, 2\pi)$.

Remark 2.5 *Note that for a robot manipulator, it is often desirable that the follower copies the motion of the leader. For these situations, the position of the follower manipulator should converge to that of the leader manipulator. However, manipulating rigid structures with two manipulators in a coordinated control scheme requires that we define a reference position for the follower through a similar reasoning as for the reference vehicle. In these applications, the orientation and length of the rigid structure interconnecting the two manipulators define the vector* $\mathbf{d}_r^m$ *from the leader manipulator to the reference manipulator.*

Chapter 3

The Observer-Controller Approach

This chapter proposes an observer-controller scheme for coordinated motion control that solves the output reference control problems of Section 2.1.5. The observer-controller approach is based on designing an *error* observer for the evolution of the coordination error, and then reconstructing the leader states based on these coordination errors and the states of the follower. The observer-controller approach is first applied to the control problem of coordinating a follower to a leader utilizing state measurements of the follower as in Definition 2.7, and then to the control problem where only position measurements are available for the follower as in Definition 2.8. The results presented in this chapter are based on Kyrkjebø and Pettersen (2003), Kyrkjebø *et al.* (2004), Kyrkjebø and Pettersen (2005*a*), Kyrkjebø *et al.* (2006*b*) and Kyrkjebø and Pettersen (2007*a*).

3.1 The Observer-controller principle

The leader-follower coordination problem where the leader is a dynamic system for which the parameters of the mathematical model, the control inputs and the internal states of the leader are unknown to the follower, requires that the states of the leader are estimated in order to coordinate the motion of the leader and follower system. The lack of model information of the leader precludes the design of model-based observers that directly estimates the states of the leader. Time-filtered derivatives of the position signals may be constructed, but this may be at the expense of robustness under noisy conditions. Thus, in this chapter we propose a model-based observer that filters the coordination errors through the dynamic model of the follower to provide estimates of the unknown states of the leader.

Model-based tracking approaches have been applied to mechanical systems by Salichs *et al.* (1991) and Dong *et al.* (2002) for mobile robots, Loría *et al.* (1997), Lefeber (2000) and Loría and Melhem (2002) for mechanical systems, Fossen and Berge (1997), Pettersen and Nijmeijer (1998), Encarnacao and Pascoal (2001) and Aguiar and Hespanha (2004) for marine systems, Al-Hiddabi and McClamroch (2002) for flight control, and many others. An output feedback tracking controller using a velocity observer design was proposed in Berghuis (1993) for robots, and this approach utilized a sliding surface (Slotine and Li (1987*b*)) to passively filter the reference states. Note that all of the tracking approach assume state information of the reference trajectory, while Rodriguez-Angeles and Nijmeijer (2001) presented an output coordination control approach for two robot manipulators based

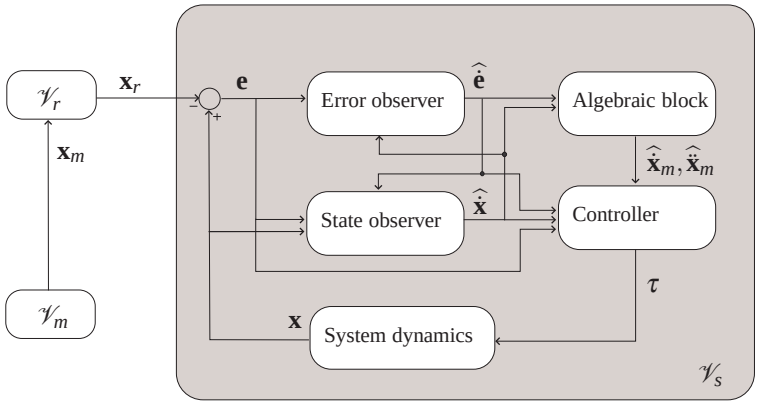

Figure 3.1: Schematic of the coordination observer-controller control scheme. The reference position $\mathcal{V}_r$ is uniquely determined by the leader system $\mathcal{V}_m$, and all the control and estimation necessary to achieve coordination is the responsibility of the follower system $\mathcal{V}_s$.

on position measurements of both the reference and the coordinating system only. This approach was later utilized in Nijmeijer and Rodriguez-Angeles (2003) for both coordinating and cooperating systems. A general overview of observers for nonlinear systems can be found in Marino and Tomei (1995) and Nijmeijer and Fossen (1999), while observers for synchronization are discussed in Nijmeijer and Mareels (1997), Pogromsky and Nijmeijer (1998) and Huijberts and Nijmeijer (2001).

In this chapter, we propose an observer-controller design that coordinates two systems in a leader-follower configuration using only the position as output information from the leader system. The parameters of the leader system are considered unknown, and model-based observers can not be designed to estimate the unknown states directly. Thus, following the approach of Nijmeijer and Rodriguez-Angeles (2003), the observer-controller design of this chapter utilizes information about the model and control input of the follower to filter the closed-loop errors of the coordination scheme to generate estimates of the derivatives of the closed-loop errors. When the states of the follower are known, either through measurements as in Section 3.2 or through a nonlinear observer as in Section 3.3, estimates of the leader states can be constructed through algebraic manipulation. The control input to the follower from the coordination control law is based on estimates of the states of the leader, and can be thought of as part of the correction term in the observer. In fact, the follower becomes a *physical observer* of the leader.

The principle of the proposed observer-controller coordination approach is shown in Figure 3.1. Note that all the coordination control responsibility is placed on the follower system. The only information that enters the coordination block from the reference is the position vector $\mathbf{x}_r$ that gives the desired position for the follower system. Based on the position of the follower $\mathbf{x}$ and the position of the reference system $\mathbf{x}_r$, a coordination

error $\mathbf{e}$ forms the basis for the coordination controller. However, derivatives of this error will be needed in the control law, and thus an error observer estimating $\dot{\mathbf{e}}$ is constructed using the dynamic model of the follower and the coordination control law. In addition, for situations where the velocity of the follower is unknown, a state observer is constructed for the follower to estimate $\dot{\mathbf{x}}$ in Section 3.3. Based on the estimated errors $\mathbf{e}$ and $\dot{\mathbf{e}}$ and the states of the follower $\mathbf{x}$ and $\dot{\mathbf{x}}$, the states of the reference system can then be found algebraically through the definition of the coordination errors.

Note that the desired position of the follower system $\mathscr{V}_s$ is at a reference position uniquely defined by the leader system $\mathscr{V}_m$. The reference system $\mathscr{V}_r$ representing this reference position can be constructed using the approach of Section 2.2.5. However, the discussion of this chapter adopts the leader system $\mathscr{V}_m$ as the reference system to simplify the illustrations and better introduce the concept of a physical observer, and to reduce the number of systems involved in the derivation of the coordination controller and observers. To utilize the concept of the reference system in the following coordination schemes, the leader states with subscripts m should thus be replaced by that of the reference system r, and the reference system should be defined in terms of the leader system following the procedure in Section 2.2.5.

3.1.1 A coordination design

The control objective of the proposed coordination observer-controller scheme is to synchronizes the states $\mathbf{x}$ and $\dot{\mathbf{x}}$ of the follower system to the states $\mathbf{x}_m$ and $\dot{\mathbf{x}}_m$ of the leader (reference) system. The leader is assumed to be a physical system where the parameters of the dynamic model and the control inputs are unknown, and where the position vector $\mathbf{x}_m$ is the only measured output. We define the coordination errors as

$$\mathbf{e} = \mathbf{x} - \mathbf{x}_m, \qquad \dot{\mathbf{e}} = \dot{\mathbf{x}} - \dot{\mathbf{x}}_m, \qquad \ddot{\mathbf{e}} = \ddot{\mathbf{x}} - \ddot{\mathbf{x}}_m \tag{3.1}$$

The unknown state derivatives of the leader $\dot{\mathbf{x}}_m$ and $\ddot{\mathbf{x}}_m$ can be passively filtered by restricting the position error $\mathbf{e}$ to lie on a sliding surface (Slotine and Li (1987*b*))

$$\dot{\mathbf{e}} + \mathbf{\Lambda}\mathbf{e} = 0 \tag{3.2}$$

where $\mathbf{\Lambda}$ is a constant matrix whose eigenvalues are strictly in the right of the half complex plane. This is achieved by replacing the unknown reference states $\dot{\mathbf{x}}_m$ and $\ddot{\mathbf{x}}_m$ with a virtual reference trajectory

$$\mathbf{y} = \mathbf{x}_m - \mathbf{\Lambda}\int_0^t \mathbf{e}\, dt \tag{3.3a}$$

$$\dot{\mathbf{y}} = \dot{\mathbf{x}}_m - \mathbf{\Lambda}\mathbf{e} \tag{3.3b}$$

$$\ddot{\mathbf{y}} = \ddot{\mathbf{x}}_m - \mathbf{\Lambda}\dot{\mathbf{e}} \tag{3.3c}$$

and defining

$$\mathbf{s} = \dot{\mathbf{x}} - \dot{\mathbf{y}} = \dot{\mathbf{e}} + \mathbf{\Lambda}\mathbf{e} \tag{3.4}$$

as a measure of tracking. The vector $\mathbf{s}$ conveys information about the boundedness and convergence of $\mathbf{x}$ and $\dot{\mathbf{x}}$, and the definition can be seen as a stable first-order differential equation in $\mathbf{e}$ with $\mathbf{s}$ as an input. For bounded initial conditions, boundedness of $\mathbf{s}$ will

imply boundedness of $\mathbf{e}$ and $\dot{\mathbf{e}}$. The formal definition of $\mathbf{y}$ in (3.3a) is equivalent to adding an internal feedback loop in the controller, but the integral term $\int_0^t \mathbf{e}\, dt$ will not be used explicitly in the controller. The passive filtering of the leader states gives additional design freedom in choosing the slope of the sliding surface through $\mathbf{\Lambda}$ that in some cases simplifies the stability analysis of the proposed coordination control schemes.

Consider now the case where the derivatives of the leader and follower system are known and measured in the control design to illustrate the coordination design. Thus, we would have state information of the reference, and state information of the follower system, and could design a coordination control law using state feedback. Write now the dynamics of (2.27) using (2.30) and (3.4) as

$$\mathbf{M}(\mathbf{x})\dot{\mathbf{s}} = -\mathbf{C}(\mathbf{x},\dot{\mathbf{x}})\mathbf{s} - \mathbf{D}(\mathbf{x},\dot{\mathbf{x}})\dot{\mathbf{s}} + \tau - \mathbf{M}(\mathbf{x})\ddot{\mathbf{y}} - \mathbf{C}(\mathbf{x},\dot{\mathbf{x}})\dot{\mathbf{y}} - \mathbf{D}(\mathbf{x},\dot{\mathbf{x}})\dot{\mathbf{y}} - \mathbf{g}(\mathbf{x}) \tag{3.5}$$

Utilizing a state feedback coordination control law inspired by Paden and Panja (1988)

$$\tau = \mathbf{M}(\mathbf{x})\ddot{\mathbf{y}} + \mathbf{C}(\mathbf{x},\dot{\mathbf{x}})\dot{\mathbf{y}} + \mathbf{D}(\mathbf{x},\dot{\mathbf{x}})\dot{\mathbf{y}} + \mathbf{g}(\mathbf{x}) - \mathbf{K}_d\mathbf{s} - \mathbf{K}_p\mathbf{e} \tag{3.6}$$

allows us to construct a Lyapunov function

$$V(t) = \frac{1}{2}\mathbf{s}^T\mathbf{M}(\mathbf{x})\mathbf{s} + \frac{1}{2}\mathbf{e}^T\mathbf{K}_p\mathbf{e}, \qquad \mathbf{K}_p = \mathbf{K}_p^T > 0 \tag{3.7}$$

where the derivative of (3.7) is

$$\dot{V}(t) = -\mathbf{s}^T\left(\mathbf{D}(\mathbf{x},\dot{\mathbf{x}}) + \mathbf{K}_d\right)\mathbf{s} - \mathbf{e}^T\mathbf{\Lambda}^T\mathbf{K}_p\mathbf{e} \tag{3.8}$$

Since $V(t)$ is positive definite, and $\dot{V}(t)$ is negative definite it follows that the equilibrium $(\mathbf{e},\mathbf{s}) = (\mathbf{0},\mathbf{0})$ would be globally exponentially stable (GES) for state feedback control, and from convergence of $\mathbf{s} \to \mathbf{0}$ and $\mathbf{e} \to \mathbf{0}$ that $\dot{\mathbf{e}} \to \mathbf{0}$.

3.2 Output reference coordination design with state feedback

The state feedback problem of Section 3.1.1 is trivial in its solution, but the control law of (3.6) can not be implemented when the states of the leader are unknown. Thus, in this section we propose an observer-controller approach to solve the coordination problem of Definition 2.7, for which only the position $\mathbf{x}_m$ is available as output information from the leader, but we have both position and velocity measurements for the follower system. The results presented here are based on Kyrkjebø and Pettersen (2007*a*).

3.2.1 Coordination control design

The control law (3.6) can not be implemented when the states of the leader $\dot{\mathbf{x}}_m$ and $\ddot{\mathbf{x}}_m$ are unknown, and thus a control law that depends on estimated values for the states $\dot{\mathbf{y}}$, $\ddot{\mathbf{y}}$ and $\mathbf{s}$ should be employed. We propose the control law

$$\tau = \mathbf{M}(\mathbf{x})\hat{\ddot{\mathbf{y}}} + \mathbf{C}(\mathbf{x},\dot{\mathbf{x}})\hat{\dot{\mathbf{y}}} + \mathbf{D}(\mathbf{x},\dot{\mathbf{x}})\hat{\dot{\mathbf{y}}} + \mathbf{g}(\mathbf{x}) - \mathbf{K}_d\hat{\mathbf{s}} - \mathbf{K}_p\mathbf{e} \tag{3.9}$$

to coordinate the states of the follower to the states of the leader. A full-state nonlinear model-based Luenberger observer (Luenberger (1971)) is designed to estimate $\widehat{\mathbf{e}}$ and $\widehat{\mathbf{s}}$ as

$$\frac{d}{dt}\widehat{\mathbf{e}} = \widehat{\mathbf{s}} - \boldsymbol{\Lambda}\widehat{\mathbf{e}} + \mathbf{L}_1\widetilde{\mathbf{e}} \tag{3.10a}$$

$$\frac{d}{dt}\widehat{\mathbf{s}} = -\mathbf{M}^{-1}(\mathbf{x})\left[\mathbf{C}(\mathbf{x},\dot{\mathbf{x}})\widehat{\mathbf{s}} + \mathbf{D}(\mathbf{x},\dot{\mathbf{x}})\widehat{\mathbf{s}} + \mathbf{K}_d\widehat{\mathbf{s}} + \mathbf{K}_p\widehat{\mathbf{e}}\right] + \mathbf{L}_2\widetilde{\mathbf{e}} \tag{3.10b}$$

where $\widetilde{\mathbf{e}} = \mathbf{e} - \widehat{\mathbf{e}}$. The closed-loop error dynamics of the system (2.27) and the controller (3.9) are

$$\mathbf{M}(\mathbf{x})\dot{\mathbf{s}} + \mathbf{C}(\mathbf{x},\dot{\mathbf{x}})\mathbf{s} + \mathbf{D}(\mathbf{x},\dot{\mathbf{x}})\mathbf{s} + \mathbf{K}_d\mathbf{s} + \mathbf{K}_p\mathbf{e} = \mathbf{C}(\mathbf{x},\dot{\mathbf{x}})\widetilde{\mathbf{s}} + \mathbf{D}(\mathbf{x},\dot{\mathbf{x}})\widetilde{\mathbf{s}} + \mathbf{K}_d\widetilde{\mathbf{s}} + \mathbf{M}(\mathbf{x})\dot{\widetilde{\mathbf{s}}} \tag{3.11}$$

where $\widetilde{\mathbf{s}} = \mathbf{s} - \widehat{\mathbf{s}}$. The estimation error dynamics can be found through the relations

$$\dot{\widetilde{\mathbf{e}}} = \frac{d}{dt}(\mathbf{e} - \widehat{\mathbf{e}}), \tag{3.12}$$

$$\dot{\widetilde{\mathbf{s}}} = \frac{d}{dt}(\mathbf{s} - \widehat{\mathbf{s}}) \tag{3.13}$$

by inserting the state-space representation of (3.11) and the observer (3.10) to give

$$\dot{\widetilde{\mathbf{e}}} = \widetilde{\mathbf{s}} - (\boldsymbol{\Lambda} + \mathbf{L}_1)\widetilde{\mathbf{e}} \tag{3.14}$$

$$\dot{\widetilde{\mathbf{s}}} = \dot{\widetilde{\mathbf{s}}} - \left(\mathbf{M}^{-1}(\mathbf{x})\mathbf{K}_p + \mathbf{L}_2\right)\widetilde{\mathbf{e}} \tag{3.15}$$

Note from (3.15) that $\dot{\widetilde{\mathbf{s}}} \neq \dot{\widetilde{\mathbf{s}}}$ through the definition of the error observer in (3.10). Assuming for simplicity that the gain matrices $\mathbf{K}_p$, $\mathbf{K}_d$ and $\mathbf{L}_1$, $\mathbf{L}_2$ are symmetric and positive definite, a change of coordinates can be introduced through

$$\overline{\mathbf{e}} = \mathbf{e} - \widetilde{\mathbf{e}} \tag{3.16}$$

$$\overline{\mathbf{s}} = \mathbf{s} - \widetilde{\mathbf{s}} \tag{3.17}$$

that gives the closed-loop error dynamics of (3.11) by using (3.14) as

$$\mathbf{M}(\mathbf{x})\dot{\overline{\mathbf{s}}} + \mathbf{C}(\mathbf{x},\dot{\mathbf{x}})\overline{\mathbf{s}} + \mathbf{D}(\mathbf{x},\dot{\mathbf{x}})\overline{\mathbf{s}} + \mathbf{K}_d\overline{\mathbf{s}} + \mathbf{K}_p\overline{\mathbf{e}} = \mathbf{M}(\mathbf{x})\mathbf{L}_2\widetilde{\mathbf{e}} \tag{3.18}$$

Note that through (3.14) and (3.16) we can write

$$\dot{\overline{\mathbf{e}}} = \frac{d}{dt}(\mathbf{e} - \widetilde{\mathbf{e}}) = \overline{\mathbf{s}} - \boldsymbol{\Lambda}\overline{\mathbf{e}} + \mathbf{L}_1\widetilde{\mathbf{e}} \tag{3.19}$$

and that the estimates of the leader states become

$$\widehat{\dot{\mathbf{y}}} = \dot{\mathbf{x}} - \widehat{\mathbf{s}} \tag{3.20}$$

$$\widehat{\ddot{\mathbf{y}}} = -\boldsymbol{\Lambda}(\widehat{\mathbf{s}} - \boldsymbol{\Lambda}\widehat{\mathbf{e}} + \mathbf{L}_1\widetilde{\mathbf{e}}) \tag{3.21}$$

3.2.2 Stability analysis

The objective of the control law of the follower is to coordinate the follower system to the leader system based on the estimates of the leader states. The leader states are indirectly estimated through the error observer of (3.10) that uses the dynamic model of the follower and its control input as parameters.

Theorem 3.1 *Consider the model (2.27), the controller (3.9) and the observer (3.10). Under Assumption 2.1, the closed-loop errors*

$$\widetilde{\eta} = \begin{bmatrix} \dot{\mathbf{e}}^T & \mathbf{e}^T & \dot{\widetilde{\mathbf{e}}}^T & \widetilde{\mathbf{e}}^T \end{bmatrix}^T \tag{3.22}$$

are globally uniformly ultimately bounded. The bound is a function of the leader acceleration $\ddot{\mathbf{x}}_m$.

Details of the proof of Theorem 3.1 are given in Appendix C.1.1.
Sketch of proof: Consider the Lyapunov function candidate

$$V(\bar{\mathbf{s}}, \bar{\mathbf{e}}, \widetilde{\mathbf{s}}, \widetilde{\mathbf{e}}) = \frac{1}{2}\bar{\mathbf{s}}^T\mathbf{M}(\mathbf{x})\bar{\mathbf{s}} + \bar{\mathbf{e}}^T\mathbf{K}_p\bar{\mathbf{e}} + \frac{1}{2}\widetilde{\mathbf{s}}^T\mathbf{P}_1\widetilde{\mathbf{s}} + \frac{1}{2}\widetilde{\mathbf{e}}^T\mathbf{L}_2\widetilde{\mathbf{e}} - \widetilde{\mathbf{e}}^T\mathbf{P}_2\widetilde{\mathbf{s}} \tag{3.23}$$

where $\mathbf{P}_1$ and $\mathbf{P}_2$ are positive definite constant matrices to be defined and (3.23) is positive definite through Property **P1** when

$$\mathbf{P}_{1,m}\mathbf{L}_{2,m} > \mathbf{P}_{2,M}^2 \tag{3.24}$$

Defining the shorthand $\mathbf{L}_3 := \mathbf{\Lambda} + \mathbf{L}_1$, and introducing a constant parameter $\varepsilon > 1$ used as a tuning parameter in the stability proof, the derivative of (3.23) along the closed-loop trajectories becomes

$$\begin{aligned}
\dot{V}(\bar{\mathbf{s}}, \bar{\mathbf{e}}, \widetilde{\mathbf{s}}, \widetilde{\mathbf{e}}) = &-\frac{1}{2}\begin{bmatrix} \bar{\mathbf{s}} \\ \bar{\mathbf{e}} \end{bmatrix}^T \overbrace{\begin{bmatrix} \mathbf{D}(\mathbf{x}, \dot{\mathbf{x}}) + \mathbf{K}_d & 0 \\ 0 & \mathbf{\Lambda}^T\mathbf{K}_p \end{bmatrix}}^{\mathbf{Q}_1} \begin{bmatrix} \bar{\mathbf{s}} \\ \bar{\mathbf{e}} \end{bmatrix} \\
&-\frac{1}{2}\begin{bmatrix} \widetilde{\mathbf{s}} \\ \widetilde{\mathbf{e}} \end{bmatrix}^T \overbrace{\begin{bmatrix} 2\mathbf{L}_1 & \left(\mathbf{M}^{-1}(\mathbf{x})\mathbf{K}_p - \mathbf{L}_3^T\mathbf{L}_1\right) \\ \left(\mathbf{M}^{-1}(\mathbf{x})\mathbf{K}_p - \mathbf{L}_3^T\mathbf{L}_1\right) & \frac{2}{\varepsilon}\mathbf{L}_2\mathbf{L}_3 - \mathbf{L}_1\left(\mathbf{M}^{-1}(\mathbf{x})\mathbf{K}_p + \mathbf{L}_2\right) \end{bmatrix}}^{\mathbf{Q}_{2,\beta}} \begin{bmatrix} \widetilde{\mathbf{s}} \\ \widetilde{\mathbf{e}} \end{bmatrix} \\
&-\frac{1}{2}\begin{bmatrix} \bar{\mathbf{s}} \\ \widetilde{\mathbf{e}} \end{bmatrix}^T \overbrace{\begin{bmatrix} \mathbf{D}(\mathbf{x}, \dot{\mathbf{x}}) + \mathbf{K}_d & -\mathbf{M}(\mathbf{x})\mathbf{L}_2 \\ -\mathbf{M}(\mathbf{x})\mathbf{L}_2 & \frac{\varepsilon-1}{\varepsilon}\mathbf{L}_2\mathbf{L}_3 \end{bmatrix}}^{\mathbf{Q}_3} \begin{bmatrix} \bar{\mathbf{s}} \\ \widetilde{\mathbf{e}} \end{bmatrix} \\
&-\frac{1}{2}\begin{bmatrix} \bar{\mathbf{e}} \\ \widetilde{\mathbf{e}} \end{bmatrix}^T \overbrace{\begin{bmatrix} \mathbf{\Lambda}^T\mathbf{K}_p & -\mathbf{L}_1^T\mathbf{K}_p \\ -\mathbf{L}_1^T\mathbf{K}_p & \frac{\varepsilon-1}{\varepsilon}\mathbf{L}_2\mathbf{L}_3 \end{bmatrix}}^{\mathbf{Q}_4} \begin{bmatrix} \bar{\mathbf{e}} \\ \widetilde{\mathbf{e}} \end{bmatrix} + \beta_N(\cdot)
\end{aligned} \tag{3.25}$$

where we have chosen $\mathbf{P}_1 = \mathbf{I}$ for simplicity, and introduced a tuning gain on the perturbation through the choice of $\mathbf{P}_2 = \mathbf{L}_1$. The perturbation term $\beta_N(\cdot)$ is now given as

$$\beta_N(\cdot) = -\left(\widetilde{\mathbf{s}}^T - \widetilde{\mathbf{e}}^T\mathbf{L}_1\right)\ddot{\mathbf{x}}_m \tag{3.26}$$

The term $\mathbf{Q}_1$ is positive definite trivially with symmetric positive definite gains $\mathbf{\Lambda}$, $\mathbf{K}_p$ and $\mathbf{K}_d$, and $\mathbf{Q}_{2,\beta}$ is positive definite when

$$\mathbf{Q}_{2,\beta} > 0 \Leftrightarrow \frac{\frac{4}{\varepsilon}\mathbf{L}_{2,m}\mathbf{L}_{3,m} - \mathbf{L}_{1,M}^2\left(\mathbf{M}_m^{-1}\mathbf{K}_{p,M} + \mathbf{L}_{2,M}\right)}{\left[\left(\mathbf{M}_m^{-1}\mathbf{K}_{p,M} - \mathbf{L}_{3,m}^T\mathbf{L}_{1,m}\right)\right]^2} > 1 \tag{3.27}$$

where the positive definiteness can be ensured through tuning the filter gain $\mathbf{\Lambda}$ of (3.2). Conditions for positive definiteness for $\mathbf{Q}_3$ and $\mathbf{Q}_4$ are

$$\mathbf{Q}_3 > 0 \quad \Leftrightarrow \quad \frac{\frac{\varepsilon-1}{\varepsilon}(\mathbf{D}_m + \mathbf{K}_{p,m})\mathbf{L}_{3,m}}{\mathbf{M}_M^2 \mathbf{L}_{2,M}} > 1 \tag{3.28}$$

$$\mathbf{Q}_4 > 0 \quad \Leftrightarrow \quad \frac{\frac{\varepsilon-1}{\varepsilon}\mathbf{\Lambda}_m^T \mathbf{L}_{2,m}\mathbf{L}_{3,m}}{\mathbf{L}_{1,M}^2 \mathbf{K}_{p,M}} > 1 \tag{3.29}$$

The perturbation term of (3.26) can thus be bounded as

$$\beta_N(\cdot) \leq (\|\widetilde{\mathbf{s}}\| + \mathbf{L}_{1,M}\|\widetilde{\mathbf{e}}\|) A_M \tag{3.30}$$

The closed-loop errors $\overline{\mathbf{s}}$, $\overline{\mathbf{e}}$, $\widetilde{\mathbf{s}}$, $\widetilde{\mathbf{e}}$, and thus $\widetilde{\eta}$ of (3.22), are globally uniformly ultimately bounded with the lower bound δ of Definition 2.1 as

$$\delta = \sqrt{1 + \mathbf{L}_{1,M}}\sqrt{A_M} \tag{3.31}$$

■

Remark 3.1 *Note that the acceleration of the leader $\ddot{\mathbf{x}}_m$ will be present as a non-vanishing disturbance in the observer-controller scheme, and thus the origin of the closed-loop error space is no longer an equilibrium. We can therefore only conclude that the closed-loop errors are ultimately bounded by some function of the leader acceleration $\ddot{\mathbf{x}}_m$.*

3.2.3 Simulation study

The observer-controller approach for coordination with only position measurements of the leader, but with state information of the follower, was simulated in the simulation environment of Appendix E with initial states and gains given in Table 3.1. In the simulations, the leader ship tracks a sine wave reference trajectory $\sin(\varpi t)$ with frequency $\varpi = 1/15$ rad/s with heading angle ψ_m along the tangent line.

Table 3.1: Initial states and gains for observer-controller scheme

Initial states for leader, follower and obs.							Observer and controller gains							
$\mathbf{x}_m$	=		[0	0	0	]^T	$\mathbf{K}_p$	=	diag[	1	1	1	]
$\mathbf{x}$	=		[−1	1.5	$\frac{\pi}{2}$	]^T	$\mathbf{K}_d$	=	diag[	40	40	10	]
$\widehat{\mathbf{x}}$	=		[0	0	0	]^T	$\mathbf{L}_1$	=	diag[	1	1	1	]
$\mathbf{\Lambda}$	=	diag[	0.3	0.3	0.3	]	$\mathbf{L}_2$	=	diag[	1.3	1.3	1.3	]

The coordination controller and observer errors in position $\mathbf{e}$ and velocity $\dot{\mathbf{e}}$ are shown in Figure 3.2, and we see that the closed-loop errors are uniformly ultimately bounded. Small oscillations are observed in the plots due to the non-vanishing perturbing acceleration $\ddot{\mathbf{x}}_m$ of the leader. Note that the performance of the observer-controller scheme can be further optimized through gain tuning, but the convergence of the scheme is here illustrated using preliminary gains that illustrates the uniform ultimate boundedness of the scheme.

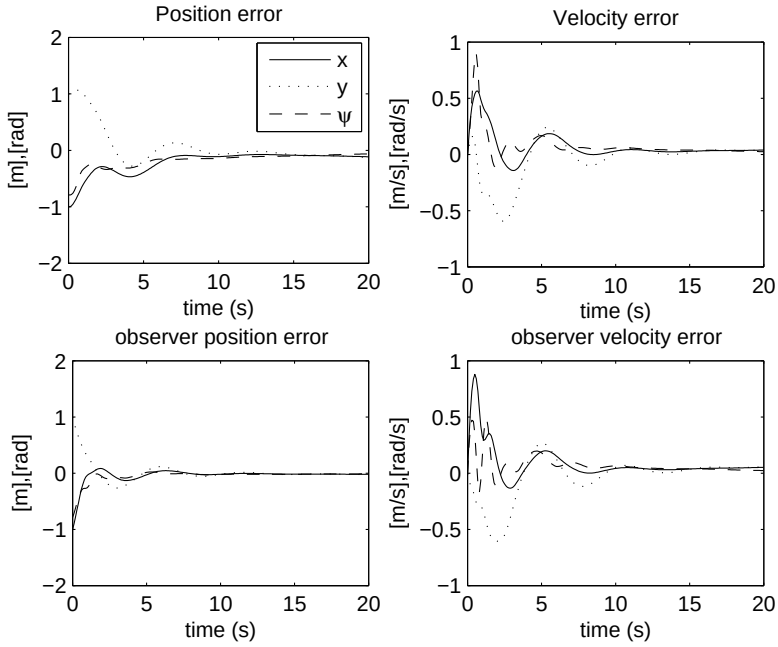

Figure 3.2: Synchronization errors in position $\mathbf{e}$ and velocity $\dot{\mathbf{e}}$ (upper row), and observer errors $\widetilde{\mathbf{e}}$ and $\widetilde{\dot{\mathbf{e}}}$ (lower row).

3.3 Output reference coordination design with output feedback

To account for situations where only the position measurement is available for *both* the leader and the follower, the observer-controller scheme of Section 3.2 is modified to remove the necessity of measuring $\dot{\mathbf{x}}$. In this section, a second nonlinear observer is introduced to estimate the velocity of the follower using the dynamic model of the follower (2.27). Simulations and experiments are presented in a back-to-back comparison of the theoretical and experimental results, and the impact from of modelling errors, external disturbances and the gain tuning process are discussed. The results of this section are based on Kyrkjebø and Pettersen (2003), Kyrkjebø *et al.* (2004) and Kyrkjebø and Pettersen (2005*a*).

3.3.1 Coordination control design

The control objective of the coordination problem of Definition 2.8 is to synchronize the states of the follower $\mathbf{x}$ and $\dot{\mathbf{x}}$ to the states of the leader $\mathbf{x}_m$ and $\dot{\mathbf{x}}_m$ based on measurements of $\mathbf{x}$ and $\mathbf{x}_m$ only. Thus, in this section we propose to extend the coordination control scheme of Section 3.2 by introducing a nonlinear model-based state observer for the unmeasured state $\dot{\mathbf{x}}$ of the follower. The presentation in this section is done under an assumption of linear dissipation in the model of (2.27) to investigate the effect of modelling errors in the back-to-back comparison between simulated and experimental results. Note, however,

that the stability results concluded in this section are valid for systems with nonlinear dissipative terms as shown in Kyrkjebø *et al.* (2006*b*).

The dissipative term $\mathbf{d}(\mathbf{x},\dot{\mathbf{x}}) = \mathbf{D}(\mathbf{x},\dot{\mathbf{x}})\dot{\mathbf{x}}$ of (2.27) in this section is assumed to include only linear dissipative terms (e.g. viscous friction, hydrodynamic skin friction)

Assumption 3.1 *The dissipative term is linear in velocity* $\dot{\mathbf{x}}$ *such that* $\mathbf{D}(\mathbf{x},\dot{\mathbf{x}})\dot{\mathbf{x}} = \mathbf{D}(\mathbf{x})\dot{\mathbf{x}}$.

Remark 3.2 *Note that Assumption 3.1 is valid for low-speed applications within robotics and marine vehicles, and in practice it is difficult to determine nonlinear dissipative terms over a wide speed regime. Thus, the assumption reflects the challenges faced when designing a nonlinear control system where model terms are cancelled; the complete model of a system (2.27) is often not available, and thus the control scheme employed must incorporate some robustness to modelling errors.*

The definition of the coordination errors from Section 3.1.1 in (3.1) gives the model (2.27) under Assumption 3.1 as

$$\mathbf{M}(\mathbf{x})\ddot{\mathbf{e}} = -\mathbf{C}(\mathbf{x},\dot{\mathbf{x}})\dot{\mathbf{e}} - \mathbf{D}(\mathbf{x})\dot{\mathbf{e}} + \tau - \mathbf{M}(\mathbf{x})\ddot{\mathbf{x}}_m - \mathbf{C}(\mathbf{x},\dot{\mathbf{x}})\dot{\mathbf{x}}_m - \mathbf{D}(\mathbf{x})\dot{\mathbf{x}}_m - \mathbf{g}(\mathbf{x}) \tag{3.32}$$

To solve the problem of Definition 2.8 where only position measurements are available for both the leader and the follower, we propose a coordination control law that depends on estimates of the unknown states as

$$\tau = \mathbf{M}(\mathbf{x})\ddot{\widehat{\mathbf{x}}}_m + \mathbf{C}\left(\mathbf{x},\widehat{\dot{\mathbf{x}}}\right)\widehat{\dot{\mathbf{x}}}_m + \mathbf{D}(\mathbf{x})\widehat{\dot{\mathbf{x}}}_m + \mathbf{g}(\mathbf{x}) - \mathbf{K}_d\widehat{\dot{\mathbf{e}}} - \mathbf{K}_p\mathbf{e} \tag{3.33}$$

To obtain estimates for the errors $\mathbf{e}$ and $\dot{\mathbf{e}}$, we propose a nonlinear model-based Luenberger observer

$$\frac{d}{dt}\widehat{\mathbf{e}} = \widehat{\dot{\mathbf{e}}} + \mathbf{L}_{\mathbf{e}1}\widetilde{\mathbf{e}} \tag{3.34a}$$

$$\frac{d}{dt}\widehat{\dot{\mathbf{e}}} = -\mathbf{M}(\mathbf{x})^{-1}\left[\mathbf{C}\left(\mathbf{x},\widehat{\dot{\mathbf{x}}}\right)\widehat{\dot{\mathbf{e}}} + \mathbf{D}(\mathbf{x})\widehat{\dot{\mathbf{e}}} + \mathbf{K}_d\widehat{\dot{\mathbf{e}}} + \mathbf{K}_p\widehat{\mathbf{e}}\right] + \mathbf{L}_{\mathbf{e}2}\widetilde{\mathbf{e}} \tag{3.34b}$$

where $\mathbf{L}_{\mathbf{e}1}, \mathbf{L}_{\mathbf{e}2}$ are positive definite gain matrices, and the estimated position/attitude and velocity coordination errors are defined as

$$\widetilde{\mathbf{e}} = \mathbf{e} - \widehat{\mathbf{e}}, \qquad \widetilde{\dot{\mathbf{e}}} = \dot{\mathbf{e}} - \widehat{\dot{\mathbf{e}}} \tag{3.35}$$

Note that in the definition of the error observer in (3.34) and (3.35), we do not utilize the measure of tracking $\mathbf{s}$ of (3.4) as in the error observer (3.10) of Section 3.2. The measure of tracking introduces a coupling between the estimates $\widehat{\mathbf{e}}$ and $\widehat{\dot{\mathbf{e}}}$ that complicates the stability analysis, and the additional design freedom introduced through the filter gain $\mathbf{\Lambda}$ in Section 3.2 is not needed in this section due to the introduction of a nonlinear state observer with additional tuning gains.

To estimate the unmeasured velocity $\dot{\mathbf{x}}$ of the follower, we propose a second nonlinear state observer

$$\frac{d}{dt}\widehat{\mathbf{x}} = \widehat{\dot{\mathbf{x}}} + \mathbf{L}_{\mathbf{x}1}\widetilde{\mathbf{x}} \tag{3.36a}$$

$$\frac{d}{dt}\widehat{\dot{\mathbf{x}}} = -\mathbf{M}(\mathbf{x})^{-1}\left[\mathbf{C}\left(\mathbf{x},\widehat{\dot{\mathbf{x}}}\right)\widehat{\dot{\mathbf{e}}} + \mathbf{D}(\mathbf{x})\widehat{\dot{\mathbf{e}}} + \mathbf{K}_d\widehat{\dot{\mathbf{e}}} + \mathbf{K}_p\mathbf{e}\right] + \mathbf{L}_{\mathbf{x}2}\widetilde{\mathbf{x}} \tag{3.36b}$$

where $\mathbf{L}_{\mathbf{x}1}, \mathbf{L}_{\mathbf{x}2}$ are positive definite gain matrices, and the estimation position/attitude and velocity errors are defined as

$$\widetilde{\mathbf{x}} = \mathbf{x} - \widehat{\mathbf{x}}, \qquad \dot{\widetilde{\mathbf{x}}} = \dot{\mathbf{x}} - \dot{\widehat{\mathbf{x}}} \tag{3.37}$$

The leader velocity and acceleration values $\dot{\widehat{\mathbf{x}}}_m$ and $\ddot{\widehat{\mathbf{x}}}_m$ are not available through direct measurement, and the velocity and acceleration values for the leader are reconstructed as in Section 3.2 based on information of the follower and the coordination closed-loop system. Estimates for $\dot{\mathbf{x}}_m$ and $\ddot{\mathbf{x}}_m$ are given as

$$\begin{aligned} \dot{\widehat{\mathbf{x}}}_m &= \dot{\widehat{\mathbf{x}}} - \dot{\widehat{\mathbf{e}}} \\ \ddot{\widehat{\mathbf{x}}}_m &= \frac{d}{dt}\left(\dot{\widehat{\mathbf{x}}} - \dot{\widehat{\mathbf{e}}}\right) = -\left(\mathbf{M}(\mathbf{x})^{-1}\mathbf{K}_p + \mathbf{L}_{\mathbf{e}2}\right)\widetilde{\mathbf{e}} + \mathbf{L}_{\mathbf{x}2}\dot{\widetilde{\mathbf{x}}} \end{aligned} \tag{3.38}$$

where the last relation stems from (3.34) and (3.36). To formulate the closed-loop error dynamics, we introduce a change of coordinates

$$\begin{aligned} \bar{\mathbf{e}} &= \mathbf{e} - \mathbf{x}_m & \widetilde{\mathbf{x}}_m &= \widetilde{\mathbf{e}} - \widetilde{\mathbf{x}} \\ \dot{\bar{\mathbf{e}}} &= \dot{\mathbf{e}} - \dot{\mathbf{x}}_m & \dot{\widetilde{\mathbf{x}}}_m &= \dot{\widetilde{\mathbf{e}}} - \dot{\widetilde{\mathbf{x}}} - \mathbf{L}_1\widetilde{\mathbf{x}}_m \end{aligned} \tag{3.39}$$

to write the closed-loop error dynamics of the system (2.27) with the controller (3.33) as

$$\begin{aligned} &\mathbf{M}(\mathbf{x})\ddot{\bar{\mathbf{e}}} + \mathbf{C}(\mathbf{x},\dot{\mathbf{x}})\dot{\bar{\mathbf{e}}} + \mathbf{D}(\mathbf{x})\dot{\bar{\mathbf{e}}} + \mathbf{K}_d\dot{\bar{\mathbf{e}}} + \mathbf{K}_p\bar{\mathbf{e}} = \mathbf{M}(\mathbf{x})\mathbf{L}_1\ddot{\widetilde{\mathbf{x}}}_m + \mathbf{D}(\mathbf{x})\mathbf{L}_1\dot{\widetilde{\mathbf{x}}}_m - \mathbf{K}_p \\ &- \mathbf{C}(\mathbf{x},\dot{\mathbf{x}})\left(\dot{\widetilde{\mathbf{x}}} + \mathbf{L}_1(\widetilde{\mathbf{x}} - \widetilde{\mathbf{x}}_m)\right) + \mathbf{C}\left(\mathbf{x}, \dot{\widetilde{\mathbf{x}}} + \mathbf{L}_1\widetilde{\mathbf{x}}\right)(\dot{\bar{\mathbf{e}}} - \mathbf{L}_1\widetilde{\mathbf{x}}_m) + \mathbf{K}_d\left(\dot{\widetilde{\mathbf{x}}} + \mathbf{L}_1(\widetilde{\mathbf{x}} + \widetilde{\mathbf{x}}_m)\right)\widetilde{\mathbf{x}}_m \end{aligned} \tag{3.40}$$

and the estimation error dynamics from the observers (3.34) and (3.36) as

$$\ddot{\widetilde{\mathbf{x}}}_m = -\mathbf{M}(\mathbf{x})^{-1}\mathbf{K}_p(\widetilde{\mathbf{x}} + \widetilde{\mathbf{x}}_m) - \mathbf{L}_1\dot{\widetilde{\mathbf{x}}}_m - \mathbf{L}_2\widetilde{\mathbf{x}}_m - \ddot{\mathbf{x}}_m \tag{3.41}$$

$$\begin{aligned} \ddot{\widetilde{\mathbf{x}}} = &-\mathbf{M}(\mathbf{x})^{-1}\mathbf{K}_p(\widetilde{\mathbf{x}} + \widetilde{\mathbf{x}}_m) - \mathbf{L}_1\dot{\widetilde{\mathbf{x}}} - \mathbf{L}_2(\widetilde{\mathbf{x}} + \widetilde{\mathbf{x}}_m) \\ &+ \mathbf{M}(\mathbf{x})^{-1}\left[\mathbf{C}\left(\mathbf{x}, \dot{\widetilde{\mathbf{x}}} + \mathbf{L}_1\widetilde{\mathbf{x}}\right) - 2\mathbf{C}(\mathbf{x},\dot{\mathbf{x}}) + \mathbf{D}(\mathbf{x})\right]\left(\dot{\widetilde{\mathbf{x}}} + \mathbf{L}_1\widetilde{\mathbf{x}}\right) \end{aligned} \tag{3.42}$$

3.3.2 Stability analysis

The objective of the control law of the follower is to coordinate the follower system to the leader based on estimates of the states of the leader and the velocity of the follower obtained through nonlinear observers. Under the assumptions that the positive definite symmetric observer gain matrices $\mathbf{L}_{\mathbf{e}1}, \mathbf{L}_{\mathbf{e}2}, \mathbf{L}_{\mathbf{x}1}, \mathbf{L}_{\mathbf{x}2}$ are chosen as

$$\mathbf{L}_{\mathbf{e}1} = \mathbf{L}_{\mathbf{x}1} := \mathbf{L}_1 \qquad \mathbf{L}_{\mathbf{e}2} = \mathbf{L}_{\mathbf{x}2} := \mathbf{L}_2 \tag{3.43}$$

the following results holds:

Theorem 3.2 *Consider the model (2.27), the controller (3.33) and the observers (3.34) and (3.36). Under Assumptions 2.1 and 3.1, the closed-loop errors*

$$\widetilde{\eta} = \begin{bmatrix} \dot{\mathbf{e}}^T & \mathbf{e}^T & \dot{\widetilde{\mathbf{e}}}^T & \widetilde{\mathbf{e}}^T & \dot{\widetilde{\mathbf{x}}}^T & \widetilde{\mathbf{x}}^T \end{bmatrix}^T \tag{3.44}$$

are semiglobally uniformly ultimately bounded. The bound is a function of the leader acceleration $\ddot{\mathbf{x}}_m$. Furthermore, under the assumption of zero acceleration of the leader, $\ddot{\mathbf{x}}_m = 0$, the closed-loop errors of (3.44) are semiglobally exponentially converging to zero.

Details of the proof of Theorem 3.2 are given in Appendix C.1.2.
Sketch of proof: Introduce the vector $\zeta \in \mathbb{R}^{6n}$ denoting the states of the error dynamics of (3.40 - 3.42) as

$$\zeta^T = \begin{bmatrix} \tilde{\mathbf{e}}^T & \bar{\mathbf{e}}^T & \dot{\tilde{\mathbf{x}}}_m^T & \tilde{\mathbf{x}}_m^T & \dot{\tilde{\mathbf{x}}}^T & \tilde{\mathbf{x}}^T \end{bmatrix} \tag{3.45}$$

Note that $\widetilde{\eta}$ is related to ζ through $\widetilde{\eta} = T\zeta$ where T is a non-singular $6n \times 6n$ matrix defined as

$$T = \begin{bmatrix} \mathbf{I} & 0 & \mathbf{I} & 0 & 0 & 0 \\ 0 & \mathbf{I} & 0 & \mathbf{I} & 0 & 0 \\ 0 & 0 & \mathbf{I} & \mathbf{L}_1 & \mathbf{I} & \mathbf{L}_1 \\ 0 & 0 & 0 & \mathbf{I} & 0 & \mathbf{I} \\ 0 & 0 & 0 & 0 & \mathbf{I} & \mathbf{L}_1 \\ 0 & 0 & 0 & 0 & 0 & \mathbf{I} \end{bmatrix} \tag{3.46}$$

Consider the Lyapunov function

$$V(\zeta) = \frac{1}{2}\zeta^T \mathbf{P}(\zeta)\,\mathbf{y} \tag{3.47}$$

where $\mathbf{P}(\zeta) = \mathbf{P}(\zeta)^T$ is given by

$$\mathbf{P}(\zeta) = \begin{bmatrix} \varepsilon_0 \begin{bmatrix} \mathbf{M}(\mathbf{x}) & \lambda_0 \mathbf{M}(\mathbf{x}) \\ \lambda_0 \mathbf{M}(\mathbf{x}) & \mathbf{K}_p + \lambda_0 \mathbf{K}_d \end{bmatrix} & 0 & 0 \\ 0 & \begin{bmatrix} \mathbf{I} & \mu(\widetilde{\mathbf{x}}_d)\mathbf{I} \\ \mu(\widetilde{\mathbf{x}}_d)\mathbf{I} & \mathbf{L}_2 \end{bmatrix} & 0 \\ 0 & 0 & \begin{bmatrix} \mathbf{I} & \gamma(\widetilde{\mathbf{x}})\mathbf{I} \\ \gamma(\widetilde{\mathbf{x}})\mathbf{I} & \mathbf{L}_2 \end{bmatrix} \end{bmatrix} \tag{3.48}$$

where $\mathbf{I} \in \mathbb{R}^{n\times n}$ is the identity matrix, $\varepsilon_0, \lambda_0, \mu_0, \gamma_0 \in \mathbb{R}$ are positive constants, and $\mu(\widetilde{\mathbf{x}}_d)$ and $\gamma(\widetilde{\mathbf{x}})$ are defined by

$$\mu(\widetilde{\mathbf{x}}_d) = \frac{\mu_0}{1 + \|\widetilde{\mathbf{x}}_d\|}, \qquad \gamma(\widetilde{\mathbf{x}}) = \frac{\gamma_0}{1 + \|\widetilde{\mathbf{x}}\|} \tag{3.49}$$

Sufficient conditions for positive definiteness of $\mathbf{P}(\zeta)$ are

$$\mathbf{K}_{d,m} > \lambda_0 \mathbf{M}_M, \qquad \mathbf{L}_{2,m} > \max\left\{\mu_0^2, \gamma_0^2\right\} \tag{3.50}$$

where $\mathbf{M}_M$ is the largest eigenvalue of $\mathbf{M}$. The time derivative of (3.47) along the error dynamics of (3.40 - 3.42) yields

$$\dot{V}(\zeta) \leq \|\zeta_N\| \left(\alpha_0 - \mathbf{Q}_{N,m}\|\zeta_N\| + \alpha_2 \|\zeta_N\|^2\right) \tag{3.51}$$

where the positive definite matrix $\mathbf{Q}_N$, the scalars α_0, α_2 and the vector ζ_N are given in Appendix C.1.2. The coordination observer-controller scheme can be treated as a perturbed system, and local uniform ultimate boundedness of ζ, and thus $\widetilde{\eta}$, can be concluded from Proposition 2.1. The size of y_2 in Proposition 2.1 can be made arbitrarily small by a proper choice of $\mathbf{L}_{1,M}$, and thus the ultimate bound for $\widetilde{\eta}$ can be made arbitrarily small. The region of attraction is given by

$$\Delta = \left\{ \mathbf{x} \in \mathbb{R}^{6n} \quad | \quad \|\mathbf{x}\| < \frac{y_2}{\|T\|}\sqrt{P_m^{-1} P_M} \right\} \tag{3.52}$$

Since the size of the region of attraction Δ is proportional to y_2, this region can be expanded by increasing y_2, and the closed-loop errors $\widetilde{\eta}$ are semiglobally uniformly ultimately bounded.

The ultimate boundedness result is due to the non-vanishing disturbance from leader acceleration $\ddot{\mathbf{x}}_m$ of Remark 3.1. Furthermore, under the assumption of constant velocity of the leader ($\ddot{\mathbf{x}}_m = 0$), the derivative of the Lyapunov function (3.51) is reduced to

$$\dot{V}(\zeta) \leq \|\zeta_N\|^2 (-\mathbf{Q}_{N,m} + \alpha_2 \|\zeta_N\|) \leq -\kappa \|\zeta_N\|^2 \tag{3.53}$$

since (3.52) guarantees that $\mathbf{Q}_{N,m} > \alpha_2 \|\zeta_N\|$. Semiglobal exponential convergence to zero of the closed-loop errors $\widetilde{\eta} = T\zeta$ for zero leader acceleration $\ddot{\mathbf{x}}_m = 0$ follows directly from (3.53). ■

In this section, the observer-controller scheme of Section 3.2 was extended with a nonlinear state observer for the follower to estimate the unknown velocity $\dot{\mathbf{x}}$ to solve the problem of Definition 2.8. The lack of velocity measurements of the follower introduced some more complexity in the stability analysis of the observer-controller scheme when employing a second state observer, due to the fact that the Coriolis- and centripetal term $\mathbf{C}(\mathbf{x}, \dot{\mathbf{x}})\dot{\mathbf{x}}$ is dependent on the unmeasured state $\dot{\mathbf{x}}$. The unknown velocity of the follower in the Coriolis- and centripetal term causes a locality in the state observers, which can not be dominated in the observer-controller design using static control gains. The region of attraction is thus reduced from a global to a semiglobal result.

Note that the properties of semiglobal ultimate boundedness and semiglobal exponential convergence of the closed-loop errors can also be shown to hold for systems with nonlinear dissipative terms (Kyrkjebø and Pettersen (2005*a*)).

3.3.3 Simulations and experiments

The observer-controller scheme where only position measurements are available from the leader and the follower were applied to the simulation and experimental environment of Appendix E. In order to validate the theoretical results, a back-to-back comparison between simulations under ideal conditions and experiments were performed. The simulations were performed under the assumption of no external disturbances and no measurement noise, and the practical experiments were performed on a model ship in a closed basin under the influence of waves and measurement noise.

Simulations and experiments are presented for the case when the leader is stationary to illustrate the exponential convergence of the scheme under a zero-acceleration assumption for the leader, and for the practical case when no such assumptions can be made on the leader acceleration, and thus the closed-loop errors are ultimately bounded.

To facilitate a direct comparison between the practical results and the simulations, the leader vessel was simulated as a virtual ship on a computer (see Remark E.1). The virtual ship was based on a theoretical ship model, and controlled using a backstepping controller from Skjetne *et al.* (2003) to track a sine wave trajectory.

Note that during the experiments with waves, only the follower vessel experienced waves as a disturbance, while the leader vessel sailed in a virtual calm sea. However, in practical replenishment operations, both ships would pursue a heading into the waves and the effect of currents, waves and wind would therefore to some extent be similar on the two ships. The experiments with waves thus serve as an extreme case of how the two ships can

experience different external disturbances, and are a measure of how robust the scheme is with regards to external disturbances.

The observer-controller coordination scheme presented is based on a model with only linear damping terms satisfying Assumption 3.1, and thus only linear damping terms are employed in the observers and the controller during simulations and experiments. Note, however, that the model ship used in experiments will experience nonlinear damping effects. The experiments thus serve as a measure how the observer-controller coordination scheme performs under modelling errors.

Note that for the experiments, only the position of the supply vessel was available for measurements, and thus convergence of the velocities $\dot{\mathbf{x}} \to \dot{\mathbf{x}}_m$ could not be verified directly. The only states available from the experimental data were $\mathbf{e}$, $\widetilde{\mathbf{e}}$, $\widetilde{\mathbf{x}}_m$ and $\dot{\widetilde{\mathbf{x}}}_m$. However, when the given experimental states compare with the corresponding states of the simulation results, it is plausible to conclude that the total state of the experimental results is comparable to the simulated results as well.

Tuning

The observer gains $\mathbf{L}_1, \mathbf{L}_2$ and the controller gains $\mathbf{K}_p, \mathbf{K}_d$ have to be chosen such that the region of convergence is large enough to ensure convergence from the initial states, and at the same time such that the ultimate bound of closed-loop errors is acceptably small for practical replenishment operations. The uniform ultimate boundedness result is of semiglobal nature due to the proportional dependence on y_2 in the bound (3.51) and region of attraction (3.52). However, for small initial estimation errors in the observers of (3.34) and (3.36), higher initial synchronization errors can be considered.

The choice of observer gains $\mathbf{L}_1$ and $\mathbf{L}_2$ in (3.34) and (3.36) is a choice between the performance of the estimator during transients, and the influence from measurement noise. Choosing the gains too low may result in poor estimates which in turn leads to poor control performance, while choosing the gains too high may result in highly fluctuating control actions. In particular, the choice of a high gain $\mathbf{L}_1$ will affect the size of the ultimate bound, while a very small gain will introduce slightly damped oscillations in the system.

The choice of controller gains $\mathbf{K}_p$ and $\mathbf{K}_d$ in (3.33) are influenced by the choice of observer gains, since the rule of thumb is that the observer should converge faster than the controller. This cannot be verified directly due to the lack of a general separation principle for nonlinear system, and can only be examined for a set point linearization of the system. Increasing the proportional gain $\mathbf{K}_p$ in the controller will lower the synchronization position errors. The derivative term $\mathbf{K}_d$ should be chosen high enough to provide sufficient damping in the system to prevent oscillations during tracking, but note that the choice of a high gain $\mathbf{K}_d$ will amplify any measurement noise on the velocity estimates.

Experiments with zero leader acceleration, $\ddot{\mathbf{x}}_m = 0$

The exponential convergence of the observer-controller coordination scheme can be observed when the leader acceleration $\ddot{\mathbf{x}}_m$ is zero, and thus include situations where the leader vessel moves at a constant non-zero velocity. However, the restriction of a constant velocity is difficult to satisfy in experiments where the leader is controlled using a tracking controller, and thus the result of exponential convergence has been verified experimentally in this section using set point regulation of the follower supply vessel to a stationary leader

ship where the velocity vector $\dot{\mathbf{x}}_m$ is constant and zero. The reference vehicle was chosen to be 1 metre off the starboard side of the leader vessel, which is chosen as the origin of the local Earth-fixed frame. An overview of initial states and gains for set point regulation is found in Table 3.2.

Table 3.2: Initial states and gains for zero leader acceleration

Initial states for main and supply ship						Observer and controller gains					
$\mathbf{x}_m$	$=$	$[$	0	-1	0 $]^T$	$\mathbf{K}_p^b$	$=$	diag$[$	35	15	5 $]$
$\mathbf{x}_r$	$=$	$[$	0	0	0 $]^T$	$\mathbf{K}_d^b$	$=$	diag$[$	70	40	10 $]$
$\mathbf{x}$	$=$	$[$	-1	-1.5	$-\frac{\pi}{2}$ $]^T$	$\mathbf{L}_1$	$=$	diag$[$	8	8	2 $]$
						$\mathbf{L}_2$	$=$	diag$[$	10	10	10 $]$

The initial state for the follower vessel was chosen to illustrate the convergence in all parts of the state $\mathbf{x} = [x, y, \psi]^T$, and the same gains were used in the experiments and simulations to facilitate a back-to-back comparison. The gains were found empirically, and note that the controller gains are expressed in the body-fixed frame to facilitate a more intuitive tuning procedure.

All errors are calculated and plotted in the NED frame, with the initial phase in the left plot and the performance after settling in the right plot. The experimental data available from the experiments are plotted in Figure 3.3, and the simulation data are plotted in Figure 3.4. The simulations are converged to zero after 40 seconds, and thus the data after settling are not shown in Figure 3.4.

The experimental results in Figure 3.3 are seen to compare well with the theoretical results of exponential convergence in the transient phase of the simulated results in Figure 3.4. The overshoot in the control errors of Figure 3.3 and Figure 3.4 are seen to be small, and the settling time is sufficient for practical applications. The closed-loop errors in the experiments show small persistent oscillations after settling, which are consistent with effects of measurement noise, modelling errors or small ripples on the water in the basin during the experiments. The experiments were also carried out under wave disturbance, and the results of these experiments compare with the results without waves, with a slight increase in the errors as expected. In all, the experimental results for position keeping compare well with the simulations, and thus support the theoretical result of exponential convergence of the closed-loop errors under the assumption of zero acceleration for the leader vessel; $\ddot{\mathbf{x}}_m = 0$.

Experiments non-zero leader acceleration

The result of ultimate boundedness of the closed-loop errors for an underway replenishment operation when the leader ship has non-zero acceleration was investigated using a desired trajectory with non-zero curvature for the main ship. The leader tracked a sine wave trajectory using the backstepping controller of Skjetne *et al.* (2003), and the follower supply ship was coordinated to the leader based on position measurements only, and independently of the desired trajectory. Note that in a practical replenishment operation, the ships would maintain a constant course and heading into the waves, and seek to keep the curvature of the trajectory at a minimum to reduce the risk of collisions. A trajectory

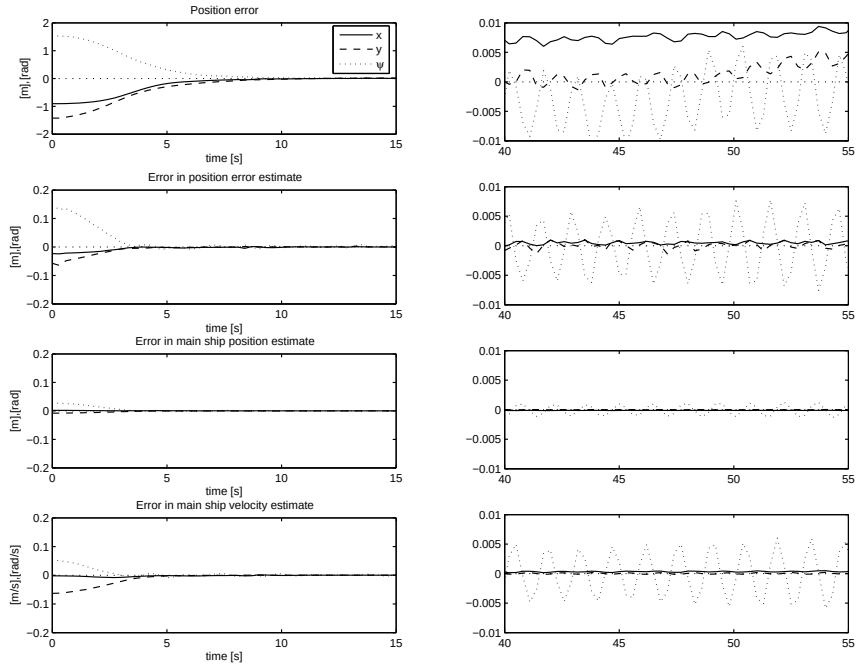

Figure 3.3: Experiment errors $\mathbf{e}$, $\widetilde{\mathbf{e}}$, $\widetilde{\mathbf{x}}_m$, $\dot{\widetilde{\mathbf{x}}}_m$, initial phase (left) and after settling (right).

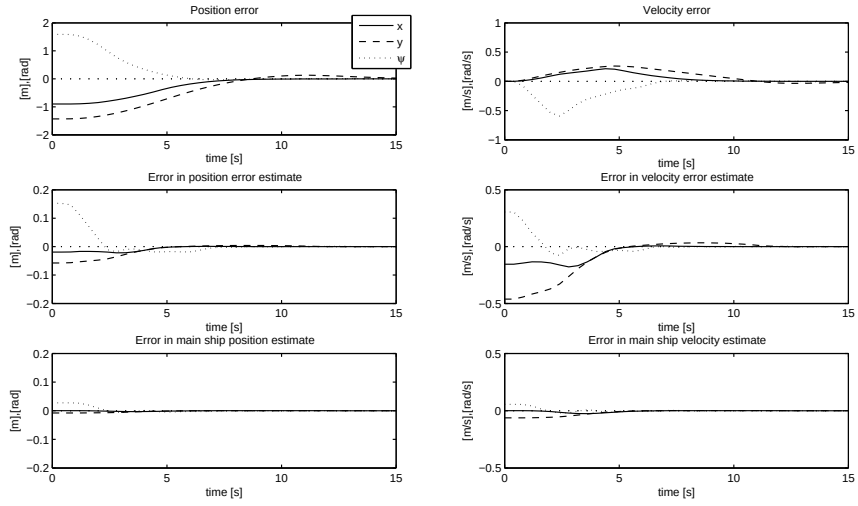

Figure 3.4: Simulation errors $\mathbf{e}$, $\tilde{\mathbf{e}}$, $\tilde{\mathbf{x}}_m$ (left), and $\dot{\mathbf{e}}$, $\dot{\tilde{\mathbf{e}}}$, $\dot{\tilde{\mathbf{x}}}_m$ (right).

with non-zero curvature is thus illustrative of situations where the leader is given greater manoeuvring freedom than in a straight line experiment, and would allow a replenishment operation to be performed in close waters or in busy fairways.

When the desired trajectory of the leader has a non-zero curvature, the forward velocity and acceleration of the reference vehicle should be different from the velocity and acceleration of the main ship due to the curvature. The supply ship's desired forward velocity relative to the main ship will therefore depend on the distance between the two ships in a curve (see Section 2.2.5). When the follower supply ship sails the inner curve, the forward velocity of the follower must be lower than that of the leader, and vice versa. An extreme case arises when the radius of the leader curve is less than the distance between the two ships, for which a follower sailing the inner curve would have to perform a backward movement.

The experiments for ship replenishment operations used a predefined curved path with a desired velocity of 0.2 m/s, corresponding to a velocity of 3.5 knots for the full scale ship. An overview of the initial states and gain matrices used in the experiments is given in Table 3.3.

Table 3.3: Initial states and gains for non-zero leader acceleration

Initial states for leader and follower ship		Observer and controller gains	
$\mathbf{x}_m = [\ 0 \quad -1 \quad 0\ ]^T$		$\mathbf{K}_p^b = \mathrm{diag}[\ 100 \quad 40 \quad 10\ ]$	
$\mathbf{x}_r = [\ 0 \quad 0 \quad 0\ ]^T$		$\mathbf{K}_d^b = \mathrm{diag}[\ 30 \quad 20 \quad 5\ ]$	
$\mathbf{x} = [\ -1 \quad 2 \quad -\frac{\pi}{2}\ ]^T$		$\mathbf{L}_1 = \mathrm{diag}[\ 8 \quad 8 \quad 2\ ]$	
$\widehat{\mathbf{x}} = [\ 0 \quad 0 \quad 0\ ]^T$		$\mathbf{L}_2 = \mathrm{diag}[\ 100 \quad 100 \quad 5\ ]$	

Figure 3.5 shows the *xy*-plot for the replenishment operation for both the experiment and the simulation. The experimental data available from the experiments are plotted in Figure 3.6, and the simulation data are plotted in Figure 3.7, while Figure 3.8 shows the additional velocity control and observer errors only available from the simulations.

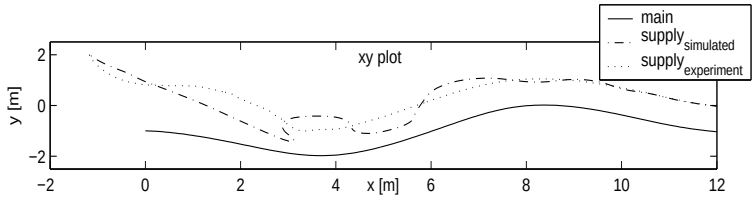

Figure 3.5: An *xy*-plot of the simulations and experiments.

The experimental results in Figure 3.6 are seen to compare well with the theoretical results of ultimate boundedness in the simulated results in Figure 3.7. Note that in the *xy*-plot of Figure 3.5 and in comparing the experiments of Figure 3.6 with the simulated results in Figure 3.7, the experiments show better performance than in the simulations. This is due to the fact that the ideal simulations presented are restricted to linear damping. The non-linear damping inherent in the model ship has a stabilizing effect, and thus much

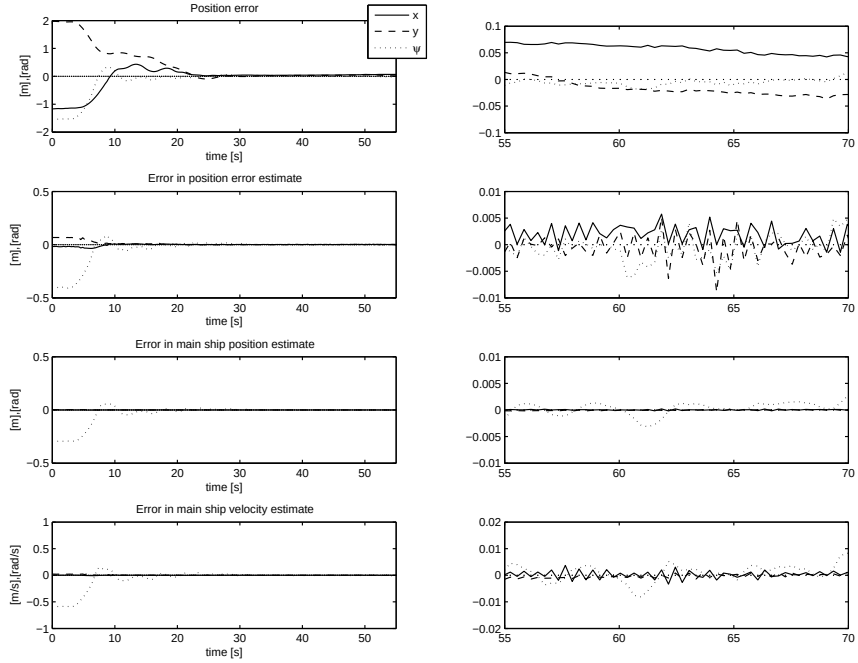

Figure 3.6: Experiment errors $\mathbf{e}$, $\widetilde{\mathbf{e}}$, $\widetilde{\mathbf{x}}_m$, $\dot{\widetilde{\mathbf{x}}}_m$, initial phase (left) and after settling (right).

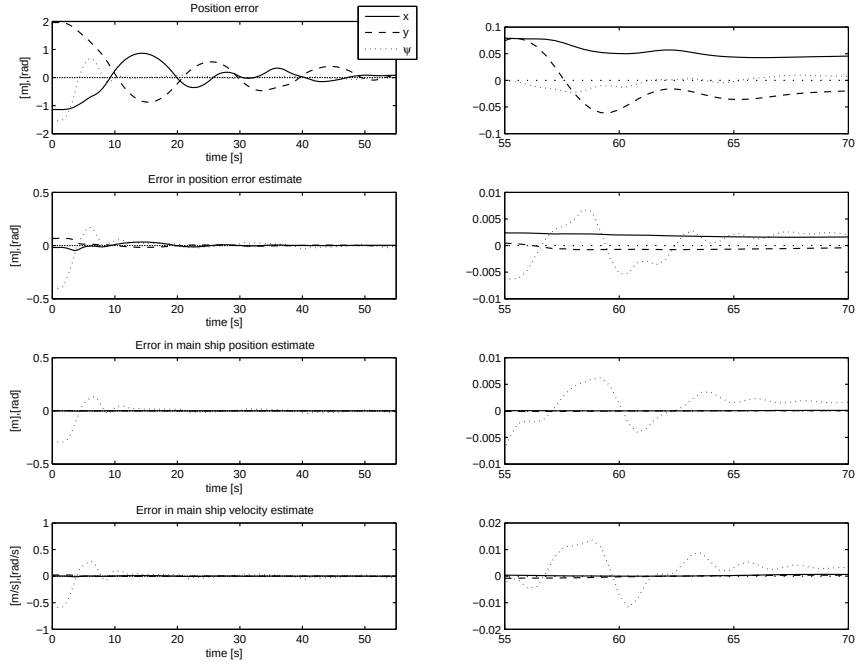

Figure 3.7: Simulation errors $\mathbf{e}$, $\widetilde{\mathbf{e}}$, $\widetilde{\mathbf{x}}_m$, $\dot{\widetilde{\mathbf{x}}}_m$, initial phase (left) and after settling (right).

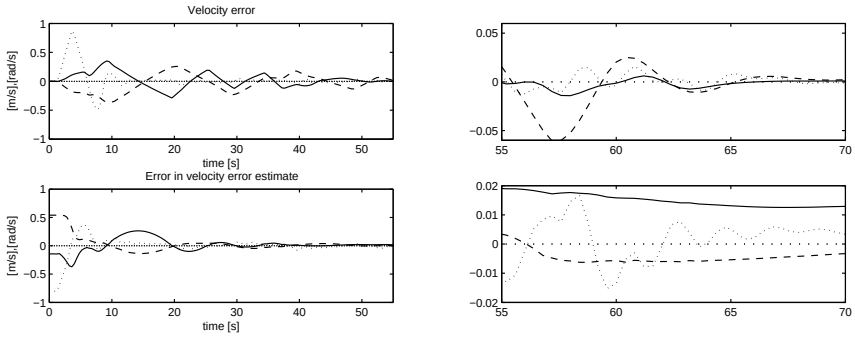

Figure 3.8: Simulation velocity errors $\dot{\mathbf{e}}$ and $\widetilde{\dot{\mathbf{e}}}$, initial phase (left) and after settling (right).

less damping is needed in the controller gain $\mathbf{K}_d$. The back-to-back comparison is shown here using gains optimized for the experiments, and thus for the simulations with linear damping only, these gains are not optimal. Similar performance as in the experiments can be shown in the simulations by increasing the $\mathbf{K}_d$ gain to compensate for the lack of nonlinear damping.

The observer accuracy diminishes slightly at the end of the path in Figure 3.6, which can be contributed to the reduced accuracy of the measurement system at the end of the basin. In all, the experimental results for motion coordination with a non-zero leader acceleration compare well with the simulations, and thus support the theoretical result of ultimately boundedness of the closed-loop errors for practical underway replenishment operations.

Discussion

Measurement noise influences the velocity estimations in the observers (with a large $\mathbf{L}_2$ in (3.34) and (3.36)), and can lead to high commanded control forces. The observer performance is affected when the commanded forces are larger than the thruster limitations, since the commanded control forces and moments are used to progress the dynamical ship model in the observer. Here, a duality of the $\mathbf{L}_2$ gain is seen; a large gain may cause saturation in the forces, while a small gain may cause larger closed-loop errors due to poor estimates.

The controller gains $\mathbf{K}_p, \mathbf{K}_d$ and observer gains $\mathbf{L}_1, \mathbf{L}_2$ are optimized for either set point regulation in Table 3.2 or underway replenishment in Table 3.3, but intermediate gains that perform well for both tasks can be found. Note that the tuning of the observer-controller scheme is a highly coupled nonlinear gain tuning problem due to the influence of observer performance on the controller performance and vice versa. Valuable input to the tuning process can be found by linearizing the system around defined set points and adopting a pole-placement scheme to shape the performance of the system, or by employing a structured gain tuning procedure based on the remarks on tuning presented earlier in this section.

Robustness of the scheme is investigated by introducing waves to the supply ship in the experiments. This does not affect the leader ship, since it is a virtual ship running on a computer, and thus the results can be seen as the ability of the control scheme to sup-

Table 3.4: Mean and maximum absolute errors for non-zero acceleration experiments

Without waves						
u_d	x_{body}[m]		y_{body}[m]		heading [deg]	
[m/s]	mean$\|\mathbf{e}\|$	max$\|\mathbf{e}\|$	mean$\|\mathbf{e}\|$	max$\|\mathbf{e}\|$	mean$\|\mathbf{e}\|$	max$\|\mathbf{e}\|$
0.1	0.0278	0.0421	0.0029	0.0128	0.4641	1.2490
0.2	0.0548	0.0783	0.0123	0.0323	0.5214	2.4064
0.3	0.0790	0.1050	0.0367	0.0896	1.1860	3.7701
With waves: JONSWAP H_s =0.01 m, T_s =0.75 s						
0.1	0.0293	0.0503	0.0048	0.0169	0.4412	1.5126
0.2	0.0555	0.0775	0.0146	0.0320	0.6818	2.2002
0.3	0.0790	0.1047	0.0408	0.0969	1.0600	4.3774

press the effects of external disturbances. The comparison between the experiments with and without disturbances during replenishment experiments is shown in Table 3.4 where the time-mean of the absolute error $\overline{\mathrm{E}} = \frac{1}{T}\int_0^t |\mathbf{e}|\,dt$ and the maximum of the absolute error E_{max} are calculated under different conditions, and the results show only small changes in performance when the follower ship is under the influence of waves. The robustness to external disturbances is particularly useful during practical underway replenishment operations, where ships operating in close proximity of each other will influence each other (e.g. through Venturi-effects).

Note that although the scheme is robust, it can not exceed the physical limitations of the ships. It can be seen that when the supply ship sails the outer curve with a velocity of 0.3 m/s in Table 3.4, the thrusters in the *y*-direction are saturated, and the errors increase.

The synchronization observer-controller scheme utilizes a theoretical model of the supply ship to construct estimates of unmeasured states for the two ships, and thus the performance of the scheme is influenced by the accuracy of the theoretical model. The model ship used in the simulations and experiments has been thoroughly modelled and tested to identify its model parameters (Skjetne *et al.* (2004*b*)), and contributing nonlinear damping terms have been identified for the model. Nevertheless, the scheme performs well under the linear damping assumption made in the control design, and thus suggests that the scheme is possesses some robustness towards modelling errors.

Experiments with two physical ships

Experiments on the coordination observer-controller scheme using two physical ships in the basin were conducted to confirm the results of the previous discussion. The experiments were conducted in the experimental setup of Appendix E with initial states and gains as given in Table 3.5, and suffered from measurement noise and measurement loss as remarked in Remark E.1. The control errors $\mathbf{e}$, observer errors $\widetilde{\mathbf{e}}$ and estimation errors $\widetilde{\mathbf{x}}_m$ from the experiments are shown in Figure 3.9.

In the experiments, the leader ship is manually steered with a joystick in sine wave trajectory, and the initial values of the observers where given from the measurements $\mathbf{e}(0) = \mathbf{x}(0) - \mathbf{x}_m(0)$ to improve robustness towards measurement noise.

The results illustrated in Figure 3.9 with two physical ships compare well with the results of the experiments using a virtual ship running on a computer as the leader. Measure-

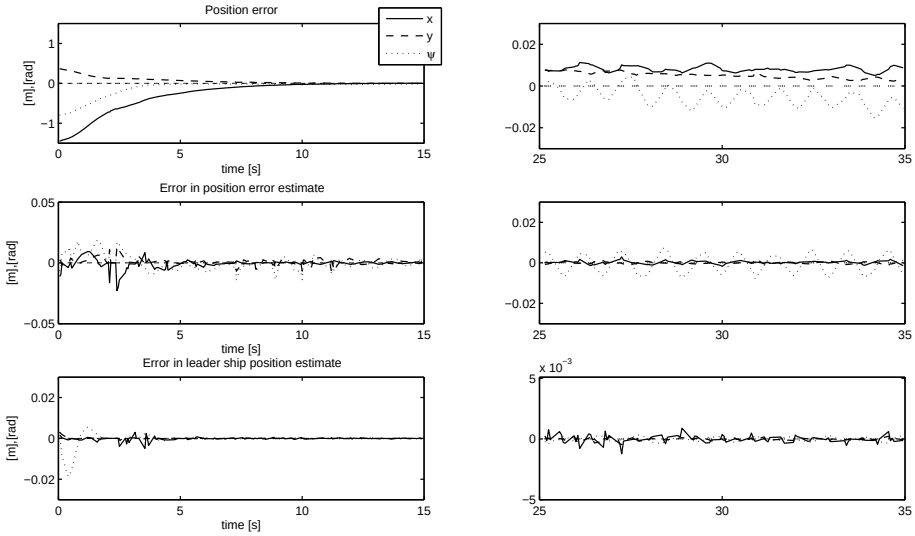

Figure 3.9: Errors from experiments with two physical ships using the observer-controller approach. Coordination errors $\mathbf{e}$ (top row), estimation errors $\widetilde{\mathbf{e}}$ (middle row) and leader ship position estimate $\widetilde{\mathbf{x}}_m$ (bottom row), with initial phase on the left and after settling on the right.

ment noise and measurement loss are more dominant in the experiments with two physical ships, but the observer-controller coordination approach performs well, and this suggests that the use of nonlinear observers filters the measurement noise sufficiently to achieve the desired performance.

Table 3.5: Initial states and gains for experiments with two physical ships

Initial states for leader and follower ship						Observer and controller gains						
$\mathbf{x}_m$	$=$	$[$	0	0	0	$]^T$	$\mathbf{K}_p^b$	$=$	$\mathrm{diag}[$	10	8	2.5	$]$
$\mathbf{x}_r$	$=$	$[$	0	-1	0	$]^T$	$\mathbf{K}_d^b$	$=$	$\mathrm{diag}[$	32	29	4	$]$
$\mathbf{x}$	$=$	$[$	-1.5	1.5	$-\frac{\pi}{2}$	$]^T$	$\mathbf{L}_1$	$=$	$\mathrm{diag}[$	8	6	4	$]$
$\widehat{\mathbf{x}}$	$=$	$[$	-1.5	1.5	$-\frac{\pi}{2}$	$]^T$	$\mathbf{L}_2$	$=$	$\mathrm{diag}[$	18	17	16	$]$

3.4 Concluding remarks

This chapter proposed an observer-controller approach to solve the motion coordination problems defined in Definitions 2.7 and 2.8. The coordination approach was based on the design of a nonlinear model-based observer that estimated the coordination errors based on position measurements, and thus indirectly provided estimates of the unknown states of the leader. The closed-loop errors were shown to be uniformly globally ultimately bounded for the situation where the velocity of the follower was available in the control design. For sit-

uations where the velocity of the follower was unknown, a second nonlinear model-based observer was used to estimate the unknown states of the follower, and uniform semiglobal ultimate boundedness of the closed-loop errors was concluded. Simulations were presented for both situations, and for the situation with unknown velocities for the follower, a back-to-back comparison between experimental results and simulations was performed to investigate the tuning procedure and robustness of the proposed coordination scheme. The stability results, simulation results and experimental results presented in this chapter suggest that the proposed observer-controller motion coordination approach is suitable for practical applications.

Chapter 4

The Virtual Vehicle Approach

This chapter proposes a virtual vehicle leader-follower coordinated motion control scheme to solve the output feedback control problems of Section 2.1.5. The virtual vehicle approach is based on using a *virtual* (sub)copy of the system to act as an estimator for the unknown states of the leader through a virtual control law. The virtual vehicle concept is first applied to the control problem of coordinating a follower to a leader utilizing state measurements of the follower as in Definition 2.7, and then to the control problem where only position measurements are available for the follower as in Definition 2.8. An illustration of how the virtual vehicle scheme can be applied to coordinate two robot manipulators is given. Furthermore, the concept of dynamic synchronization is proposed to design a smooth behaviour for the follower during formation changes. The results presented in this chapter are based on Kyrkjebø *et al.* (2006*a*), Kyrkjebø and Pettersen (2006*a*), Kyrkjebø and Pettersen (2006*b*) and Kyrkjebø and Pettersen (2007*b*).

4.1 The Virtual vehicle principle

The purpose of the virtual vehicle is to alleviate the information requirements on the leader. The leader is a dynamic system manoeuvring freely in the motion coordination scheme, and the parameters of the mathematical model, the control inputs and internal states of the leader are unknown to the follower. The virtual vehicle is designed to stabilize its trajectories to the position of a reference vehicle through a kinematic control law, and through the definition of the virtual control law, the coordination control law of the follower is provided with an estimate of the states of the leader. Note that the reference vehicle of Section 2.2.5 is utilized as the desired position of the follower with respect to the leader.

A virtual system approach has been utilized both as an abstraction vehicle (cf. Crowley (1989), Salichs *et al.* (1991)) and as an intermediate level between the desired trajectories of a system and the controller. The virtual system can be considered as a low-level controller in a two-level control structure (cf. Fradkov *et al.* (1991), Gusev *et al.* (1998)), and was used in Sakaguchi *et al.* (1999) as the mapping of a physical vehicle on an entry-ramp on a main lane in order to do merging control of autonomous mobile robots, and in Egerstedt *et al.* (2001) to control a reference point on a planned path. The latter approach has been utilized in Hu *et al.* (2003) to combine the task of path following and obstacle avoid-

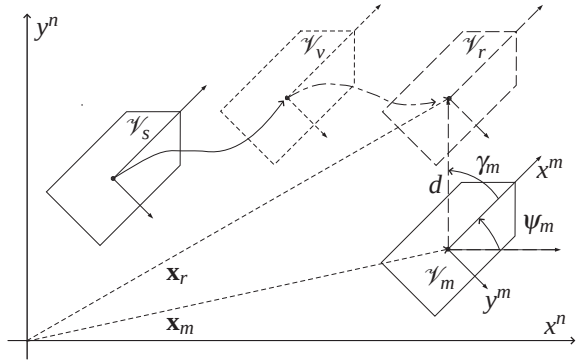

Figure 4.1: Virtual vehicle $\mathcal{V}_v$, reference vehicle $\mathcal{V}_r$ and the leader $\mathcal{V}_m$ and follower vehicle $\mathcal{V}_s$.

ance, and in Cheng *et al.* (2004) with a modified goal point to improve practical robustness to path diversity.

The virtual system approach of Sakaguchi *et al.* (1999) for mobile robots has its parallel in the approach of Encarnacao and Pascoal (2001) for marine vessels in the use of a path parameterization variable mapping the leader vessel on the desired path of the follower, while the mobile platform control approach of Egerstedt *et al.* (2001) can be related to the manoeuvring approach of Skjetne *et al.* (2004*c*) applied to marine vessels where the tracking problem is subdivided into a geometric and a dynamic task with a path variable, which can be viewed as virtual vehicle.

In this chapter, the virtual system approach is utilized to design a virtual vehicle that follows the behaviour of the leader vehicle based on position feedback only, and provide a velocity output through the controller design. The states of the virtual vehicle can thus be used in the coordination controller to control the follower to the virtual vehicle. The proposed virtual vehicle approach imposes a cascaded structure in the control system, as opposed to the observer-controller approach proposed in Chapter 3 where the observers and controller are closely interconnected.

The virtual vehicle approach is presented in this section for motion control applications in the plane using a three-degree-of-freedom fully actuated vehicle, but Section 4.4 shows how the schemes can be applied to control n-degree-of-freedom robot manipulators. The concepts of the virtual vehicle and the reference vehicle are illustrated in Figure 4.1 together with the physical follower and leader vehicles. The vehicles in Figure 4.1 are defined as follows

$\mathcal{V}_m$ The leader vehicle where only the position $\mathbf{x}_m$ is available as output.

$\mathcal{V}_r$ The reference vehicle shifted a distance d in the direction given by γ_m relative to the position of the leader vehicle.

$\mathcal{V}_v$ A virtual vehicle controlled to track the reference vehicle $\mathcal{V}_r$ through a kinematic control law.

$\mathcal{V}_s$ The follower vehicle coordinating to the leader vessel.

Note that the physical vehicles are the leader vehicle $\mathscr{V}_m$, and the follower vehicle $\mathscr{V}_s$ coordinating its motion to the leader. The reference vehicle is a mathematical reference constructed by shifting the position of the leader vehicle to the desired position of the follower vehicle in relation to the leader, and the virtual vehicle is a virtual reference vehicle controlled to this shifted position through a kinematic control law. Through the use of a virtual vehicle as an intermediate controlled vehicle in the motion coordination scheme, the physical follower vehicle is controlled to the leader using the known velocity of the virtual reference. Note that the principle of using a virtual vehicle as a state estimator of the leader states can be extended to any number of followers providing the introduction of a collision avoidance scheme for the followers.

4.1.1 A virtual vehicle design

The only measurement available from the leader vessel is the position/heading measurements $\mathbf{x}_m$, and due to the lack of information about the parameters of the mathematical model and the control input to the leader vessel, model-based observers are not readily constructed for the leader states. Thus, a virtual vehicle is designed as an intermediate controlled vehicle $\mathscr{V}_v$ stabilizing to the reference vehicle $\mathscr{V}_r$ based on position measurement feedback from the leader vehicle $\mathscr{V}_m$ to provide estimates of the unmeasured states of the leader. The virtual vehicle design presented in this section is based on Kyrkjebø *et al.* (2006*a*) and Kyrkjebø and Pettersen (2006*b*).

As in Gusev *et al.* (1998), the first step (kinematic level) considers the velocities ν_v of the virtual vehicle as the control inputs, and the control law is designed such that convergence of the virtual trajectories to the reference trajectories is ensured. In a way, the trajectories $\mathbf{x}_v$ and velocities ν_v can be considered as estimates of $\mathbf{x}_r$ and ν_r. Thus, the virtual vehicle becomes a kind of kinematic estimator of the leader states through the position feedback loop.

The virtual vehicle can be defined by its kinematic model from (2.49) as

$$\dot{\mathbf{x}}_v = \mathbf{J}(\mathbf{x}_v)\,\nu_v \tag{4.1}$$

Based on Assumption 2.1, the velocity and acceleration of the reference vehicle are assumed bounded and satisfying

$$\sup_t \|\nu_r\| = V_M < \infty \tag{4.2}$$

$$\sup_t \|\dot{\nu}_r\| = A_M < \infty \tag{4.3}$$

with known constants V_M and A_M. The kinematics of the reference vehicle in (2.62) is given by

$$\dot{\mathbf{x}}_r = \mathbf{J}(\mathbf{x}_m)\,\nu_r \tag{4.4}$$

We define the tracking errors for the virtual vehicle

$$\mathbf{e}_v = \mathbf{x}_v - \mathbf{x}_r, \qquad \dot{\mathbf{e}}_v = \dot{\mathbf{x}}_v - \dot{\mathbf{x}}_r = \mathbf{J}(\mathbf{x}_v)\,\nu_v - \mathbf{J}(\mathbf{x}_m)\,\nu_r \tag{4.5}$$

To stabilize the virtual vehicle to the reference vehicle, we propose a virtual vehicle control law

$$\nu_v = -\mathbf{J}^{-1}(\mathbf{x}_v)\,\mathbf{L}_1\mathbf{e}_v - \mathbf{J}^{-1}(\mathbf{x}_v)\,\mathbf{L}_2\mathbf{z} \tag{4.6}$$

where $\mathbf{L}_1$ and $\mathbf{L}_2$ are symmetric positive gain matrices, and with the integral term

$$\dot{\mathbf{z}} = \mathbf{e}_v \tag{4.7}$$

The closed-loop error equation thus beomes

$$\dot{\mathbf{e}}_v = -\mathbf{L}_1\mathbf{e}_v - \mathbf{L}_2\mathbf{z} - \mathbf{J}(\mathbf{x}_m)\,\nu_r \tag{4.8}$$

Theorem 4.1 *The closed-loop error dynamics (4.7-4.8) of system (4.1) satisfying assumption (4.2) with the control law (4.6) are uniformly globally practically asymptotically stable.*

Details of the proof of Theorem 4.1 are given in Appendix C.2.1.
Sketch of proof: Consider the Lyapunov function candidate

$$V_v(\mathbf{z},\,\mathbf{e}_v) = \frac{1}{2}\mathbf{e}_v^T\mathbf{e}_v + \frac{1}{2}\mathbf{z}^T\mathbf{L}_2\mathbf{z} + \frac{1}{2}\mathbf{z}^T\mathbf{e}_v \tag{4.9}$$

which is positive definite for $\mathbf{L}_{2,m} > 1/4$. Note that $\mathbf{L}_{i,m}$ (resp. $\mathbf{L}_{i,M}$) designates the minimum (resp. maximum) eigenvalue of $\mathbf{L}_i$. Differentiating along the closed-loop trajectories we get

$$\dot{V}_v(\mathbf{z},\,\mathbf{e}_v) = -\mathbf{e}_v^T\left(\mathbf{L}_1 - \frac{1}{2}\mathbf{I}\right)\mathbf{e}_v - \frac{1}{2}\mathbf{z}^T\mathbf{L}_2\mathbf{z} - \frac{1}{2}\mathbf{z}^T\mathbf{L}_1\mathbf{e}_v - \left(\mathbf{e}_v^T + \frac{1}{2}\mathbf{z}^T\right)\mathbf{J}(\mathbf{x}_m)\,\nu_r \tag{4.10}$$

Using (4.2), and the relation $2|ab| \leq (\lambda a^2 + b^2/\lambda)$ for any real a, b and any positive constant λ, it follows that

$$\begin{aligned}\dot{V}_v(\mathbf{z},\,\mathbf{e}_v) \leq &-\left(\mathbf{L}_{1,m} - \frac{1}{2} - \frac{\lambda}{4}\mathbf{L}_{1,M} - \frac{3V_M}{2\,\|(\mathbf{e}_v,\mathbf{z})\|}\right)\|\mathbf{e}_v\|^2 \\ &-\frac{1}{2}\left(\mathbf{L}_{2,m} - \frac{1}{2\lambda}\mathbf{L}_{1,M} - \frac{3V_M}{\|(\mathbf{e}_v,\mathbf{z})\|}\right)\|\mathbf{z}\|^2\end{aligned} \tag{4.11}$$

since $\|\mathbf{J}(\mathbf{x})\| \leq 1$. Designing the gain matrices $\mathbf{L}_1$ and $\mathbf{L}_2$ as $\mathbf{L}_{i,M} \leq \ell\,\mathbf{L}_{i,m}$, $i \in \{1,2\}$, for some $\ell > 0$, it follows through $\lambda = 2/\ell$ and δ_v as any given positive constant that any gain matrices satisfying

$$\mathbf{L}_{1,m} = 3 + \frac{3V_M}{\delta_v} \tag{4.12}$$

$$\mathbf{L}_{2,m} = 2 + \frac{3\ell^2}{4} + \left(1 + \frac{\ell^2}{4}\right)\frac{3V_M}{\delta_v} \tag{4.13}$$

generate the following bound on the derivative of V_v:

$$\|\mathbf{e}_v\|^2 + \|\mathbf{z}\|^2 \geq \delta_v^2 \quad \Rightarrow \quad \dot{V}_v(\mathbf{z},\mathbf{e}_v) \leq -\|\mathbf{e}_v\|^2 - \|\mathbf{z}\|^2\,. \tag{4.14}$$

Note that V_v is positive definite and radially unbounded for this choice of gains. Due to the linear dependency of $\mathbf{L}_{1,m}$ and $\mathbf{L}_{2,m}$ in $1/\delta_v$, the error dynamics of (4.7 - 4.8) are uniformly practically asymptotically stable through Corollary 2.1, which implies that the region to which solutions converge – from any initial condition – can be reduced as much as desired by enlarging $\mathbf{L}_{1,m}$ and $\mathbf{L}_{2,m}$. ■

4.2 Output reference coordination design with state feedback

The section proposes a motion coordination control law for the follower vehicle to coordinate to the motion of the virtual vehicle proposed in Section 4.1.1. The virtual vehicle acts as a reference to the coordination control law, and is stabilized to the reference vehicle through the virtual control law (4.6). In this section, we assume that only position measurements of the leader vehicle are available to the follower, while the states of the follower vehicle are known as in the problem of Definition 2.7. The results presented here are based on Kyrkjebø *et al.* (2006*a*).

4.2.1 Follower vehicle design

The velocity information from the virtual vehicle design of Section 4.1.1 can be utilized in the design of a coordination controller for the follower vehicle $\mathscr{V}_s$ to follow the virtual vehicle $\mathscr{V}_v$ in Figure 4.1. Note that the body-fixed velocity ν_v is now known through the definition of the control law (4.6), and the velocity $\dot{\mathbf{x}}_v$ of the virtual vehicle in the NED frame can be obtained through the kinematic relationship (4.1). Furthermore, due to the virtual vehicle controller design, an expression for the acceleration of the virtual vehicle will be partially available for control purposes. The variables available from the virtual vehicle design to the coordination controller are

$$\dot{\mathbf{x}}_v = \mathbf{J}(\mathbf{x}_v)\,\nu_v = -\mathbf{L}_1\mathbf{e}_v - \mathbf{L}_2\mathbf{z} \tag{4.15}$$

$$\ddot{\mathbf{x}}_v = -\mathbf{L}_1\dot{\mathbf{e}}_v - \mathbf{L}_2\mathbf{e}_v = \left(\mathbf{L}_1^2 - \mathbf{L}_2\right)\mathbf{e}_v + \mathbf{L}_1\mathbf{L}_2\mathbf{z} + \mathbf{L}_1\mathbf{J}(\mathbf{x}_m)\,\nu_r \tag{4.16}$$

We define the coordination errors as

$$\mathbf{e} = \mathbf{x} - \mathbf{x}_v, \qquad \dot{\mathbf{e}} = \dot{\mathbf{x}} - \dot{\mathbf{x}}_v, \qquad \ddot{\mathbf{e}} = \ddot{\mathbf{x}} - \ddot{\mathbf{x}}_v \tag{4.17}$$

Using the sliding surface from Slotine and Li (1987*a*) as a passive filtering of the virtual vehicle states, we can design a virtual reference trajectory as

$$\dot{\mathbf{y}}_v = \dot{\mathbf{x}}_v - \mathbf{\Lambda}\mathbf{e} \tag{4.18}$$

$$\ddot{\mathbf{y}}_v = \ddot{\mathbf{x}}_v - \mathbf{\Lambda}\dot{\mathbf{e}} \tag{4.19}$$

where $\mathbf{\Lambda} > 0$ is a positive definite design matrix. Let us denote

$$\ddot{\mathbf{y}}'_v = \left(\mathbf{L}_1^2 - \mathbf{L}_2\right)\mathbf{e}_v + \mathbf{L}_1\mathbf{L}_2\mathbf{z} - \mathbf{\Lambda}\dot{\mathbf{e}} \tag{4.20}$$

and thus

$$\ddot{\mathbf{y}}_v = \ddot{\mathbf{y}}'_v + \mathbf{L}_1\mathbf{J}(\mathbf{x}_m)\,\nu_r \tag{4.21}$$

where $\ddot{\mathbf{y}}'_v$ is available for control design. Defining

$$\mathbf{s} = \dot{\mathbf{x}} - \dot{\mathbf{y}}_v = \dot{\mathbf{e}} + \mathbf{\Lambda}\mathbf{e} \tag{4.22}$$

as a measure of tracking gives the following dynamic model for the follower from (2.27)

$$\mathbf{M}(\mathbf{x})\,\dot{\mathbf{s}} = -\mathbf{C}(\mathbf{x},\dot{\mathbf{x}})\,\mathbf{s} - \mathbf{D}(\mathbf{x},\dot{\mathbf{x}})\,\mathbf{s} + \tau - \mathbf{M}(\mathbf{x})\,\ddot{\mathbf{y}}_v - \mathbf{C}(\mathbf{x},\dot{\mathbf{x}})\,\dot{\mathbf{y}}_v - \mathbf{D}(\mathbf{x},\dot{\mathbf{x}})\,\dot{\mathbf{y}}_v - \mathbf{g}(\mathbf{x}) \tag{4.23}$$

To coordinate the motion of the follower vehicle to the virtual vehicle, we propose a coordination control law for the follower vehicle

$$\tau = \mathbf{M}(\mathbf{x})\,\ddot{\mathbf{y}}_v' + \mathbf{C}(\mathbf{x},\dot{\mathbf{x}})\,\dot{\mathbf{y}}_v + \mathbf{D}(\mathbf{x},\dot{\mathbf{x}})\,\dot{\mathbf{y}}_v + \mathbf{g}(\mathbf{x}) - \mathbf{K}_d\mathbf{s} - \mathbf{K}_p\mathbf{e} \tag{4.24}$$

where $\mathbf{K}_p$ and $\mathbf{K}_d$ are symmetric positive gain matrices. This gives the closed-loop errors

$$\mathbf{M}(\mathbf{x})\,\dot{\mathbf{s}} + \mathbf{C}(\mathbf{x},\dot{\mathbf{x}})\,\mathbf{s} + \mathbf{D}(\mathbf{x},\dot{\mathbf{x}})\,\mathbf{s} + \mathbf{K}_d\mathbf{s} + \mathbf{K}_p\mathbf{e} = -\mathbf{M}(\mathbf{x})\,\mathbf{L}_1\mathbf{J}(\mathbf{x}_m)\,v_r \tag{4.25}$$

Theorem 4.2 *The closed-loop error dynamics (4.25) of system (2.27) with the control law (4.24) are uniformly globally practically asymptotically stable.*

Sketch of proof: Consider the following Lyapunov function candidate

$$V_e(\mathbf{e},\,\mathbf{s}) = \frac{1}{2}\mathbf{s}^T\mathbf{M}(\mathbf{x})\,\mathbf{s} + \frac{1}{2}\mathbf{e}^T\mathbf{K}_p\mathbf{e} \tag{4.26}$$

Differentiating along the closed-loop trajectories we get

$$\dot{V}_e(\mathbf{e},\,\mathbf{s}) \quad = \quad -\mathbf{s}^T\left[\mathbf{D}(\mathbf{x},\dot{\mathbf{x}}) + \mathbf{K}_d\right]\mathbf{s} - \mathbf{e}^T\mathbf{\Lambda}^T\mathbf{K}_p\mathbf{e} - \mathbf{s}^T\mathbf{M}(\mathbf{x})\,\mathbf{L}_1\mathbf{J}(\mathbf{x}_m)\,v_r \tag{4.27}$$

Let δ_e be any given positive constant. Then, it holds that, for all $\|\mathbf{e}\|^2 + \|\mathbf{s}\|^2 \geq \delta_e^2$,

$$\dot{V}_e(\mathbf{e},\,\mathbf{s}) \leq -\left[\mathbf{D}_m + \mathbf{K}_{d,m} - \frac{1}{2\delta_e}\mathbf{M}_M\mathbf{L}_{1,M}\right]\|\mathbf{s}\|^2 - \left[\mathbf{\Lambda}_m\mathbf{K}_{p,m} - \frac{1}{2\delta_e}\mathbf{M}_M\mathbf{L}_{1,M}\right]\|\mathbf{e}\|^2 \tag{4.28}$$

Proceeding as in the proof of Theorem 4.1 in Section 4.1.1, Corollary 2.1 can be invoked by observing that the choice of $\mathbf{K}_{d,m}$ and $\mathbf{K}_{p,m}$ can be made as affine functions of $1/\delta_e$ to conclude uniform global practical asymptotic stability. ■

4.2.2 Stability analysis of the overall system

The control law of the follower coordinates the follower vehicle to the virtual vehicle based on a computed virtual reference velocity from the virtual vehicle controller. The virtual vehicle is in turn stabilized to the reference vehicle parallel to the leader vehicle. Thus, we must analyse the stability of the overall system from the follower to the leader to conclude any stability properties for the coordination control scheme.

Theorem 4.3 *Consider the vehicle model (2.27) satisfying Properties **P1**-**P4**, the virtual vehicle control law (4.6) and the coordination controller (4.24). Under Assumptions 2.1 and 2.2, the overall closed-loop system is uniformly globally practically asymptotically stable.*

Sketch of proof: Take as a positive definite Lyapunov function candidate

$$V(\widetilde{\eta}) = \frac{1}{2}\widetilde{\eta}^T\mathbf{P}\,\widetilde{\eta} \tag{4.29}$$

where

$$\mathbf{P} = \begin{bmatrix} \mathbf{K}_p & 0 & 0 & 0 \\ 0 & \mathbf{M}(\mathbf{x}) & 0 & 0 \\ 0 & 0 & \mathbf{L}_2 & \frac{1}{2}\mathbf{I} \\ 0 & 0 & \frac{1}{2}\mathbf{I} & \mathbf{I} \end{bmatrix} \tag{4.30}$$

is a composition of the Lyapunov functions (4.9) and (4.26) of Section 4.1.1 and 4.2.1. Differentiating along the closed-loop trajectories we get

$$\dot{V}(\widetilde{\eta}) \quad = \quad -\widetilde{\eta}^T \mathbf{Q}\,\widetilde{\eta} + \beta(\mathbf{s},\,\mathbf{e}_v,\,\mathbf{z},\,\nu_r) \tag{4.31}$$

where

$$\mathbf{Q} = \begin{bmatrix} \mathbf{\Lambda}^T\mathbf{K}_p & 0 & 0 & 0 \\ 0 & \mathbf{D}(\mathbf{x},\dot{\mathbf{x}}) + \mathbf{K}_d & 0 & 0 \\ 0 & 0 & \frac{1}{2}\mathbf{L}_2 & \frac{1}{4}\mathbf{L}_1 \\ 0 & 0 & \frac{1}{4}\mathbf{L}_1 & \mathbf{L}_1 - \frac{1}{2}\mathbf{I} \end{bmatrix} \tag{4.32}$$

and

$$\beta(\mathbf{s},\,\mathbf{e}_v,\,\mathbf{z},\,\nu_r) = -\mathbf{s}^T\mathbf{M}(\mathbf{x})\mathbf{L}_1\mathbf{J}(\mathbf{x}_m)\,\nu_r - \frac{1}{2}\mathbf{z}^T\mathbf{J}(\mathbf{x}_m)\,\nu_r - \mathbf{e}_v^T\mathbf{J}(\mathbf{x}_m)\,\nu_r \tag{4.33}$$

Let δ be any given positive constant such that

$$\|\widetilde{\eta}\| \geq \delta \quad \Rightarrow \quad \|\beta(\mathbf{s},\,\mathbf{e}_v,\,\mathbf{z},\,\nu_r)\| \leq \frac{V_M}{\delta}\left(\mathbf{M}_M\mathbf{L}_{1,M}\|\mathbf{s}\|^2 + \frac{\|\mathbf{z}\|^2}{2} + \frac{\|\mathbf{e}_v\|^2}{2}\right). \tag{4.34}$$

Consequently, in view of the proofs of Theorem 4.1 and 4.2, and repeating a similar reasoning as for (4.11) and (4.28) while choosing the minimum eigenvalue of the gain matrices $\mathbf{K}_p$, $\mathbf{K}_d$, $\mathbf{L}_1$ and $\mathbf{L}_2$ large enough, it holds that

$$\dot{V}(\widetilde{\eta}) \leq -\|\widetilde{\eta}\|^2, \qquad \forall\|\widetilde{\eta}\| \geq \delta. \tag{4.35}$$

Since the dependency on the bound on β (and on the gain matrices) in $1/\delta$ is again affine, uniform global practical asymptotic stability follows from Corollary 2.1. ■

4.2.3 Simulation study

The virtual vehicle coordination approach with only position measurements of the leader vehicle, but with state information of the follower vehicle, was simulated in the simulation setup of Appendix E with initial states and gains as given in Table 4.1. In the simulations, the leader ship tracks a sine wave reference trajectory $\sin(\varpi t)$ with frequency $\varpi = 1/15$ with heading angle ψ_m along the tangent line.

Table 4.1: Initial states and gains for the state feedback virtual vehicle scheme

Initial states and filter gain						Controller gains				
$\mathbf{x}_m$	$=$	$[$ 2	4	0	$]^T$	$\mathbf{K}_p$	$=\mathrm{diag}[$ 70	140	70	$]$
$\mathbf{x}$	$=$	$[$ 0	0	0	$]^T$	$\mathbf{K}_d$	$=\mathrm{diag}[$ 100	100	50	$]$
$\mathbf{x}_v$	$=$	$[$ 1	0.5	$\frac{\pi}{4}$	$]^T$	$\mathbf{L}_1$	$=\mathrm{diag}[$ 0.8	1.6	1.6	$]$
$\mathbf{\Lambda}$	$=\mathrm{diag}[$ 0.3	0.3	0.3	$]$		$\mathbf{L}_2$	$=\mathrm{diag}[$ 0.55	0.55	0.55	$]$

Figure 4.2 shows stability of the trajectories of the follower to the reference vehicle in the upper plot, and an *xy*-plot of the vehicles during the simulation in the lower plot. Figure 4.3 shows the control errors during the simulation.

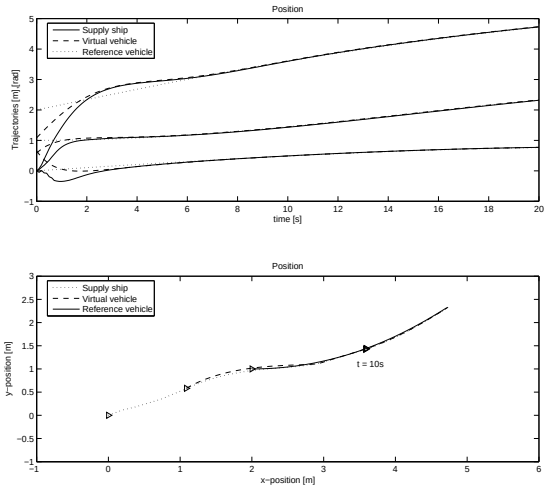

Figure 4.2: Trajectories of the follower $\mathbf{x}$, the virtual vehicle $\mathbf{x}_v$ and the reference vehicle $\mathbf{x}_r$ in the upper plot, and the xy-plot of the vehicles with special marks at initial states and at time $t = 10$ s in the lower plot.

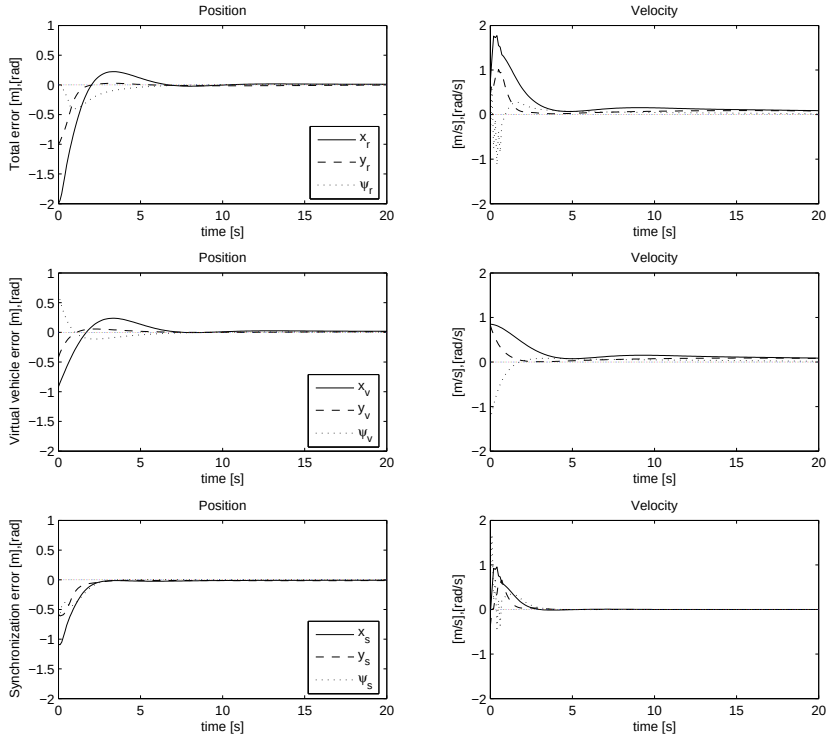

Figure 4.3: The total errors $\mathbf{x} - \mathbf{x}_r$ in the upper row, the virtual vehicle control errors $\mathbf{x}_v - \mathbf{x}_r$ in the middle row, and the synchronization errors $\mathbf{x} - \mathbf{x}_v$ in the lower row, with positions on the left and velocities on the right.

From Figure 4.3 we see that the virtual vehicle control errors $\mathbf{e}_v = \mathbf{x}_v - \mathbf{x}_r$, the synchronization errors $\mathbf{e} = \mathbf{x} - \mathbf{x}_v$ and the overall control errors $\mathbf{x} - \mathbf{x}_r$ are practically asymptotically stable. We observe small oscillations, especially in the velocity errors, due to the unknown velocity of the leader ship. However, due to the practical stability property of the closed-loop system, the magnitude of these oscillations can be arbitrarily reduced within control saturation limits by enlarging the control gains.

4.3 Output reference coordination design with output feedback

To account for situations where only position measurements are available for the follower vehicle, the control scheme of Section 4.2 is in this section modified to remove the necessity of measuring $\dot{\mathbf{x}}$. The results of this section are based on Kyrkjebø and Pettersen (2006*b*).

4.3.1 Follower vehicle design

This section considers the case when the velocity of the follower is unknown, and use a filtered estimate as introduced by Kelly (1993) to provide an estimate of $\dot{\mathbf{x}}$ to the control law. The filtered estimates preserves the cascaded structure of the virtual vehicle scheme, and thus allow the virtual vehicle and the follower vehicle to be tuned separately. The variables available from the virtual vehicle design to the coordination controller are $\dot{\mathbf{x}}_v$ from (4.16) and $\ddot{\mathbf{x}}_v$ from (4.16) as in Section 4.2.

We define the synchronization errors as

$$\mathbf{e} = \mathbf{x} - \mathbf{x}_v, \qquad \dot{\mathbf{e}} = \dot{\mathbf{x}} - \dot{\mathbf{x}}_v, \qquad \ddot{\mathbf{e}} = \ddot{\mathbf{x}} - \ddot{\mathbf{x}}_v \tag{4.36}$$

and denote

$$\ddot{\mathbf{x}}_v' = \left(\mathbf{L}_1^2 - \mathbf{L}_2\right)\mathbf{e}_v + \mathbf{L}_1\mathbf{L}_2\mathbf{z} \tag{4.37}$$

such that

$$\ddot{\mathbf{x}}_v = \ddot{\mathbf{x}}_v' + \mathbf{L}_1\mathbf{J}\left(\mathbf{x}_m\right)\nu_r \tag{4.38}$$

where $\ddot{\mathbf{x}}_v'$ is available for control design. Using the relationship $\dot{\mathbf{x}} = \dot{\mathbf{e}} + \dot{\mathbf{x}}_v$ we can rewrite (2.27) as

$$\mathbf{M}\left(\mathbf{x}\right)\ddot{\mathbf{e}} = -\mathbf{C}\left(\mathbf{x},\dot{\mathbf{x}}\right)\dot{\mathbf{e}} - \mathbf{d}\left(\mathbf{x},\dot{\mathbf{x}}\right) + \tau - \mathbf{M}\left(\mathbf{x}\right)\ddot{\mathbf{x}}_v - \mathbf{C}\left(\mathbf{x},\dot{\mathbf{x}}\right)\dot{\mathbf{x}}_v - \mathbf{g}\left(\mathbf{x}\right) \tag{4.39}$$

To coordinate the follower to the virtual vehicle based only on output feedback from the follower, we propose a coordination control law inspired by the tracking control law of Wen and Bayard (1988), but modified with a filtered estimate ϑ of $\dot{\mathbf{e}}$ from Kelly (1993) and Loría and Ortega (1995))

$$\tau = \mathbf{M}\left(\mathbf{x}\right)\ddot{\mathbf{x}}_v' + \mathbf{C}\left(\mathbf{x},\dot{\mathbf{x}}_v\right)\dot{\mathbf{x}}_v + \mathbf{d}\left(\mathbf{x},\dot{\mathbf{x}}_v\right) + \mathbf{g}\left(\mathbf{x}\right) - \mathbf{K}_d\,\vartheta - \mathbf{K}_p\mathbf{e} \tag{4.40}$$

where $\mathbf{K}_p$ and $\mathbf{K}_d$ are symmetric positive definite gain matrices. The filtered estimate is defined as

$$\vartheta = \operatorname{diag}\left\{\frac{b_i p}{p + a_i}\right\}\mathbf{e} \tag{4.41}$$

where p denotes the differential operator, and

$$\mathbf{A} := \operatorname{diag}\left\{a_i\right\}, \qquad \mathbf{B} := \operatorname{diag}\left\{b_i\right\} \tag{4.42}$$

such that

$$\dot{\vartheta} = -\mathbf{A}\vartheta + \mathbf{B}\dot{\mathbf{e}} \tag{4.43}$$

Although (4.43) has the form of a differential equation driven by the unknown input $\dot{\mathbf{e}}$, it can be implemented using an internal filter state $\mathbf{x}_c$ as

$$\dot{\mathbf{x}}_c = -\mathbf{A}(\mathbf{x}_c + \mathbf{B}\mathbf{e}) \tag{4.44}$$

to obtain ϑ through

$$\vartheta = \mathbf{x}_c + \mathbf{B}\mathbf{e} \tag{4.45}$$

Using the Mean Value Theorem (cf. Khalil (2002)), we can write as in Paulsen and Egeland (1995)

$$\mathbf{d}(\mathbf{x},\dot{\mathbf{x}}) - \mathbf{d}(\mathbf{x},\dot{\mathbf{x}}_v) = \left.\frac{\partial \mathbf{d}(\mathbf{x},\mathbf{y})}{\partial \mathbf{y}}\right|_{\mathbf{y}=\xi} \dot{\mathbf{e}} := \mathbf{D}\,\dot{\mathbf{e}} \tag{4.46}$$

where ξ is on the line segment between $\dot{\mathbf{x}}$ and $\dot{\mathbf{x}}_v$. Note that

$$\xi = \theta\dot{\mathbf{x}} + (1-\theta)\dot{\mathbf{x}}_v = \theta\dot{\mathbf{e}} + \dot{\mathbf{x}}_v, \qquad 0 < \theta < 1 \tag{4.47}$$

Assumption 2.2 suggests

$$\|\mathbf{d}(\mathbf{x},\dot{\mathbf{x}}) - \mathbf{d}(\mathbf{x},\dot{\mathbf{x}}_v)\| \leq \left\| \left.\frac{\partial \mathbf{d}(\mathbf{x},\mathbf{y})}{\partial \mathbf{y}}\right|_{\mathbf{y}=\xi} \right\| \|\dot{\mathbf{e}}\| \leq \beta_d(\|\xi\|)\,\|\dot{\mathbf{e}}\| \tag{4.48}$$

To investigate the stability of the dissipative terms, we will in this section restrict the dissipative forces to linear and quadratic terms as in Assumption 2.3 to give

$$\beta_d(\|\xi\|) \leq k_{D1} + k_{D2}(\|\dot{\mathbf{e}}\| + \|\dot{\mathbf{x}}_v\|) \tag{4.49}$$

through (4.47). Using Property **P2**, the error dynamics can be written

$$\mathbf{M}(\mathbf{x})\ddot{\mathbf{e}} = -\mathbf{C}(\mathbf{x},\dot{\mathbf{x}})\dot{\mathbf{e}} - \mathbf{C}(\mathbf{x},\dot{\mathbf{x}}_v)\dot{\mathbf{e}} - \left.\frac{\partial \mathbf{d}(\mathbf{x},\mathbf{y})}{\partial \mathbf{y}}\right|_{\mathbf{y}=\xi} \dot{\mathbf{e}} - \mathbf{K}_d\vartheta - \mathbf{K}_p\mathbf{e} - \mathbf{M}(\mathbf{x})\mathbf{L}_1\mathbf{J}(\mathbf{x}_m)\,\nu_r \tag{4.50}$$

To investigate the stability of error-dynamics of the follower vehicle design, we formulate the Lyapunov function candidate

$$V_e(\mathbf{e},\dot{\mathbf{e}},\vartheta) = \frac{1}{2}\dot{\mathbf{e}}^T\mathbf{M}(\mathbf{x})\dot{\mathbf{e}} + \frac{1}{2}\mathbf{e}^T\mathbf{K}_p\mathbf{e} + \frac{1}{2}\vartheta^T\mathbf{K}_d\mathbf{B}^{-1}\vartheta + \varepsilon\mathbf{e}^T\mathbf{M}(\mathbf{x})\dot{\mathbf{e}} - \varepsilon\vartheta^T\mathbf{M}(\mathbf{x})\dot{\mathbf{e}} \tag{4.51}$$

The Lyapunov function $V(\mathbf{e},\dot{\mathbf{e}},\vartheta)$ can be shown to be positive definite through partitioning V as $V = W_1 + W_2$ (cf. Loría and Ortega (1995)) where

$$\begin{aligned} W_1 &= \frac{1}{4}\dot{\mathbf{e}}^T\mathbf{M}(\mathbf{x})\dot{\mathbf{e}} + \frac{1}{4}\mathbf{e}^T\mathbf{K}_p\mathbf{e} + \frac{1}{4}\vartheta^T\mathbf{K}_d\mathbf{B}^{-1}\vartheta + \varepsilon\mathbf{e}^T\mathbf{M}(\mathbf{x})\dot{\mathbf{e}} - \varepsilon\vartheta^T\mathbf{M}(\mathbf{x})\dot{\mathbf{e}} \\ W_2 &= \frac{1}{4}\dot{\mathbf{e}}^T\mathbf{M}(\mathbf{x})\dot{\mathbf{e}} + \frac{1}{4}\mathbf{e}^T\mathbf{K}_p\mathbf{e} + \frac{1}{4}\vartheta^T\mathbf{K}_d\mathbf{B}^{-1}\vartheta \end{aligned} \tag{4.52}$$

Writing W_1 in matrix form as

$$W_1 = \frac{1}{4}\begin{bmatrix}\mathbf{e}\\ \dot{\mathbf{e}}\end{bmatrix}^T \overbrace{\begin{bmatrix}\mathbf{K}_p & 2\varepsilon\mathbf{M}\\ 2\varepsilon\mathbf{M} & \frac{1}{2}\mathbf{M}\end{bmatrix}}^{\mathbf{P}_1} \begin{bmatrix}\mathbf{e}\\ \dot{\mathbf{e}}\end{bmatrix} + \frac{1}{4}\begin{bmatrix}\dot{\mathbf{e}}\\ \vartheta\end{bmatrix}^T \overbrace{\begin{bmatrix}\frac{1}{2}\mathbf{M} & -2\varepsilon\mathbf{M}\\ -2\varepsilon\mathbf{M} & \mathbf{K}_d\mathbf{B}^{-1}\end{bmatrix}}^{\mathbf{P}_2} \begin{bmatrix}\dot{\mathbf{e}}\\ \vartheta\end{bmatrix} \tag{4.53}$$

we see that W_1 is positive definite if

$$\frac{1}{2}\sqrt{\frac{\mathbf{K}_{p,m}}{2\mathbf{M}_M}} > \varepsilon, \qquad \frac{1}{2}\sqrt{\frac{\mathbf{K}_{d,m}}{2\mathbf{B}_M\mathbf{M}_M}} > \varepsilon \tag{4.54}$$

and W_2 is trivially positive definite. Note that the constant ε is not used in the controller, but only in the stability proof. Differentiating along the closed-loop trajectories, we get

$$\begin{aligned}\dot{V}_e(\mathbf{e},\dot{\mathbf{e}},\vartheta) = &-\vartheta^T\mathbf{K}_d\mathbf{B}^{-1}\mathbf{A}\vartheta - \dot{\mathbf{e}}^T\mathbf{C}(\mathbf{x},\dot{\mathbf{x}}_v)\dot{\mathbf{e}} - \dot{\mathbf{e}}^T\mathbf{D}\dot{\mathbf{e}} - \dot{\mathbf{e}}^T\mathbf{M}(\mathbf{x})\mathbf{L}_1\mathbf{J}(\mathbf{x}_m)\nu_r \\ &+\varepsilon\Big[\dot{\mathbf{e}}^T\mathbf{M}(\mathbf{x})\dot{\mathbf{e}} - \dot{\mathbf{e}}^T\mathbf{B}^T\mathbf{M}(\mathbf{x})\dot{\mathbf{e}} - \mathbf{e}^T\mathbf{K}_p\mathbf{e} + \vartheta^T\mathbf{K}_d\vartheta - (\mathbf{e}-\vartheta)^T\mathbf{D}\dot{\mathbf{e}} - \mathbf{e}^T\mathbf{K}_d\vartheta \\ &+\vartheta^T\mathbf{K}_p\mathbf{e} + \vartheta^T\mathbf{A}^T\mathbf{M}(\mathbf{x})\dot{\mathbf{e}} + (\mathbf{e}-\vartheta)^T\left(\mathbf{C}^T(\mathbf{x},\dot{\mathbf{x}}_v) - \mathbf{C}(\mathbf{x},\dot{\mathbf{x}}_v) + \mathbf{C}(\mathbf{x},\dot{\mathbf{e}})\right)\dot{\mathbf{e}}\Big]\end{aligned} \tag{4.55}$$

To further investigate the stability properties of the virtual vehicle design using only output feedback from the follower vehicle as presented in this section, we will combine the Lyapunov function of the virtual vehicle in (4.9) and the follower vehicle (4.51) and investigate the overall stability of the system.

4.3.2 Stability analysis of the overall system

In this section, we will show that the follower synchronizes to the virtual vehicle based on a computed virtual reference velocity from the virtual vehicle, and that the virtual vehicle is in turn stabilized to the reference vehicle parallel to the leader vessel.

Theorem 4.4 *Consider the model (2.27), the virtual vehicle control law (4.6), the coordination control law (4.40) and the velocity filter (4.43). Under Assumptions 2.1 and 2.3 and with gains satisfying (4.54), the closed-loop errors*

$$\widetilde{\eta} = [\mathbf{e}_v, \mathbf{z}, \dot{\mathbf{e}}, \mathbf{e}, \vartheta]^T \tag{4.56}$$

are uniformly semi-globally practically asymptotically stable.

Details of the proof of Theorem 4.4 can be found in Appendix C.2.2.
Sketch of proof: Combining the Lyapunov functions of (4.9) and (4.51) as

$$V(\widetilde{\eta}) = V_v(\mathbf{z},\mathbf{e}_v) + V_e(\mathbf{e},\dot{\mathbf{e}},\vartheta) \tag{4.57}$$

gives a region to which the solutions converge

$$\|\widetilde{\eta}\| \geq \delta = \max\{\delta_1 + \delta_2\} \tag{4.58}$$

Note that δ_1 can be designed through the choice of minimum eigenvalues for the gain matrices $\mathbf{L}_1$ and $\mathbf{L}_2$ as

$$\mathbf{L}_{1,m} = \frac{3+3\frac{V_M}{\delta_1}}{1-2\mathbf{M}_m\ell\frac{V_M}{\delta_1}}, \quad \mathbf{L}_{2,m} = 2 + \left(\frac{\ell}{4} + \frac{2\mathbf{M}_m\ell V_M}{\delta_1}\right)\mathbf{L}_{1,m} + 3\frac{V_M}{\delta_1} \tag{4.59}$$

and δ_2 can be designed through a proper choice of $\mathbf{B}_m$ in

$$\delta_2 = \frac{b-\sqrt{b^2-4ac}}{2a} \tag{4.60}$$

where

$$a := \mathbf{C}_V\left(\mathbf{L}_{1,M}+\mathbf{L}_{2,M}\right), \quad b := \frac{\varepsilon}{3}\mathbf{B}_m^T\mathbf{M}_m + k_d, \quad c := \left(\mathbf{M}_M\mathbf{L}_{1,M}+\frac{3}{2}\right)V_M \tag{4.61}$$

Through the dependence of the gains in the radius $1/\delta$ and by invoking Corollary 2.1, the closed-loop errors can be shown to be uniformly practically asymptotically stable. The region of attraction contains the set

$$\|\widetilde{\eta}\| \leq \Delta = \min\left\{\Delta_1+\Delta_2\right\}\sqrt{\frac{\alpha_1}{\alpha_2}} \tag{4.62}$$

where

$$\begin{aligned}\Delta_1 = \min\Bigg\{ & \frac{\mathbf{B}_m\mathbf{M}_m - 3\mathbf{M}_M}{6\left(k_{D2}+\mathbf{C}_M+\left(\frac{1}{2}k_{D2}+\mathbf{C}_V\right)\left(\mathbf{L}_{1,M}+\mathbf{L}_{2,M}\right)\right)}, \\ & \frac{\mathbf{K}_{d,m}\mathbf{A}_m - 2\varepsilon\mathbf{K}_{d,M}\mathbf{B}_M}{\varepsilon\mathbf{B}_M\left(k_{D2}+2\mathbf{C}_V\right)\left(\mathbf{L}_{1,M}+\mathbf{L}_{2,M}\right)}, \frac{\mathbf{K}_{p,m}}{\left(k_{D2}+2\mathbf{C}_V\right)\left(\mathbf{L}_{1,M}+\mathbf{L}_{2,M}\right)}\Bigg\}\end{aligned} \tag{4.63}$$

and

$$\Delta_2 = \frac{b+\sqrt{b^2-4ac}}{2a} \tag{4.64}$$

The positive constants α_1 and α_2 are given by

$$\alpha_1 = \frac{1}{4}\min\left\{\mathbf{M}_m, \frac{\mathbf{K}_{d,m}}{\mathbf{B}_M}, \mathbf{K}_{p,m}, \frac{1}{4}, \mathbf{L}_{2,m}\right\} \tag{4.65}$$

and

$$\alpha_2 = \max\left\{\left[\left(\varepsilon+\frac{1}{2}\right)\mathbf{M}_M\right], \left[\frac{\varepsilon}{2}\mathbf{M}_M+\frac{1}{2}\mathbf{K}_{p,M}\right], \frac{1}{2}\left[\varepsilon\mathbf{M}_M+\frac{\mathbf{K}_{d,M}}{\mathbf{B}_m}\right], 1, \left[\mathbf{L}_{2,M}+\frac{1}{2}\right]\right\} \tag{4.66}$$

We can enlarge the region of attraction by increasing Δ through a suitable choice of $\mathbf{K}_{p,m}$, $\mathbf{K}_{d,m}$, $\mathbf{A}_m$ and $\mathbf{B}_m$, and can conclude with semiglobal stability. Thus, the closed-loop errors $\widetilde{\eta}$ as defined in (4.56) are uniformly semiglobally practically asymptotically stable. ■

4.3.3 Simulations and experiments

The virtual vehicle coordination approach with only position measurements of both the leader and the follower was simulated in the simulation setup of Appendix E with initial states and gains as given in Table 4.2. In the simulations, the distance between the leader and the reference vehicle was given by $d = 2$m with $\gamma_m = \frac{\pi}{2}$, and the leader ship tracked a sine wave reference trajectory $\sin(\varpi t)$ with frequency $\varpi = 1/15$ rad/s with heading angle ψ_m along the tangent line. From Figure 4.4 we see that the closed-loop errors $\widetilde{\eta}$ are practically asymptotically stable. Small oscillations are observed in the plots due to the unknown velocities of the leader and the follower ship. Due to the practical stability property of the closed-loop system, the magnitude of these oscillations can be arbitrarily reduced by enlarging the gains within control saturations limits.

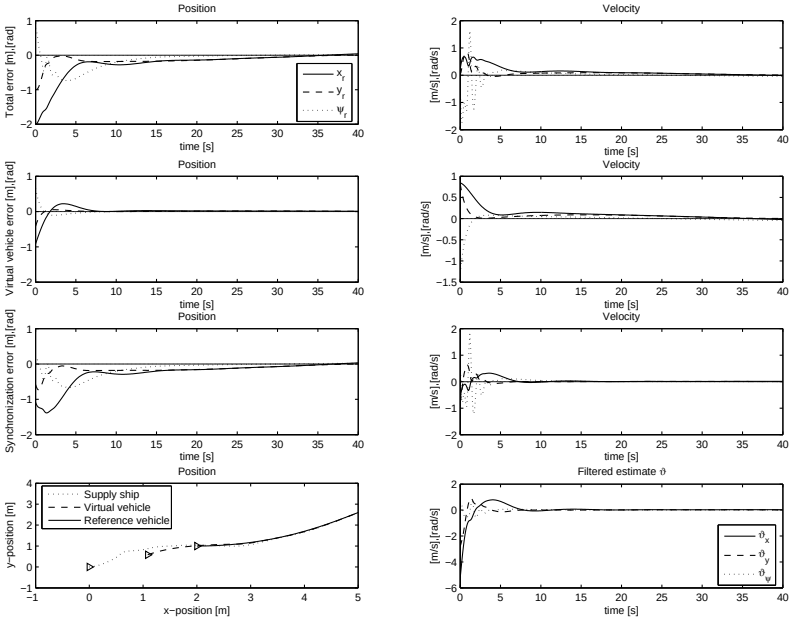

Figure 4.4: Simulation errors $\mathbf{x} - \mathbf{x}_r$ (row 1), virtual vehicle control errors $\mathbf{x}_v - \mathbf{x}_r$ (row 2), synchronization errors $\mathbf{x} - \mathbf{x}_v$ (row 3), in positions (left) and velocities (right). The lower plots show *xy*-plot of the vehicles on the left with special marks at initial states, and the filtered velocity estimate ϑ on the right.

Table 4.2: Initial states and gains for the output feedback virtual vehicle scheme

Initial states and filter gains							Controller gains						
$\mathbf{x}_m$	$=$		$[$	2	4	0	$]^T$	$\mathbf{K}_p = \mathrm{diag}[$	9	24	6	$]$
$\mathbf{x}_v$	$=$		$[$	1	0.5	$\frac{\pi}{4}$	$]^T$	$\mathbf{K}_d = \mathrm{diag}[$	4	16	32	$]$
$\mathbf{A}$	$=$	$\mathrm{diag}[$	2	2	5	$]$		$\mathbf{L}_1 = \mathrm{diag}[$	0.8	1.6	1.6	$]$
$\mathbf{B}$	$=$	$\mathrm{diag}[$	6	6	6	$]$		$\mathbf{L}_2 = \mathrm{diag}[$	0.55	0.55	0.55	$]$

Experiments with two physical ships

To verify the theoretical simulation results presented in Figure 4.4, the virtual vehicle coordination scheme with only position measurements was experimentally tested with two model ships in the experimental setup of Appendix E with initial states and gains given in Table 4.3. The distance between the leader and the reference vehicle was chosen as 2 m with $\gamma_m = \frac{\pi}{2}$, and Figure 4.5 illustrates the experimental results. The leader ship was manually steered with a joystick in a curved path with a velocity of approximately 0.1m/s.

Note that due to the presence of two model ships in the experiments, the quality of the measurement data was poor (see Remark E.1). Frequent position losses prohibited the collection of long time-series of data, and the performance of the coordination scheme could not be investigated except for the convergence of the follower to the reference vehicle

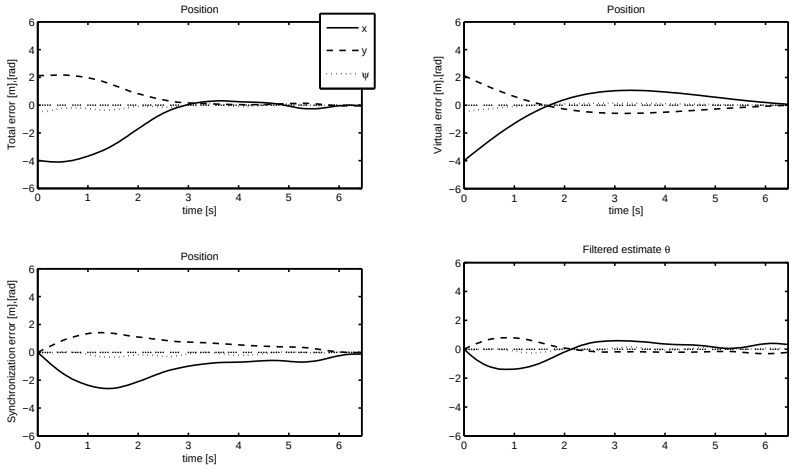

Figure 4.5: Experimental errors $\mathbf{x} - \mathbf{x}_r$ (top left), virtual vehicle control errors $\mathbf{x}_v - \mathbf{x}_r$ (top right), synchronization errors $\mathbf{x} - \mathbf{x}_v$ (bottom left) and the filtered estimate θ (bottom right).

Table 4.3: Initial states and gains for the output feedback virtual vehicle scheme in experiments with two model ships

Initial states and filter gains							Controller gains					
$\mathbf{x}$	$=$		$[$	-4	4	$-\frac{\pi}{2}$ $]^T$	$\mathbf{K}_p$	$=$ diag$[$	5	5	0.5	$]$
$\mathbf{x}_v$	$=$		$[$	-4	4	$-\frac{\pi}{2}$ $]^T$	$\mathbf{K}_d$	$=$ diag$[$	15	15	10	$]$
$\mathbf{A}$	$=$	diag$[$	2	2	2	$]$	$\mathbf{L}_1$	$=$ diag$[$	0.8	0.8	0.8	$]$
$\mathbf{B}$	$=$	diag$[$	6	6	6	$]$	$\mathbf{L}_2$	$=$ diag$[$	1	1	1	$]$

alongside the leader. No quantitative results could be obtained after convergence due to loss of measurement data.

The loss of data was mainly due to the principle of measurement; active infrared markers on each model ship are detected through a camera system. When the two ships are aligned in the basin, the markers can in some situations overlap between ships from the camera perspective, and cause an ambiguity in the position fixes for the two ships. Thus, position measurements of the ships are unavailable or invalid for periods of time. Increasing the distance d between the ships gives increases stability of measurements, but renders little room for manoeuvring in the basin. Furthermore, position measurements through the camera system are also influence by the detection of "false" markers; reflections of markers in the water that are identified as real markers by the camera system.

The experimental results presented here are thus only an illustration of the convergence of the virtual vehicle coordination scheme when applied to a underway replenishment problem with two model ships in a basin. No conclusion on the performance of the scheme can be made from the experimental results due to the poor quality of measurements, and thus a back-to-back comparison with simulations under ideal conditions to validate the theoretical results was not feasible.

4.4 A virtual manipulator design

The virtual vehicle approach was illustrated for motion control in the plane using a three-degree-of-freedom fully actuated vehicle in Section 4.1, but is not limited to mobile vehicle control in a two-dimensional plane. This sections shows how the virtual vehicle, or virtual manipulator, approach can be applied to control *n*-degree-of-freedom robot manipulators. The results presented in this section are based on Kyrkjebø and Pettersen (2007*b*).

In practice, robot manipulators are often equipped with high-precision position sensors such as encoders, but velocity or acceleration measurements are not so readily available, and are often contaminated with noise when obtained from low-quality tachometers or through numerical differentiation techniques. Model-based observers utilize the nonlinear dynamic model of the manipulator to reconstruct velocity and acceleration information, and may produce estimates less contaminated by noise than simple differentiation techniques. However, the dynamic model of a robot manipulator is not always known, and thus alternative approaches to model-based observers must be employed to estimate the velocity and acceleration of the manipulator. Differentiation and model-based estimation approaches to the problem of output trajectory control of robot manipulators can be found extensively in literature (cf. Kelly (1993), Loría and Ortega (1995), De Queiroz *et al.* (1997), Loría and Melhem (2002)).

In this section, we propose to utilize the known kinematics of a leader manipulator with unknown dynamics to estimate the unknown states of the leader manipulator. The estimates are constructed using a virtual manipulator that is stabilized to the leader manipulator through a kinematic control procedure. Hence, the available information (kinematics) is utilized to estimate the unknown states of the leader, while the requirement of knowing the parameters of the more complex dynamic model is lifted.

This section considers leader-follower coordination control for fully actuated robot manipulators with $n \leq 6$ joints, where the only available measurement from the leader is the position vector. The leader robot is driven by an input torque τ_m that is designed to drive the operational space coordinates $\mathbf{x}_m, \dot{\mathbf{x}}_m \in \mathbb{R}^m$ to a desired trajectory $\mathbf{x}_d, \dot{\mathbf{x}}_d \in \mathbb{R}^m$. The input torque as well as the dynamical model and its parameters are considered unknown for the leader, and thus a model-based observer for the leader is not readily constructed. There is no guarantee that the leader follows the desired trajectory perfectly, and thus the follower can not simply track the desired trajectory $\mathbf{x}_d, \dot{\mathbf{x}}_d$, but must *synchronize* its states $\mathbf{x}, \dot{\mathbf{x}}$ to the leader states $\mathbf{x}_m, \dot{\mathbf{x}}_m$ to achieve coordination.

The relationship between joint angles $\mathbf{q}$ and operational space coordinates $\mathbf{x}$ is known through the direct kinematics equation. The direct kinematic equation of (2.41)

$$\mathbf{x} = \mathbf{f}(\mathbf{q}) \tag{4.67}$$

is assumed known for both manipulators. The nonlinear function $\mathbf{f}(\cdot)$ allows computation of the operational space variables from knowledge of the joint space variables.

Note that the proposed virtual manipulator design of this section coordinates two robot manipulators in the operational space, and not in the joint space as in Rodriguez-Angeles and Nijmeijer (2001) and Bondhus *et al.* (2004). Hence, we formulate the coordination scheme in the task space of the robot manipulator, which is more suitable to applications where the robot manipulators should follow a geometrically specified motion, or in applications where two robots should manipulate large rigid structures. Thus, we inherently

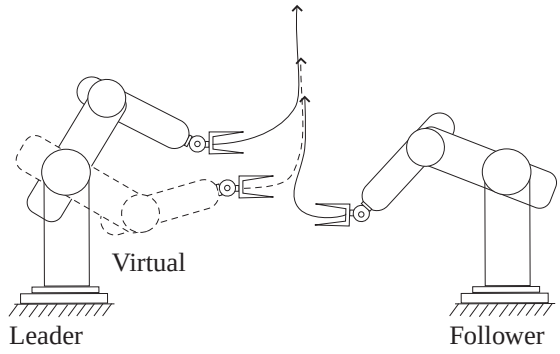

Figure 4.6: Leader, follower and virtual manipulator

assume that the image of the forward kinematics of the leader must be contained within the image of the forward kinematics of the follower. Note also that if measurements of the operational space position variables $\mathbf{x}$ and $\mathbf{x}_m$ are available, the virtual manipulator design does not require that the direct kinematic function $\mathbf{f}(\cdot)$ is known explicitly.

In this section, the dynamic model of the leader manipulator with mass and inertia parameters is considered unknown, as well as the velocity and acceleration of the leader manipulator. The position and orientation of the leader manipulator $\mathbf{q}_m$ is known and measured, and the kinematic equation $\mathbf{x}_m = \mathbf{f}_m(\mathbf{q}_m)$ and the differential kinematics relationship through the Jacobian matrix $\mathbf{J}_m(\mathbf{q}_m)$ is considered known. No knowledge of the desired trajectory of the leader is assumed.

The parameters of the dynamic model of the follower manipulator are considered known, as well as its position and orientation vector $\mathbf{q}$. The proposed virtual manipulator design in this section is done in the framework of Section 4.2 and Definition 2.7, assuming that the velocity vector $\dot{\mathbf{q}}$, the kinematic relationship $\mathbf{f}(\mathbf{q})$ and differential kinematic relationship through the Jacobian matrix $\mathbf{J}(\mathbf{q})$ in (2.42) are known for the follower manipulator. In practice, this relates to the problem of synchronizing a known robot manipulator to an unknown robot manipulator where only the length and type of the joints are known, and where only the joint position and orientation vector $\mathbf{q}_m$ is measured. However, the virtual manipulator approach is easily adopted to the design of Section 4.3 to solve the problem of Definition 2.8 where the restriction of knowing the velocity of the follower manipulator is lifted.

4.4.1 Virtual manipulator

The virtual manipulator design is based on replacing the concept of a virtual vehicle in Section 4.1 with a virtual manipulator that stabilizes itself to the leader manipulator as illustrated in Figure 4.6. This virtual manipulator is based on the differential kinematic relationship of the leader through the Jacobian relationship

$$\dot{\mathbf{x}}_v = \mathbf{J}_m(\mathbf{q}_v)\,\dot{\mathbf{q}}_v \tag{4.68}$$

and uses the virtual joint velocity $\dot{\mathbf{q}}_v$ as a control input. The control objective is to coordinate the follower manipulator to the leader manipulator using a virtual manipulator as an state estimator for the leader. In the discussion of this section, we adopt the leader manipulator as a motion reference for the follower manipulator, and thus the two manipulators will perform the same movement in the operational space. See Remark 2.5 for a discussion on problems where the motion of the manipulators should not be exactly copied, but instead defined through a reference manipulator.

4.4.2 Virtual manipulator design

The only measurement available from the leader is the joint position vector $\mathbf{q}_m$ which translates directly into the position and orientation vector $\mathbf{x}_m$ through the relationship in (2.41). The virtual manipulator is designed as an intermediate controlled manipulator that is stabilized to the leader manipulator based on position measurement only. The virtual manipulator is thus a state estimator for the leader.

As in Section 4.1.1, the first step considers the velocity $\dot{\mathbf{q}}_v$ of the virtual manipulator as the control input to ensure convergence of the virtual trajectories to the leader trajectories. Thus, the trajectories $\mathbf{x}_v$ and velocities $\dot{\mathbf{q}}_v$ can be considered as estimates of $\mathbf{x}_m$ and $\dot{\mathbf{q}}_m$, and the virtual manipulator becomes a kinematic estimator of the leader states through the position feedback loop.

The virtual manipulator is defined by its differential kinematic model in (4.68), and in this section we adopt assumptions on the states of the leader similar to the ones defined in Assumption 2.1 as

$$\sup_t \|\dot{\mathbf{q}}_m\| = V_M < \infty \tag{4.69}$$

$$\sup_t \|\ddot{\mathbf{q}}_m\| = A_M < \infty \tag{4.70}$$

We define the virtual manipulator errors in the operational space as

$$\mathbf{e}_v = \mathbf{x}_v - \mathbf{x}_m = \mathbf{f}_m(\mathbf{q}_v) - \mathbf{f}_m(\mathbf{q}_m) \tag{4.71}$$

and

$$\dot{\mathbf{e}}_v = \dot{\mathbf{x}}_v - \dot{\mathbf{x}}_m = \mathbf{J}_m(\mathbf{q}_v)\dot{\mathbf{q}}_v - \mathbf{J}_m(\mathbf{q}_m)\dot{\mathbf{q}}_m \tag{4.72}$$

To stabilize the virtual vehicle to the leader, we propose the virtual control law

$$\dot{\mathbf{q}}_v = -\mathbf{J}_m^{-1}(\mathbf{q}_v)\mathbf{L}_1\mathbf{e}_v - \mathbf{J}_m^{-1}(\mathbf{q}_v)\mathbf{L}_2\mathbf{z} \tag{4.73}$$

where $\mathbf{L}_1$ and $\mathbf{L}_2$ are symmetric positive gain matrices, and

$$\dot{\mathbf{z}} = \mathbf{e}_v \tag{4.74}$$

Thus, we can write (4.72) as

$$\dot{\mathbf{e}}_v = -\mathbf{L}_1\mathbf{e}_v - \mathbf{L}_2\mathbf{z} - \mathbf{J}_m(\mathbf{q}_m)\dot{\mathbf{q}}_m \tag{4.75}$$

The closed-loop errors (4.74 - 4.75) are now in the form of (4.7 - 4.8), and we can adopt Theorem 4.1 of Section 4.1.1 to show that the virtual manipulator control scheme is uniformly practically asymptotically stable.

4.4.3 Follower manipulator design

The velocity information from the virtual manipulator design of Section 4.4.2 can now be used in a coordination controller for the follower manipulator to follow the virtual manipulator of (4.68) as in Section 4.3.1. Note that the joint velocity $\dot{\mathbf{q}}_v$ is now known through the definition of the control law of (4.73), and through the differential kinematic relationship of (4.68) we can obtain the velocity $\dot{\mathbf{x}}_v$ of the virtual manipulator. Furthermore, due to the design of the virtual controller (4.73), an expression for the acceleration of the virtual manipulator will be partially available for control purposes. The variables available from the virtual manipulator design to the coordination controller are

$$\dot{\mathbf{x}}_v = \mathbf{J}_m(\mathbf{q}_v)\,\dot{\mathbf{q}}_v = -\mathbf{L}_1\mathbf{e}_v - \mathbf{L}_2\mathbf{z} \tag{4.76}$$

$$\ddot{\mathbf{x}}_v = -\mathbf{L}_1\dot{\mathbf{e}}_v - \mathbf{L}_2\mathbf{e}_v = \left(\mathbf{L}_1^2 - \mathbf{L}_2\right)\mathbf{e}_v + \mathbf{L}_1\mathbf{L}_2\mathbf{z} + \mathbf{L}_1\mathbf{J}_m(\mathbf{q}_m)\,\dot{\mathbf{q}}_m \tag{4.77}$$

Recognizing that (4.76 - 4.77) are in the form of (4.15 - 4.16), we can adopt Theorem 4.2 of Section 4.2.1 to show that the coordination closed-loop errors are uniformly globally practically asymptotically stable. Furthermore, we can adopt Theorem 4.3 of Section 4.3 to show that the overall closed-loop system is uniformly globally practically asymptotically stable.

4.4.4 Simulation study

The operational space synchronization scheme with virtual velocity estimates was tested in a simulation environment in MATLAB using a two-link manipulator structure from Sciavicco and Siciliano (1996). The leader manipulator tracked an operational space rectilinear path from $\mathbf{x}_d(0) = [0.2, 0.2]^T$ to $\mathbf{x}_d(t_f) = [0.1, -0.6]^T$ with a trapezoidal velocity profile and a trajectory duration of $t_f = 25$ s. The maximum velocity was restricted to 1 m/s, and an inverse dynamic trajectory tracking scheme in the operational space was employed for the leader manipulator.

The leader robot parameters were taken from (Sciavicco and Siciliano, 1996, Section 6.7) as $a_1 = a_2 = 1$ m, $l_1 = l_2 = 0.5$ m, $m_{l_1} = m_{l_2} = 50$ kg, $I_{l_1} = I_{l_2} = 10$ kg·m^2, $k_{r_1} = k_{r_2} = 100$, $m_{m_1} = m_{m_2} = 5$ kg, and $I_{m_1} = I_{m_2} = 0.001$ kg·m^2. Data for the two equal joint actuators were chosen as $F_{m_1} = F_{m_2} = 0.001$ N·m·s/rad, $R_{a_1} = R_{a_2} = 10$ ohm, $k_{t_1} = k_{t_2} = 2$ N·m/A, and $k_{v_1} = k_{v_2} = 2$ V·s/rad. The control gains of the leader trajectory tracking controller were $\mathbf{K}_p = 200\,\mathbf{I}$ and $\mathbf{K}_d = 150\,\mathbf{I}$.

The follower parameters were chosen equal to the leader parameters, apart from $a_1 = a_2 = 1.2$ m. The control gains were chosen as $\mathbf{L}_1 = 1\,\mathbf{I}$, $\mathbf{L}_2 = 1\,\mathbf{I}$ for the virtual manipulator, and $\mathbf{K}_p = 700\,\mathbf{I}$, $\mathbf{K}_d = 450\,\mathbf{I}$ for the follower manipulator using a sliding surface gain of $\mathbf{\Lambda} = 0.1\,\mathbf{I}$. Plots of the errors are shown in Figure 4.7, and the initial states were chosen as $\mathbf{x}(0) = [0.5,\ 0.5]^T$ for the follower, $\mathbf{x}_v(0) = [0.9,\ 0.0]^T$ for the virtual manipulator and as $\mathbf{x}_m(0) = [0.7,\ 0.2]^T$ for the leader to illustrate convergence.

The virtual manipulator control errors $\mathbf{e}_v = \mathbf{x}_v - \mathbf{x}_m$, the coordination control errors $\mathbf{e} = \mathbf{x} - \mathbf{x}_v$ and the overall control errors $\mathbf{x} - \mathbf{x}_r$ are seen in Figure 4.7 to be practically asymptotically stable. Small oscillations in the virtual velocity errors are observed due to the unknown velocity of the leader manipulator, but due to the practical stability property of the closed-loop system the magnitude of these oscillations can be arbitrarily reduced within control saturation limits by enlarging the control gains.

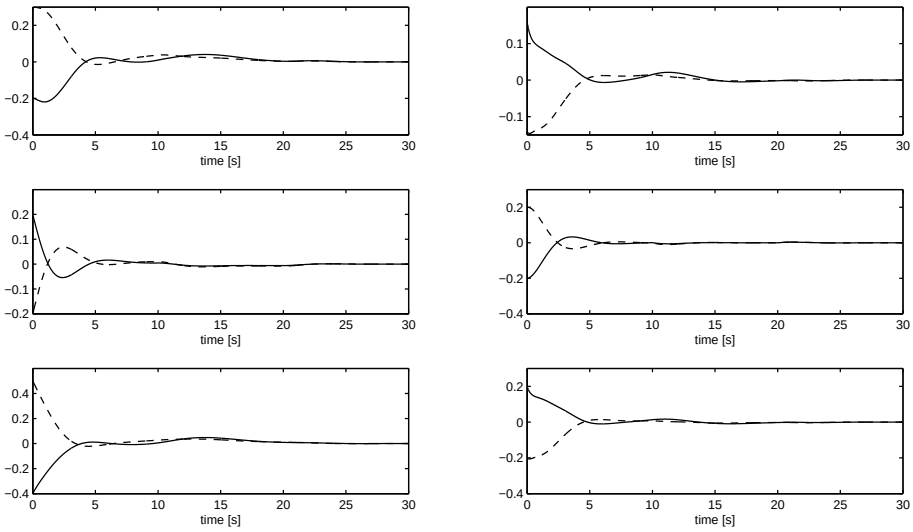

Figure 4.7: The total errors $\mathbf{x} - \mathbf{x}_m$ in the upper row, the virtual manipulator control errors $\mathbf{x}_v - \mathbf{x}_m$ in the middle row, and the coordination errors $\mathbf{x} - \mathbf{x}_v$ in the lower row, with positions [m] on the left and velocities [m/s] on the right.

4.5 Dynamic synchronization

Leader-follower coordination control of vehicles in a formation requires that the followers maintain a fixed static position relative to the leader. However, in the phase when the followers are approaching or changing their desired position in a formation, the behaviour of the follower is dynamic relative to the leader. This is also the case in docking operations when the target is moving, which can be considered a special dynamic case of leader-follower coordination control. The behaviour during this approach phase is usually specified through the tuning of static control gains, and in order to minimize overshoot or uncontrolled motions which could possibly lead to collisions, the control gains are often chosen conservatively low. This may severely limit the performance of the control scheme at the same time as it does not guarantee a safe approaching behaviour for different initial conditions.

A dynamic surface control (DSC) scheme is utilized in Swaroop *et al.* (2000) and Girard and Hedrick (2001) to avoid the explosion of terms associated with integrator backstepping techniques and the model differentiation required in a multiple sliding surface control approach. In Swaroop *et al.* (2000), the regulation and tracking problem in a formation is addressed, but no special care is taken to specify the transient behaviour of the vessels when they are approaching or changing their position in a formation, or when docking to a moving vessel. In Girard and Hedrick (2001), the transition between manoeuvres from a communication protocol view is addressed, but no dynamic behaviour that guarantees the followers a stable approach to the leader is proposed.

The concept of dynamical synchronization is defined in Efimov (2005) as when the

synchronization error obeys oscillatory differential equations, and is used in an adaptive scheme to synchronize two Lurie systems in oscillatory motion. In this section, we utilize the idea of Efimov (2005) in the concept of *dynamic synchronization*, where the synchronization error is designed to satisfy *some* differential equation, not necessarily oscillatory.

Reference models have been used extensively throughout the literature to filter step inputs. However, the reference model approach is not readily applicable to systems where the reference input is dynamic rather than a step input. Thus, in this section we propose a dynamic synchronization scheme to specify the behaviour of the follower during the transient phase of approaching, or changing position, relative to a leader. To specify the dynamic synchronization behaviour, a smooth reference model-based on a first-order filter in cascade with a stable second-order mass-spring-damper system is used to filter the synchronization *error* of the closed-loop system. This imposes a controlled dynamic synchronization behaviour on the follower relative to the leader in the approach phase.

4.5.1 The dynamic synchronization design

The synchronization problem of coordinating a follower to a leader suggests that the relationship between of the follower and the leader will be dynamic in the transient phase. Thus, in this section we propose to describe this dynamic relationship in the form of a differential equation

$$\dot{\boldsymbol{\varepsilon}} = \mathbf{f}_{\varepsilon}(\boldsymbol{\varepsilon}) \tag{4.78}$$

to control the behaviour of the follower while changing position relative to the leader. Note that dynamic synchronization is particularly suited for docking operations to a moving leader.

In this section, we restrict the coordination reference for the follower to a motion parallel to the motion of the leader (see Section 2.2.5) to simplify the presentation. Furthermore, the dynamic synchronization scheme is presented utilizing state feedback of the follower and state measurements of the leader to focus on the concept of dynamic synchronization rather than on state estimation.

In the presentation of this section, we will utilize the concepts of a reference and a virtual vehicle as defined in Figure 4.1 of Section 4.1. We define the dynamic synchronization errors

$$\boldsymbol{\varepsilon} = \mathbf{x}_v - \mathbf{x}_r, \qquad \dot{\boldsymbol{\varepsilon}} = \dot{\mathbf{x}}_v - \dot{\mathbf{x}}_r, \qquad \ddot{\boldsymbol{\varepsilon}} = \ddot{\mathbf{x}}_v - \ddot{\mathbf{x}}_r \tag{4.79}$$

where $\mathbf{x}_r$ is the position of the reference vehicle, and $\mathbf{x}_v$ the position of a virtual vehicle that will be used as a motion reference for the follower. Thus, the dynamic synchronization error $\boldsymbol{\varepsilon}$ defines the desired dynamic behaviour of the follower relative to the leader. We propose a 1st order low-pass filter cascaded with a stable mass-damper-spring system (which is used as a reference filter in Fossen (2002)) to define the dynamic behaviour in the dynamic synchronization scheme

$$\boldsymbol{\varepsilon}^{(3)} + (2\boldsymbol{\Delta} + \mathbf{I})\boldsymbol{\Omega}\ddot{\boldsymbol{\varepsilon}} + (2\boldsymbol{\Delta} + \mathbf{I})\boldsymbol{\Omega}^2\dot{\boldsymbol{\varepsilon}} + \boldsymbol{\Omega}^3\boldsymbol{\varepsilon} = \boldsymbol{\Omega}^3\boldsymbol{\varepsilon}_r \tag{4.80}$$

for designed filter constants $\boldsymbol{\Delta} > 0$ and $\boldsymbol{\Omega} > 0$, and where $\boldsymbol{\varepsilon}_r$ is the desired value for $\boldsymbol{\varepsilon}$ since

$$\lim_{t\to\infty} \boldsymbol{\varepsilon}(t) = \boldsymbol{\varepsilon}_r \tag{4.81}$$

Note that (4.80) guarantees that (4.79) are smooth signals, and that (4.80) can be written as a linear time invariant system

$$\dot{\bar{\varepsilon}} = \mathbf{A}\bar{\varepsilon} + \mathbf{B}\varepsilon_r, \qquad \bar{\varepsilon} = \begin{bmatrix} \varepsilon & \dot{\varepsilon} & \ddot{\varepsilon} \end{bmatrix}^T \tag{4.82}$$

where

$$\mathbf{A} = \begin{bmatrix} \mathbf{0} & \mathbf{I} & \mathbf{0} \\ \mathbf{0} & \mathbf{0} & \mathbf{I} \\ -\boldsymbol{\Omega}^3 & (2\boldsymbol{\Delta}+\mathbf{I})\boldsymbol{\Omega}^2 & -(2\boldsymbol{\Delta}+\mathbf{I})\boldsymbol{\Omega} \end{bmatrix} \tag{4.83}$$

and

$$\mathbf{B} = \begin{bmatrix} \mathbf{0} & \mathbf{0} & \boldsymbol{\Omega}^3 \end{bmatrix}^T \tag{4.84}$$

We define the synchronization control errors as

$$\mathbf{e} = \mathbf{x} - \mathbf{x}_v, \qquad \dot{\mathbf{e}} = \dot{\mathbf{x}} - \dot{\mathbf{x}}_v, \qquad \ddot{\mathbf{e}} = \ddot{\mathbf{x}} - \ddot{\mathbf{x}}_v \tag{4.85}$$

where the states of the virtual vehicle are given from (4.79)

$$\mathbf{x}_v = \mathbf{x}_r + \varepsilon, \qquad \dot{\mathbf{x}}_v = \dot{\mathbf{x}}_r + \dot{\varepsilon}, \qquad \ddot{\mathbf{x}}_v = \ddot{\mathbf{x}}_r + \ddot{\varepsilon} \tag{4.86}$$

Using the definition of the measure of tracking (3.4) of Section 3.1.1

$$\mathbf{s} = \dot{\mathbf{x}} - \dot{\mathbf{y}} = \dot{\mathbf{e}} + \boldsymbol{\Lambda}\mathbf{e} \tag{4.87}$$

where

$$\dot{\mathbf{y}} = \dot{\mathbf{x}}_m - \boldsymbol{\Lambda}\mathbf{e} \tag{4.88}$$

allows us to write the dynamics of (2.27)

$$\mathbf{M}(\mathbf{x})\dot{\mathbf{s}} = -\mathbf{C}(\mathbf{x},\dot{\mathbf{x}})\mathbf{s} - \mathbf{D}(\mathbf{x},\dot{\mathbf{x}})\dot{\mathbf{s}} + \tau - \mathbf{M}(\mathbf{x})\ddot{\mathbf{y}} - \mathbf{C}(\mathbf{x},\dot{\mathbf{x}})\dot{\mathbf{y}} - \mathbf{D}(\mathbf{x},\dot{\mathbf{x}})\dot{\mathbf{y}} - \mathbf{g}(\mathbf{x}) \tag{4.89}$$

Proposing the state feedback coordination control law

$$\tau = \mathbf{M}(\mathbf{x})\ddot{\mathbf{y}} + \mathbf{C}(\mathbf{x},\dot{\mathbf{x}})\dot{\mathbf{y}} + \mathbf{D}(\mathbf{x},\dot{\mathbf{x}})\dot{\mathbf{y}} + \mathbf{g}(\mathbf{x}) - \mathbf{K}_d\mathbf{s} - \mathbf{K}_p\mathbf{e} \tag{4.90}$$

and constructing a Lyapunov function

$$V(t) = \frac{1}{2}\mathbf{s}^T\mathbf{M}(\mathbf{x})\mathbf{s} + \frac{1}{2}\mathbf{e}^T\mathbf{K}_p\mathbf{e}, \qquad \mathbf{K}_p = \mathbf{K}_p^T > 0 \tag{4.91}$$

we get the derivative along the closed-loop trajectories

$$\dot{V}(t) = -\mathbf{s}^T(\mathbf{D}(\mathbf{x},\dot{\mathbf{x}}) + \mathbf{K}_d)\mathbf{s} - \mathbf{e}^T\boldsymbol{\Lambda}^T\mathbf{K}_p\mathbf{e} \tag{4.92}$$

Since $V(t)$ is positive definite, and $\dot{V}(t)$ is negative definite it follows that the equilibrium $(\mathbf{e},\mathbf{s}) = (\mathbf{0},\mathbf{0})$ is uniformly globally exponentially stable (UGES), and from convergence of $\mathbf{s} \to \mathbf{0}$ and $\mathbf{e} \to \mathbf{0}$ that $\dot{\mathbf{e}} \to \mathbf{0}$.

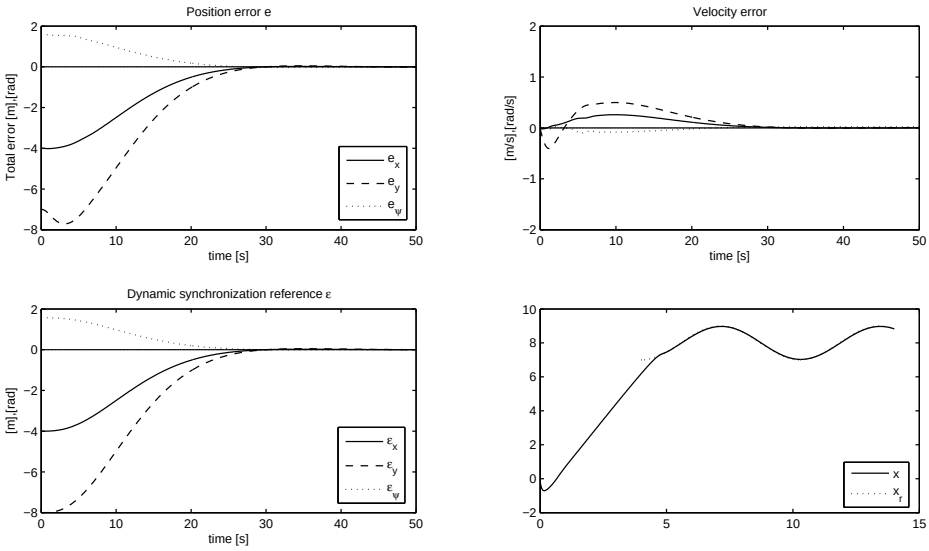

Figure 4.8: Position errors $\mathbf{e}$ (top left), velocity errors $\dot{\mathbf{e}}$ (top right), dynamic synchronization reference $\varepsilon(t)$ (bottom left), *xy*-plot of the follower $\mathbf{x}$ and leader $\mathbf{x}_m$ (bottom right)

Table 4.4: Initial states and gains for the dynamic synchronization scheme

Initial states and sliding surface gain							Controller and reference filter gains						
$\mathbf{x}_m$	$=$		$[$	4	7	0 $]^T$	$\mathbf{K}_p$	$=$	diag$[$	50	150	50 $]$
$\mathbf{x}$	$=$		$[$	0	0	$-\frac{\pi}{2}$ $]^T$	$\mathbf{K}_d$	$=$	diag$[$	14	14	14 $]$
							$\mathbf{\Delta}$	$=$	diag$[$	0.77	0.77	0.77 $]$
$\mathbf{\Lambda}$	$=$	diag$[$	0.8	0.8	0.8	$]$	$\mathbf{\Omega}$	$=$	diag$[$	0.2	0.2	0.2 $]$

4.5.2 Simulation study

The dynamic synchronization approach was simulated in the simulation setup of Appendix E for a docking situation where the follower is docking to a moving leader vessel. In this situation, the reference position $\mathbf{x}_r$ coincides with the leader position $\mathbf{x}_m$, and control objective is thus to synchronize the follower states $\mathbf{x}$ and $\dot{\mathbf{x}}$ to the leader states $\mathbf{x}_m$ and $\dot{\mathbf{x}}_m$. Initial states and gains for the simulation are given in Table 4.4, and the simulation results are shown in Figure 4.8.

In the simulations, the leader ship tracks a sine wave reference trajectory $\sin(\varpi t)$ with frequency $\varpi = 1/45$ with heading angle ψ_m along the tangent line. We see in Figure 4.8 that the synchronization closed-loop errors $\mathbf{e}$ and $\dot{\mathbf{e}}$ converges smoothly to the origin through to the design of the dynamic reference system $\varepsilon(t)$ as smooth signals.

4.6 Concluding remarks

This chapter proposed a virtual vehicle approach to the motion coordination problems defined in Definition 2.7 and 2.8. The coordination approach was based on the design of a virtual vehicle that estimated the unknown states of a leader based on position measurements only. The closed-loop errors were shown to be globally practically asymptotically stable for the situation where the velocity of the follower was available in the control design. For situations where the velocity of the follower was unknown, a stable first-order velocity filter was used to estimate the unknown states of the follower, and semiglobal practical asymptotic stability of the closed-loop errors was concluded. Simulations were presented for both approaches, and for the situation with unknown velocities for the follower, experimental results illustrated the convergence of the proposed coordination scheme. The motion coordination scheme was furthermore applied to robot manipulators in a separate section to illustrate the application of the virtual vehicle approach to manipulating structures. The stability results, simulation results and experimental results presented in this chapter suggest that the proposed virtual vehicle motion coordination approach is suitable for practical applications. Furthermore, a dynamic synchronization scheme was proposed to impose a smooth behaviour on the follower when changing position relative to the leader.

Chapter 5

Comparison of the observer-controller and virtual vehicle schemes

This chapter presents a discussion on the proposed observer-controller coordination scheme of Chapter 3 and the virtual vehicle coordination scheme of Chapter 4. The schemes are compared in terms of estimation principle; the approach taken to estimate the unknown states of the leader through the use of an observer or a controlled virtual vehicle, and in terms of performance and robustness; the ability to suppress disturbances, modelling errors, measurement noise and the practical bounds to which the schemes converge.

5.1 Estimation principle

The estimation principles of the observer-controller scheme and the virtual vehicle scheme are based on the notion of estimating the unknown states of the leader through a system that mimics (or simulates) the behaviour of the leader. In the virtual vehicle scheme, this system is a *virtual* system; a virtual vehicle that is constructed to stabilize to the output of the leader, and which in turn provides estimates of the states of the leader to the follower. For the observer-controller scheme, the mimicking system is the follower itself, and through the observers and controller the follower becomes a *physical* observer of the leader.

The information constraints imposed on the proposed coordination schemes by allowing the parameters of the mathematical model of the leader to be unknown, and also through the fact that only the position is available from the leader as output, suggest that the coordination schemes will not make the closed-loop errors converge to an equilibrium point at the origin, but rather to a bounded or practically stable solution close to the origin. In particular, the presence of non-vanishing perturbations due to the unknown states renders the schemes at best ultimately bounded or practically stable. The results proposed in this thesis are presented on the premise that for many applications this is sufficient. Physical limitations such as measurement noise and the resolution of measurement instruments may suggest that an equilibrium point at the origin can not be stabilized, or energy considerations on the actuators may suggest that the system errors should not be controlled to exactly zero, but rather to a sufficiently small neighbourhood around zero. Friction or external disturbances may perturb the systems so that zero is an unattainable equilibrium, or neglected high-order nonlinearities in the model may cause the system to deviate from

an ideal reference. In these situations it is often enough to ensure that the region to which the solutions converge is sufficiently small to meet the performance demands.

Imposing in addition information constraints on the follower in situations where the velocity of the follower is unknown broadens the range of applications that is suitable for the motion coordination schemes of Chapters 3 and 4. In many systems, velocity sensors are expensive, not easily fitted to the application or contaminated with noise, and thus coordination schemes must be designed that do not rely on accurate velocity measurements. In addition, coordination schemes that can maintain the fundamental stability properties with a reduced set of measurements during temporary loss of measurements or in case of permanent measurement failure have an increased robustness towards failures. The lack of velocity measurements of a system typically reduces stability results from global to semiglobal when using static control gains, and thus the region of attraction for the coordination schemes is reduced from global to a region that can be tuned through control gains. The region of attraction can, however, be increased as much as desired, and thus for most applications this presents no practical drawback in regards to performance. Note also that a global solution to the observer design problem for Euler-Lagrange systems has recently been presented in Børhaug and Pettersen (2006) using time-varying control gains, which suggests that the global region of attraction can be maintained even for systems without velocity measurements.

5.1.1 The observer-controller principle

The observer-controller coordination approach of Chapter 3 relies on a nonlinear observer constructed from the known mathematical model of the follower to provide estimates of the unknown states of the leader. The nonlinear observer is designed to estimate the evolution of the coordination *error* rather than the leader states, since there is no information of the parameters of the mathematical model of the leader to allow the design of a model-based observer that estimates the leader states directly.

Luenberger (1971) suggests that "Almost any System is an Observer". If the available outputs of a system are used as inputs to drive another system, the second system will almost always serve as an observer of the first system in that its states will tend to track the states of the first system. Conceptually, in the observer-controller approach of Chapter 3, the leader is the first system with only output information. The follower is the second system driven by the outputs of the leader, and becomes a *physical* observer tracking the states of the leader. The correction terms used as feedback in the observer are the estimation error $\widetilde{\mathbf{e}}$ and the control input τ, which is based on the estimated states of the leader. In this way, the coordination error is filtered through the nonlinear dynamics of the follower, and the follower thus becomes a nonlinear model-based observer of the leader states.

5.1.2 The virtual vehicle principle

The virtual vehicle coordination approach of Chapter 4 relies on a virtual vehicle that is stabilized to the output of the leader through a virtual control law. The virtual vehicle is based on the kinematics of the follower and disregards any dynamic information of the states, and thus the design of the virtual vehicle and the follower vehicle control schemes can be separated. Through the stabilization, the states of the virtual vehicle become estimates of the states of the leader, and can be used as feedback in the coordination control law of the

follower. Note that there is an inherent attenuation of slowly varying disturbances in the virtual vehicle scheme through the integral term present in the kinematic control law. The virtual vehicle is based on a kinematic control law, and thus becomes a kinematic observer of the states of the leader.

5.1.3 Discussion

In the observer-controller approach of Chapter 3, the error dynamics of the observer and of the coordination controller are closely interconnected due to the interplay between the error observer and the coordination (error) controller. The analysis of the stability properties of the observer-controller scheme is involved due to the couplings between the observer and the controller, and gain tuning is a complex and tedious task where observer gains influence controller performance, and vice versa. Adding a second nonlinear state observer to estimate the velocity of the follower adds further complexity, but preserves the principles of the stability analysis and the gain tuning procedure.

The virtual vehicle approach of Chapter 4 is based on a cascaded structure; the virtual vehicle controller and the follower coordination controller are designed separately, and stability of each of the systems can to some extent be analysed separately. Only the perturbation term from the design of the virtual vehicle is carried through the dynamics of the follower, and must be ensured to be bounded to conclude stability of the overall system. Thus, gain tuning is a design task for the virtual vehicle to specify the performance of the kinematic observer, while gain tuning of the coordination control law of the follower is done utilizing information about the gains from the virtual vehicle design. Removing the velocity measurements of the follower and utilizing a filtered estimate of the coordination velocity error in the coordination control law of the follower complicates the stability analysis, but the cascaded structure of the overall design is kept in the gain tuning process.

The estimator in the virtual vehicle approach is a designed kinematic vehicle; a filter based on the kinematics of the follower, but utilizing no dynamic model information of the follower. Thus, it is possible to tune the gains of the virtual vehicle to achieve performance that is not consistent with the system dynamics of the follower. Care should thus be taken in tuning the virtual vehicle so that the reference trajectory for the coordination control law of the follower does not exceed any limitations of the actuators of the follower. Thus, the challenge faced when tuning the virtual vehicle is similar to the one of designing a reference trajectory; the tracking problem must be feasible.

The error observer in the observer-controller scheme is based on the dynamic model of the follower, and thus the model-based observer guarantees that the estimates of the states are consistent with the dynamics of the follower. The observer may thus be tuned to maximize performance, and energy considerations in regard to the actuators of the follower should be optimized through the tuning of controller gains. Note, however, that maximizing the performance of the observer to follow any transients has some negative effects on noise sensitivity in systems experiencing measurement noise.

In the observer-controller approach where the velocity of the follower is unknown, a second nonlinear model-based state observer is employed to estimate the velocity of the leader. This nonlinear state observer augments the error dynamics of the system, but the principles of the stability analysis are preserved, and gain tuning can be simplified by assuming that the observer gains are equal for the error and state observer. In the virtual vehicle approach, a filtered estimate of the coordination velocity error is used instead of a

nonlinear model-based state observer. Hence, the cascaded tuning process in the approach is preserved.

Note that the coordination approach of Chapter 3 leads to uniform ultimate boundedness of the closed-loop errors, while Chapter 4 yields practical asymptotic stability of the closed-loop errors. In this lies the difference that in the observer-controller schemes, the region of attraction is linked to the size of the ultimate bound. The size of the ultimate bound can thus not be reduced *independently* from the size of the region of attraction by tuning some parameter, and thus the closed-loop error dynamics of the observer-controller scheme are uniformly ultimately bounded rather practically asymptotically stable as discussed in Section 2.1. Note also that uniform practical asymptotic stability guarantees that the transient behaviour of the closed-loop system remains within a small neighbourhood of the origin at all time, which is a property that can not always be guaranteed for uniformly ultimately bounded systems. For most practical applications, and for the application used as a motion coordination example in this thesis (Section 1.1.2), these differences present no practical implications in terms of performance.

5.2 Performance comparison

To investigate the performance of the proposed coordination approaches of Chapter 3 and 4, the two schemes were applied to the simulation setup of Appendix E. The velocity of the follower was assumed known in the simulations to focus on the estimation principles for estimating the leader states, rather than the model-based nonlinear state observer of Section 3.3 and the filtered estimate of Section 4.3. In the simulations, the leader tracks a sine wave reference trajectory $\sin(\varpi t)$ with frequency $\varpi = 1/10$ rad/s with heading angle ψ_d along the tangent line. Initial values are chosen equal for both schemes and are found in Table 5.1 and 5.2. The reference vehicle is chosen at a distance $d = 1$ m and at an angle $\gamma_m = -\frac{\pi}{2}$ relative to the leader for the simulations.

The leader controller is tuned poorly, and tracking performance in the *xy*-plot of Figure 5.1 and 5.2 is seen to be poor. This is done deliberately to illustrate that the follower has no knowledge of the desired trajectory for the leader, but coordinates to the leader using only the available output information; position. Thus, coordination between the follower and the leader is independent of the tracking performance of the leader.

The plots of Figures 5.1 and 5.2 are constructed to compare the two schemes subfigure by subfigure, except for the plot on the bottom left which shows information that is not readily compared between the two schemes. In the top five rows, the plots show the transient behaviour on the left, and the behaviour after settling on the right.

The topmost plots show the total coordination errors in position $\mathbf{x} - \mathbf{x}_r$, and the second row shows the total coordination control errors in velocity $\dot{\mathbf{x}} - \dot{\mathbf{x}}_r$. The third row in Figure 5.1 shows the estimation error $\widetilde{\mathbf{e}} = \mathbf{e} - \widehat{\mathbf{e}}$ due to the nature of the error observer employed, while the third row in Figure 5.2 shows the difference $\mathbf{e} - \mathbf{e}_v$ as the estimation error for the virtual vehicle approach. Row four in Figure 5.1 shows the observer state $\widehat{\mathbf{e}}$ for the observer-controller scheme, while row four in Figure 5.2 shows the virtual error $\mathbf{e}_v = \mathbf{x}_v - \mathbf{x}_r$. The fifth row in both figures shows the control forces τ applied to the follower in the simulations. An *xy*-plot is shown at the bottom right in both schemes, while the bottom left subfigure shows the observer velocity error $\widetilde{\mathbf{s}}$ in Figure 5.1, and the follower control errors $\mathbf{e} = \mathbf{x} - \mathbf{x}_v$ in Figure 5.2.

A quantitative comparison between two different control schemes is difficult due to the fact that choosing optimal gains for both schemes requires a clearly specified optimality criterion that may not exist. Weighting the control performance in terms of control errors against the energy consumption of the actuators may distinguish the two control schemes, but in critical coordination operations, such as the underway replenishment scheme, energy considerations are insignificant to the concern of ensuring a safe operation in terms of safety of personnel, safety margins in the equipment (tension rigs) and smooth behaviour.

In the comparison between the control schemes of Chapter 3 and 4, the gains are tuned such that the schemes converge to a bounded region about the origin of approximately the same size. This region is chosen to be small enough for the schemes to be suitable for practical operations, while adhering to the limitations of the measurement system in the experimental setup described in Appendix E. Note, however, that no control saturations are imposed on the control forces in the transient phase of the simulations shown in Figures 5.1 and 5.2 to illustrate the difference in the applied forces during the simulations. The settling time of the two approaches is chosen fast enough such that the reference motion provided by the virtual vehicle to the follower is challenging for the follower during the transient phase. Hence, large control forces may be demanded from the follower during the transient phase to coordinate to the leader. The comparison presented in this section is thus only a qualitative comparison between different aspects of the two control schemes proposed in this thesis in simulations.

5.2.1 Observer-controller performance

The performance of the observer-controller scheme proposed in Chapter 3 is shown in Figure 5.1 with initial states and gains given in Table 5.1. The convergence of the scheme to a bounded region about the origin is seen in the top row of Figure 5.1, where the control errors are well below 0.05 m after the settling phase of the simulations. The transient behaviour for in both position and heading converges relatively fast to a bounded region for the fully actuated model ship. The coordination errors in velocity given in row two show again the boundedness of the scheme, and the velocities are kept smooth during the transient phase. This is partly due to the use of a nonlinear model-based filter in the observer. The observer errors in row three are also small, bounded and smooth, as is reflected in the observer estimate of the error in row four, and in the observer velocity error in the bottom left subfigure.

Table 5.1: Initial states and gains for the observer-controller scheme

Initial states for leader, follower and obs.							Observer and controller gains						
$\mathbf{x}_m$	$=$	$[$	0	0	0	$]^T$	$\mathbf{K}_p$	$=$	$\text{diag}[$	20	50	20	$]$
$\mathbf{x}$	$=$	$[$	-2	2	$\frac{\pi}{4}$	$]^T$	$\mathbf{K}_d$	$=$	$\text{diag}[$	10	20	20	$]$
$\widehat{\mathbf{x}}$	$=$	$[$	-2.1	1.9	$-\frac{3\pi}{8}$	$]^T$	$\mathbf{L}_1$	$=$	$\text{diag}[$	4	4	2	$]$
$\mathbf{\Lambda}$	$=$	$\text{diag}[$	0.1	0.1	0.1	$]$	$\mathbf{L}_2$	$=$	$\text{diag}[$	4.1	4.1	2.1	$]$

The control forces are seen to be high in the transient phase of the simulations as shown in row five, and this suggests that gains are tuned a bit too aggressively to be suitable for a practical applications. The control gains are in the simulations presented in this chap-

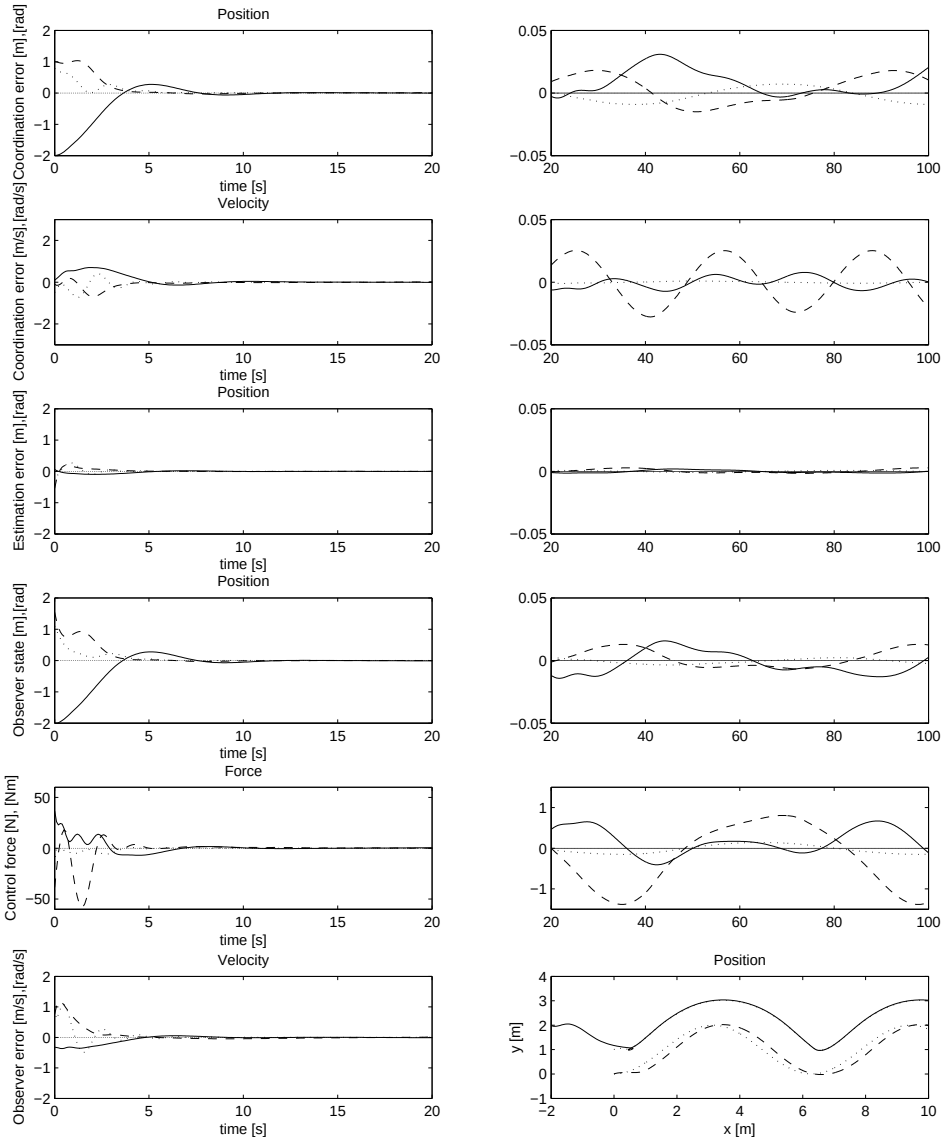

Figure 5.1: Observer-controller simulation errors $\mathbf{x} - \mathbf{x}_r$ (top row), $\dot{\mathbf{x}} - \dot{\mathbf{x}}_r$ (second row), $\widetilde{\mathbf{e}}$ (third row), $\widehat{\mathbf{e}}$ (fourth row), control forces τ (fifth row) and $\widetilde{\mathbf{s}}$ (bottom left) and an *xy*-plot of the simulations (bottom right) with the follower (solid) and reference vehicle (dotted) in the upper part, and the leader (dashed) and its desired trajectory (dotted) in the lower part.

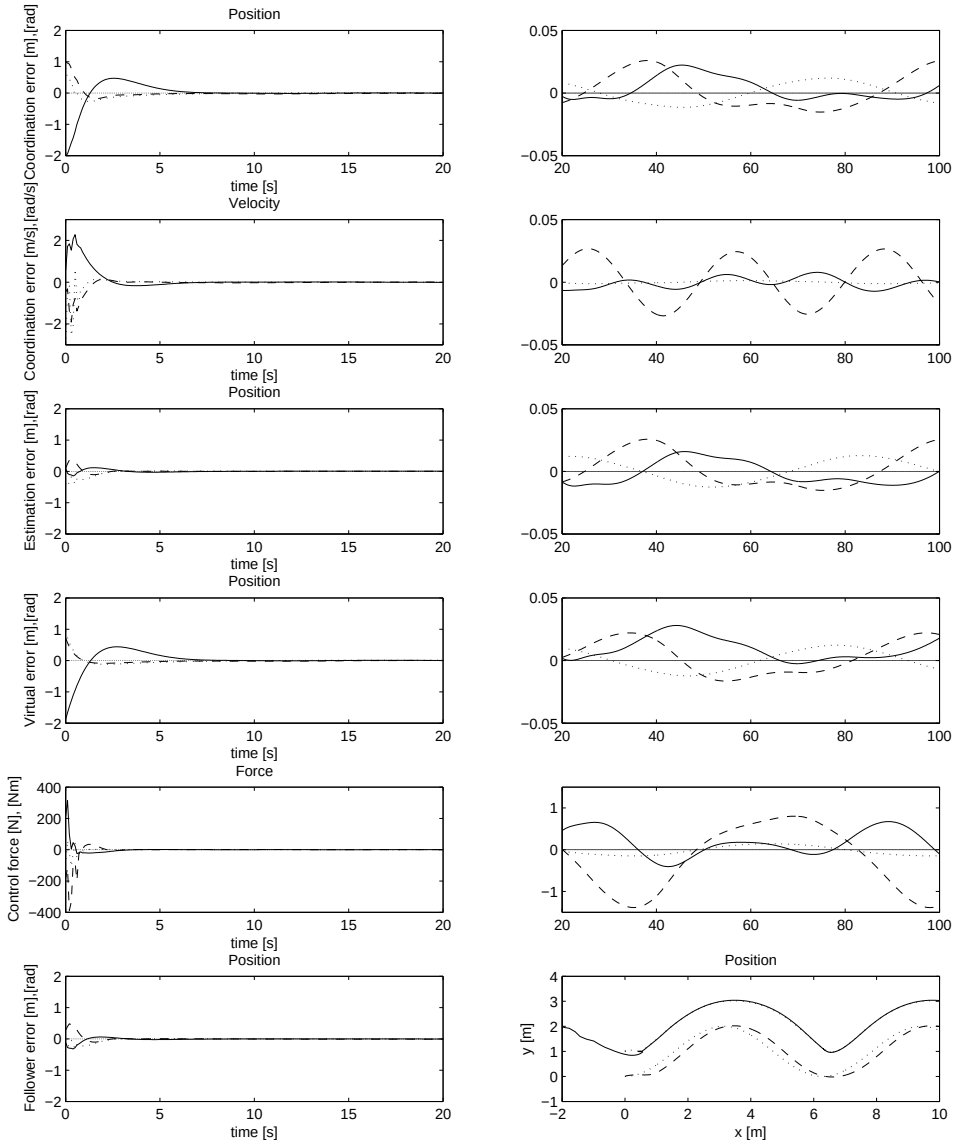

Figure 5.2: Virtual vehicle simulation errors $\mathbf{x} - \mathbf{x}_r$ (top row), $\dot{\mathbf{x}} - \dot{\mathbf{x}}_r$ (second row), $\mathbf{e} - \mathbf{e}_v$ (third row), $\mathbf{x}_v$ (fourth row), control forces τ (fifth row) and $\mathbf{e}_v$ (bottom left) and an *xy*-plot of the simulations (bottom right) with the follower (solid) and reference vehicle (dotted) in the upper part, and the leader (dashed) and its desired trajectory (dotted) in the lower part.

ter chosen large to clearly illustrate the difference in applied control forces between the observer-controller scheme and the virtual vehicle scheme. Note, however, that the control forces are low and suitable for practical experiments after the initial transient phase. This suggests that the use of excessive control forces during the transient phase may be avoided by imposing a smooth transient behaviour through e.g. the dynamic synchronization approach proposed in Section 4.5.

The observer-controller scheme performs well in the simulations, and the performance of the scheme can be tuned through adjusting the controller gains, although this comes with the added price of needing to adjust the observer gains as well.

5.2.2 Virtual vehicle performance

The performance of the virtual vehicle scheme proposed in Chapter 4 is shown in Figure 5.2 with initial states and gains given in Table 5.2. The convergence of the scheme to a bounded region about the origin is seen in the top row of Figure 5.2, where the control errors are well below 0.05 m after the settling phase of the simulations. The transient behaviour converges relatively fast for both position and heading. The coordination errors in velocity given in row two show again convergence to a bounded region, while the velocities are less smooth during the transient phase than for the observer-controller scheme. This is partly because the virtual vehicle scheme uses only the kinematics, and no smoothing second-order dynamics, of the virtual vehicle to estimate the unknown leader states. The estimation errors in row three are small, bounded and smooth, and slightly larger than those of the observer-controller scheme, although they are not readily compared directly due to the difference in the estimation approach and the tuning of the two schemes. The behaviour of the virtual vehicle control errors in row four are designed through the gain tuning, and thus show a smooth and bounded behaviour.

Table 5.2: Initial states and gains for the virtual vehicle scheme

Initial states for leader, follower and virt.						Controller gains				
$\mathbf{x}_m$	$=$	$\begin{bmatrix} 0 & 0 & 0 \end{bmatrix}^T$				$\mathbf{K}_p$	$=\text{diag}\begin{bmatrix} 140 & 280 & 70 \end{bmatrix}$			
$\mathbf{x}$	$=$	$\begin{bmatrix} -2 & 2 & \frac{\pi}{4} \end{bmatrix}^T$				$\mathbf{K}_d$	$=\text{diag}\begin{bmatrix} 100 & 100 & 50 \end{bmatrix}$			
$\mathbf{x}_v$	$=$	$\begin{bmatrix} -2.1 & 1.9 & -\frac{3\pi}{8} \end{bmatrix}^T$				$\mathbf{L}_1$	$=\text{diag}\begin{bmatrix} 1 & 2 & 2 \end{bmatrix}$			
$\mathbf{\Lambda}$	$=\text{diag}\begin{bmatrix} 0.1 & 0.1 & 0.1 \end{bmatrix}$					$\mathbf{L}_2$	$=\text{diag}\begin{bmatrix} 0.55 & 0.55 & 0.55 \end{bmatrix}$			

The control forces are seen to be very high in the transient phase of the simulations as shown in row five, and this clearly illustrate the difference in applied control forces between the observer-controller scheme and the virtual vehicle scheme. The virtual vehicle is designed to provide a smooth and bounded, but challenging, reference to the follower, and since the behaviour of the kinematic estimator is not filtered through a dynamic model, large control forces are demanded in the follower to coordinate to the virtual vehicle. Note, however, that the control forces are low and suitable for practical experiments after the initial transient phase, and comparable to the control forces demanded when employing the observer-controller scheme.

The performance of the control scheme of the follower is shown in the bottom left subfigure, and illustrates that the follower is able to track the virtual vehicle.

5.2.3 Discussion

The observer-controller scheme of Chapter 3 and the virtual vehicle scheme of Chapter 4 are simulated in a scenario using the same initial conditions. The performance of both schemes has been tuned to show similar coordination performance, and thus the control errors are seen to be comparable in size after the initial settling phase.

Most of the difference between the two schemes lies within their transient behaviour and control efforts in that the observer-controller scheme gives a smoother behaviour due to the inherent model-based filter which is based on the system dynamics, and thus provides smoother estimates that are used in the control scheme. However, the convergence time of the observer is difficult to specify explicitly, and is inherently strongly coupled with the controller performance. Tuning the observer gains is interlinked with tuning the controller gains, and thus the gain tuning process is somewhat tedious and time-consuming.

The virtual vehicle approach is easily tuned through the cascaded design, where the performance and transient behaviour of the estimator, the virtual vehicle, can be designed independently of the coordination controller of the follower. However, care should be taken to design the kinematic control law of the virtual vehicle within the control limitations of the follower.

5.3 Robustness in practical applications

The comparison between the observer-controller scheme of Chapter 3 and the virtual vehicle scheme of Chapter 4 in this chapter has focused on comparing the two schemes in terms of principle and performance in an ideal simulation environment as described in Appendix E. However, in a practical application, a number of disturbances and limitations are introduced to the coordination control schemes that may affect the performance of the schemes differently due to the difference in estimation principle. In this section, we will focus on the impact of external disturbances, measurement noise, actuator limitations and modelling errors to the coordination control schemes presented in Chapters 3 and 4.

Note that in addition to being robust to disturbances, limitations and modelling errors, a practical implementation of an automatic control system will require additional system components to be implemented. Error-handling systems, fault-tolerance within the systems, power-management systems (PMS), thrust allocation systems, redundant sensor systems and often trained personnel operating designated operator stations are instrumental in ensuring safe and reliable operation of an automatic control system within a wide range of operating conditions.

5.3.1 Disturbances and actuator limitations

In this section, we will focus our treatment of the disturbances and limitations introduced to the control system in a surface application for marine vessels as described in Section 1.1.2. Disturbances and limitations to a specific application are particular in nature, and thus an impact analysis for each application should be carried out when implementing the coordination control schemes proposed in this thesis. However, disturbances and limitations enter the mathematical model of an Euler-Lagrange system (2.27)

$$\mathbf{M}(\mathbf{x})\ddot{\mathbf{x}} + \mathbf{C}(\mathbf{x},\dot{\mathbf{x}})\dot{\mathbf{x}} + \mathbf{d}(\mathbf{x},\dot{\mathbf{x}}) + \mathbf{g}(\mathbf{x}) = \tau \tag{5.1}$$

in similar ways for many different applications, and thus some general comments regarding the sensitivity of the proposed motion coordination schemes to external disturbances and actuator limitations may be made. The disturbances and limitations addressed in this section enter the model (5.1) through

$\mathbf{M}(\cdot)$, $\mathbf{C}(\cdot)$, $\mathbf{d}(\cdot)$, $\mathbf{g}(\cdot)$ - model parameter errors in the mathematical model of the system.

$\mathbf{x}$ - disturbances that affect the position input to the mathematical model of the system. Typically, measurement noise from the position measurement systems and wave disturbances are included in this term in a surface vessel application.

$\dot{\mathbf{x}}$ - disturbances that affect the velocity input to the mathematical model of the system. Typically, currents that increase or decrease the vessels relative velocity to the surrounding fluid are included in this term in a surface vessel application.

τ - disturbances and limitations affecting the force input to the mathematical model. The force vector can be divided into the applied control forces τ_c subject to actuator limitations and the sum of external forces $\mathbf{w}$ representing the impact from wind, waves and possibly currents as $\tau = \tau_c + \mathbf{w}$ for a surface vessel application. Note that disturbances through the force vector τ may viewed as a perturbation in the acceleration $\ddot{\mathbf{x}}$ of the system through the inertia matrix $\mathbf{M}(\mathbf{x})$.

The external forces affecting the performance of an automatic control system for a surface vessel are mainly due to wind, waves and ocean currents (Fossen (2002)). Wind is the movement of air relative to the surface, and can be compensated for in extreme conditions by utilizing filtered estimates of the wind speed and wind direction from wind sensors. Note that due to the large inertia of surface vessels, wind gusts are usually not compensated for in control systems (Fossen (2002)). Wind-induced disturbances are usually described as a generalized force vector $\mathbf{w}_{wind}$.

Waves are caused by tidal effects or the wind generating wavelets on the ocean surface, and can be separated into a low-frequency part (LF) and a wave-frequency part (WF) (Strand (1999)). The LF part can be utilized in the feedback control design, while the WF part should not be compensated for by the thrusters to avoid unnecessary wear and tear of the propulsion system. Wave-induced LF disturbances are usually simulated by introducing a generalized force vector $\mathbf{w}_{wave}$ (Fossen (2002)).

Note that the position measurements will include contributions from WF wave motions, and thus we may define the position measurement equation

$$\mathbf{y} = \mathbf{x} + \mathbf{x}_\omega + \mathbf{v}_y \tag{5.2}$$

where $\mathbf{x}_\omega$ is the contribution from WF wave motions and $\mathbf{v}_y$ consists of measurement noise.

Ocean currents are generated by gravity, wind friction and water density variations in the system of ocean waters, and affects the hydrodynamic forces experienced by the vessel due to a change of relative velocity between the surface vessel and the surrounding fluid (Fossen (2002)). Different models for describing the influence of ocean currents to a surface vessel can be found in the literature, and the different approaches are usually distinguished by how the disturbance is introduced to the mathematical model of the vessel.

The model of a marine vessel in the body-fixed reference frame (2.48) can be separated into a rigid-body part and a hydrodynamic part as

$$\overbrace{\mathbf{M}_{RB}\dot{\nu}+\mathbf{C}_{RB}(\nu)\nu}^{\text{rigid-body terms}}+\overbrace{\mathbf{M}_{A}\dot{\nu}+\mathbf{C}_{A}(\nu_r)\nu_r+\mathbf{D}(\nu_r)\nu_r}^{\text{hydrodynamic terms}}=\tau_{\nu} \tag{5.3}$$

where $\nu_r = \nu - \nu_c$, and where the current velocity vector ν_c is introduced to distinguish the hydrodynamic terms depending on the velocity of the vessel relative to the fluid as in Fossen (2002). Note that the term $\mathbf{M}_A\dot{\nu}$ assumes that the contribution from the derivative of the current velocity (usually modelled as a 1st-order Gauss-Markov process) is small and negligible ($\dot{\nu}_c \approx \mathbf{0}$) (Fossen (2002)), and thus the influence of ocean currents on the mathematical model of the surface vessel is only through the hydrodynamic terms depending on the velocity vector ν_r. This modelling approach have been utilized by Skjetne *et al.* (2004*a*) and Refsnes *et al.* (2006), while Sørensen (2002) accounted for the effects from $\dot{\nu}_c$ through a hydrodynamic force vector in the body-fixed frame

$$\tau_H = -\mathbf{M}_A\dot{\nu}_r - \mathbf{C}_A(\nu_r)\nu_r - \mathbf{d}(\nu_r) \tag{5.4}$$

Note that the disturbances due to ocean currents can now be introduced to the mathematical model through a force vector rather than through a perturbation on the relative velocity of the vessel. Thus, we can collect the unmodelled external forces from wind, waves and ocean currents together in a slowly varying bias term as in Strand (1999)

$$\mathbf{b} = \tau_H^n + \mathbf{w}_{wind} + \mathbf{w}_{wave} \tag{5.5}$$

where τ_H^n is the representation of (5.4) in the NED frame.

Thus, external disturbances, measurement noise and actuator limitations enter the model (5.1) as perturbations on the position input $\mathbf{x}$, the velocity input $\dot{\mathbf{x}}$ or the force vector τ (and thus the acceleration $\ddot{\mathbf{x}}$), while model parameter errors in the model matrices of (5.1) will in general affect observer and controller performance through residual terms in the feedback linearization designs.

5.3.2 Simulation study

The observer-controller scheme of Chapter 3 and the virtual vehicle scheme of Chapter 4 utilize two different estimation techniques to estimate the unknown states of the leader. In this section, we present a discussion on how robust the two proposed coordination schemes are to model parameter errors, disturbances, actuator limitations and measurement noise.

Simulation results are presented using the simulation setup of Section 5.2, and we distinguish between two different mathematical models used in the simulations. The simulation model is a mathematical representation of the surface vessel used to simulate the behaviour of the surface vessel, while the control model is the mathematical model utilized in the controllers and observers of the coordination control schemes. Typically, model parameter errors are introduced to the control model to investigate the effect of modelling errors, while disturbances are added to the simulation model to investigate the robustness of the control schemes under the influence of external disturbances and actuator limitations. Measurement noise is added to the control model to reduce the quality of measurements as seen by the control system.

Note that all gains and initial conditions are kept as in Table 5.1 and 5.2 to allow a direct comparison with the results in Figure 5.1 and 5.2.

Model parameter errors Synchronization approaches utilizing tracking or manoeuvring controllers for all participants in a group requires that all participants have knowledge of the parameters of the mathematical model to employ nonlinear model-based controllers. In the coordination schemes presented in Chapter 3 and 4, only the follower is responsible for the control action necessary to coordinate the systems, and thus only errors in the parameters of the mathematical model of the follower will affect the performance of the control schemes in practical operations.

To investigate the robustness of the proposed schemes to errors in the model parameters, we increase the parameters of the control model of the follower ship in (E.1) and (E.2) by 50%, while the parameters of the simulation model are unchanged. Furthermore, to address the fact that the most uncertain term in the mathematical model of a surface vessel is the damping term, we restrict the damping in the control model to linear damping (E.3), and thus disregard the nonlinear damping term (E.4). Note the speed of the vehicle is nominally approximately 0.2 m/s along the path, with peaks of up to 0.8 m/s in unconstrained motion during the transient phase. Thus, the assumption of only linear damping imposed on the control model represents a significant difference in regards to the simulation model.

The performance of the two proposed coordination schemes in the situation of model parameter errors and a linear damping assumption for the control model is shown in Figure 5.3. The performance is seen to be similar to the performance of Figures 5.1 and 5.2, except for a small increase in the velocity errors during the transient phase for the virtual vehicle scheme, which suggests that the proposed coordination control schemes are robust towards model parameter errors. This is also supported by the practical experiments presented in Chapter 3 and 4.

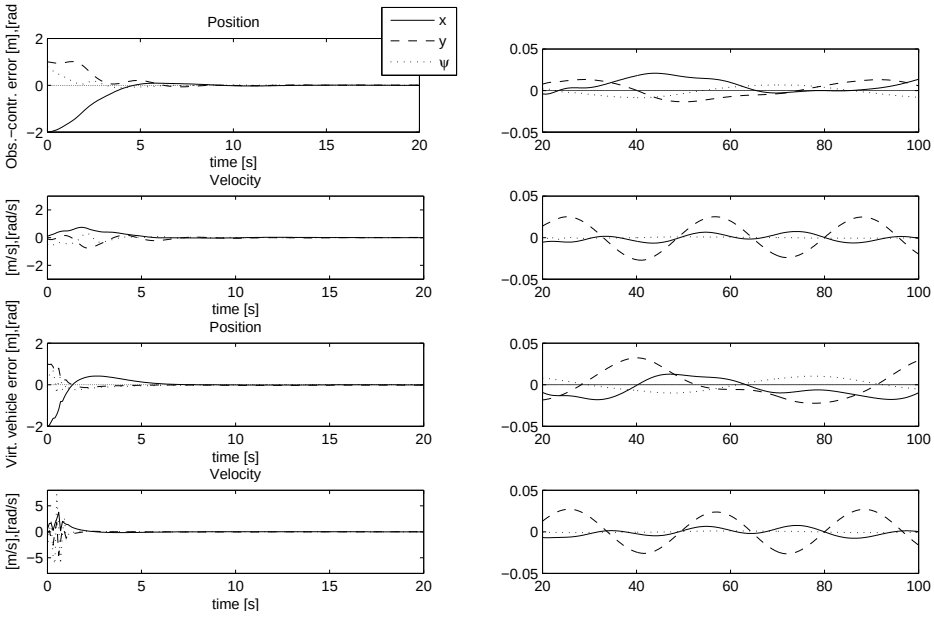

Figure 5.3: Performance of the observer-controller scheme (top rows) and virtual vehicle scheme (bottom rows) under model parameter errors.

External velocity disturbances To investigate the robustness of the coordination control schemes towards external disturbances in the velocity terms, we introduce a slowly varying ocean current v_c^n in the inertial frame with nominal speed 0.2 m/s from the starboard side of the surface vessel

$$v_c^n = -\begin{bmatrix} 0 \\ 0.2 \\ 0 \end{bmatrix} - \begin{bmatrix} 0.1 \\ 0.1 \\ 0.1 \end{bmatrix} \sin(0.1\,t) \tag{5.6}$$

in the simulation model of the surface vessel. The control model of the follower has no knowledge of this external velocity disturbance; $v = v_r$. The nominal speed of the follower vessel is approximately 0.2 m/s in surge, and the external disturbance from ocean currents is thus chosen large in the simulations compared to the nominal speed of the vessel. This choice is made to emphasize the effect of the velocity disturbance to better illustrate the impact on the coordination control schemes.

The performance of the observer-controller scheme and the virtual vehicle scheme is shown in Figure 5.4. We see that the performance of the virtual vehicle scheme is similar to that of the ideal simulations in Figures 5.1 and 5.2, while the performance of the observer-controller scheme is slightly worse than in the ideal case. This is mainly due to the performance of the model-based observer in the observer-controller scheme that performs worse when the behaviour of the simulation model is different than that of the control model, and thus the estimates of the unknown states of the leader are less accurate. Note that the performance of the observer-controller scheme can be improved through gain tuning to achieve similar performance as for the virtual vehicle scheme.

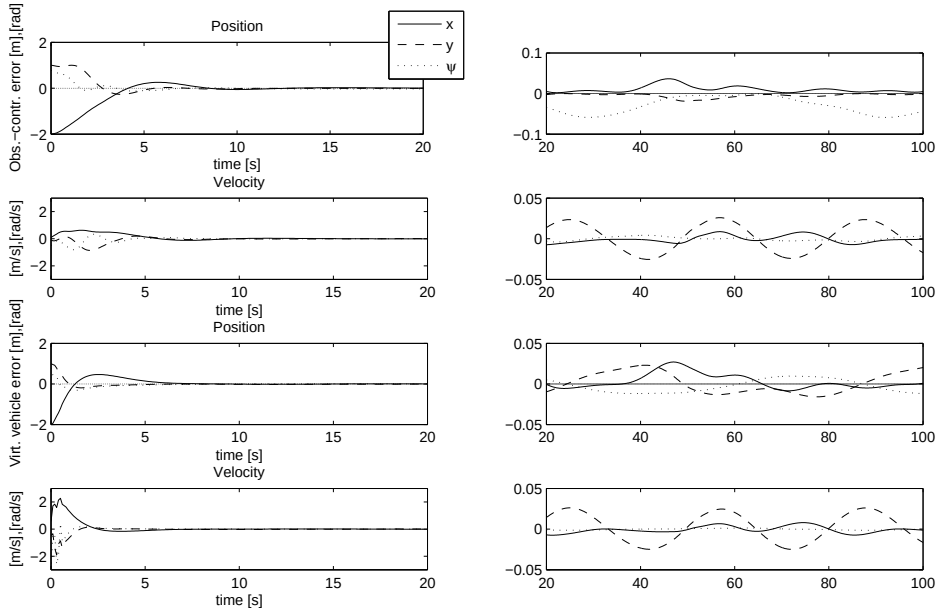

Figure 5.4: Performance of the observer-controller scheme (top rows) and virtual vehicle scheme (bottom rows) under velocity disturbances.

External force disturbances External force disturbances may influence the coordination control scheme through a hydrodynamic force vector as defined in (5.4), or through a slowly varying bias term as defined in (5.5). To investigate the effect of external force disturbances, we will utilize a bias term inspired by Skjetne (2005) and Strand (1999) as

$$\mathbf{w} = \begin{bmatrix} 0 \\ 0.1 \\ 0 \end{bmatrix} + \begin{bmatrix} 0.05 \\ 0.05 \\ 0.05 \end{bmatrix} \sin(0.1\,t) + \mathbf{w}_b \tag{5.7}$$

with the additional zero-mean Gaussian bounded disturbance vector $\mathbf{w}_b$ with a standard deviation of 0.05 N. The performance of the coordination control schemes is shown in Figure 5.5, and we see that the performance of the virtual vehicle approach is slightly worse than in the ideal case of Figures 5.1 and 5.2, while the observer-controller performance is more severely affected in terms of performance.

Any external force disturbances are seen by the observer-controller coordination scheme as an unknown perturbation in acceleration, and appears in the error dynamics of the error observer (3.10) in the same way as the unknown leader acceleration term $\ddot{\mathbf{x}}_m$. Thus, unmodelled force disturbances directly influence the size of the bound on the closed-loop errors, as is clearly seen in Figure 5.5. Note, however, that the sized of this bound can be reduced through gain tuning to yield similar performance as for the virtual vehicle scheme. Note also that the definition of the virtual vehicle control law (4.6) introduces an integral term in the estimation scheme, and thus the influence from slowly varying external disturbances are partly attenuated by the kinematic control law in the virtual vehicle control scheme.

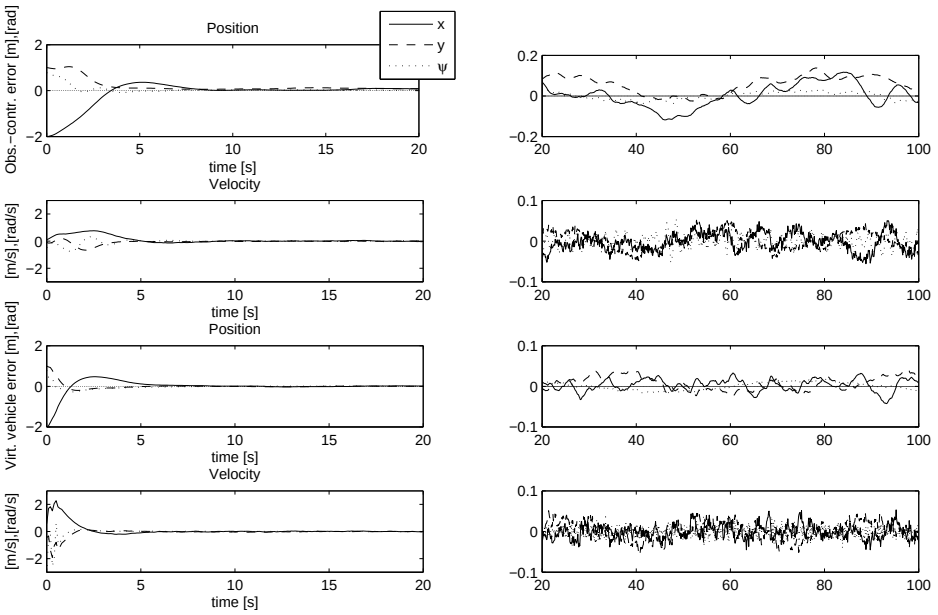

Figure 5.5: Performance of the observer-controller scheme (top rows) and virtual vehicle scheme (bottom rows) under force disturbances.

Measurement noise To investigate the effect of measurement noise and small perturbations caused by external disturbances such as WF motions generated by waves, we introduce noise and small periodic disturbances for both the follower and the leader vessel in the measurement equation (5.2)

$$\mathbf{y} = \mathbf{x} + \begin{bmatrix} 0.01 \\ 0.01 \\ 0.01 \end{bmatrix} \sin(t) + \mathbf{v}_y \tag{5.8}$$

where the zero-mean Gaussian disturbance vector $\mathbf{v}_y$ has a standard deviation of 0.02 m.

The performance of the coordination control schemes is shown in Figure 5.6 when reducing the quality of the position measurements. Both the observer-controller scheme and the virtual vehicle scheme reflects the reduced quality of the measurements, and most notably is the increased velocity errors in the virtual vehicle scheme. This is due to the estimation principle of the virtual vehicle scheme that does not employ any model-based filter based on the mathematical model of the surface vessel, and thus there is no inherent noise filtering in the virtual vehicle scheme.

Measurement noise directly adds to the size of the bounded region to which the coordination schemes converge. The size of this bounded region may be reduced through gain tuning or by introducing a band-limited filter (wave filter) in the control scheme. Note, however, that there is a lower limit to the size of this bounded region that will depend on the size of the measurement noise and non-vanishing perturbations present in the closed-loop system.

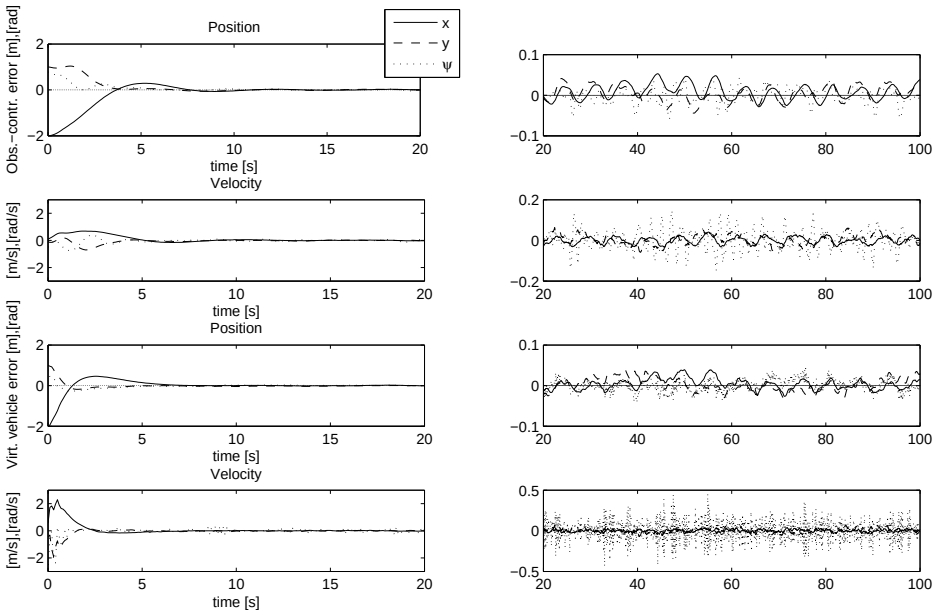

Figure 5.6: Performance of the observer-controller scheme (top rows) and virtual vehicle scheme (bottom rows) under the influence of periodic wave-frequency motions and measurement noise.

Actuator limitations Limitations on the available control force from the actuators are one of the limiting factors in terms of transient performance, and may also be the determining factor in how robust automatic control systems are towards external disturbances. In practical applications, there must be sufficient control forces available to both meet the performance demands of the operation, while at the same time reduce the impact from external disturbances. To investigate the effect of control saturations, we employ force saturations on the available control force from the actuators of the follower surface vessel of 2 N in surge, 1.5 N in sway and 1.5 Nm in yaw as determined by the physical model ship described in Appendix E.

The performance of the coordination control scheme under actuator limitations is shown in Figure 5.7. Note the change in the length of the time vector plotted in the transient phase and after settling. We see that the force saturations severely increases the length of the transient phase due to the limited amount of force available, while the performance after the transient phase is similar to the performance shown in Figures 5.1 and 5.2. Note that in the simulations presented in this section and in Section 5.2, the demanded control forces to coordinate the follower to the leader are close to the force limitations due to the definition of the desired trajectory for the leader. Thus, the increased length of the transient phase is expected when limitations are imposed on the available control forces of the follower.

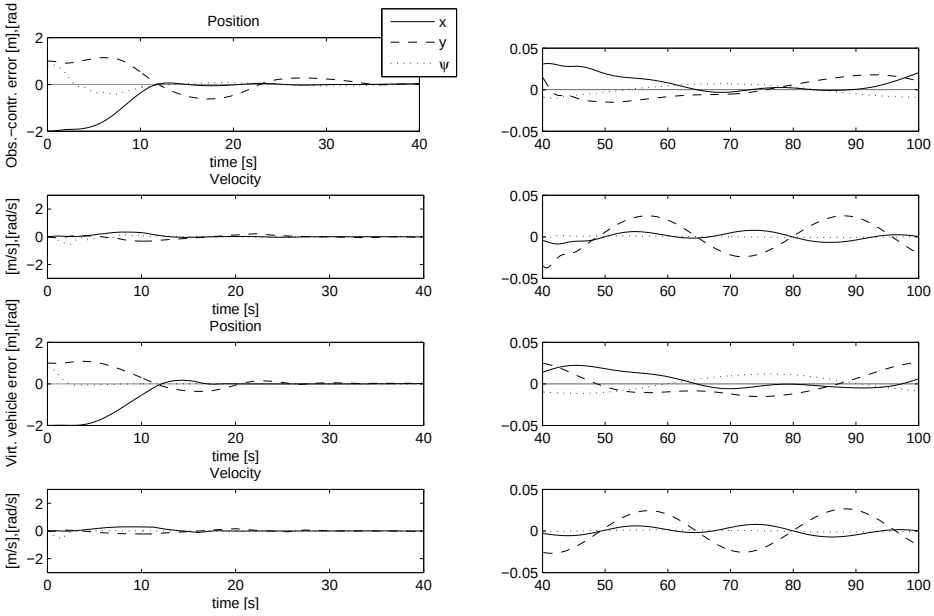

Figure 5.7: Performance of the observer-controller scheme (top rows) and virtual vehicle scheme (bottom rows) subject to actuator limitations of 2 N in surge, 1.5 N in sway and 1.5 Nm in yaw.

5.3.3 Discussion

Both the observer-controller scheme of Chapter 3 and the virtual vehicle scheme of Chapter 4 show robustness towards model parameter errors as illustrated in Figure 5.3. The effect of model parameter errors in the control model does not significantly influence the performance of the schemes after the initial transient phase, and thus the coordination schemes may be suited for practical implementation in systems with model uncertainties.

External velocity disturbances affect the performance of the model-based observer in the observer-controller scheme due to the unexpected behaviour of the system which is not reflected in the control model utilized in the observer. The effect of disturbances in velocity is less visible in the virtual vehicle scheme since the kinematic observer does not depend on the velocity of the system. Note, however, that the external velocity disturbance introduced to the simulations shown in Figure 5.4 is large to emphasize the effect of the disturbance, and can be attenuated by using a different set of observer and control gains in the observer-controller scheme. In all, the coordination schemes show robustness towards external velocity disturbances.

External force disturbances add to the non-vanishing perturbation term in the observer-controller scheme, and thus directly influence the size of the bounded region to which the solutions converge as seen in Figure 5.5. The size of this bound can be reduced by tuning the control gains, or by redesigning the control system to include an integral term or an adaptive bias estimation algorithm to counteract slowly varying disturbances appearing as external forces to the control system. The performance of the virtual vehicle scheme is less affected by the introduction of a slowly varying disturbance force term due to the integral action provided through the definition of the kinematic control law.

The observer-controller scheme utilizes a model-based observer to provide estimates of the errors used in the control scheme. Under the influence of measurement noise, the measurements are filtered through this second-order filter (the dynamic model of the follower), and thus wild-points and noisy measurements are attenuated intrinsically in the observer-controller scheme. The observer is a separate model-based dynamic system that provides estimates of the unknown states of the leader whether it is updated with measurements or not, and thus provides some robustness towards measurement noise in practical applications.

The virtual vehicle scheme utilizes a virtual kinematic control law to estimate the unknown states of the leader. Under the influence of measurement noise on the leader position measurements, there is no model-based filter to filter the measurements, and thus the scheme is more sensitive to fast transients in the measurement signals, which is confirmed in the experiment presented in Section 4.3.3 and in the velocity errors of Figure 5.6. Note that this issue can be addressed by designing a separate filter to remove wild-points and band-limit the measurement signal to reduce the influence of measurement noise.

The overall performance of the coordination control schemes is shown in Figure 5.8, where the model parameter errors, the velocity and force disturbances and the measurement noise defined in this section are imposed on the follower simultaneously. We see that the impact from the external disturbances influences the performance of the coordination control schemes similarly, although the observer-controller scheme suffers from the increased size of the non-vanishing perturbation due to the force disturbances using control gains of Table 5.1. Note that the performance of the observer-controller scheme can be improved to show a level of performance similar to that of the virtual vehicle scheme by

tuning the control gains. Note also that the combined disturbance vector imposed on the follower in Figure 5.8 is larger than the available control forces from the actuators of the model surface vessel, and thus no force limitations are imposed on the control schemes in Figure 5.8.

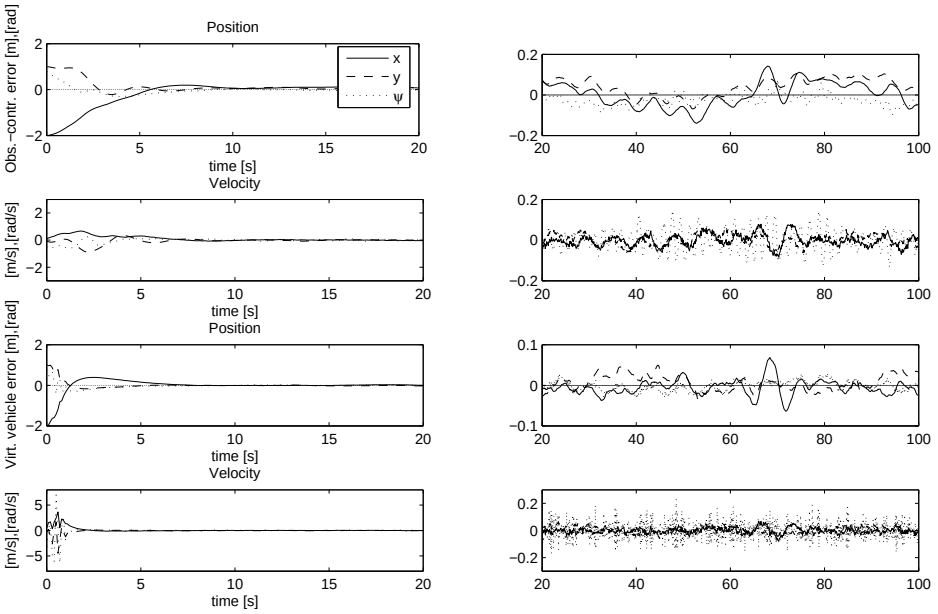

Figure 5.8: Performance of the observer-controller scheme (top rows) and virtual vehicle scheme (bottom rows) under model parameter errors, velocity disturbances, force disturbances and measurement noise.

In all, both the observer-controller scheme and the virtual vehicle scheme are shown to exhibit robustness towards external disturbances, measurement noise and actuator limitations. The performance of both schemes is sensitive to the performance of the estimation schemes, and thus care should be taken in tuning the coordination control schemes. The observer-controller scheme is sensitive to the tuning of the observer, and a choice between the convergence rate and the sensitivity towards disturbances has to be made. In the virtual vehicle scheme, care should be taken in designing the virtual vehicle kinematic velocity such that it only demands velocities and accelerations within the range of the actuators of the follower, and hence provides a reference trajectory that complies with the system dynamics of the follower.

Note that although the discussion on robustness in this section is carried out in the framework of the application presented in Section 1.1.2 using the simulation setup of Appendix E, the results are an indication of the robustness of the schemes in different applications within the Euler-Lagrange framework. Note also that the simulation study presented in this section does not necessarily reflect the true magnitude and nature of disturbances encountered in a full-scale operation, and should thus be regarded as a indication of the impact of external disturbances only. A full-scale feasibility study should be carried out for each practical implementation.

5.4 Concluding remarks

The observer-controller scheme of Chapter 3 and the virtual vehicle scheme of Chapter 4 are both suited to provide motion coordination for mechanical systems, and are solutions to the problems defined in Definitions 2.7 and 2.8. They both rely solely on position output information of the leader, and thus for applications where the parameters of the mathematical model of the leader are unknown, and the velocity and acceleration are unavailable, the follower can still follow the motion of the leader using the proposed motion coordination schemes. Furthermore, for applications where the velocity measurements of the follower are unavailable or unreliable, the proposed coordination schemes maintain the fundamental stability properties within a semiglobal region of attraction. Both schemes show a level of performance that is suitable for practical applications, and are distinguished rather by concept than by performance. The observer-controller scheme is robust and reliable, although it is tedious and time-consuming to tune, while the virtual vehicle scheme is cascaded in nature and provides an easy gain-tuning process, although somewhat sensitive to measurement noise without additional filtering.

Chapter 6

Conclusions

This thesis has presented two motion coordination approaches for mechanical systems within the Euler-Lagrange system framework. The proposed leader-follower coordination schemes rely only on position measurements from the leader, and thus do not require knowledge of predefined paths, model parameters, control inputs or velocity and acceleration measurements of the leader. The leader system is free to manoeuvre independently of the follower, and the follower is responsible for the control action necessary to coordinate to the leader. Both of the proposed coordination schemes were applied using both state feedback and output feedback from the follower to increase the usefulness of the schemes in practical applications, and to provide robustness towards loss or poor quality of velocity measurements.

The proposed observer-controller scheme was based on the design of a nonlinear model-based observer that estimated the coordination errors, and together with state information of the follower, the unknown states of the leader could be reconstructed. The observer-controller scheme used the coordination controller as part of the correction term in the error observer, and thus the follower became a physical observer of the leader. The closed-loop errors of the proposed observer-controller scheme were shown to be uniformly globally ultimately bounded when utilizing state feedback from the follower. Furthermore, for the output feedback design, a second nonlinear model-based observer was designed to estimate the velocity of the follower, and the closed-loop errors were shown to be uniformly semi-globally ultimately bounded.

The proposed virtual vehicle scheme was based on the design of an intermediate virtual system that was stabilized to the leader. Thus, through the design of a virtual control law, estimates of the unknown states of the leader were available to the coordination controller of the follower. The virtual vehicle coordination control scheme was based on a cascaded design, and thus the virtual control law and the coordination control law of the follower could be tuned separately. The closed-loop errors of the proposed virtual vehicle control scheme were shown to be uniformly globally practically asymptotically stable when utilizing state feedback from the follower. Furthermore, for the output feedback design, a first-order velocity filter was designed to estimate the velocity of the follower, and the closed-loop errors were shown to be uniformly semi-globally practically asymptotically stable.

The proposed coordination schemes are distinguished rather by concept than by performance. The observer-controller scheme is model-based and reliable, although it is tedious and time-consuming to tune, while the virtual vehicle scheme is cascaded in nature and provides an easy gain-tuning process, although somewhat sensitive to measurement noise without additional filtering.

The proposed coordination approaches were applied to the underway replenishment problem to verify the theoretical results in simulations and practical experiments. The proposed control schemes performed well in simulations under ideal conditions, and clearly illustrated the theoretical stability results through convergence of the closed-loop errors to a bounded region about the origin. In practical experiments with model ships in a closed basin, the theoretical results were confirmed through convergence of the closed-loop errors. However, the experimental setup was not well suited to experiments with two physical model ships simultaneously, and thus only a qualitative estimate of the bounded region about the origin could be obtained through experiments. In all, both through the simulations and practical experiments, the proposed coordination schemes were seen to be suitable for practical applications.

Bibliography

Aguiar, A. P. and J. P. Hespanha (2004). Logic-based switching control for trajectory-tracking and path-following of underactuated autonomous vehicles with parametric modeling uncertainty. In: *Proc. American Control Conf.* Boston, MA.

Aguiar, A. P., D. B. Dacic, J. P. Hespanha and P. Kokotovic (2004). Path-following or reference-tracking?. In: *Proc. 5th IFAC/EURON Symp. on Intelligent Autonomous Vehicles,*. Lisbon, Portugal.

Al-Hiddabi, S. A. and N. H. McClamroch (2002). Tracking and maneuver regulation control for nonlinear nonminimum phase systems: Application to flight control. *IEEE Trans. on Control Systems Technology* **10**(6), 780 – 792.

Balch, T. and R. C. Arkin (1998). Behavior-based formation control of multirobot teams. *IEEE Trans. on Robotics and Autmation*.

Berghuis, H. (1993). Model-based Robot Control: from Theory to Practice. PhD thesis. University of Twente. The Netherlands.

Berghuis, H. and H. Nijmeijer (1994). Robust control of robots via linear estimated state feedback. *IEEE Trans. on Automatic Control* **39**(10), 2159 – 2162.

Bill, R. G. and W. F. Herrnkind (1976). Drag reduction by formation movement in spiny lobsters. *Science* **193**, 1146 – 1148.

Blekhman, I.I. (1971). *Synchronization of Dynamical Systems*. in Russian, English translation in ASME Press, New York: Synchronization in Science and Technology. Nauka, Moscow.

Blekhman, I.I., A.L. Fradkov, H. Nijmeijer and Yu.A. Pogromsky (1997). On self-synchronization and controlled synchronization. *Systems and Control Letter* **31**, 299 – 305.

Bondhus, A. K., K. Y. Pettersen and H. Nijmeijer (2004). Master-slave synchronization of robot manipulators. In: *Proc. 6th IFAC Symp. on Nonlinear Control Systems*. Stuttgart, Germany. pp. 591 – 596.

Børhaug, E. and K. Y. Pettersen (2006). A UGAS observer for n-DOF Euler-Lagrange systems. In: *Proc. American Control Conf.* Minneapolis, Minnesota, USA.

Brown, S.H. and R. Alvestad (1978). Simulation of maneuvering control during underway replenishment. *Journal of Hydronautics* **12**(3), 109 – 117.

Brunt, M. (1998). Coordination of Redundant Systems. PhD thesis. Technical University Delft. The Netherlands.

Caccavale, F., P. Chiacchio and S. Chiaverini (1998). A quaternion-based regulator for cooperative manipulators. In: *Proc. 1998 IEEE Int. Conf. on Control Applications*. Trieste, Italy. pp. 557 – 561.

Camazine, S., J.-L. Deneubourg, N. R. Franks, J. Sneyd, G. Theraulaz and E. Bonabeau (2001). *Self-Organization in Biological Systems*. Princeton studies in complexity. Princeton University Press.

Celikovský, S. and G. Chen (2005). Secure synchronization of a class of chaotic systems from a nonlinear observer approach. *IEEE Trans. on Automatic Control* **50**(1), 76 – 83.

Chaillet, A. (2006). Staiblité et Robustesse des Cascades Non-linéaires et Application aux Systèmes Mécaniques. PhD thesis. L'Université Paris XI Orsay. Supélec, France.

Chaillet, A. and A. Loría (2006). Uniform semiglobal practical asymptotic stability for non-autonomous cascaded systems and applications. *Submitted to Automatica*.

Chen, H. (2003). Probabilistic Evaluation of FPSO-Tanker Collision in Tandem Offloading Operation. PhD thesis. Norwegian University of Science and Technology, Department of Marine Technology. Trondheim, Norway.

Chen, Y. H. and G. Leitman (1987). Robustness of uncertain systems in the absence of matching assumptions. *Int. Journal of Control* **45**, 1527 – 1542.

Cheng, G., J. Gu, T. Bai and O Majdalawieh (2004). A new efficient control algorithm using potential field: extension to robot path tracking. In: *Canadian Conf. on Electrical and Computer Engineering*. pp. 2035 – 2040.

Connolly, T. H. and F. Pfeiffer (1994). Cooperating manipulator control using dual quaternion coordinates. In: *Proc. 33rd IEEE Conf. on Decision and Control*. Lake Buena Vista, FL USA. pp. 2417 – 2418.

Crowley, J.L. (1989). Asynchronous control of orientation and displacement in a robot vehicle. In: *Proc. 1989 IEEE Int. Conf. on Robotics and Automation*. Scottsdale, AZ, USA. pp. 1277 – 1282.

Danielsen, A. L., E. Kyrkjebø and K. Y. Pettersen (2004). MVT: A marine visualization toolbox for matlab. In: *Proc. IFAC Conf. on Control Applications in Marine Systems*. Ancona, Italy. pp. 515 – 519.

De Queiroz, M.S., Jun Hu, D.M. Dawson and S.R. Burg, T.and Donepudi (1997). Adaptive position/force control of robot manipulators without velocity measurements: theory and experimentation. *IEEE Trans. on Systems, Man and Cybernetics, Part B* **27**(5), 796 – 809.

Dimmick, J.G., R. Alvestad and S.H. Brown (1978). Two-block romeo (simulation of ship steering control for underway replenishment). In: *Proc. 28th IEEE Vehicular Technology Conf.*. New York. pp. 382 – 389.

Dong, S., H.N. Dong and S.K. Tso (2002). Tracking stabilization of differential mobile robots using adaptive synchronized control. In: *Proc. IEEE Conf. Robotics and Automation*. Washington DC. pp. 2638–2643.

Efimov, D. V. (2005). Dynamical adaptive synchronization. In: *Proc. 44th IEEE Conf. on Decision and Control and European Control Conf.* Sevilla, Spain.

Egerstedt, M., X. Hu and A. Stotsky (2001). Control of mobile platforms using a virtual vehicle approach. *IEEE Trans. on Automatic Control* **46**(11), 1777 – 1782.

Encarnacao, P. and A. Pascoal (2001). Combined trajectory tracking and path following: An application to the coordinated control of autonomous marine craft. In: *Proc. 40th IEEE Conf. on Decision and Control*. Orlando, FL, USA. pp. 964 – 969.

FAS (1999). Underway replenishment (UNREP) - navy ships. [online]. Available: http://www.fas.org/man/dod-101/sys/ship/unrep.htm. [2003, November 4th].

Fax, J. A. and R. M. Murray (2004). Information flow and cooperative control of vehicle formations. *IEEE Trans. on Automatic Control* **49**(9), 1455 – 1466.

Flakstad Ihle, I.-A. (2006). Coordinated Control of Marine Craft. PhD thesis. Norwegian University of Science and Technology, Department of Engineering Cybernetics. Trondheim, Norway.

Fossen, T. I. (2002). *Marine Control Systems: Guidance, Navigation, and Control of Ships, Rigs and Underwater Vehicles*. Marine Cybernetics. Trondheim, Norway.

Fossen, T. I. and S. P. Berge (1997). Nonlinear vectorial backstepping design for global exponential tracking of marine vessels in the presence of actuator dynamics. In: *Proc. 36th IEEE Conf. on Decision and Control*. pp. 4237 – 4242.

Fradkov, A.L., S.V. Gusev and I.A. Makarov (1991). Robust speed-gradient adaptive control algorithms for manipulators and mobile robots. In: *Proc. 30th IEEE Conf. on Decision and Control*. Brighton, England. pp. 3095 – 3096.

Frenet, J. (1847). Sur les fonctions qui servent à déterminer l'attraction des sphéroides quelconques. Programme d'une thèse sur quelque propriétés des courbes à double courbure. PhD thesis. Université Toulouse, France.

Frezza, R. (1999). Path following for air vehicles in coordinated flight. In: *Proc. 1999 IEEE/ASME Int. Conf. on Advanced Intelligent Mechatronics*. Atlanta, GA, USA. pp. 884 – 889.

Frezza, R. (2000). How much does one need to know about a curve in order to follow it with a nonholonomic vehicle?. In: *Proc. Int. Conf. on Mathematical Theory of Networks and Systems*. Perpignan, France. MTNS 2000.

Ghabcheloo, R., A. Pascoal, C. Silvestre and I. Kaminer (2006). *Group Coordination and Cooperative Control*. Chap. Coordinated Path Following Control of Multiple Vehicles Subject to Bidirectional Communication Constraints. Vol. 336 of *Lecture Notes in Control and Information Systems*. Springer Verlag. Tromsø, Norway.

Girard, A. R. and J. K. Hedrick (2001). Dynamic positioning of ships using nonlinear dynamic surface control. In: *Proc. 5th IFAC Symp. on Nonlinear Control Systems*. Saint-Petersburg, Russia. pp. 1134 – 1140.

Giulietti, F., L. Pollini and M. Innocenti (2000). Autonomous formation flight. *IEEE Control Systems Magazine* pp. 34 – 44.

Goldstein, H., C. Poole and J. Safko (2002). *Classical Mechanics*. 3rd ed.. Pearson Education, Addison Wesley.

Gusev, S.V., I.A. Makarov, I.E. Paromtchik, V.A. Yakubovich and C. Laugier (1998). Adaptive motion control of a noholonomic vehicle. In: *Proc. 1998 IEEE Int. Conf. on Robotics and Automation*. pp. 3285 – 3290.

Harre, I. (2000). AIS adding new quality to VTS systems. *Journal of Navigation* **53**(3), 527 – 539.

Hauser, J. and R. Hindman (1995). Manoeuvre regulation from trajectory tracking: Feedback linearizable systems. In: *Proc. IFAC Symp. on Nonlinear Control Systems Design*. Lake Tahoe, CA, USA. pp. 595 – 600.

Hill, D. D. (1989). Underway replenishment. [online]. Available: http://www.globalsecurity.org/military/library/report/1989/HDD.htm. [2004, July 4th].

Hills, J.W. and J.F. Jensen (1998). Telepresence technology in medicine: Principles and applications. *Proc. IEEE* **86**, 569 – 580.

Hu, X., D.F. Alarcon and T. Gustavi (2003). Sensor-based navigation coordination for mobile robots. In: *Proc. 42nd IEEE Conf. on Decision and Control, 2003.*. pp. 6375 – 6380.

Huijberts, H. J. C. and H. Nijmeijer (2001). An observer view on synchronization. Lecture notes.

Huijberts, H. J. C., H. Nijmeijer and R. Willems (2000). Regulation and controlled synchronization for complex dynamical systems. *Int. Journal of Robust Nonlinear Control* **10**, 363–377.

Huygens, C. (1673). *Horoloquium Oscilatorium*. Paris, France.

Justh, E. W. and P. S. Krishnaprasad (2004). Equilibria and steering laws for planar formations. *Systems & Control Letters* (52), 25 – 38.

Kang, W. and H. Yeh (2002). Co-ordinated attitude control of mulit-satellite systems. *Int. Journal of Robust and Nonlinear Control* **12**, 185 – 205.

Kelly, R. (1993). A simple set-point robot controller by using only position measurements. In: *Proc. IFAC World Congress*. Vol. 6. Sydney, Australia. pp. 173 – 176.

Khalil, H. K. (1996). *Nonlinear Systems*. 2nd ed.. Prentice Hall. New Jersey.

Khalil, H. K. (2002). *Nonlinear Systems*. 3rd ed.. Prentice Hall. New Jersey.

Khatib, O. (1987). A unified approach for motion and force control of robot manipulators: The operational space formulation. *IEEE Journal of Robotics and Automation* **RA-3**(1), 43 – 53.

Knudsen, K. A. (2004). Experimental verification of a control system for rendezvous operations. Technical report. Department of Engineering Cybernetics, Norwegian University of Science and Technology. Norway.

Kocarev, L., K. S. Halle, K. Eckert and L. O. Chua (1992). Experimental demonstration of secure communication via chaotic synchronization. *Int. Journal of Bifurcations and Chaos* **2**, 709 – 713.

Kristiansen, R., A. Loría, A. Chaillet and P. J. Nicklasson (2006). *Group Coordination and Cooperative Control*. Chap. Output Feedback Control of Relative Translation in a Leader-Follower Spacecraft Formation, pp. 131 – 151. Vol. 336 of *Lecture Notes in Control and Information Systems*. Springer Verlag. Tromsø, Norway.

Krogstad, T. R. and J. T. Gravdahl (2006). *Group Coordination and Cooperative Control*. Chap. Coordinated Attitude Control of Satellites in Formation, pp. 153 – 170. Vol. 336 of *Lecture Notes in Control and Information Systems*. Springer Verlag. Tromsø, Norway.

Kumon, M., R. Washiazaki, J. Sato, R. Kohzava, I. Mizumoto and Z. Iwai (2002). Controlled synchronization of two 1-DOF coupled oscillators. In: *Proc. 15th IFAC World Congress on Automatic Control*. Barcelona, Spain.

Kyrkjebø, E. and K. Y. Pettersen (2003). Ship replenishment using synchronization control. In: *Proc. 6th IFAC Conf. on Manoeuvring and Control of Marine Craft*. Girona, Spain. pp. 286–291.

Kyrkjebø, E. and K. Y. Pettersen (2005*a*). Output synchronization control of Euler-Lagrange systems with nonlinear damping terms. In: *Proc. 44th IEEE Conf. on Decision and Control and European Control Conf.* Sevilla, Spain. pp. 4951 – 4957.

Kyrkjebø, E. and K. Y. Pettersen (2005*b*). Tracking from a synchronization perspective. In: *Proc. 17th IMACS World Congress on Scientific Computation, Applied Mathematics and Simulation*. Paris, France.

Kyrkjebø, E. and K. Y. Pettersen (2006*a*). Leader-follower dynamic synchronization of surface vessels. In: *Proc. 7th IFAC Conference on Manoeuvring and Control of Marine Craft*. Lisboa, Portugal.

Kyrkjebø, E. and K. Y. Pettersen (2006*b*). A virtual vehicle approach to output synchronization control. In: *Proc. 45th Conf. on Decision and Control*. San Diego, USA.

Kyrkjebø, E. and K. Y. Pettersen (2007*a*). Leader-follower synchronization control of Euler-Lagrange systems with leader position measurements only. In: *Proc. Mediterranean Conf. on Control and Automation*. Athens, Greece. *Submitted*.

Kyrkjebø, E. and K. Y. Pettersen (2007*b*). Operational space synchronization of two robot manipulators through a virtual velocity estimate. In: *Proc. 46th Conf. on Decision and Control*. Submitted. New Orleans, USA. *Submitted*.

Kyrkjebø, E., E. Panteley, A. Chaillet and K. Y. Pettersen (2006*a*). *Group Coordination and Cooperative Control*. Chap. A Virtual Vehicle Approach to Underway Replenishment, pp. 171 – 189. Vol. 336 of *Lecture Notes in Control and Information Systems*. Springer Verlag. Tromsø, Norway.

Kyrkjebø, E., K. Y. Pettersen, M. Wondergem and H. Nijmeijer (2006*b*). Output synchronization control of ship replenishment operations: Theory and experiments. *Control Engineering Practice* **15**(6), 741 – 755.

Kyrkjebø, E., M. Wondergem, K. Y. Pettersen and H. Nijmeijer (2004). Experimental results on synchronization control of ship rendezvous operations. In: *Proc. IFAC Conf. on Control Applications in Marine Systems*. Ancona, Italy. pp. 453 – 458.

Lawton, J. R. and R. W. Beard (2002). Synchronized multiple spacecraft rotations. *Automatica* (38), 1359 – 1364.

Lefeber, A. A. J. (2000). Tracking Control of Nonlinear Mechanical Systems. PhD thesis. University of Twente, The Netherlands.

Leonard, N.E. and E. Fiorelli (2001). Virtual leaders, artificial potentials and coordinated control of groups. In: *Proc. 40th IEEE Conf. on Decision and Control*. Vol. 3. Orlando, FL, USA. pp. 2968 – 2973.

Levine, J. (2004). On the synchronization of a pair of independent windshield wipers. *IEEE Trans. on Control Systems Technology* **12**(5), 787 – 795.

Lindegaard, K.-P. (2003). Acceleration Feedback in Dynamic Positioning. PhD thesis. Norwegian University of Science and Technology, Department of Engineering Cybernetics. Trondheim, Norway.

Lissaman, P. B. S and C. A. Shollenberger (1970). Formation flight of birds. *Science* **168**, 1003 – 1005.

Lizarralde, F., J.T. Wen and L. Hsu (1995). Quaternion-based coordinated control of a subsea mobile manipulator with only position measurements. In: *Proc. 34th IEEE Conf. on Decision and Control*. New Orleans, LA USA. pp. 3996 – 4001.

Loría, A. (1996). Commande par retour de sortie des système Euler-Lagrange/On Output Feedback Control of Euler-Lagrange Systems. PhD thesis. Université de Technologie de Compiègne. France.

Loría, A. and E. Panteley (2006). *Advanced Topics in Control Theory*. Chap. Stability, told by its developers. Lecture Notes in Control and Information Systems. Springer Verlag. London.

Loría, A. and K. Melhem (2002). Position feedback global tracking control of el systems: A state transformation approach. *IEEE Trans. on Automatic Control* **47**(5), 841 – 847.

Loría, A. and R. Ortega (1995). On tracking control of rigid and flexible joints robots. *Appl Math Comp Sci, special issue on Mathematical Methods in Robotics* **5**(2), 101 – 113.

Loría, A., H. Nijmeijer and O. Egeland (1998). Controlled synchronization of two pendula: A cascaded structure approach. *IEEE Trans. on Control Systems Technology*.

Loría, A., R. Kelly, R. Ortega and V. Santibanez (1997). On global output feedback regulation of euler-lagrange systems with bounded inputs. *IEEE Trans. on Automatic Control* **42**(8), 1138 – 1143.

Luenberger, D. G. (1971). An introduction to observers. *IEEE Trans. on Automatic Control* **16**(6), 596 – 602.

Marino, R. and P. Tomei (1995). *Nonlinear Control Design: Geometric, Adaptive and Robust*. Prentice Hall.

Martinez, D. R. and E. Klinghammer (1970). The behavior of the whale *Orcinus orca*: a review of the literature. *Z. Tierpsychol* **27**, 828 – 839.

May, R. M. (1979). Flight formations in geese and other birds. *Nature* **282**, 778 – 780.

McTaggart, K., D. Cumming, C. C. Hsiung and L. Li (2002). Seakeeping of two ships in close proximity. *Ocean Engineering*.

Miller, M.O. and J. A. Combs (1999). The next underway replenishment system. *Naval Engineers Journal* **111**(2), 45–55.

Naylor, A. W. and G. R. Sell (1982). *Linear Operator Theory in Engineering and Science*. Vol. 40 of *Applied Mathematical Sciences*. 2nd ed.. Springer-Verlag, Inc.. New York.

Newton, Sir I. (1687). *Philosophiae Naturalis Principia Mathematica*.

Nijmeijer, H. and A. Rodriguez-Angeles (2003). *Synchronization of Mechanical Systems*. Vol. 46. World Scientific Series on Nonlinear Science, Series A.

Nijmeijer, H. and I.M.Y. Mareels (1997). An observer looks at synchronization. *IEEE Trans. on Circuits and Systems I 44* pp. 882 – 890.

Nijmeijer, H. and T. I. Fossen (1999). *New Directions in Nonlinear Observer Design*. Vol. 244 of *Lecture Notes in Control and Information Sciences*. Springer Verlag. London.

Nijmeijer, Henk and Arjan Van der Schaft (1990). *Nonlinear Dynamical Control Systems*. Springer-Verlag. New York.

NROTC (2003). Underway replenishment. [online]. Available: http://www.unc.edu/depts/nrotc/classes/classinfo /NAVS52/12 Underway Replenishment.ppt. [2003, March 13].

Øgren, P., E. Fiorelli and N. E. Leonard (2004). Cooperative control of mobile sensor networks: Adaptive gradient climbing in a distributed environment. *IEEE Trans. on Automatic Control* **49**(8), 1292 – 1302.

Olfati-Saber, R. and R.M. Murray (2002). Graph rigidity and distributed formation stabilization of multi-vehicle systems. In: *Proc. 41st IEEE Conf. on Decision and Control*. Vol. 3. pp. 2965 – 2971.

Ortega, R., A. Loria, R. Kelly and L. Praly (1994). On passivity-based output feedback global stabilization of euler-lagrange systems. In: *Proc. 33rd IEEE Conf. on Decision and Control*. Buena Vista, FL USA. pp. 381 – 386.

Ortega, R. and M. W. Spong (1989). Adaptive motion control of rigid robots: A tutorial. *Automatica* **25**(6), 877 – 888.

Paden, B. and R. Panja (1988). Globally asymptotically stable "pd +" controller for robot manipulators. *Int. Journal of Control* **47**(6), 1697 – 1712.

Paley, D., N. Leonard and R. Sepulchre (2004). Collective motion: Bistability and trajectory tracking. In: *Proc. 43rd IEEE Conf. on Decision and Control*. Paradise Island, The Bahamas.

Parkinson, B. W. and J. J. (Eds.) Spilker (1995). *Global Positioning System: Theory and Applications*. American Institute of Aeronautics and Astronautics, Inc.. Washington, DC, USA.

Partridge, B. L. (1982). The structure and function of fish schools. *Scientific American* **246**, 114 – 123.

Partridge, B. L. and T.J. Pitcher (1979). Evidence against a hydrodynamic function for fish schools. *Nature* **279**, 418 – 419.

Paulsen, M. J. and O. Egeland (1995). Tracking controller and velocity observer for mechanical systems with nonlinear damping terms. In: *Proc. 3rd European Control Conf*. Rome, Italy.

Pettersen, K. Y. and H. Nijmeijer (1998). Tracking control of an underactuated surface vessel. In: *Proc. 37th IEEE Conf. on Decision and Control*. Tampa, FL, USA. pp. 4561 – 4566.

Pogromsky, Yu. A. and H. Nijmeijer (1998). Observer based robust synchronization of dynamical systems. *Int. Journal on Bifurcation and Chaos* pp. 2243–2254.

Refsnes, J. E., A. J. Sørensen and K. Y. Pettersen (2006). Robust observer design for underwater vehicles. In: *Proc. 2006 IEEE Int. Conf. on Control Applications*. Munich, Germany. pp. 313 – 319.

Rodriguez-Angeles, A. (2002). Synchronization of Mechanical Systems. PhD thesis. Eindhoven University of Technology. The Netherlands.

Rodriguez-Angeles, A. and H. Nijmeijer (2001). Coordination of two robot manipulators based on position measurements only. *Int. Journal of Control* **74**, 1311 – 1323.

Sagatun, S. I. (1992). Modeling and Control of Underwater Vehicles: A Lagrangian Approach. PhD thesis. Norwegian University of Science and Technology, Department of Engineering Cybernetics. Trondheim, Norway.

Sakaguchi, T., A. Uno and S. Tsugawa (1999). Inter-vehicle communications for merging control. In: *Proc. IEEE Int. Vehicle Electronics Conf*. pp. 365 – 370.

Salichs, M.A., E.A. Puente, D. Gachet and L. Moreno (1991). Trajectory tracking for a mobile robot - an application to contour following. In: *Proc. Int. Conf. on Industrial Electronics, Control and Instrumentation*. Kobe. pp. 1067 – 1070.

Sciavicco, L. and B. Siciliano (1996). *Modeling and Control of Robot Manipulators*. McGraw-Hill Series in Electrical and Computer Engineering. McGraw-Hill.

Seiler, P., A. Pant and J. K. Hedrick (2004). String instabilities in formation flight: Limitations due to integral constraints. *Journal of Dynamic Systems, Measurement, and Control* **126**(4), 873 – 879.

Sepulchre, R., D. A. Paley and N. E. Leonard (2006). *Group Coordination and Cooperative Control*. Chap. Group Coordination and Coopertive Control of Steered Particles in the Plane, pp. 217 – 232. Vol. 336 of *Lecture Notes in Control and Information Systems*. Springer Verlag. Tromsø, Norway.

Skjetne, R. (2005). The Maneuvering Problem. PhD thesis. Dep. of Engineering Cybernetics, Norwegian University of Science and Technology.

Skjetne, R., I.-A. F. Ihle and T. I. Fossen (2003). Formation control by synchronizing multiple maneuvering systems. In: *Proc. 6th IFAC Conf. on Manoeuvring and Control of Marine Craft*. Girona, Spain. pp. 280–285.

Skjetne, R., Ø. N. Smogeli and T. I. Fossen (2004*a*). A nonlinear ship maneuvering model: Identification and adaptive control with experiments for a model ship. *Modeling, Identification and Control* **25**(1), 3 – 27.

Skjetne, R., Ø. Smogeli and T. I. Fossen (2004*b*). Modelling, identification and adaptive maneuvering of cybership II: A complete design with experiments. In: *Proc. IFAC Conf. on Control Applications in Marine Systems*. Ancona, Italy. pp. 203 – 208.

Skjetne, R., S. Moi and T. I. Fossen (2002). Nonlinear formation control of marine craft. In: *Proc. 41st IEEE Conf. On Decision and Control*. Las Vegas, Nevada. pp. 1699–1704.

Skjetne, R., T. I. Fossen and P. Kokotovic (2004*c*). Robust output maneuvering for a class of nonlinear systems. *Automatica* **40**(3), 373 – 383.

Slotine, J.-J. E. and W. Li (1987*a*). Adaptive manipulator control a case study. In: *Proc. 1987 IEEE Int. Conf. on Robotics and Automation*. pp. 1392 – 1400.

Slotine, J.-J. E. and W. Li (1987*b*). On the adaptive control of robot manipulators. *The Int. Journal of Robotics Research* **6**(3), 49 – 59.

Slotine, J.-J. E. and W. Li (1991). *Applied Nonlinear Control*. Prentice Hall. New Jersey, US.

Sørensen, A. J. (2002). Marine cybernetics: Modelling and control. Technical report. Marine Technology Centre. Trondheim, Norway.

Spong, M. W. and M. Vidyasagar (1989). *Robot Dynamics and Control*. John Wiley & Sons. New York.

Stilwell, D. J. and B. E. Bishop (2000). Platoons of underwater vehicles; communication, feedback and decentralized control. *IEEE Control Systems Magazine* pp. 45 – 52.

Stilwell, D. J. and B. E. Bishop (2002). Redundant manipulator techniques for path planning and control of a platoon of autonomous vehicles. In: *Proc. 41st IEEE Conf. Decision and Control*. Las Vegas, USA. pp. 2093 – 2098.

Strand, J. P. (1999). Nonlinear Position Control Systems Design for Marine Vessels. PhD thesis. Norwegian University of Science and Technology, Department of Engineering Cybernetics. Trondheim, Norway.

Swaroop, D., J.K. Hedrick, P.P. Yip and J.C Gerdes (2000). Dynamic surface control for a class of nonlinear systems. *IEEE Transactions on Automatic Control* **45**(10), 1893 – 1899.

Tan, K.K., S. Y. Lim, S. Huang, H.F Dou and T. S. Giam (2004). Coordinated motion control of moving gantry stages for precision applications based on an observer-augmented composite controller. *IEEE Trans. on Control Systems Technology* **12**(6), 984 – 989.

Teel, A. R. (1996). A nonlinear small gain theorem for the analysis of control systems with saturation. *IEEE Trans. on Automatic Control* **41**(9), 1256 – 1270.

Treherne, J. E. and W. A. Foster (1981). Group transmission of predator avoidance in a marine insect: the Trafalgar Effect. *Animal Behaviour* **29**, 911 – 917.

Uhrin, J. and G.J. Thaler (1976). Design of a nonlinear speed control system. In: *Proc. IEEE Milwaukee Symp. on Automatic Computation and Control*. New York. pp. 179 – 183.

USCG (2005). Uscg navigation center: The automatic identification system. [online]. Available: http://www.navcen.uscg.gov/enav/ais/default.htm. [2006, December 28th].

Wang, P. K. C., A. Sparks and S. Banda (1996). Co-ordination and control of multiple microspacecraft moving in formation. *The Journal ofthe Astronautical Sciences* **44**, 315 – 355.

Weisstein, Eric (2006). From *MathWorld*–a wolfram web resource. [online]. Available: http://mathworld.wolfram.com/. [2006, February 8th].

Wen, J. T. and D. S. Bayard (1988). New class of control laws for robotic manipulators. *Int. Journal of Control* **47**(5), 1361 – 1385.

Wiehs, D. (1973). Hydromechanics of fish schooling. *Nature* **241**, 290 – 291.

Wondergem, M. (2004). Experimental results on synchronization control of ship rendezvous operations. Technical report. Eindhoven University of Technology. The Netherlands.

Xi, Ning and T. J. Tarn (2000). Stability analysis of non-time referenced internet-based telerobotic systems. *Robotics and Autonomous Systems* **32**, 172 – 178.

Yamaguchi, H., T. Arai and G. Beni (2001). A distributed control scheme for multiple robotic vehicles to make group formations. *Robotics and Autonomous Systems* **36**, 125 – 147.

Young, N. (1988). *An introduction to Hilbert space*. Cambridge Mathematical Textbooks.

Appendix A

Mathematical tools and definitions

This appendix summarizes some of the preliminaries vital in order to understand the mathematics involved in some of the chapters in this thesis. The section is merely a summary of other people's ideas, definitions, theorems and corollaries that can mostly be found in standard textbooks, but are nevertheless included to make the thesis more self-contained.

A.1 Notation and terminology

This section defines the notation of sets, functions and terms used frequently throughout the thesis. It is worth mentioning that a *Proposition* (statement which is to be proved) that has been proved through a *Proof* (rigorous mathematical argument) is called a *Theorem* (statement that can be demonstrated to be true), sometimes using a *Lemma* (short theorem used in proving a larger theorem). A *Corollary* is an immediate consequence of a result already proved, and usually state more complicated theorems in a language simpler to use and apply. This is different from an *Axiom* or *Postulate* (proposition regarded as self-evidently true without proof) or *Conjecture* and *Hypothesis* (propositions which are consistent with known data, but have neither been verified nor shown to be false) (cf. Weisstein (2006)). A *Definition* is the creation of a new mathematical object, while a *Property* is used to characterize and distinguish between objects.

The system considered in this appendix is

$$\dot{\mathbf{x}} = f(t, \mathbf{x}), \quad \mathbf{x}(t_0) = \mathbf{x}_0. \tag{A.1}$$

Definition A.1 ***(Lipschitz Condition)*** *The Lipschitz condition is*

$$||f(t, \mathbf{x}) - f(t, \mathbf{y})|| \leq L_U ||\mathbf{x} - \mathbf{y}|| \tag{A.2}$$

for all $(t, \mathbf{x})$ *and* $(t, \mathbf{y})$ *in some neighbourhood of* $(t_0, \mathbf{x}_0)$ *for any norm* $||\cdot||$.

This guarantees *existence* and *uniqueness* of solutions of Equation (A.1), and that the system has a bounded derivative f'; the slope of the function f is limited by L_U. Lipschitz is stronger than *continuity*, but weaker than *continuous differentiability*.

Definition A.2 *A class* C^k*, or* ***smooth****, function has continuous partial derivatives up to and including order k; a* C^0 *function is a continuous function. If defined for all k, then it is* C^∞.

Thus, the following relation holds

$$C^1 \Rightarrow L \Rightarrow C^0 \tag{A.3}$$

where L is a Lipschitz system.

Definition A.3 ***(Analytic)*** *An* ***analytic*** *function in $\mathscr{R}$ is expandable in a power series in its arguments about each point in $\mathscr{R}$ (Nijmeijer and der Schaft (1990)); in effect, the complex function is* ***complex differentiable*** *at every point in $\mathscr{R}$, and thus infinitely differentiable in $\mathscr{R}$ (Weisstein (2006)).*

This is a stronger result than smooth ($\in C^\infty$).

Definition A.4 *A class $\mathscr{K}$* ***continuous*** *function $\alpha : [0,a) \to [0,\infty)$ is* ***strictly increasing*** *and $\alpha(0) = 0$.*

Definition A.5 *A class $\mathscr{K}_\infty$* ***continuous*** *function $\alpha : [0,\infty) \to [0,\infty)$ is* ***strictly increasing*** *and $\alpha(0) = 0$, and $\alpha(t) \to \infty$ as $t \to \infty$.*

Definition A.6 *A class $\mathscr{KL}$* ***continuous*** *function $\beta : [0,a) \times [0,\infty) \to [0,\infty)$ is* ***strictly increasing*** *(class $\mathscr{K}$) for each fixed $t \geq 0$, and decreasing for each fixed $\mathbf{x} > 0$, and $\beta(\mathbf{x},t) \to 0$ as $t \to \infty$.*

A class $\mathscr{K}$ function f starts in zero, and increases forever with $f' > 0$. The gain function γ of Teel (1996) is only continuous and nondecreasing, and thus allows for the identically zero function or $\gamma(s) = min\{s,1\}$ for $s \geq 0$. A class $\mathscr{K}_\infty$ is defined for all positive values of t, and is unbounded. A class $\mathscr{KL}$ function is strictly increasing (class $\mathscr{K}$ for each fixed t, and decreasing for each $\mathbf{x}$, while $\lim_{t\to\infty} \beta(\mathbf{x},t) = 0$ (Khalil (2002)).

Definition A.7 ***(Supremum)*** *The supremum* $\sup S$ *is the* ***least upper bound*** *of a set S, defined as a* ***unique*** *quantity M such that no member of the set exceeds M, but if ε is any positive quantity, however small, there is a member that exceeds $M - \varepsilon$.*

Supremum is the least upper bound of a set; that is, the uniquely largest value contained in a set. Note that $\sup \mathscr{R}$ does not exist. Conversely, infimum is the greatest lower bound of a set; denoted $\inf \mathscr{R}$ which neither exists.

Definition A.8 ***(Autonomous)*** *An autonomous or time invariant system does not depend on time* ***explicitly****, and is invariant to time shifts in the time origin, since changing the time variable from t to $\tau = t - a$ does not change the right-hand side of $\dot{\mathbf{x}} = f(\mathbf{x})$ (Khalil (2002)). If the system is not autonomous, it is said to be* ***nonautonomous*** *or time varying.*

Note that a system that exhibits influence from a time varying unknown or known signal is also time varying. If a disturbance depends on time, e.g. waves, or the reference for the system changes with time, the system is nonautonomous. Since the leader position variable $\mathbf{x}_m(t)$ in this thesis depends on time, the leader system is nonautonomous or time varying.

Definition A.9 ***(Affine system)*** *A* ***input-linear*** *or* ***affine*** *system is described as*

$$\dot{\mathbf{x}}(t) = f(\mathbf{x}(t)) + \sum_{i=1}^{m} g_i(\mathbf{x}(t))\, u_i(t) \tag{A.4}$$

together with some output relation only depending on the state. The functions f and g_i are smooth (Nijmeijer and der Schaft (1990)).

The distinctive feature is that the control $u = (u_1, u_2, ..., u_m)$ appears *linearly* (or better, affine) in the differential equation. Also, a homogeneous equation is e.g. $\mathbf{G}u = 0$, while a non-homogeneous equation is $\mathbf{G}u + b = 0$, where a system of non-homogeneous linear equations is said to be affine.

Definition A.10 ***(Exogenous variable)*** *A prescribed know control function (Nijmeijer and der Schaft (1990)).*

Definition A.11 ***(Manifold)*** *A manifold is a Euclidean (Cartesian) topological space (Weisstein (2006)).*

This can be compared to seeing the Earth as flat, although it is a sphere. A manifold is an object which is nearly "flat" on small scales.

Definition A.12 ***(Diffeomorphism)*** *A diffeomorphism is a map between manifolds which is differentiable and has a differentiable inverse (Weisstein (2006)); both ϕ and ϕ^{-1} are smooth maps (Marino and Tomei (1995)), and ϕ is a diffeomorphism if it is smooth and its inverse ϕ^{-1} exists and is smooth.*

Definition A.13 ***(Vector field)*** *A vector field f in $U \subset R$ is a function which assigns to each point $p \in U$ a vector f_p (Marino and Tomei (1995)).*

One can think of this as a vector $f(x)$ emanating from every point x (Slotine and Li (1991)).

Definition A.14 ***(Lie derivatives)*** *If f is a vector field on U and h is a smooth function on U, then $f(h)$ is a smooth function on U defined as*

$$f(h)(p) = \sum_{i=1}^{n} f_i(p) \left(\frac{\partial h}{\partial x_i} \right)(p) \tag{A.5}$$

and called the ***Lie derivative*** *of the function h along the vector field f, and denoted $L_f h$ (Marino and Tomei (1995)).*

A.2 Norms and inequalities

Or rather tips and tricks? While linear control is often straightforward and – in lack of a better word – linear, nonlinear control is all about the tips and tricks one learns through experience and practice, and through reading other people's work. We state here some of the "tools-of-the-trade" that have proven themselves useful in the topic of nonlinear control. We begin with the definition of an *inner product*.

Definition A.15 (Naylor and Sell (1982)) *Let X be a vector (linear) space, complex or real. An inner product on X is a mapping that associates with each pair of vectors $\mathbf{x}, \mathbf{y}$ a number, real or complex, denoted by $(\mathbf{x}, \mathbf{y})$, that satisfies*

$$(\mathbf{x} + \mathbf{y}, \mathbf{z}) = (\mathbf{x}, \mathbf{z}) + (\mathbf{y}, \mathbf{z}); \quad \textit{(Additivity)} \tag{A.6}$$

$$(\lambda \mathbf{x}, \mathbf{y}) = \lambda (\mathbf{x}, \mathbf{y}); \quad \textit{(Homogenity)} \tag{A.7}$$

$$(\mathbf{x}, \mathbf{y}) = (\mathbf{x}, \mathbf{y}); \quad \textit{(Symmetry)} \tag{A.8}$$

$$(\mathbf{x}, \mathbf{x}) > 0, \textit{when } \mathbf{x} \neq 0. \quad \textit{(Positive Definiteness)} \tag{A.9}$$

The abstract inner product $(\mathbf{x},\mathbf{y})$ has its definition for vectors in $\mathbb{R}^n$ as $\mathbf{x}^T\mathbf{y}$.

Definition A.16 (Young (1988)) *The norm $\|\cdot\|$ of a vector $\mathbf{x}$ in an inner product space X is defined to be*

$$\|\mathbf{x}\| = (\mathbf{x},\mathbf{x})^{\frac{1}{2}} = \sqrt{(\mathbf{x},\mathbf{x})} \tag{A.10}$$

Definition A.17 (Young (1988)) *An inner product space (or pre-Hilbert space) is a pair $(X,(\cdot,\cdot))$, where X is a vector space and $(\cdot,\cdot)$ is an inner product on X.*

An important inequality was stated by the German mathematician Herman Amadeus Schwartz (1843–1921) as

Theorem A.1 (Schwartz Inequality (Naylor and Sell (1982))) *Let $(\mathbf{x},\mathbf{y})$ be an inner product on a vector space X. Then, for $\|\mathbf{x}\|$ and $\|\mathbf{y}\|$ as defined in (A.10),*

$$|(\mathbf{x},\mathbf{y})| \leq \|\mathbf{x}\|\,\|\mathbf{y}\|, \tag{A.11}$$

with equality iff $\mathbf{x}$ and $\mathbf{y}$ are linearly independent. This is sometimes known as the Cauchy-Schwartz inequality (Young (1988)) or the Buniakowsky Inequality, and is a special case of the Holder Inequality (Naylor and Sell (1982)) with $p = q = 2$.

Remark A.1 *It follows from Schwartz Inequality in Theorem A.1 that (Naylor and Sell (1982))*

$$\|\mathbf{x}+\mathbf{y}\|^2 \leq (\|\mathbf{x}\| + \|\mathbf{y}\|)^2 \tag{A.12}$$

and also that

$$0 \leq (\mathbf{x}-\lambda\mathbf{y},\mathbf{x}-\lambda\mathbf{y}) = \|\mathbf{x}\|^2 - \frac{|(\mathbf{x},\mathbf{y})|^2}{\|\mathbf{y}\|^2} \tag{A.13}$$

Theorem A.2 (Parallelogram Law (Young (1988))) *For vectors $\mathbf{x}$ and $\mathbf{y}$ in an inner product space X*

$$\|\mathbf{x}+\mathbf{y}\|^2 + \|\mathbf{x}-\mathbf{y}\|^2 = 2\|\mathbf{x}\|^2 + 2\|\mathbf{y}\|^2 \tag{A.14}$$

Theorem A.3 (Triangle Inequality (Weisstein (2006))) *For vectors $\mathbf{x}$ and $\mathbf{y}$ in an inner product space X*

$$\|\mathbf{x}\| - \|\mathbf{y}\| \leq \|\mathbf{x}+\mathbf{y}\| \leq \|\mathbf{x}\| + \|\mathbf{y}\| \tag{A.15}$$

Theorem A.4 (Young's Inequality (Weisstein (2006))) *For $\mathbf{x}$ and $\mathbf{y}$ and any real $p > 1$, we have*

$$\|\mathbf{xy}\| \leq \frac{1}{p}\|\mathbf{x}\|^p + \frac{p-1}{p}\|\mathbf{y}\|^{\frac{p}{p-1}} \tag{A.16}$$

Corollary A.1 *It follows from Young's Inequality in Theorem A.4 that for $p = 2$*

$$\|\mathbf{xy}\| \leq \frac{1}{2}\|\mathbf{x}\|^2 + \frac{1}{2}\|\mathbf{y}\|^2 \tag{A.17}$$

We can state the following proposition very useful in Lyapunov analysis

Proposition A.1 *For $\mathbf{x},\mathbf{y} > 0$, $\lambda > 0$ and $p > 1, q > 0$ we have*

$$\mathbf{x}^{p-1}\mathbf{y}^q \leq \lambda\mathbf{x}^p + \frac{\mathbf{y}^{pq}}{\lambda^{p-1}} \tag{A.18}$$

Note also that we have

Proposition A.2 *For* $\lambda > 0$,

$$\mathbf{xy} \leq \frac{\lambda}{2}\mathbf{x}^2 + \frac{1}{2\lambda}\mathbf{y}^2 \tag{A.19}$$

or as norms

$$\|\mathbf{xy}\| \leq \frac{\lambda}{2}\|\mathbf{x}\|^2 + \frac{1}{2\lambda}\|\mathbf{y}\|^2 \tag{A.20}$$

which agrees with Corollary A.1 for $\lambda = 1$.

Appendix B

Reference kinematics

A reference vehicle at a position relative to the leader is designed to provide a reference for the leader-follower coordinated synchronization control law of the follower. The position of the reference vehicle is uniquely determined by the position and heading of the leader vehicle through (2.56) as

$$\mathbf{x}_r = \mathbf{x}_m + \mathbf{J}(\mathbf{x}_m)\,\mathbf{d}_r^m \tag{B.1}$$

In this section, we develop the differential kinematics for a general reference vehicle model with an arbitrary heading assignment, i.e. the heading angle of the reference vehicle ψ_r can be different from the heading angle of the leader vessel ψ_m.

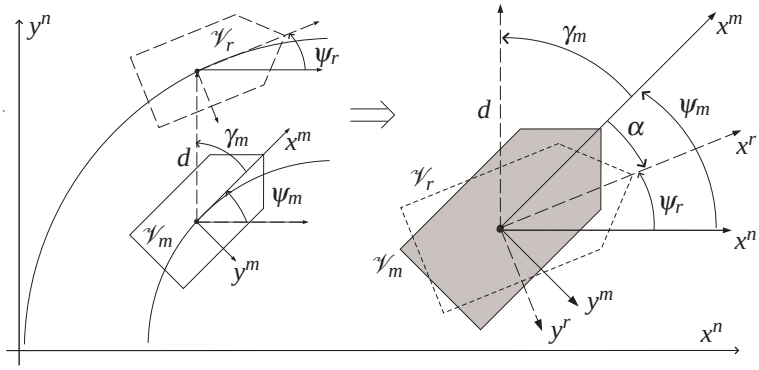

Figure B.1: The reference vehicle $\mathscr{V}_r$ at the distance d and angle γ_m from the leader $\mathscr{V}_m$.

The differential kinematic model of the leader vehicle $\mathscr{V}_m$ with the position/heading vector $\mathbf{x}_m$ can be written as

$$\dot{\mathbf{x}}_m = \mathbf{J}(\mathbf{x}_m)\,\nu_m \tag{B.2}$$

and for a fully actuated 3DOF vehicle takes the form

$$\begin{aligned} \dot{x}_m &= u_m \cos\psi_m - v_m \sin\psi_m \\ \dot{y}_m &= u_m \sin\psi_m + v_m \cos\psi_m \\ \dot{\psi}_m &= r_m \end{aligned} \tag{B.3}$$

Let d (= const) be the desired (required) distance between the leader and the follower vessel, and γ_m (= const) the angle between the body x-axis of the leader and the vector d, positive counterclockwise, as shown in Figure B.1. We can calculate the "position" χ of the leader in the body frame[1] of the leader

$$\chi_m^m = \mathbf{J}^T(\mathbf{x}_m)\,\mathbf{x}_m \tag{B.4}$$

Superscripts denote the reference frames, and subscripts denote which vehicle position and heading vector that is described. We will use χ to denote position/heading in the body frames with no immediate physical interpretation, and $\mathbf{x}$ as the position/heading of vehicles in the NED frame. Thus, $\mathbf{x}_m$ is the position vector of the leader vehicle m in the NED frame, while χ_m^m is the position vector of the leader vehicle in its own body frame. We have that the position vector of the reference vehicle in the NED frame can be written as

$$\mathbf{x}_r = \mathbf{J}(\mathbf{x}_r)\,\chi_r^r \tag{B.5}$$

The position vector of the reference vehicle in the body frame of the leader can be written as

$$\chi_r^m = \chi_m^m + \mathbf{d}_r^m \tag{B.6}$$

where

$$\mathbf{d}_r^m = \begin{bmatrix} d\cos\gamma_m \\ d\sin\gamma_m \\ \alpha \end{bmatrix} \tag{B.7}$$

with the distance d and rotation α separating the two frames. The angle α is the desired difference in heading between the leader vessel and the reference vehicle, and defined in the body frame. Expressed in the NED frame, (B.6) becomes

$$\mathbf{x}_r = \mathbf{J}(\mathbf{x}_m)\,\chi_r^m = \mathbf{x}_m + \mathbf{J}(\mathbf{x}_m)\,\mathbf{d}_r^m \tag{B.8}$$

Taking the time derivative through

$$\dot{\mathbf{J}}(\mathbf{x}_m) = \mathbf{J}(\mathbf{x}_m)\,\mathbf{S}(r_m) \tag{B.9}$$

where $\mathbf{S}(r_m)$ is the skew-symmetric matrix

$$\mathbf{S}(r_m) = \begin{bmatrix} 0 & -r_m & 0 \\ r_m & 0 & 0 \\ 0 & 0 & 0 \end{bmatrix} \tag{B.10}$$

we get

$$\dot{\mathbf{x}}_r = \dot{\mathbf{x}}_m + \mathbf{J}(\mathbf{x}_m)\,\mathbf{S}(r_m)\,\mathbf{d}_r^m + \mathbf{J}(\mathbf{x}_m)\,\dot{\mathbf{d}}_r^m \tag{B.11}$$

[1] Note that the position of the vehicle in the body-frame does not have any immediate physical interpretation as the integral $\int_0^t v^b dt$, but its mathematical representation is still valid.

In component form this is equivalent to

$$\dot{x}_r = u_m \cos\psi_m - v_m \sin\psi_m - dr_m \cos\gamma_m \sin\psi_m - dr_m \sin\gamma_m \cos\psi_m \tag{B.12a}$$
$$\dot{y}_r = u_m \sin\psi_m + v_m \cos\psi_m + dr_m \cos\gamma_m \cos\psi_m - dr_m \sin\gamma_m \sin\psi_m \tag{B.12b}$$
$$\dot{\psi}_r = r_m + \dot{\alpha} \tag{B.12c}$$

By investigating (B.12a) more closely, we can rewrite this as

$$\begin{aligned}\dot{x}_r &= \cos\psi_m (u_m - dr_m \sin\gamma_m) - \sin\psi_m (v_m + dr_m \cos\gamma_m) \\ &= \sqrt{(u_m - dr_m \sin\gamma_m)^2 + (v_m + dr_m \cos\gamma_m)^2}\,(\cos\psi_m \cos\alpha - \sin\psi_m \sin\alpha)\end{aligned} \tag{B.13}$$

where we have

$$\cos\alpha = \frac{u_m - dr_m \sin\gamma_m}{\sqrt{(u_m - dr_m \sin\gamma_m)^2 + (v_m + dr_m \cos\gamma_m)^2}} \tag{B.14}$$

$$\sin\alpha = \frac{v_m - dr_m \cos\gamma_m}{\sqrt{(u_m - dr_m \sin\gamma_m)^2 + (v_m + dr_m \cos\gamma_m)^2}} \tag{B.15}$$

Similarly, we can rewrite (B.12b) as

$$\begin{aligned}\dot{y}_r &= \sin\psi_m (u_m - dr_m \sin\gamma_m) + \cos\psi_m (v_m + dr_m \cos\gamma_m) \\ &= \sqrt{(u_m - dr_m \sin\gamma_m)^2 + (v_m + dr_m \cos\gamma_m)^2}\,(\sin\psi_m \cos\alpha + \cos\psi_m \sin\alpha)\end{aligned} \tag{B.16}$$

and by using that

$$\tan\alpha = \frac{\sin\alpha}{\cos\alpha} = \frac{u_m - dr_m \sin\gamma_m}{v_m + dr_m \cos\gamma_m} \tag{B.17}$$

we get

$$\dot{\alpha} = \frac{(\dot{u}_m - d\dot{r}_m \sin\gamma_m)(v_m + dr_m \cos\gamma_m) - (u_m - dr_m \sin\gamma_m)(\dot{v}_m + d\dot{r}_m \cos\gamma_m)}{(v_m + dr_m \cos\gamma_m)^2} \cos^2\alpha \tag{B.18}$$

The differential kinematic relationship for the reference vehicle can thus be written as

$$\begin{aligned}\dot{x}_r &= \sqrt{(u_m - dr_m \sin\gamma_m)^2 + (v_m + dr_m \cos\gamma_m)^2}\cos(\psi_m + \alpha) \\ \dot{y}_r &= \sqrt{(u_m - dr_m \sin\gamma_m)^2 + (v_m + dr_m \cos\gamma_m)^2}\sin(\psi_m + \alpha) \\ \dot{\psi}_r &= \dot{\psi}_m + \dot{\alpha}\end{aligned} \tag{B.19}$$

Appendix C

Details of Proofs

C.1 The Observer-controller approach

C.1.1 Proof of Theorem 3.1

Consider the Lyapunov function candidate

$$V_1(\bar{\mathbf{s}},\bar{\mathbf{e}}) = \frac{1}{2}\bar{\mathbf{s}}^T\mathbf{M}(\mathbf{x})\bar{\mathbf{s}} + \bar{\mathbf{e}}^T\mathbf{K}_p\bar{\mathbf{e}} \tag{C.1}$$

and differentiate along the closed-loop trajectories while using (3.18) and (3.19) to get

$$\dot{V}_1(\bar{\mathbf{s}},\bar{\mathbf{e}}) = -\bar{\mathbf{s}}^T\left(\mathbf{D}(\mathbf{x},\dot{\mathbf{x}}) + \mathbf{K}_d\right)\bar{\mathbf{s}} - \bar{\mathbf{e}}^T\boldsymbol{\Lambda}^T\mathbf{K}_p\bar{\mathbf{e}} + \bar{\mathbf{s}}^T\mathbf{M}(\mathbf{x})\mathbf{L}_2\tilde{\mathbf{e}} + \tilde{\mathbf{e}}^T\mathbf{L}_1^T\mathbf{K}_p\bar{\mathbf{e}} \tag{C.2}$$

Furthermore, consider the Lyapunov function candidate

$$V_2(\tilde{\mathbf{s}},\tilde{\mathbf{e}}) = \frac{1}{2}\tilde{\mathbf{s}}^T\mathbf{P}_1\tilde{\mathbf{s}} + \frac{1}{2}\tilde{\mathbf{e}}^T\mathbf{L}_2\tilde{\mathbf{e}} - \tilde{\mathbf{e}}^T\mathbf{P}_2\tilde{\mathbf{s}} \tag{C.3}$$

where $\mathbf{P}_{1,2}$ are positive definite constants to be defined. Equation (C.3) is positive definite for

$$\mathbf{P}_{1,m}\mathbf{L}_{2,m} > \mathbf{P}_{2,M}^2 \tag{C.4}$$

Differentiating along the closed-loop trajectories and using (3.14) yields

$$\dot{V}_2(\tilde{\mathbf{s}},\tilde{\mathbf{e}}) = -\tilde{\mathbf{s}}^T\mathbf{P}_2\tilde{\mathbf{s}} - \tilde{\mathbf{e}}^T\mathbf{L}_2\left(\boldsymbol{\Lambda}+\mathbf{L}_1\right)\tilde{\mathbf{e}} + \tilde{\mathbf{e}}^T\left(\mathbf{L}_2 + \left(\boldsymbol{\Lambda}+\mathbf{L}_1\right)^T\mathbf{P}_2\right)\tilde{\mathbf{s}} + \left(\tilde{\mathbf{s}}^T\mathbf{P}_1 - \tilde{\mathbf{e}}^T\mathbf{P}_2\right)\dot{\tilde{\mathbf{s}}} \tag{C.5}$$

Combining (C.1) and (C.3) in

$$V(\bar{\mathbf{s}},\bar{\mathbf{e}},\tilde{\mathbf{s}},\tilde{\mathbf{e}}) = \frac{1}{2}\bar{\mathbf{s}}^T\mathbf{M}(\mathbf{x})\bar{\mathbf{s}} + \bar{\mathbf{e}}^T\mathbf{K}_p\bar{\mathbf{e}} + \frac{1}{2}\tilde{\mathbf{s}}^T\mathbf{P}_1\tilde{\mathbf{s}} + \frac{1}{2}\tilde{\mathbf{e}}^T\mathbf{L}_2\tilde{\mathbf{e}} - \tilde{\mathbf{e}}^T\mathbf{P}_2\tilde{\mathbf{s}} \tag{C.6}$$

and defining the shorthand

$$\mathbf{L}_3 := \boldsymbol{\Lambda} + \mathbf{L}_1 \tag{C.7}$$

the derivative along the closed-loop trajectories becomes

$$\begin{aligned}\dot{V}(\bar{\mathbf{s}},\bar{\mathbf{e}},\tilde{\mathbf{s}},\tilde{\mathbf{e}}) = &-\frac{1}{2}\begin{bmatrix}\bar{\mathbf{s}}\\ \bar{\mathbf{e}}\end{bmatrix}^T \overbrace{\begin{bmatrix}\mathbf{D}(\mathbf{x},\dot{\mathbf{x}})+\mathbf{K}_d & 0\\ 0 & \boldsymbol{\Lambda}^T\mathbf{K}_p\end{bmatrix}}^{\mathbf{Q}_1}\begin{bmatrix}\bar{\mathbf{s}}\\ \bar{\mathbf{e}}\end{bmatrix}\\ &-\frac{1}{2}\begin{bmatrix}\tilde{\mathbf{s}}\\ \tilde{\mathbf{e}}\end{bmatrix}^T \overbrace{\begin{bmatrix}2\mathbf{P}_2 & -\left(\mathbf{L}_2+\mathbf{L}_3^T\mathbf{P}_2\right)\\ -\left(\mathbf{L}_2+\mathbf{L}_3^T\mathbf{P}_2\right) & \frac{2}{\varepsilon}\mathbf{L}_2\mathbf{L}_3\end{bmatrix}}^{\mathbf{Q}_2}\begin{bmatrix}\tilde{\mathbf{s}}\\ \tilde{\mathbf{e}}\end{bmatrix}\\ &-\frac{1}{2}\begin{bmatrix}\bar{\mathbf{s}}\\ \tilde{\mathbf{e}}\end{bmatrix}^T \overbrace{\begin{bmatrix}\mathbf{D}(\mathbf{x},\dot{\mathbf{x}})+\mathbf{K}_d & -\mathbf{M}(\mathbf{x})\mathbf{L}_2\\ -\mathbf{M}(\mathbf{x})\mathbf{L}_2 & \frac{\varepsilon-1}{\varepsilon}\mathbf{L}_2\mathbf{L}_3\end{bmatrix}}^{\mathbf{Q}_3}\begin{bmatrix}\bar{\mathbf{s}}\\ \tilde{\mathbf{e}}\end{bmatrix}\\ &-\frac{1}{2}\begin{bmatrix}\bar{\mathbf{e}}\\ \tilde{\mathbf{e}}\end{bmatrix}^T \overbrace{\begin{bmatrix}\boldsymbol{\Lambda}^T\mathbf{K}_p & -\mathbf{L}_1^T\mathbf{K}_p\\ -\mathbf{L}_1^T\mathbf{K}_p & \frac{\varepsilon-1}{\varepsilon}\mathbf{L}_2\mathbf{L}_3\end{bmatrix}}^{\mathbf{Q}_4}\begin{bmatrix}\bar{\mathbf{e}}\\ \tilde{\mathbf{e}}\end{bmatrix}+\beta(\cdot)\end{aligned} \tag{C.8}$$

where the constant parameter $\varepsilon > 1$ is not used in the controller, but only as a parameter in the stability proof. The perturbation term $\beta(\cdot)$ is given as

$$\beta(\cdot) = \left(\tilde{\mathbf{s}}^T\mathbf{P}_1 - \tilde{\mathbf{e}}^T\mathbf{P}_2\right)\dot{\tilde{\mathbf{s}}} \tag{C.9}$$

The term $\mathbf{Q}_1$ is positive definite trivially with symmetric positive definite gains $\boldsymbol{\Lambda}$, $\mathbf{K}_p$ and $\mathbf{K}_d$, and the conditions for positive definiteness for $\mathbf{Q}_3$ and $\mathbf{Q}_4$ are

$$\mathbf{Q}_3 > 0 \quad \Leftrightarrow \quad \frac{\frac{\varepsilon-1}{\varepsilon}\left(\mathbf{D}_m+\mathbf{K}_{p,m}\right)\mathbf{L}_{3,m}}{\mathbf{M}_M^2\mathbf{L}_{2,M}} > 1 \tag{C.10}$$

$$\mathbf{Q}_4 > 0 \quad \Leftrightarrow \quad \frac{\frac{\varepsilon-1}{\varepsilon}\boldsymbol{\Lambda}_m^T\mathbf{L}_{2,m}\mathbf{L}_{3,m}}{\mathbf{L}_{1,M}^2\mathbf{K}_{p,M}} > 1 \tag{C.11}$$

To analyze positive definiteness of $\mathbf{Q}_2$, we must first analyse the perturbing term $\beta(\cdot)$ of (C.9). We recognize that

$$\tilde{\mathbf{s}} = \hat{\dot{\mathbf{y}}} - \dot{\mathbf{y}} \tag{C.12}$$

and use (3.3b) to write

$$\beta(\cdot) = \left(\tilde{\mathbf{s}}^T\mathbf{P}_1 - \tilde{\mathbf{e}}^T\mathbf{P}_2\right)\left(\dot{\hat{\dot{\mathbf{x}}}}_m - \ddot{\mathbf{x}}_m\right) \tag{C.13}$$

Choosing the estimation update law as

$$\dot{\hat{\dot{\mathbf{x}}}}_m = -\left(\mathbf{M}^{-1}(\mathbf{x})\mathbf{K}_p + \mathbf{L}_2\right)\tilde{\mathbf{e}} \tag{C.14}$$

and using (3.16) so that

$$\dot{\hat{\dot{\mathbf{y}}}} = \dot{\hat{\dot{\mathbf{x}}}}_m - \boldsymbol{\Lambda}\dot{\hat{\mathbf{e}}} = -\left(\mathbf{M}^{-1}(\mathbf{x})\mathbf{K}_p + \mathbf{L}_2\right)\tilde{\mathbf{e}} - \boldsymbol{\Lambda}\left(\hat{\mathbf{s}} - \boldsymbol{\Lambda}\hat{\mathbf{e}} + \mathbf{L}_1\tilde{\mathbf{e}}\right) \tag{C.15}$$

Inserting this in the observer (3.15) as

$$\dot{\hat{\mathbf{s}}} - \dot{\hat{\dot{\mathbf{y}}}} = \dot{\tilde{\mathbf{s}}} - \dot{\tilde{\mathbf{s}}} = \left(\mathbf{M}^{-1}(\mathbf{x})\mathbf{K}_p + \mathbf{L}_2\right)\tilde{\mathbf{e}} \tag{C.16}$$

gives the velocity and acceleration estimates used in the controller as

$$\widehat{\dot{\mathbf{y}}} = \dot{\mathbf{x}} - \widehat{\mathbf{s}} \tag{C.17}$$

$$\widehat{\ddot{\mathbf{y}}} = -\mathbf{\Lambda}\left(\widehat{\mathbf{s}} - \mathbf{\Lambda}\widehat{\mathbf{e}} + \mathbf{L}_1\widetilde{\mathbf{e}}\right) \tag{C.18}$$

The perturbation term can now be written using (C.14) as

$$\beta(\cdot) = -\widetilde{\mathbf{s}}^T\mathbf{P}_1\left(\mathbf{M}^{-1}(\mathbf{x})\mathbf{K}_p + \mathbf{L}_2\right)\widetilde{\mathbf{e}} + \widetilde{\mathbf{e}}^T\mathbf{P}_2\left(\mathbf{M}^{-1}(\mathbf{x})\mathbf{K}_p + \mathbf{L}_2\right)\widetilde{\mathbf{e}} - \left(\widetilde{\mathbf{s}}^T\mathbf{P}_1 - \widetilde{\mathbf{e}}^T\mathbf{P}_2\right)\ddot{\mathbf{x}}_m \tag{C.19}$$

Remark C.1 *Note that the acceleration of the leader $\ddot{\mathbf{x}}_m$ is present in (C.19) as non-vanishing disturbance, and thus the origin of the closed-loop error space is no longer an equilibrium.*

Equation (C.19) can be written as

$$\beta(\cdot) = \beta_Q(\cdot) + \beta_N(\cdot) \tag{C.20}$$

where

$$\beta_Q(\cdot) = -\widetilde{\mathbf{s}}^T\mathbf{P}_1\left(\mathbf{M}^{-1}(\mathbf{x})\mathbf{K}_p + \mathbf{L}_2\right)\widetilde{\mathbf{e}} + \widetilde{\mathbf{e}}^T\mathbf{P}_2\left(\mathbf{M}^{-1}(\mathbf{x})\mathbf{K}_p + \mathbf{L}_2\right)\widetilde{\mathbf{e}} \tag{C.21}$$

and

$$\beta_N(\cdot) = -\left(\widetilde{\mathbf{s}}^T\mathbf{P}_1 - \widetilde{\mathbf{e}}^T\mathbf{P}_2\right)\ddot{\mathbf{x}}_m \tag{C.22}$$

The terms of $\beta_Q(\cdot)$ can be incorporated in $\mathbf{Q}_2$ to give a new matrix $\mathbf{Q}_{2,\beta}$ defined as

$$\mathbf{Q}_{2,\beta} = \begin{bmatrix} 2\mathbf{P}_2 & \mathbf{P}_1\left(\mathbf{M}^{-1}(\mathbf{x})\mathbf{K}_p - \mathbf{L}_2\right) - \left(\mathbf{L}_2 + \mathbf{L}_3^T\mathbf{P}_2\right) \\ \mathbf{P}_1\left(\mathbf{M}^{-1}(\mathbf{x})\mathbf{K}_p - \mathbf{L}_2\right) - \left(\mathbf{L}_2 + \mathbf{L}_3^T\mathbf{P}_2\right) & \frac{2}{\varepsilon}\mathbf{L}_2\mathbf{L}_3 - \mathbf{P}_2\left(\mathbf{M}^{-1}(\mathbf{x})\mathbf{K}_p + \mathbf{L}_2\right) \end{bmatrix} \tag{C.23}$$

Choosing for simplicity $\mathbf{P}_1 = \mathbf{I}$, and we have that $\mathbf{Q}_{2,\beta}$ is positive definite for the choice of $\mathbf{P}_2 = \mathbf{L}_1$ when

$$\mathbf{Q}_{2,\beta} > 0 \Leftrightarrow \frac{\frac{4}{\varepsilon}\mathbf{L}_{2,m}\mathbf{L}_{3,m} - \mathbf{L}_{1,M}^2\left(\mathbf{M}_m^{-1}\mathbf{K}_{p,M} + \mathbf{L}_{2,M}\right)}{\left[\left(\mathbf{M}_m^{-1}\mathbf{K}_{p,M} - \mathbf{L}_{3,m}^T\mathbf{L}_{1,m}\right)\right]^2} > 1 \tag{C.24}$$

where the positive definiteness can be ensured through tuning the filter gain $\mathbf{\Lambda}$ of (3.2) in (C.7).

The perturbing term of (3.26) can thus be bounded as

$$\beta_N(\cdot) \leq \left(\|\widetilde{\mathbf{s}}\| + \mathbf{L}_{1,M}\|\widetilde{\mathbf{e}}\|\right)A_M \tag{C.25}$$

with the ultimate bound δ in Definition 2.1 as

$$\delta = \sqrt{1 + \mathbf{L}_{1,M}}\sqrt{A_M} \tag{C.26}$$

C.1.2 Proof of Theorem 3.2

By inserting the controller (3.33) into the model (2.27) under Assumption 3.1, and by subtracting $\mathbf{M}(\mathbf{x})\ddot{\mathbf{x}}_m + \mathbf{C}(\mathbf{x},\dot{\mathbf{x}})\dot{\mathbf{x}}_m + \mathbf{D}(\mathbf{x})\dot{\mathbf{x}}_m$ on each side, the closed-loop error dynamics of the controller becomes

$$\begin{aligned}\mathbf{M}(\mathbf{x})\ddot{\mathbf{e}} + \mathbf{C}\left(\mathbf{x},\widehat{\dot{\mathbf{x}}}\right)\dot{\mathbf{e}} + \mathbf{D}(\mathbf{x})\dot{\mathbf{e}} + \mathbf{K}_d\dot{\mathbf{e}} + \mathbf{K}_p\mathbf{e} &= \mathbf{M}(\mathbf{x})\left(\widehat{\ddot{\mathbf{x}}}_m - \ddot{\mathbf{x}}_m\right) \\ &+ \mathbf{C}\left(\mathbf{x},\widehat{\dot{\mathbf{x}}}\right)\widehat{\dot{\mathbf{x}}}_m - \mathbf{C}(\mathbf{x},\dot{\mathbf{x}})\dot{\mathbf{x}}_m + \mathbf{D}(\mathbf{x})\widehat{\dot{\mathbf{x}}}_m - \mathbf{D}(\mathbf{x})\dot{\mathbf{x}}_m - \mathbf{K}_d\left(\widehat{\dot{\mathbf{e}}} - \dot{\mathbf{e}}\right)\end{aligned} \tag{C.27}$$

The Coriolis and Centripetal terms can be collected as

$$\mathbf{C}\left(\mathbf{x},\widehat{\dot{\mathbf{x}}}\right)\widehat{\dot{\mathbf{x}}}_m - \mathbf{C}(\mathbf{x},\dot{\mathbf{x}})\dot{\mathbf{x}}_m = \mathbf{C}(\mathbf{x},\dot{\mathbf{x}})\left(\widetilde{\dot{\mathbf{e}}} - 2\widetilde{\dot{\mathbf{x}}}\right) + \mathbf{C}\left(\mathbf{x},\widehat{\dot{\mathbf{x}}}\right)\left(\widetilde{\dot{\mathbf{x}}} + \dot{\mathbf{e}} - \widetilde{\dot{\mathbf{e}}}\right) \tag{C.28}$$

from Property **P2**, and due to

$$\widehat{\dot{\mathbf{x}}}_m - \dot{\mathbf{x}}_m = \widetilde{\dot{\mathbf{e}}} - \widetilde{\dot{\mathbf{x}}}, \qquad \widehat{\ddot{\mathbf{x}}}_m - \ddot{\mathbf{x}}_m = \frac{d}{dt}\left(\widetilde{\dot{\mathbf{e}}} - \widetilde{\dot{\mathbf{x}}}\right) \tag{C.29}$$

the resulting error dynamics from (C.27) is

$$\begin{aligned}\mathbf{M}(\mathbf{x})\ddot{\mathbf{e}} + \mathbf{C}\left(\mathbf{x},\widehat{\dot{\mathbf{x}}}\right)\dot{\mathbf{e}} + \mathbf{D}(\mathbf{x})\dot{\mathbf{e}} + \mathbf{K}_d\dot{\mathbf{e}} + \mathbf{K}_p\mathbf{e} &= \mathbf{M}(\mathbf{x})\frac{d}{dt}\left(\widetilde{\dot{\mathbf{e}}} - \widetilde{\dot{\mathbf{x}}}\right) \\ + \mathbf{C}(\mathbf{x},\dot{\mathbf{x}})\left(\widetilde{\dot{\mathbf{e}}} - 2\widetilde{\dot{\mathbf{x}}}\right) + \mathbf{C}\left(\mathbf{x},\widehat{\dot{\mathbf{x}}}\right)\left(\widetilde{\dot{\mathbf{x}}} + \dot{\mathbf{e}} - \widetilde{\dot{\mathbf{e}}}\right) + \mathbf{D}(\mathbf{x})\left(\widetilde{\dot{\mathbf{e}}} - \widetilde{\dot{\mathbf{x}}}\right) + \mathbf{K}_d\widetilde{\mathbf{e}}\end{aligned} \tag{C.30}$$

From the observers of (3.34) and (3.36), the estimation error dynamics becomes

$$\frac{d}{dt}\widetilde{\mathbf{e}} = \widetilde{\dot{\mathbf{e}}} - \mathbf{L}_1\widetilde{\mathbf{e}} \tag{C.31a}$$

$$\frac{d}{dt}\widetilde{\dot{\mathbf{e}}} = \mathbf{M}(\mathbf{x})^{-1}\left[\mathbf{C}\left(\mathbf{x},\widetilde{\dot{\mathbf{x}}}\right)\widetilde{\dot{\mathbf{x}}} - 2\mathbf{C}(\mathbf{x},\dot{\mathbf{x}})\widetilde{\dot{\mathbf{x}}} - \mathbf{D}(\mathbf{x})\widetilde{\dot{\mathbf{x}}} - 2\mathbf{K}_p\widetilde{\mathbf{e}}\right] + \mathbf{L}_2\widetilde{\mathbf{x}} - 2\mathbf{L}_2\widetilde{\mathbf{e}} - \ddot{\mathbf{x}}_m \tag{C.31b}$$

and

$$\frac{d}{dt}\widetilde{\mathbf{x}} = \widetilde{\dot{\mathbf{x}}} - \mathbf{L}_{\mathbf{x}1}\widetilde{\mathbf{x}} \tag{C.32a}$$

$$\frac{d}{dt}\widetilde{\dot{\mathbf{x}}} = \mathbf{M}(\mathbf{x})^{-1}\left[\mathbf{C}\left(\mathbf{x},\widetilde{\dot{\mathbf{x}}}\right)\widetilde{\dot{\mathbf{x}}} - 2\mathbf{C}(\mathbf{x},\dot{\mathbf{x}})\widetilde{\dot{\mathbf{x}}} - \mathbf{D}(\mathbf{x})\widetilde{\dot{\mathbf{x}}} - \mathbf{K}_p\widetilde{\mathbf{e}}\right] - \mathbf{L}_2\widetilde{\mathbf{e}} \tag{C.32b}$$

By defining a new set of coordinates

$$\begin{aligned}\bar{\mathbf{e}} &= \mathbf{e} - \mathbf{x}_m & \widetilde{\mathbf{x}}_m &= \widetilde{\mathbf{e}} - \widetilde{\mathbf{x}} \\ \dot{\bar{\mathbf{e}}} &= \dot{\mathbf{e}} - \dot{\mathbf{x}}_m & \dot{\widetilde{\mathbf{x}}}_m &= \widetilde{\dot{\mathbf{e}}} - \widetilde{\dot{\mathbf{x}}} - \mathbf{L}_1\widetilde{\mathbf{x}}_m\end{aligned} \tag{C.33}$$

the synchronization closed-loop error dynamics of (C.30) can be rewritten as

$$\begin{aligned}\mathbf{M}(\mathbf{x})\ddot{\bar{\mathbf{e}}} + \mathbf{C}(\mathbf{x},\dot{\mathbf{x}})\dot{\bar{\mathbf{e}}} + \mathbf{D}(\mathbf{x})\dot{\bar{\mathbf{e}}} + \mathbf{K}_d\dot{\bar{\mathbf{e}}} + \mathbf{K}_p\bar{\mathbf{e}} &= \mathbf{M}(\mathbf{x})\mathbf{L}_1\dot{\widetilde{\mathbf{x}}}_m + \mathbf{D}(\mathbf{x})\mathbf{L}_1\widetilde{\mathbf{x}}_m - \mathbf{K}_p \\ - \mathbf{C}(\mathbf{x},\dot{\mathbf{x}})\left(\dot{\widetilde{\mathbf{x}}} + \mathbf{L}_1(\widetilde{\mathbf{x}} - \widetilde{\mathbf{x}}_m)\right) + \mathbf{C}\left(\mathbf{x},\dot{\widetilde{\mathbf{x}}} + \mathbf{L}_1\widetilde{\mathbf{x}}\right)(\dot{\widetilde{\mathbf{e}}} - \mathbf{L}_1\widetilde{\mathbf{x}}_m) + \mathbf{K}_d\left(\dot{\widetilde{\mathbf{x}}} + \mathbf{L}_1(\widetilde{\mathbf{x}} + \widetilde{\mathbf{x}}_m)\right)\widetilde{\mathbf{x}}_m\end{aligned} \tag{C.34}$$

and the estimation closed-loop error dynamics of (C.31) and (C.32) as

$$\ddot{\widetilde{\mathbf{x}}}_m = -\mathbf{M}(\mathbf{x})^{-1}\mathbf{K}_p(\widetilde{\mathbf{x}} + \widetilde{\mathbf{x}}_m) - \mathbf{L}_1\dot{\widetilde{\mathbf{x}}}_m - \mathbf{L}_2\widetilde{\mathbf{x}}_m - \ddot{\mathbf{x}}_m \tag{C.35}$$

$$\begin{aligned}\ddot{\widetilde{\mathbf{x}}} = &-\mathbf{M}(\mathbf{x})^{-1}\mathbf{K}_p(\widetilde{\mathbf{x}} + \widetilde{\mathbf{x}}_m) - \mathbf{L}_1\dot{\widetilde{\mathbf{x}}} - \mathbf{L}_2(\widetilde{\mathbf{x}} + \widetilde{\mathbf{x}}_m) \\ &+ \mathbf{M}(\mathbf{x})^{-1}\left[\mathbf{C}\left(\mathbf{x},\dot{\widetilde{\mathbf{x}}} + \mathbf{L}_1\widetilde{\mathbf{x}}\right) - 2\mathbf{C}(\mathbf{x},\dot{\mathbf{x}}) + \mathbf{D}(\mathbf{x})\right]\left(\dot{\widetilde{\mathbf{x}}} + \mathbf{L}_1\widetilde{\mathbf{x}}\right)\end{aligned} \tag{C.36}$$

Stability analysis

Consider the vector $\zeta \in \mathbb{R}^{6n}$ as defined in (3.45) and take the Lyapunov function

$$V(\zeta) = \frac{1}{2}\zeta^T \mathbf{P}(\zeta)\,\mathbf{y} \tag{C.37}$$

where $\mathbf{P}(\zeta) = \mathbf{P}(\zeta)^T$ is given by

$$\mathbf{P}(\zeta) = \begin{bmatrix} \varepsilon_0 \begin{bmatrix} \mathbf{M}(\mathbf{x}) & \lambda_0 \mathbf{M}(\mathbf{x}) \\ \lambda_0 \mathbf{M}(\mathbf{x}) & \mathbf{K}_p + \lambda_0 \mathbf{K}_d \end{bmatrix} & 0 & 0 \\ 0 & \begin{bmatrix} \mathbf{I} & \mu(\widetilde{\mathbf{x}}_d)\mathbf{I} \\ \mu(\widetilde{\mathbf{x}}_d)\mathbf{I} & \mathbf{L}_2 \end{bmatrix} & 0 \\ 0 & 0 & \begin{bmatrix} \mathbf{I} & \gamma(\widetilde{\mathbf{x}})\mathbf{I} \\ \gamma(\widetilde{\mathbf{x}})\mathbf{I} & \mathbf{L}_2 \end{bmatrix} \end{bmatrix} \tag{C.38}$$

where $\mathbf{I} \in \mathbb{R}^{n\times n}$ is the identity matrix, $\varepsilon_0, \lambda_0, \mu_0, \gamma_0 \in \mathbb{R}$ are positive constants

$$\lambda_0 > 0, \qquad \mu_0 > 0, \qquad \gamma_0 > 0, \qquad \varepsilon_0 > 0 \tag{C.39}$$

to be determined, and $\mu(\widetilde{\mathbf{x}}_d)$ and $\gamma(\widetilde{\mathbf{x}})$ are defined by

$$\mu(\widetilde{\mathbf{x}}_d) = \frac{\mu_0}{1+\|\widetilde{\mathbf{x}}_d\|}, \qquad \gamma(\widetilde{\mathbf{x}}) = \frac{\gamma_0}{1+\|\widetilde{\mathbf{x}}\|} \tag{C.40}$$

Sufficient conditions for positive definiteness of $\mathbf{P}(\zeta)$ are

$$\mathbf{K}_{d,m} > \lambda_0 \mathbf{M}_M, \qquad \mathbf{L}_{2,m} > \max\left\{\mu_0^2, \gamma_0^2\right\} \tag{C.41}$$

where $\mathbf{M}_M$ is the largest eigenvalue of $\mathbf{M}$. By choosing the minimum eigenvalues of the gain matrices $\mathbf{L}_{1,m}, \mathbf{L}_{2,m}, \mathbf{K}_{p,m}, \mathbf{K}_{d,m}$ to satisfy a set of lower bounds, and together with the boundedness of $\mu(\widetilde{\mathbf{x}}_m)$ and $\gamma(\widetilde{\mathbf{x}})$, this implies that there exists constants $\mathbf{P}_m$ and $\mathbf{P}_M$ such that

$$\frac{1}{2}\mathbf{P}_m \|\zeta\|^2 \le V(\zeta) \le \frac{1}{2}\mathbf{P}_M \|\zeta\|^2 \tag{C.42}$$

The time derivative of (3.47) along the error dynamics of (3.40 - 3.42) yields

$$\dot{V}(\zeta) = -\zeta^T \mathbf{Q}(\zeta)\,\zeta + \beta(\zeta, \dot{\mathbf{x}}, \ddot{\mathbf{x}}_m) \tag{C.43}$$

where

$$\begin{aligned} \beta(\zeta, \dot{\mathbf{x}}, \ddot{\mathbf{x}}_m) &= \varepsilon_0 \left[\dot{\widetilde{\mathbf{e}}}^T + \lambda_0 \widetilde{\mathbf{e}}^T\right] \mathbf{C}\left(\mathbf{x}, \dot{\widetilde{\mathbf{x}}} + \mathbf{L}_1 \widetilde{\mathbf{x}}\right) \left[\dot{\widetilde{\mathbf{e}}} - L_1 \widetilde{\mathbf{x}}_m\right] - \varepsilon_0 \lambda_0 \widetilde{\mathbf{e}}^T \mathbf{C}(\mathbf{x}, \dot{\mathbf{x}})\,\dot{\widetilde{\mathbf{e}}} \\ &- \varepsilon_0 \left[\dot{\widetilde{\mathbf{e}}}^T + \lambda_0 \widetilde{\mathbf{e}}^T\right] \mathbf{C}(\mathbf{x}, \dot{\mathbf{x}}) \left[\dot{\widetilde{\mathbf{x}}} + \mathbf{L}_1(\widetilde{\mathbf{x}} - \widetilde{\mathbf{x}}_m)\right] - \varepsilon_0 \left[\dot{\widetilde{\mathbf{e}}}^T + \lambda_0 \widetilde{\mathbf{e}}^T\right] \mathbf{D}(\mathbf{x}) \left[\dot{\widetilde{\mathbf{e}}} - \mathbf{L}_1 \widetilde{\mathbf{x}}_m\right] \\ &+ \left[\dot{\widetilde{\mathbf{x}}}^T + \gamma \widetilde{\mathbf{x}}^T\right] \mathbf{M}^{-1}(\mathbf{x}) \left[\mathbf{C}\left(\mathbf{x}, \dot{\widetilde{\mathbf{x}}} + \mathbf{L}_1 \widetilde{\mathbf{x}}\right) - 2\mathbf{C}(\mathbf{x}, \dot{\mathbf{x}}) - \mathbf{D}(\mathbf{x})\right] \left[\dot{\widetilde{\mathbf{x}}} + L_1 \widetilde{\mathbf{x}}\right] \\ &+ \varepsilon_0 \lambda_0 \widetilde{\mathbf{e}}^T \dot{\mathbf{M}}(\mathbf{x})\,\dot{\widetilde{\mathbf{e}}} + \dot{\gamma} \widetilde{\mathbf{x}}^T \dot{\widetilde{\mathbf{x}}} + \dot{\mu} \widetilde{\mathbf{x}}_m^T \dot{\widetilde{\mathbf{x}}}_m - \left[\dot{\widetilde{\mathbf{x}}}_m^T + \mu \widetilde{\mathbf{x}}_m^T\right] \ddot{\mathbf{x}}_m \end{aligned} \tag{C.44}$$

and $\mathbf{Q}(\zeta) = \mathbf{Q}(\zeta)^T$ is given by

$$\mathbf{Q} = \begin{bmatrix} \mathbf{Q}_{11} & \mathbf{Q}_{12} & \mathbf{Q}_{13} \\ \mathbf{Q}_{12}^T & \mathbf{Q}_{22} & \mathbf{Q}_{23} \\ \mathbf{Q}_{13}^T & \mathbf{Q}_{23}^T & \mathbf{Q}_{33} \end{bmatrix} \tag{C.45}$$

with the block matrices

$$\mathbf{Q}_{11} = \varepsilon_0 \begin{bmatrix} \mathbf{K}_m - \lambda_0 \mathbf{M} & 0 \\ 0 & \lambda_0 \mathbf{K}_p \end{bmatrix} \tag{C.46}$$

$$\mathbf{Q}_{12} = \frac{\varepsilon_0}{2} \begin{bmatrix} -\mathbf{M}(\mathbf{x})\mathbf{L}_1 & \mathbf{K}_p - \mathbf{K}_m\mathbf{L}_1 \\ -\lambda_0 \mathbf{M}(\mathbf{x})\mathbf{L}_1 & \lambda_0 (\mathbf{K}_p - \mathbf{K}_m\mathbf{L}_1) \end{bmatrix} \tag{C.47}$$

$$\mathbf{Q}_{13} = \frac{\varepsilon_0}{2} \begin{bmatrix} -\mathbf{K}_m & -\mathbf{K}_m\mathbf{L}_1 \\ -\lambda_0 \mathbf{K}_m & -\lambda_0 \mathbf{K}_m\mathbf{L}_1 \end{bmatrix} \tag{C.48}$$

$$\mathbf{Q}_{22} = \begin{bmatrix} \mathbf{L}_1 - \mu_0 \mathbf{I} & \frac{1}{2}\left(\mathbf{M}^{-1}(\mathbf{x})\mathbf{K}_p + \mu \mathbf{L}_1\right) \\ \frac{1}{2}\left(\mathbf{M}^{-1}(\mathbf{x})\mathbf{K}_p + \mu \mathbf{L}_1\right)^T & \mu\left(\mathbf{M}^{-1}(\mathbf{x})\mathbf{K}_p + \mathbf{L}_2\right) \end{bmatrix} \tag{C.49}$$

$$\mathbf{Q}_{23} = \begin{bmatrix} 0 & \frac{1}{2}\mathbf{M}^{-1}(\mathbf{x})\mathbf{K}_p \\ \frac{1}{2}\left(\mathbf{M}^{-1}\mathbf{K}_p + \mathbf{L}_2\right) & \frac{1}{2}\left((\mu+\gamma)\mathbf{M}^{-1}\mathbf{K}_p + \gamma \mathbf{L}_2\right) \end{bmatrix} \tag{C.50}$$

$$\mathbf{Q}_{33} = \begin{bmatrix} \mathbf{L}_1 - \gamma \mathbf{I} & \frac{1}{2}\left(\mathbf{M}^{-1}(\mathbf{x})\mathbf{K}_p + \gamma \mathbf{L}_1\right) \\ \frac{1}{2}\left(\mathbf{M}^{-1}(\mathbf{x})\mathbf{K}_p + \gamma \mathbf{L}_1\right)^T & \gamma\left(\mathbf{M}^{-1}(\mathbf{x})\mathbf{K}_p + \mathbf{L}_2\right) \end{bmatrix} \tag{C.51}$$

From the definition in (3.49) it follows that

$$\dot{\mu}\, \tilde{\mathbf{x}}_m^T \dot{\tilde{\mathbf{x}}}_m = -\mu \left(\frac{\tilde{\mathbf{x}}_m^T \dot{\tilde{\mathbf{x}}}_m}{1 + \|\tilde{\mathbf{x}}_m\|} \right) \dot{\tilde{\mathbf{x}}}_m^T \tilde{\mathbf{x}}_m \leq \mu_0 \left\| \dot{\tilde{\mathbf{x}}}_m \right\|^2 \tag{C.52}$$

$$\dot{\gamma}\, \tilde{\mathbf{x}}^T \dot{\tilde{\mathbf{x}}} = -\gamma \left(\frac{\tilde{\mathbf{x}}^T \dot{\tilde{\mathbf{x}}}}{1 + \|\tilde{\mathbf{x}}\|} \right) \dot{\tilde{\mathbf{x}}}^T \tilde{\mathbf{x}} \leq \gamma_0 \left\| \dot{\tilde{\mathbf{x}}} \right\|^2 \tag{C.53}$$

where μ_0 and γ_0 are upper bounds on $\mu(\tilde{\mathbf{x}}_d)$ and $\gamma(\tilde{\mathbf{x}})$, respectively. The definition of the inertia matrix $\mathbf{M}(\mathbf{x})$ implies that

$$\dot{\mathbf{M}}(\mathbf{x}) = \frac{d}{dt}\mathbf{M}(\mathbf{x}) = \frac{\partial \mathbf{M}(\mathbf{x})}{\partial \mathbf{x}} \dot{\mathbf{x}} \tag{C.54}$$

and since $0 < \mathbf{M}_m \leq \|\mathbf{M}(\mathbf{x})\| \leq \mathbf{M}_M$ and the fact that $\mathbf{x}$ only appears as an argument of trigonometric functions in $\mathbf{M}(\mathbf{x})$ it can be concluded that

$$\mathbf{M}_{pm} \|\dot{\mathbf{x}}\| \leq \left\| \dot{\mathbf{M}}(\mathbf{x}) \right\| \leq \mathbf{M}_{pM} \|\dot{\mathbf{x}}\| \tag{C.55}$$

Using Properties P3 and P4, and introducing the vector ζ_N as

$$\zeta_N^T = \left[\|\vec{\mathbf{e}}\|,\ \|\overline{\mathbf{e}}\|,\ \left\|\dot{\tilde{\mathbf{x}}}_m\right\|,\ \|\tilde{\mathbf{x}}_m\|,\ \left\|\dot{\tilde{\mathbf{x}}}\right\|,\ \|\tilde{\mathbf{x}}\| \right] \tag{C.56}$$

an upper bound for (C.43) is

$$\dot{V}(\zeta) \leq \|\zeta_N\| \left(\alpha_0 - \mathbf{Q}_{N,m} \|\zeta_N\| + \alpha_2 \|\zeta_N\|^2 \right) \tag{C.57}$$

where $\mathbf{Q}_{N,m}$ is the minimum eigenvalue of the matrix $\mathbf{Q}_N = \mathbf{Q}_N^T$ given by

$$\mathbf{Q}_N = \begin{bmatrix} \mathbf{Q}_{11_N} & \mathbf{Q}_{12_N} & \mathbf{Q}_{13_N} \\ \mathbf{Q}_{12_N}^T & \mathbf{Q}_{22_N} & \mathbf{Q}_{23_N} \\ \mathbf{Q}_{13_N}^T & \mathbf{Q}_{23_N}^T & \mathbf{Q}_{33_N} \end{bmatrix} \tag{C.58}$$

where

$$\mathbf{Q}_{11_N} = \varepsilon_0 \begin{bmatrix} \mathbf{K}_{d,m} + \mathbf{D}_M - \lambda_0 \mathbf{M}_M & q_{12} \\ q_{12} & \lambda_0 \mathbf{K}_{p,m} \end{bmatrix} \tag{C.59}$$

$$\mathbf{Q}_{12_N} = \frac{\varepsilon_0}{2} \begin{bmatrix} -\mathbf{M}_M \mathbf{L}_{1,M} - \mathbf{D}_M \mathbf{L}_{1,M} & \mathbf{K}_{p,M} - \mathbf{K}_{d,M} \mathbf{L}_{1,M} - \mathbf{C}_M V_M \\ -\lambda_0 \mathbf{M}_M \mathbf{L}_{1,M} & q_{24} \end{bmatrix} \tag{C.60}$$

$$\mathbf{Q}_{13_N} = \frac{\varepsilon_0}{2} \begin{bmatrix} \mathbf{C}_M V_M - \mathbf{K}_{d,M} & \mathbf{C}_M V_M \mathbf{L}_{1,M} - \mathbf{K}_{d,M} \mathbf{L}_{1,M} \\ \lambda_0 \left(\mathbf{C}_M V_M - \mathbf{K}_{d,M} \right) & \lambda_0 \left(\mathbf{C}_M V_M \mathbf{L}_{1,M} - \mathbf{K}_{d,M} \mathbf{L}_{1,M} \right) \end{bmatrix} \tag{C.61}$$

$$\mathbf{Q}_{22_N} = \begin{bmatrix} L_{1,m} - 2\mu_0 & \frac{1}{2} \left(\mathbf{M}_m^{-1} \mathbf{K}_{p,M} + \mu_0 \mathbf{L}_{1,M} \right) \\ \frac{1}{2} \left(\mathbf{M}_m^{-1} \mathbf{K}_{p,M} + \mu_0 \mathbf{L}_{1,M} \right) & \mu_0 \left(\mathbf{M}_m^{-1} \mathbf{K}_{p,m} + \mathbf{L}_{2,m} \right) \end{bmatrix} \tag{C.62}$$

$$\mathbf{Q}_{23_N} = \begin{bmatrix} 0 & \frac{1}{2} \mathbf{M}_m^{-1} \mathbf{K}_{p,M} \\ \frac{1}{2} \left(\mathbf{M}_m^{-1} \mathbf{K}_{p,M} + L_{2,M} \right) & \frac{1}{2} \left((\mu_0 + \gamma_0) \mathbf{M}_m^{-1} \mathbf{K}_{p,M} + \gamma_0 \mathbf{L}_{2,M} \right) \end{bmatrix} \tag{C.63}$$

$$\mathbf{Q}_{33_N} = \begin{bmatrix} L_{1,m} - 2\gamma_0 + 2\mathbf{M}_m^{-1} \mathbf{C}_M V_M + \mathbf{M}_m^{-1} \mathbf{D}_M & q_{56} \\ q_{56} & q_{66} \end{bmatrix} \tag{C.64}$$

$$q_{12} = \frac{1}{2} \lambda_0 \left(\mathbf{C}_M V_M - \mathbf{M}_M V_M + \mathbf{D}_M \right) \tag{C.65}$$

$$q_{24} = \lambda_0 \left(\mathbf{K}_{p,M} - \mathbf{K}_{d,M} \mathbf{L}_{1,M} - \mathbf{C}_M V_M - \mathbf{D}_M \mathbf{L}_{1,M} \right) \tag{C.66}$$

$$q_{56} = \frac{1}{2} \left(\mathbf{M}_m^{-1} \mathbf{K}_{p,M} + \gamma_0 \mathbf{L}_{1,M} \right) + \mathbf{M}_m^{-1} \mathbf{C}_M V_M \left(\mathbf{L}_{1,M} + \gamma_0 \right) + \mathbf{M}_m^{-1} \mathbf{D}_M \left(\mathbf{L}_{1,M} + \gamma_0 \right) \tag{C.67}$$

$$q_{66} = \gamma_0 \left(\mathbf{M}_m^{-1} \mathbf{K}_{p,m} + \mathbf{L}_{2,m} + 2\mathbf{M}_m^{-1} \mathbf{C}_M V_M \mathbf{L}_{1,m} + \mathbf{M}_m^{-1} \mathbf{D}_M \mathbf{L}_{1,m} \right) \tag{C.68}$$

and α_0 and α_2 are positive scalars given by

$$\alpha_0 = (1 + \sqrt{\mu_0}) \sqrt{A_M} \tag{C.69}$$

$$\begin{aligned} \alpha_2 = & \sqrt{8 \, \mathbf{M}_m^{-1} C_M \Lambda_M} \left(\sqrt{\gamma_0} + \sqrt{\mathbf{L}_{1,M}} \right) + \sqrt{\varepsilon_0 C_M} \left(1 + \sqrt{\lambda_0} \right) \left(\mathbf{L}_{1,M} + 2\sqrt{\mathbf{L}_{1,M}} \right) \\ & + \varepsilon_0 \left(\sqrt{C_M} \left(1 + 2\sqrt{\mathbf{L}_{1,M}} \right) + \sqrt{\lambda_0 \left(\mathbf{M}_{pM} + C_M \right)} \right) \\ & + \sqrt{\varepsilon_0 \lambda_0} \left(2\sqrt{C_M} \left(1 + \sqrt{\mathbf{L}_{1,M}} \right) + \sqrt{\mathbf{M}_{pM} + C_M} \right) \\ & + \mathbf{M}_m^{-1} C_M \left(5 + \sqrt{\gamma_0 + 2\mathbf{L}_{1,M}} + \sqrt{\gamma_0 \mathbf{L}_{1,M} + \mathbf{L}_{1,M}^2 + \gamma_0} + \mathbf{L}_{1,M} \sqrt{\gamma_0} + \sqrt{8 \, \gamma_0 \mathbf{L}_{1,M}} \right) \end{aligned} \tag{C.70}$$

Choosing the gains $\mathbf{K}_p, \mathbf{K}_d, \mathbf{L}_1, \mathbf{L}_2$ and the constants $\varepsilon_0, \lambda_0, \mu_0, \gamma_0$ such that $\mathbf{Q}_N$ is positive definite suggests that the coordination observer-controller scheme can be treated as a perturbed system. Equation (3.47) together with (3.51) and Proposition 2.1 allows the conclusion of local uniform ultimate boundedness of ζ_N and consequently of ζ. Through the coordinate transformation defined by (3.46) it follows that the original state $\widetilde{\eta}$ in (3.44) is locally uniformly ultimately bounded. Moreover, since α_2 depends explicitly on $\mathbf{L}_{1,M}$, y_2 in Proposition 2.1 can be made arbitrarily small by a proper choice of $\mathbf{L}_{1,M}$, and thus the ultimate bound for $\widetilde{\eta}$ can be made arbitrarily small. Also note that the region of attraction is given by

$$\Delta = \left\{ \mathbf{x} \in \mathbb{R}^{6n} \quad | \quad \|\mathbf{x}\| < \frac{y_2}{\|T\|} \sqrt{P_m^{-1} P_M} \right\} \tag{C.71}$$

Since the size of the region of attraction Δ is proportional to y_2, this region can be expanded by increasing y_2. Thus the closed-loop errors $\widetilde{\eta}$ are semiglobally uniformly ultimately bounded.

The ultimate boundedness result is due to the non-vanishing disturbance from leader acceleration $\ddot{\mathbf{x}}_m$. Under the assumption of constant velocity of the leader ($\ddot{\mathbf{x}}_m = 0$), the derivative of the Lyapunov function (3.51) is reduced to

$$\dot{V}(\zeta) \leq \|\zeta_N\|^2 (-\mathbf{Q}_{N,m} + \alpha_2 \|\zeta_N\|) \leq -\kappa \|\zeta_N\|^2 \tag{C.72}$$

since (C.71) guarantees that $\mathbf{Q}_{N,m} > \alpha_2 \|\zeta_N\|$. Semiglobal exponential convergence to zero of the closed-loop errors $\widetilde{\eta} = T\zeta$ for leader acceleration $\ddot{\mathbf{x}}_m = 0$ follows directly from (C.72).

C.2 The Virtual vehicle approach

C.2.1 Proof of Theorem 4.1

Consider the Lyapunov function candidate

$$V_v(\mathbf{z},\, \mathbf{e}_v) = \frac{1}{2}\mathbf{e}_v^T\mathbf{e}_v + \frac{1}{2}\mathbf{z}^T\mathbf{L}_2\mathbf{z} + \frac{1}{2}\mathbf{z}^T\mathbf{e}_v \tag{C.73}$$

which is positive definite for $\mathbf{L}_{2,m} > 1/4$. Differentiating along the closed-loop trajectories

$$\dot{V}_v(\mathbf{z},\, \mathbf{e}_v) = -\mathbf{e}_v^T\left(\mathbf{L}_1 - \frac{1}{2}\mathbf{I}\right)\mathbf{e}_v - \frac{1}{2}\mathbf{z}^T\mathbf{L}_2\mathbf{z} - \frac{1}{2}\mathbf{z}^T\mathbf{L}_1\mathbf{e}_v - \left(\mathbf{e}_v^T + \frac{1}{2}\mathbf{z}^T\right)\mathbf{J}(\mathbf{x}_m)\,v_r \tag{C.74}$$

It follows through Proposition A.2 that

$$-\frac{1}{2}\mathbf{z}^T\mathbf{L}_1\mathbf{e}_v \leq \frac{1}{2}\left(\frac{\lambda}{2}\mathbf{L}_{1,M}\|\mathbf{e}_v\|^2 - \frac{1}{2\lambda}\mathbf{L}_{1,M}\|\mathbf{z}\|^2\right) \tag{C.75}$$

and the relation using (4.2)

$$-\left(\mathbf{e}_v^T + \frac{1}{2}\mathbf{z}^T\right)\mathbf{J}(\mathbf{x}_m)\,v_r \leq \left(\|(\mathbf{e},\mathbf{z})\| + \frac{1}{2}\|(\mathbf{e},\mathbf{z})\|\right)V_M \leq \frac{3V_M}{2\|(\mathbf{e},\mathbf{z})\|}\left(\mathbf{e}^T\mathbf{e} + \mathbf{z}^T\mathbf{z}\right) \tag{C.76}$$

that (C.73) can be rewritten as

$$\begin{aligned}\dot{V}_v(\mathbf{z},\, \mathbf{e}_v) \leq &-\left(\mathbf{L}_{1,m} - \frac{1}{2} - \frac{\lambda}{4}\mathbf{L}_{1,M} - \frac{3V_M}{2\|(\mathbf{e}_v,\mathbf{z})\|}\right)\|\mathbf{e}_v\|^2 \\ &-\frac{1}{2}\left(\mathbf{L}_{2,m} - \frac{1}{2\lambda}\mathbf{L}_{1,M} - \frac{3V_M}{\|(\mathbf{e}_v,\mathbf{z})\|}\right)\|\mathbf{z}\|^2\end{aligned} \tag{C.77}$$

since $\|\mathbf{J}(\mathbf{x})\| \leq 1$. Designing the gain matrices $\mathbf{L}_1$ and $\mathbf{L}_2$ as $\mathbf{L}_{i,M} \leq \ell\,\mathbf{L}_{i,m}$, $i \in \{1,2\}$, for some $\ell > 0$, it follows through $\lambda = 2/\ell$ and δ_v as any given positive constant that the choice

$$\mathbf{L}_{1,m} - \frac{1}{2} - \frac{\lambda}{4}\mathbf{L}_{1,M} - \frac{3V_M}{2\|(\mathbf{e}_v,\mathbf{z})\|} = 1 \tag{C.78}$$

gives

$$\left(1-\frac{2}{4\ell}\ell\right)\mathbf{L}_{1,m}-\frac{1}{2}-\frac{3V_M}{2\delta_v}=1 \qquad \Rightarrow \qquad \mathbf{L}_{1,m}=3+\frac{3V_M}{\delta_v} \tag{C.79}$$

and the choice

$$\frac{1}{2}\left(\mathbf{L}_{2,m}-\frac{1}{2\lambda}\mathbf{L}_{1,m}-\frac{3V_M}{\|(\mathbf{e}_v,\mathbf{z})\|}\right)=1 \tag{C.80}$$

gives

$$\frac{1}{2}\left(\mathbf{L}_{2,m}-\frac{\ell^2}{4}\mathbf{L}_{1,m}-\frac{3V_M}{\delta_v}\right)=1 \qquad \Rightarrow \qquad \mathbf{L}_{2,m}=2+\frac{3\ell^2}{4}+\left(1+\frac{\ell^2}{4}\right)\frac{3V_M}{\delta_v} \tag{C.81}$$

The choices of (C.78) and (C.80) generates the following bound of the derivative of V_v:

$$\|\mathbf{e}_v\|^2+\|\mathbf{z}\|^2\geq\delta_v^2 \quad \Rightarrow \quad \dot{V}_v(\mathbf{z},\mathbf{e}_v)\leq-\|\mathbf{e}_v\|^2-\|\mathbf{z}\|^2. \tag{C.82}$$

C.2.2 Proof of Theorem 4.4

Sketch of proof: We can combine the Lyapunov functions as

$$V(\widetilde{\eta})=V_v(\mathbf{z},\mathbf{e}_v)+V_e(\mathbf{e},\dot{\mathbf{e}},\vartheta) \tag{C.83}$$

and write the derivative of (C.83) by bounding the terms as

$$\begin{aligned}\dot{V}(\widetilde{\eta})\leq&-\frac{\varepsilon}{2}\begin{bmatrix}\|\mathbf{e}\|\\\|\dot{\mathbf{e}}\|\end{bmatrix}^T\overbrace{\begin{bmatrix}\frac{1}{2}\mathbf{K}_{p,m} & -k_{D1}\\ -k_{D1} & \frac{1}{3}\mathbf{B}_m^T\mathbf{M}_m\end{bmatrix}}^{\mathbf{Q}_1}\begin{bmatrix}\|\mathbf{e}\|\\\|\dot{\mathbf{e}}\|\end{bmatrix}\\&-\frac{\varepsilon}{2}\begin{bmatrix}\|\mathbf{e}\|\\\|\vartheta\|\end{bmatrix}^T\overbrace{\begin{bmatrix}\frac{1}{2}\mathbf{K}_{p,m} & -\mathbf{K}_{d,M}-\mathbf{K}_{p,M}\\ -\mathbf{K}_{d,M}-\mathbf{K}_{p,M} & \frac{1}{2\varepsilon}\mathbf{K}_{d,m}\mathbf{B}_M^{-1}\mathbf{A}_m\end{bmatrix}}^{\mathbf{Q}_2}\begin{bmatrix}\|\mathbf{e}\|\\\|\vartheta\|\end{bmatrix}\\&-\frac{\varepsilon}{2}\begin{bmatrix}\|\vartheta\|\\\|\dot{\mathbf{e}}\|\end{bmatrix}^T\overbrace{\begin{bmatrix}\frac{1}{2\varepsilon}\mathbf{K}_{d,m}\mathbf{B}_M^{-1}\mathbf{A}_m & -k_{D1}-\mathbf{A}_M^T\mathbf{M}_M\\ -k_{D1}-\mathbf{A}_M^T\mathbf{M}_M & \frac{1}{3}\mathbf{B}_m^T\mathbf{M}_m\end{bmatrix}}^{\mathbf{Q}_3}\begin{bmatrix}\|\vartheta\|\\\|\dot{\mathbf{e}}\|\end{bmatrix}\\&-\Lambda_{\mathbf{e}_v}\|\mathbf{e}_v\|^2-\Lambda_{\mathbf{z}}\|\mathbf{z}\|^2-(\varepsilon\Lambda_{\dot{\mathbf{e}}1}+\Lambda_{\dot{\mathbf{e}}2})\|\dot{\mathbf{e}}\|^2-\Lambda_{\mathbf{e}}\|\mathbf{e}\|^2-\varepsilon\Lambda_{\vartheta}\|\vartheta\|^2\end{aligned} \tag{C.84}$$

where

$$\begin{aligned}
\Lambda_{\mathbf{e}_v} =& L_{1,m} - \frac{1}{2} - \frac{\lambda}{4} L_{1,M} - \frac{\left(\mathbf{M}_M \mathbf{L}_{1,M} + \frac{3}{2}\right) V_M}{\|[\mathbf{e}_v, \mathbf{z}, \dot{\mathbf{e}}]\|} \\
\Lambda_{\mathbf{z}} =& \frac{1}{2}\left(L_{2,m} - \frac{1}{2\lambda} L_{1,M} - \frac{\left(\mathbf{M}_M \mathbf{L}_{1,M} + \frac{3}{2}\right) V_M}{\|[\mathbf{e}_v, \mathbf{z}, \dot{\mathbf{e}}]\|} \right) \\
\Lambda_{\dot{\mathbf{e}}1} =& \frac{1}{3}\mathbf{B}_m^T \mathbf{M}_m - \mathbf{M}_M - k_{D2}\left(\|\mathbf{e}\| + \|\vartheta\|\right) - k_{D2}\|\dot{\mathbf{x}}_v\| - \mathbf{C}_M\left(\|\mathbf{e}\| + \|\vartheta\|\right) - 2\mathbf{C}_V\|\dot{\mathbf{x}}_v\| \\
\Lambda_{\dot{\mathbf{e}}2} =& \frac{\varepsilon}{3}\mathbf{B}_m^T \mathbf{M}_m + k_d - \mathbf{C}_V\|\dot{\mathbf{x}}_v\| - \frac{\left(\mathbf{M}_M \mathbf{L}_{1,M} + \frac{3}{2}\right) V_M}{\|[\mathbf{e}_v, \mathbf{z}, \dot{\mathbf{e}}]\|} \\
\Lambda_{\mathbf{e}} =& \frac{1}{2}\mathbf{K}_{p,m} - \frac{1}{2}k_{D2}\|\dot{\mathbf{x}}_v\| - \mathbf{C}_V\|\dot{\mathbf{x}}_v\| \\
\Lambda_{\vartheta} =& \frac{1}{2}\mathbf{K}_{d,m}\mathbf{B}_M^{-1}\mathbf{A}_m - \varepsilon\mathbf{K}_{d,M} - \frac{\varepsilon}{2}k_{D2}\|\dot{\mathbf{x}}_v\| - \varepsilon\mathbf{C}_V\|\dot{\mathbf{x}}_v\|
\end{aligned} \tag{C.85}$$

through

$$\left(\mathbf{M}_M \mathbf{L}_{1,M}\|\dot{\mathbf{e}}\| + \|\mathbf{e}_v\| + \frac{1}{2}\|\mathbf{z}\|\right) V_M \leq \frac{\left(\mathbf{M}_M \mathbf{L}_{1,M} + \frac{3}{2}\right) V_M}{\|[\mathbf{e}_v, \mathbf{z}, \dot{\mathbf{e}}]\|}\left(\|\mathbf{e}_v\|^2 + \|\mathbf{z}\|^2 + \|\dot{\mathbf{e}}\|^2\right) \tag{C.86}$$

Positive definiteness requires

$$\begin{aligned}
\mathbf{Q}_1 > 0 \Leftrightarrow & \mathbf{K}_{p,m}\mathbf{B}_m\mathbf{M}_m > 6\, k_{D1}^2 \\
\mathbf{Q}_2 > 0 \Leftrightarrow & \frac{\mathbf{K}_{p,m}\mathbf{K}_{d,m}\mathbf{A}_m}{4\mathbf{B}_M\left[\mathbf{K}_{p,m} + \mathbf{K}_{d,m}\right]^2} > \varepsilon \\
\mathbf{Q}_3 > 0 \Leftrightarrow & \frac{\mathbf{K}_{d,m}\mathbf{A}_m\mathbf{B}_m\mathbf{M}_m}{6\mathbf{B}_M\left[k_{D1} + \mathbf{A}_M\mathbf{M}_M\right]^2} > \varepsilon
\end{aligned} \tag{C.87}$$

Through the definition of $\dot{\mathbf{x}}_v$ in (4.16) constants are positive for

$$\begin{aligned}
\Lambda_{\dot{\mathbf{e}}1} > 0 \Leftrightarrow & \frac{\mathbf{B}_m\mathbf{M}_m - 3\mathbf{M}_M}{6\left(k_{D2} + \mathbf{C}_M + \left(\frac{1}{2}k_{D2} + \mathbf{C}_V\right)\left(\mathbf{L}_{1,M} + \mathbf{L}_{2,M}\right)\right)} > \|\widetilde{\eta}\| \\
\Lambda_{\vartheta} > 0 \Leftrightarrow & \frac{\mathbf{K}_{d,m}\mathbf{A}_m - 2\varepsilon\mathbf{K}_{d,M}\mathbf{B}_M}{\varepsilon\mathbf{B}_M\left(k_{D2} + 2\mathbf{C}_V\right)\left(\mathbf{L}_{1,M} + \mathbf{L}_{2,M}\right)} > \|\widetilde{\eta}\| \\
\Lambda_{\mathbf{e}} > 0 \Leftrightarrow & \frac{\mathbf{K}_{p,m}}{\left(k_{D2} + 2\mathbf{C}_V\right)\left(\mathbf{L}_{1,M} + \mathbf{L}_{2,M}\right)} > \|\widetilde{\eta}\|
\end{aligned} \tag{C.88}$$

where

$$\begin{aligned}
\Delta_1 = \min\Bigg\{ & \frac{\mathbf{B}_m\mathbf{M}_m - 3\mathbf{M}_M}{6\left(k_{D2} + \mathbf{C}_M + \left(\frac{1}{2}k_{D2} + \mathbf{C}_V\right)\left(\mathbf{L}_{1,M} + \mathbf{L}_{2,M}\right)\right)}, \\
& \frac{\mathbf{K}_{d,m}\mathbf{A}_m - 2\varepsilon\mathbf{K}_{d,M}\mathbf{B}_M}{\varepsilon\mathbf{B}_M\left(k_{D2} + 2\mathbf{C}_V\right)\left(\mathbf{L}_{1,M} + \mathbf{L}_{2,M}\right)}, \frac{\mathbf{K}_{p,m}}{\left(k_{D2} + 2\mathbf{C}_V\right)\left(\mathbf{L}_{1,M} + \mathbf{L}_{2,M}\right)}\Bigg\}
\end{aligned} \tag{C.89}$$

Choose the minimum eigenvalues of the gain matrices $\mathbf{L}_1$ and $\mathbf{L}_2$ large enough using the same reasoning as in Section 4.1.1, and satisfying

$$\mathbf{L}_{1,m} = \frac{3+3\frac{V_M}{\delta_1}}{1-2\mathbf{M}_m\ell\frac{V_M}{\delta_1}}, \quad \mathbf{L}_{2,m} = 2+\left(\frac{\ell}{4}+\frac{2\mathbf{M}_m\ell V_M}{\delta_1}\right)\mathbf{L}_{1,m}+3\frac{V_M}{\delta_1} \tag{C.90}$$

ensures that $\Lambda_{\mathbf{e}_v}$ and $\Lambda_{\mathbf{z}}$ are positive as

$$\|\widetilde{\eta}\| \geq \delta_1 \Rightarrow \Lambda_{\mathbf{e}_v} = \Lambda_{\mathbf{z}} = 1 \tag{C.91}$$

The region δ_1 to which the solutions converge can be reduced by enlarging $\mathbf{L}_{1,m}$ and $\mathbf{L}_{2,m}$. Defining constants

$$a := \mathbf{C}_V\left(\mathbf{L}_{1,M}+\mathbf{L}_{2,M}\right), \quad b := \frac{\varepsilon}{3}\mathbf{B}_m^T\mathbf{M}_m + k_d, \quad c := \left(\mathbf{M}_M\mathbf{L}_{1,M}+\frac{3}{2}\right)V_M \tag{C.92}$$

the term $\Lambda_{\dot{\mathbf{e}}2}$ is positive when $b > 2\sqrt{ac}$, and the two distinct roots are

$$\Delta_2 = \frac{b+\sqrt{b^2-4ac}}{2a}, \qquad \delta_2 = \frac{b-\sqrt{b^2-4ac}}{2a} \tag{C.93}$$

such that

$$\Delta_2 > \|\widetilde{\eta}\| > \delta_2 \tag{C.94}$$

The lower bound δ_2 can be decreased and the upper bound Δ_2 can be increased by increasing the gain $\mathbf{B}_m$ in b, and

$$\lim_{\mathbf{B}_m\to\infty}\Delta_2 = \infty, \qquad \lim_{\mathbf{B}_m\to\infty}\delta_2 = 0 \tag{C.95}$$

The region to which the solutions converge is thus $\delta = \max\{\delta_1+\delta_2\}$. Through the dependence of the gains in the radius $1/\delta$ and by Corollary 2.1 the closed-loop errors are uniformly practically asymptotically stable.

To investigate the region of attraction there exists positive constants α_1 and α_2 such that

$$\alpha_1\|\widetilde{\eta}\|^2 \leq V(t,\widetilde{\eta}) \leq \alpha_2\|\widetilde{\eta}\|^2 \tag{C.96}$$

since from (4.54)

$$V \geq \frac{1}{4}\left[\mathbf{M}_m\|\dot{\mathbf{e}}\|^2+\mathbf{K}_{p,m}\|\mathbf{e}\|^2+\frac{\mathbf{K}_{d,m}}{\mathbf{M}_M}\|\vartheta\|^2+\mathbf{L}_{2,m}\|\mathbf{z}\|^2+\|\mathbf{e}_v\|^2\right] \tag{C.97}$$

and thus

$$\alpha_1 = \frac{1}{4}\min\left\{\mathbf{M}_m, \frac{\mathbf{K}_{d,m}}{\mathbf{B}_M}, \mathbf{K}_{p,m}, \frac{1}{4}, \mathbf{L}_{2,m}\right\} \tag{C.98}$$

Similarly, an upper bound on V is

$$V \leq \left[\left(\varepsilon+\frac{1}{2}\right)\mathbf{M}_M\right]\|\dot{\mathbf{e}}\|^2+\left[\frac{\varepsilon}{2}\mathbf{M}_M+\frac{1}{2}\mathbf{K}_{p,M}\right]\|\mathbf{e}\|^2+\frac{1}{2}\left[\varepsilon\mathbf{M}_M+\frac{\mathbf{K}_{d,M}}{\mathbf{B}_m}\right]\|\vartheta\|^2+\|\mathbf{e}\|^2+\left[\mathbf{L}_{2,M}+\frac{1}{2}\right]\|\mathbf{z}\|^2 \tag{C.99}$$

and thus

$$\alpha_2 = \max\left\{\left[\left(\varepsilon+\frac{1}{2}\right)\mathbf{M}_M\right], \left[\frac{\varepsilon}{2}\mathbf{M}_M+\frac{1}{2}\mathbf{K}_{p,M}\right], \frac{1}{2}\left[\varepsilon\mathbf{M}_M+\frac{\mathbf{K}_{d,M}}{\mathbf{B}_m}\right], 1, \left[\mathbf{L}_{2,M}+\frac{1}{2}\right]\right\} \tag{C.100}$$

The region of attraction thus contains the set

$$\|\widetilde{\eta}\| \leq \Delta = \min\{\Delta_1+\Delta_2\}\sqrt{\frac{\alpha_1}{\alpha_2}} \tag{C.101}$$

The region of attraction can be enlarged by increasing Δ through a suitable choice of $\mathbf{K}_{p,m}$, $\mathbf{K}_{d,m}$, $\mathbf{A}_m$ and $\mathbf{B}_m$, and thus suggest semiglobal stability. The closed-loop errors of (4.7-4.8), (4.43) and (4.50) are uniformly semiglobally practically asymptotically stable. ■

Appendix D

Additional background

This appendix presents an overview of the single-object motion control schemes used throughout the literature. These control schemes have been the basis for the development of a large class of multi-object coordination schemes, and the schemes are compared to the motion coordination schemes proposed in this thesis.

D.1 Tracking approaches

This section presents and classifies a number of tracking approaches. Many of the definitions are used interchangeably in literature among different authors, and an attempt is made to give an overview of the different approaches. This section is based on Kyrkjebø and Pettersen (2005*b*).

The definition of tracking can be stated in compliance with Fossen (2002) as

Definition D.1 *When the objective is to force the system output* $y(t) \in \mathbb{R}^{\mathrm{m}}$ *to track a desired ideal output* $y_d(t) \in \mathbb{R}^{\mathrm{m}}$*, it will be defined as a tracking problem.*

The problem of controlling the output of a system to a reference can be viewed with different applications in mind. One of the approaches is the *point stabilization* problem, or parking problem (Frezza (2000)), that consists of steering an object to a desired end configuration irrespective of the system behaviour between the initial state and the end configuration. In this problem the reference y_d is stationary, and it is common to refer to y_d as a set point, and to the problem as a *regulation* problem Khalil (1996).

In the *path following* problem the reference is non-stationary, and the objective is to have the object reach and follow a predefined geometric curve. In the definition of Encarnacao and Pascoal (2001) the path is stated without any temporal specifications, while in the definition of Skjetne *et al.* (2004*c*), Aguiar *et al.* (2004), Frezza (2000) and Fossen (2002) the path is parameterized with a continuous path variable. Using the definition of a parameterized path from Fossen (2002) as

Definition D.2 *A parameterized path is defined as a geometric curve* $\mathbf{y}_d(\theta) \in \mathbb{R}^m$ *with* $m \geq 1$ *parameterized by a continuous path variable* θ*.*

the path-following objective for the system can be stated for the desired geometric path

$$y_d(\theta) \in \mathbb{R}^{\mathrm{m}} : \theta \in [0, \infty) \tag{D.1}$$

as driving the path following error

$$e_P(t) = y(t) - y_d(\theta(t)), \qquad t \geq 0. \tag{D.2}$$

to zero (Aguiar *et al.* (2004)). Note that there may be constraints on θ that reflects the physical limitations in velocity and acceleration of the objects. The trajectory tracking problem is a specialization of the path following problem where the path has been parameterized in terms of time ($\theta(t) = t$), and the trajectory tracking error reduces to

$$e_T(t) = y(t) - y_d(t), \qquad t \geq 0. \tag{D.3}$$

To further define the motion coordination problem, Skjetne (2005) has defined the manoeuvring problem inspired by Hauser and Hindman (1995), where the manoeuvre is a curve in the input and state space that is consistent with the system dynamics

$$y_d = \{(x_d(\theta), u_d(\theta)) \in \mathbb{R}^n \times \mathbb{R}^r : \theta \in \mathbb{R}\} \tag{D.4}$$

for the system $\dot{x} = f(x,u)$ with $x \in \mathbb{R}^n$ and $u \in \mathbb{R}^r$ if

$$\frac{dx_d(\theta)}{d\theta} = f(x_d(\theta), u_d(\theta)) \qquad \theta \in \mathbb{R} \tag{D.5}$$

The specific parameterization used is unimportant - the manoeuvre y_d is the curve, and thus an infinite number of trajectories may give rise to the same manoeuvre. The manoeuvring problem consists of two tasks; the geometric task to force the path following error to zero

$$\lim_{t\to\infty} |y(t) - y_d(\theta(t))| = 0, \qquad \theta(t) \in \mathbb{R} \tag{D.6}$$

and the dynamic task that takes care of any time, speed or acceleration assignments consistent with the system dynamics (Skjetne *et al.* (2004*c*)).

Al-Hiddabi and McClamroch (2002) designed a manoeuvre regulation controller from a trajectory tracking controller by introducing a suitable state projection, and applied the results to the flight control problem, while a recent result in Aguiar *et al.* (2004) highlighted the fundamental difference between manoeuvring and trajectory tracking by demonstrating that performance limitations in trajectory tracking due to unstable zero-dynamics can be removed in the manoeuvring problem, and that the trajectory tracking approach introduces performance limitations that are not a consequence of the problem to be solved, but rather of how the problem solution is approached.

Hauser and Hindman (1995) addressed the problem of converting a stable tracking law to a stable manoeuvring law through a projection mapping onto the manoeuvre to select the appropriate trajectory time for feedback linearizable nonlinear systems, and applied this technique in a flight control problem. Skjetne *et al.* (2004*c*) used the mapping of Hauser and Hindman (1995) to solve the output manoeuvring problem for multiple vehicles using a speed assignment as the dynamic task parameterization, and then synchronized the parameterization variable θ for each vehicle along their reference trajectories. This guarantees that every vehicle is synchronized to the others with respect to the path parameterization variable.

Encarnacao and Pascoal (2001) combined the trajectory tracking and path following problem in coordinated control of an autonomous surface craft (ASC) and an autonomous

underwater vehicle (AUV) in a leader-follower scheme. In order to coordinate their behaviour despite deviations due to wind, waves and currents, the authors forced the follower - the AUV - to track a projection of the leader - the ASC - on a two-dimensional nominal path. The approach guarantees that the AUV converges to the nominal path, and on that path tracks the projection of the ASC. In this way, the time parameterization of the path - the trajectory - is only available in an implicit manner depending on the actual position of the ASC through the projection mapping.

Tracking control in terms of path following, trajectory tracking or manoeuvring is sufficient in control applications where the reference is a predefined curve not subject to any disturbances. If the reference for tracking control is generated by a physical system with disturbances modelled by

$$\begin{aligned} \dot{x}_d &= f_d(t, x_d, u_d, w_d) \\ y_d &= h_d(t, x_d, u_d, w_d) \end{aligned} \tag{D.7}$$

with $x_d \in \mathbb{R}^n$ as the state, $u_d \in \mathbb{R}^r$ as the control input, $w_d \in \mathbb{R}^s$ as a disturbance input and $y_d \in \mathbb{R}^m$ as the output, some sort of feedback from the actual states of the reference system must be introduced to account for the effect of these disturbances in order to assure good tracking behaviour. If the tracking systems with disturbances are modelled similarly as

$$\begin{aligned} \dot{x} &= f(t, x, u, w) \\ y &= h(t, x, u, w) \end{aligned} \tag{D.8}$$

the *multi-object tracking problem* can be stated as

Definition D.3 *When the objective is to force the system output $y(t, x, u, w) \in \mathbb{R}^m$ to track a dynamic desired output $y_d(t, x_d, u_d, w_d) \in \mathbb{R}^m$ to provide a joint motion, it will be defined as a multi-object tracking problem.*

An *asymptotic multi-object tracking* scheme is feasible in the absence of input disturbance w and w_d, or for certain types of disturbance inputs where it is possible to achieve asymptotic disturbance rejection (Khalil (1996)). The asymptotic multi-object tracking problem is thus to drive the tracking error

$$e(t) = y(t, x, u, w) - y_d(t, x_d, u_d, w_d) \tag{D.9}$$

to zero asymptotically as

$$\lim_{t \to \infty} |y(t, x, u, w) - y_d(t, x_d, u_d, w_d)| = 0. \tag{D.10}$$

For general time-varying disturbance input $w(t)$ and $w_d(t)$ it might only be possible to achieve asymptotic disturbance attenuation, and thus the control law can only achieve uniform ultimate boundedness or practical asymptotic stability of the multi-object tracking errors. Note that local, global or semiglobal results obtained through the motion control law refer not only to the size of the initial state, but also to the size of the exogenous signals y_d and w (Khalil (1996)).

There is a fundamental difference between a tracking scheme where the different objects have individual tracking controllers that controls each object to predefined paths, and

a tracking scheme utilizing some sort of feedback to synchronize the tracking objects to the actual states of the reference object. Synchronization is only present in the planning phase for pure trajectory tracking or manoeuvring schemes, while the manoeuvring scheme of Skjetne *et al.* (2004*c*) and the combined path following and trajectory tracking approach of Encarnacao and Pascoal (2001) synchronize the planned behaviour during the execution of the scheme. Both the latter approaches synchronize the objects to points on predefined paths, rather than to arbitrary points in space. In this thesis, the objects are synchronized to the motion (position and velocity) of the reference object, regardless of whether this follows a predefined path or not. The objects are synchronized in the whole state space, not only in their forward motion with respect to the predefined paths. This circumvents the need for any knowledge of planned manoeuvres altogether.

Appendix E

Simulation and experimental environments

This section provides an overview of the mathematical models used in simulations and practical experiments for the Underway Replenishment operation to validate the proposed coordination schemes of Chapter 3 and 4. The mathematical models are available from extensive model tests, and can be found in Skjetne *et al.* (2004*a*), Wondergem (2004) and Knudsen (2004).

E.1 Simulation environment

Simulations of the Underway Replenishment operations were performed in MATLAB using the mathematical models of the model surface ships Cybership II and Cybership III of Section E.3. Simulations serve as an illustration of the theoretical stability properties of the proposed coordination schemes of Chapter 3 and 4, and were performed in an ideal environment with no waves, winds, currents or measurement noise. In the simulations, a reference vehicle (see Section 2.2.5) was designed to provide a desired position and heading for the follower vessel, and the leader was controlled to track a sine trajectory to illustrate coordination of the ships for a non-trivial manoeuvre. The trajectory and the mathematical model of the leader were unknown to the follower, and only the position and heading of the leader were available as output. The mathematical model of the follower was considered known in the coordination schemes, and the velocity of the follower was considered known in the motion coordination schemes of Sections 3.2 and 4.2, and unknown for Sections 3.3 and 4.3.

E.2 Experimental environment

Experiments were performed in the Marine Cybernetics Laboratory (MClab) at NTNU (see Figure E.1). The MClab is approximately $40\text{m} \times 6.45\text{m} \times 1.5\text{m}$, and is equipped with a ProReflex motion capture system that gives 6 DOF position and orientation measurements for the two surface vessel models. The ProReflex system consists of four infrared cameras, four or five active markers on each model ship and a computer (NyPosPC) which sends the 6DOF measurement position data to the vessels via a wireless Ethernet connection.

Figure E.1: Pictures of Cybership II (left) and basin (right) in MClab, NTNU.

A limitation in the experimental setup limits the number of vessels that can receive real-time position measurements to only one, and thus for experiments with two physical models in the basin, only the follower vessel receives position information of the two ships. In this scenario, the leader is manually controlled using a joystick based on visual feedback only. To allow a direct comparison between the theoretical results and the performance in practice, a different experimental setup utilized a non-physical virtual model ship running on a computer, and controlled to track the desired sine wave trajectory. In this setup, only the follower vessel manoeuvres in the basin, while the leader vessel exists only as a mathematical model with a controller running on a computer.

Remark E.1 *Note that the scenario with only one model ship greatly improves the performance of the position measurement system in the basin in terms of availability of measurements. However, no ship interaction through drag forces between the ships, known as the Venturi-effect (cf. McTaggart* et al. *(2002)), are experienced in this scenario, and only the follower ship experiences waves and disturbances, and only the position measurements of the follower are contaminated by measurement noise during the experiments.*

In the scenario where both the leader and the follower vessels are physical model ships, both ships experience disturbances, waves, and both positions are contaminated by measurement noise. However, limitations in the camera-based position measurement system causes frequent drop-outs of position measurements when there are two physical ships is the basin, which greatly reduces the quality of the measurement. Furthermore, due to the limitation on the distribution of position measurements, only the follower can receive position measurements. Thus, the leader must be controlled manually using a joystick which renders the comparison between theoretical simulations and practical performance in experiments difficult.

Measurement errors for a single marker were less than 4 mm, but when the distance from the camera was increased, or there were two physical ships in the basin with active markers, an increasing rate of measurement drop-outs was experienced, and the accuracy of the measurements decreased.

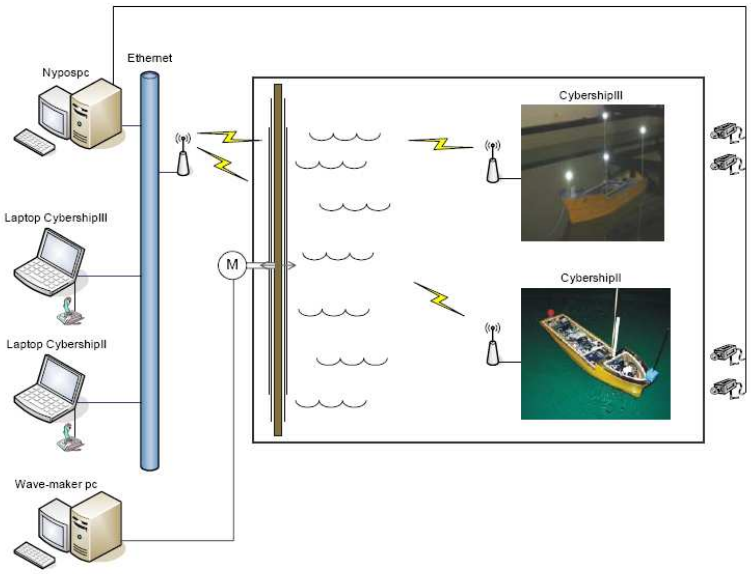

Figure E.2: The MClab experimental setup (Knudsen (2004)).

Each ship has an onboard PC, and communicates with an assigned laptop PC through a wireless Ethernet link (Figure E.2). The model Cybership III was assigned as the leader vessel (designated as the *main* vessel in the underway replenishment scenario) in the experiments, and was manually steered by joystick control through a Fujitsu-Siemens Lifebook E with a Pentium M processor and 512 MB RAM running Microsoft Windows XP Professional. The model ship Cybership II was assigned as the follower vessel (designated as the *supply* vessel in the underway replenishment scenario), and was interfaced using a Dell Latitude D800 laptop with a 1.6 GHz Intel Pentium M processor, 512 MB RAM running Microsoft Windows XP Professional.

A wave maker system consisting of a single flap covering the width of the basin was available for generating waves in the experiments through a controlled motor which moves the flap with a predefined wave spectrum. The wave-maker system was set to give waves with a JONSWAP (Joint North Sea Wave Project) spectrum during the designated experiments with waves. The significant wave high was set to 0.01m and the peak-period to 0.75s.

E.2.1 Cybership II

The surface ship Cybership II is a Froude scaled (1:70) model supply vessel with length 1.3m and weight 24kg. The ship is actuated through two rpm-controlled screws with two rudders at the stern, and an rpm-controlled tunnel bow thruster (Figure E.3). The maximum actuated forces are 2 N in surge, 1.5 N in sway and 1.5 Nm in yaw, and the KPL

thrust-allocation algorithm of Lindegaard (2003) is employed for actuation in all degrees of freedom. The onboard PC is a 300 MHz embedded board computer with 128 MB SDRAM running QNX Neutrino RTOS.

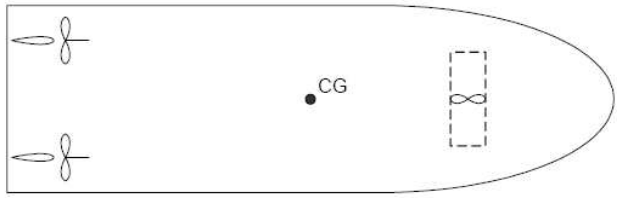

Figure E.3: Cybership II thruster configuration (Knudsen (2004)).

E.2.2 Cybership III

The surface ship Cybership III is a Froude scaled (1:30) model offshore vessel primarily built for testing dynamic positioning (DP) systems. It is equipped with two azimuth thrusters at the stern, and one azimuth thruster and one tunnel thruster in the bow (Figure E.4). The onboard PC is a NS GX1-300 MMX with 512 MB SDRAM and it is running QNX Neutrino 6.2 RTOS. The overall length is 2.3m and the weight is approx. 75kg.

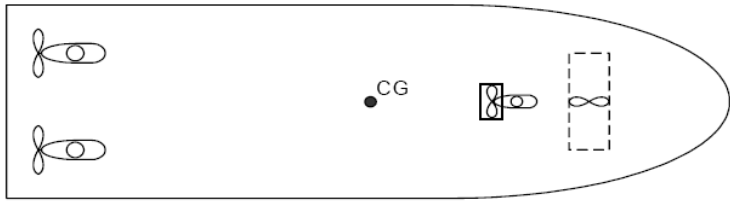

Figure E.4: Cybership III thruster configuration (Knudsen (2004)).

E.2.3 Control implementation

The software is developed using rapid prototyping and automatic code generation with Opal RT-Lab and Matlab/Simulink. Opal RT-Lab builds a distributed model from the Simulink model and loads this model to the target PC onboard the vessel where it is compiled. The experiments are controlled and monitored using a LabView interface. Figure E.5 shows a simplified sketch of the implementation architecture in the experimental setup. The LabView interface controls and monitors the follower vessel during experiments, and allows the user to change the distance between the reference vehicle and the leader ship online, and to reset experiments and logging variables. Figure E.6 shows a screenshot of the LabView interface during experiments. Note that a graphical visualization tool is also available for the data collected in the experiments (Danielsen *et al.* (2004)).

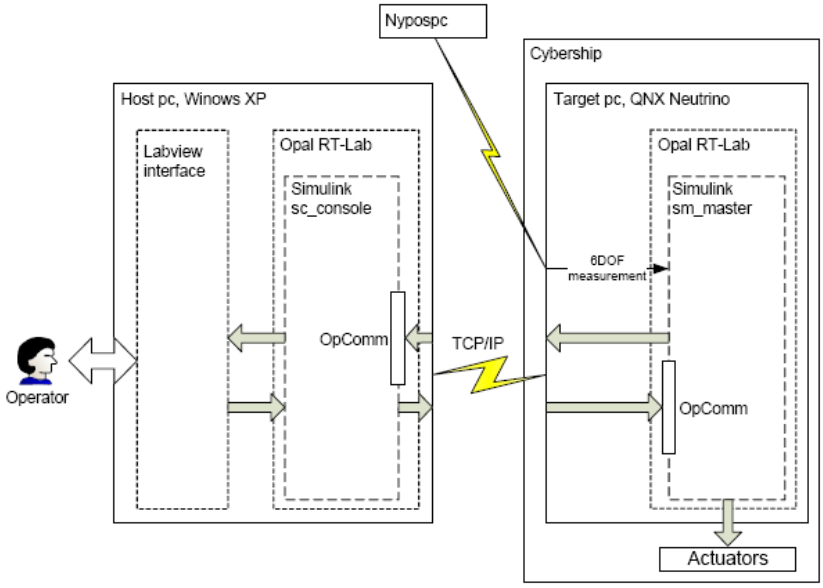

Figure E.5: Implementation architecture for control implementation (Knudsen (2004)).

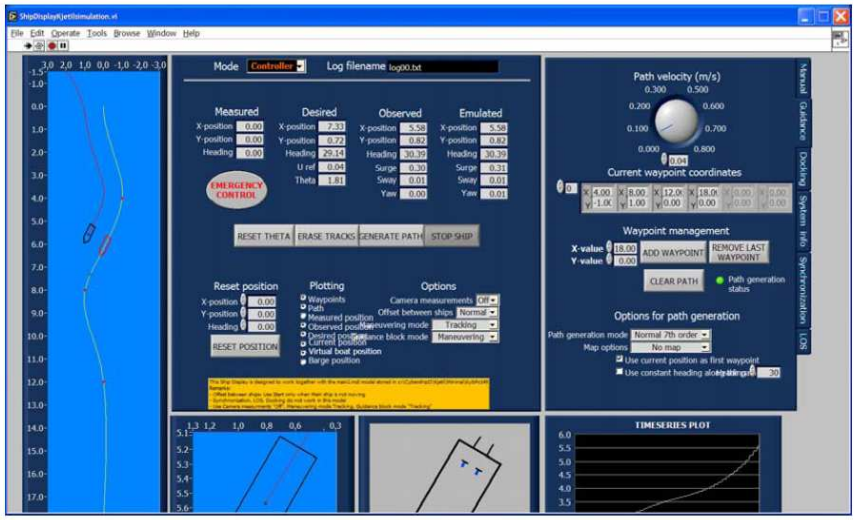

Figure E.6: LabView interface during experiments (Knudsen (2004)).

E.3 Mathematical models

The mathematical models of Cybership II and Cybership III are obtained through model tests using force sensors, and hydrodynamic software computations. The mathematical models are given in the body reference frame, and body-fixed velocities are $\nu = [u, v, r]^T$ in surge, sway and yaw. Note that for surface ships considered in a 3DOF situation on the surface with heave, pitch and roll negligible, the gravity and buoyancy vector $\mathbf{g}(\mathbf{x})$ of (2.27) is zero.

E.3.1 Cybership II

The inertia matrix $\mathbf{M}_\nu$, Coriolis and centrifugal matrix $\mathbf{C}_\nu(\nu)$, and the nonlinear damping matrix $\mathbf{D}_\nu(\nu) = \mathbf{D}_l + \mathbf{D}_n(\nu)$ of (2.27) for the surface ship model Cybership II are

$$\mathbf{M}_\nu = \begin{bmatrix} 25.8 & 0 & 0 \\ 0 & 33.8 & 1.0115 \\ 0 & 1.0115 & 2.76 \end{bmatrix} \tag{E.1}$$

$$\mathbf{C}_\nu(\nu) = \begin{bmatrix} 0 & 0 & -33.8v - 1.0115r \\ 0 & 0 & 25.8u \\ 33.8v + 1.0115r & -25.8u & 0 \end{bmatrix} \tag{E.2}$$

$$\mathbf{D}_l = \begin{bmatrix} 0.72 & 0 & 0 \\ 0 & 0.8896 & 7.25 \\ 0 & 0.0313 & 1.90 \end{bmatrix} \tag{E.3}$$

$$\mathbf{D}_n(\nu) = \begin{bmatrix} 1.33|u| + 5.87u^2 & 0 & 0 \\ 0 & 36.5|v| + 0.805|r| & 0.845|v| + 3.45|r| \\ 0 & 3.96|v| - 0.130|r| & -0.080|v| + 0.75|r| \end{bmatrix} \tag{E.4}$$

E.3.2 Cybership III

The inertia matrix $\mathbf{M}_\nu$, Coriolis and centrifugal matrix $\mathbf{C}_\nu(\nu)$, and the nonlinear damping matrix $\mathbf{D}_\nu(\nu) = \mathbf{D}_l + \mathbf{D}_n(\nu)$ of (2.27) for the surface ship model Cybership III are

$$\mathbf{M}_\nu = \begin{bmatrix} 76.9 & 0 & 0 \\ 0 & 76.9 & 2.77 \\ 0 & 2.77 & 20.4 \end{bmatrix} \tag{E.5}$$

$$\mathbf{C}_\nu(\nu) = \begin{bmatrix} 0 & 0 & -76.9v + 1.07r \\ 0 & 0 & 0.006u \\ 76.9v - 1.07r & -0.006u & 0 \end{bmatrix} \tag{E.6}$$

$$\mathbf{D}_l = \begin{bmatrix} 12.2 & 0 & 0 \\ 0 & 11.9 & 0.59 \\ 0 & 0.59 & 4.37 \end{bmatrix} \tag{E.7}$$

Note that the nonlinear damping terms have not been identified for Cybership III, and that these terms are in general difficult to identify. Due to the manual control with a joystick of Cybership III during experiments, the lack of identified nonlinear damping effects have no practical significance for the experiments.